NOTICE

The quality of this microform is heavily dependent upon the quality of the original thesis submitted for microfilming. Every effort has been made to ensure the highest quality of reproduction possible.

If pages are missing, contact the university which granted the degree.

Some pages may have indistinct print especially if the original pages were typed with a poor typewriter ribbon or if the university sent us an inferior photocopy.

Reproduction in full or in part of this microform is governed by the Canadian Copyright Act, R.S.C. 1970, c. C-30, and subsequent amendments.

AVIS

La qualité de cette microforme dépend grandement de la qualité de la thèse soumise au microfilmage. Nous avons tout fait pour assurer une qualité supérieure de reproduction.

S'il manque des pages, veuillez communiquer avec l'université qui a conféré le grade.

La qualité d'impression de certaines pages peut laisser à désirer, surtout si les pages originales ont été dactylographiées à l'aide d'un ruban usé ou si l'université nous a fait parvenir une photocopie de qualité inférieure.

La reproduction, même partielle, de cette microforme est soumise à la Loi canadienne sur le droit d'auteur, SRC 1970, c. C-30, et ses amendements subséquents.

Canada

A Dinuclear Approach to Phosphate Diester Hydrolysis

Daphne C. Wahnon

A thesis submitted to the Faculty of Graduate Studies and Research of McGill University in partial fulfillment of the requirements for the degree of Doctor of Philosophy

June, 1995
Department of Chemistry
McGill University
Montréal, Québec, Canada

ISBN 0-612-08164-8

Canada

To my parents,
Angel and Amalia

Abstract

The catalysis of the transesterification reaction of 2-hydroxypropyl *p*-nitrophenyl phosphate HPNP by a series of copper(II) complexes is investigated. Dichloro-[(bis(benzimidazol-2-ylmethyl)amine)copper(II)]·CH_3OH (Cu(N3)) and chloro-[(bis(benzimidazol-2ylmethyl)hydroxyethylamine)copper(II)] chloride·3(H_2O) (Cu(N3OH)) are the most reactive mononuclear catalysts for promoting HPNP cleavage. A second order dependence on catalyst and a second order hydroxide dependence is observed for the transesterification reaction of HPNP promoted by Cu(N3). A mechanism is proposed in which a dimerized complex provides double Lewis acid activation followed by nucleophilic attack of the internal alkoxide of HPNP.

A dinuclear copper(II) complex dichloro-[(N,N,N',N'-tetrakis(2-benzimidazolyl)-2-hydroxy-1,3-di-aminopropane)dicopper(II)] chloride LCu_2 is also shown to be extremely reactive in promoting the cleavage of HPNP. LCu_2 (2 mM) cleaves HPNP with an observed pseudo first order rate constant of 3.9×10^{-3} s^{-1} at pH 7 and 25°C. The half-life for this reaction is 3 mins. LCu_2 is as effective as Cu(N3) and Cu(N3OH) for promoting the transesterification reaction of HPNP. A mechanism is proposed which involves double Lewis acid activation and facilitation of nucleophilic attack by the internal alkoxide of HPNP. A value for the rate enhancement expected by a double Lewis acid mechanism 6×10^6 in the cleavage reaction of phosphate diesters is reported. The novel compound LCu_2DMP is synthesized and characterized. The structure of LCu_2DMP provides supporting evidence for the mechanism proposed.

Two novel and structurally interesting dinuclear cobalt(III) complexes, μ-dimethylphosphato-di-μ-hydroxy-bis[(1,4,7-triazacylononane)cobalt(III)] triperchlorate $tacn_2Co_2(OH)_2DMP$ and μ-(methyl-*p*-nitro-phenylphosphato)-di-μ-hydroxy-bis[(1,4,7-triazacylononane)cobalt(III)] triperchlorate $tacn_2Co_2(OH)_2MPNP$ are synthesized and characterized. The second order rate constant for the hydroxide catalyzed hydrolysis of the doubly coordinated methyl (*p*-nitrophenyl) phosphate MPNP is 1.1×10^6 $M^{-1}s^{-1}$ at 45 °C. The proposed mechanism involves double Lewis activation of the phosphate diester and nucleophilic attack by a bridging oxy nucleophile. The breakdown of the species formed by this nucleophilc attack involves Co - O bond cleavage. Oxygen labeling experiments, pH-rate data and the identified reaction products are consistent with the proposed mechanism. A rate acceleration of 6×10^{11} fold is observed for the hydrolysis of the P-O bond in $tacn_2Co_2OH_2MPNP$ over the background hydrolysis rate of MPNP.

Résumé

La catalyse de la réaction de transestérification du 2-hydroxypropyl *p*-nitrophenyl phosphate HPNP par une série de complexes de cuivre(II) a été étudiée. Le [(bis(benzimidazol-2-ylmethyl)amine)copper(II)]·CH_3OH (Cu(N3)) et le chloro-[(bis(benzimidazol-2ylmethyl)hydroxyethylamine)copper(II)] chloride·3(H_2O) (Cu(N3OH)) sont les catalyseurs mononucléaires les plus réactifs pour promouvoir le clivage du HPNP. Un caractère de second ordre du catalyseur ainsi que de l'ion hydroxyde est observé pour la réaction de transestérification du HPNP promue par le Cu(N3). Le mécanisme proposé fait intervenir un complexe dimerisé qui fournit une activation double par les acides de Lewis suivi par une attaque nucléophilique par l'alcoolate interne du HPNP.

Un complexe de cuivre(II) dinucléaire dichloro-[(N,N,N',N'-tetrakis(2-benzimidazolyl)-2-hydroxy-1,3-di-aminopropane)dicopper(II)] chloride LCu_2 a aussi démontré une extrême réactivité dans la promotion du cleavage du HPNP. LCu_2 (2 mM) clive le HPNP avec une constante du pseudo-premier ordre de 3.9×10^{-3} s^{-1} à pH 7 et 25 °C. La demi-vie pour cette réaction est 3 mins. Le LCu_2 est aussi efficace que le Cu(N3) et le Cu(N3OH) pour promouvoir la transestérification du HPNP. Un mécanisme, comprenant une activation double par acide de Lewis, facilité par l' attaque nucléophilique de l' alcoolate interne du HPNP, est proposé. Une valeur pour l' accroissement du taux attendu avec un mécanisme d' activation double par des acides de Lewis, dans la réaction du clivage du diesters de phosphate, est rapportée. Le nouveau composé LCu_2DMP est synthétisé et caractérisé. La structure observée pour le LCu_2DMP est en accord avec le mécanisme proposé.

Deux nouveaux complexes dinucléaires de cobalt(III), de structures intéressantes, le μ-dimethylphosphato-di-μ-hydroxy-bis[(1,4,7-triazacylononane)cobalt(III)] triperchlorate $tacn_2Co_2OH_2DMP$ et le μ-(methyl-*p*-nitro-phenylphosphato)-di-μ-hydroxy-bis[(1,4,7-triazacylononane)cobalt(III)] triperchlorate $tacn_2Co_2OH_2MPNP$, sont synthétisés et caractérisés. La constante de deuxième ordre pour l'hydrolyse du MPNP catalysée par l' hydroxyde, doublement coordonné, est de 1.1×10^6 M^{-1} s^{-1} à 45 °C. Le mécanisme proposé procède par une activation double inité par les acides de Lewis du diester de phosphate et une attaque nucléophile par un oxygène ponté. L'espèce formée suite à cette attaque nucléophile conduit à une rupture du lien Co-O. Les expériences à l'oxygène marqué, la variance de la vitesse en function du pH ainsi que l'identification des produits de la réaction sont en accord avec le mécanisme proposé. Un taux d'accélération de la réaction de 6×10^{11} fois est observé pour l'hydrolyse du lien P-O dans le $tacn_2Co_2OH_2MPNP$ comparativement à l'hydrolyse du MPNP sans catalyseur.

Acknowledgments

I would like to acknowledge my research supervisor Prof. Jik Chin for his advice and support throughout this endeavour.

I would like to thank :

Dr. Bryan Takasaki, James Connolly, Dr. Nick Williams, Dr. Jung Hee Kim, Dr. Barry Linkletter, Jin Seog Seo, Mary Jane Young, Phillip Hurst, Mark Wall, William Cheung, Dan Williams, Dr. Vrej Jubian, Karen Mrejen, and Dr. Stephen Kawai for their friendship and helpful discussions.

Dr. Rosemary Hynes and Dr. Anne-Marie Lebuis for the X-ray structure determinations.

Paul Jones for translating the abstract.

Nick Williams and James Connolly for their helpful criticisms, comments and proof reading of the manuscript.

James Connolly for his invaluable assistance throughout the years in areas too numerous and diverse to mention.

I extend a special thanks to Curtis Keith and Christophe Farès, two undergraduate students who assisted me in my first years of research at McGill.

I wish to thank my parents and family for their love, support, and encouragement throughout my studies. A special thanks to my friends Jean Baldwin, Michelle Meszaros and Darlene Trojansek and to Paul Jones for always making life interesting and enjoyable.

Glossary of symbols and abbreviations

Å	angstrom
°C	degrees Celsius
δ	chemical shift
ApA	adenyl (3'-5') adenosine
bamp	2,6-(bis-aminomethyl)pyridine
BDNPP	bis(dinitrophenyl) phosphate
BNPP	bis(*p*-nitrophenyl) phosphate
bpy	2,2' - bypyridine or 2,2'-dipyridyl
Bz	benzimidazole
c-AMP	2',3'-cyclic adenosinemonophosphate
CHES	2-(cyclcohexylamino)ethanesulfonic acid
Cu(N3)	dichloro-[(bis(benzimidazol-2-ylmethyl)amine)copper(II)]·CH3OH
Cu(N3OH)	chloro-[(bis(benzimidazol-2-ylmethyl)hydroxyethylamine)copper(II)] chloride
Cu(N3DMP)	dimethylphosphato-methanol-[(bis(benzimidazol-2-ylmethyl)amine)copper(II)] perchlorate
cyclen	1,4,7,10-tetraazacyclododecane
dApdA	2' - deoxyadenyl (3'-5') -2'-deoxyadenosine
DIEN	diethylenetriamine
DMF	dimethylformamide
DMP	dimethyl phosphate
DNA	deoxyribonucleic acid
DNase	doexyribonuclease
DPA	2,2' - dipyridylamine
DPP	diphenyl phosphate
DSS	3-(trimethylsilyl)-1-propanesulfonic acid
EDTA	ethylenediaminetetracetic acid
EPNP	ethyl (*p*-nitrophenol)phosphate
EPPS	4-(2-hydroxyethyl)-1-piperazinepropanesulfonic acid
eq.	equation

HEPES	4-(2-hydroxyethyl) -1-piperazineethanesulfonic acid
HIV	human immunodeficiency virus
HPNP	2-hydroxypropyl *p*-nitrophenyl phosphate
hr(s)	hour(s)
Hz	hertz
K	equilibrium constant
K_d	dissociation constant
k	rate constant
k_o	observed rate constant
µL	microlitre(s)
L	ligand
LCu_2	dichloro-[(N,N,N',N'-terakis(2-benzimidazolyl)-2-hydroxy-1,3-diaminopropane)dicopper(II)] chloride
LCu_2DMP	µ-dimethylphosphato-[(N,N,N',N'-terakis(2-benzimidazolyl)-2-hydroxy-1,3-diaminopropane)dicopper(II)] diperchlorate
LFE	linear free enery relationship
MES	4-morpholineethanesulfonic acid
min(s)	minute(s)
mL	millilitre(s)
M	molar
mM	millimolar
MMP	methyl phosphate
mol	mole
mmol	millimole
MPNP	methyl (*p*-nitrophenyl)phosphate
mRNA	messenger RNA
neo	neocuproine
nm	nanometer
poly (A)	poly(adenylic acid)
poly (U)	poly(uridylic acid)
ppt	precipitate
Py	pyridine
R	correlation coefficient
RNA	ribonucleic acid
RNase	ribonuclease

s	second(s)
tacd	1,5,9-triazacyclododecane
tach	1,3,5-triaminocyclohexyl
tacn	1,4,7-triazacyclononane
tacn2Co2(OH)3	tri-m-hydroxo-bis[(1,4,7-triazacylononane)dicobalt(III)] trinitrate
tacn2Co2(OH)2DMP	μ-(dimethylphosphato)-di-μ-hydroxy-bis[(1,4,7-triazacylononane)dicobalt(III)] triperchlorate
tacn2Co2(OH)2MPNP	μ-(methyl-*p*-nitro-phenylphosphato)-di-μ-hydroxy-bis[(1,4,7-triazacylononane)dicobalt(III)] triperchlorate
TBP	trigonal bypyramidal
tcmc	1,4,7,10-tetrazacyclododecane-1,4,7,10 - tetramethylamide
TER	2,2' - 6,6" - terpyridine
tren	tris(2-aminoethyl)amine
tRNA	transfer RNA
trpn	tris-(3-aminopropyl)amine
UpU	uridyl(3'-5')uridine
Uv-vis	ultraviolet-visible
vs.	versus
W	2,12-dimethyl-3,7,11,17-tetraazabicyclo[11.3.1]-heptadeca-1(17),2,11,13,15-pentaene

Structure of ligands

cyclen

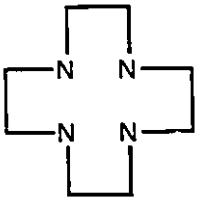

DIEN

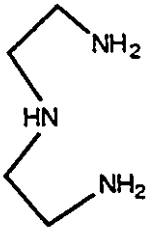

DPA

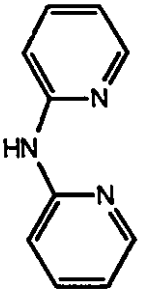

L

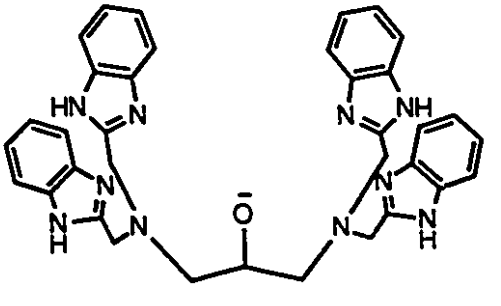

N3

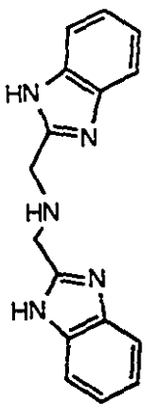

N3OH

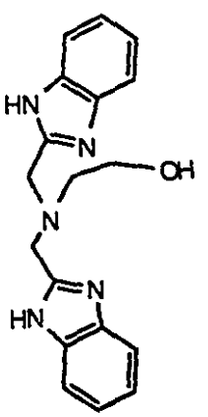

neo

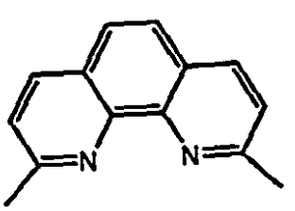

tacd

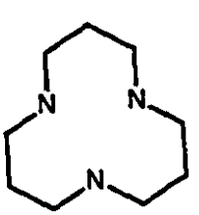

tach

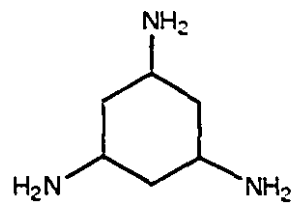

tacn

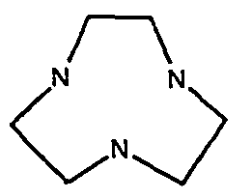

tcmc

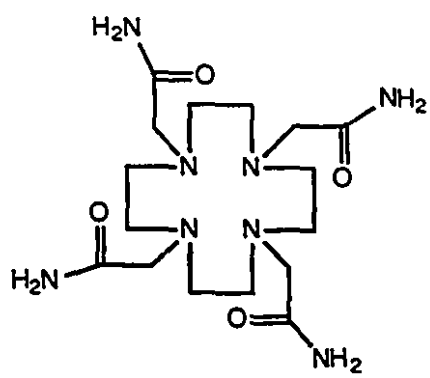

TER

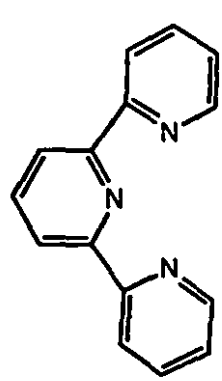

tren

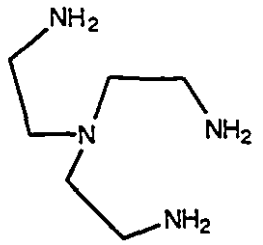

trpn

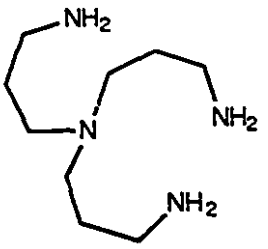

W

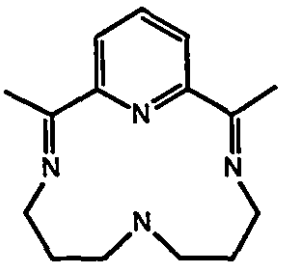

Introduction

1 DNA and RNA

The nucleic acids, deoxyribonucleic acid (DNA) and ribonucleic acid (RNA), are the biopolymers responsible for the storage and transfer of genetic information. The flow of genetic information occurs from DNA to RNA by the process of transcription. Translation of the information leads to the synthesis of important proteins. While the genes of all organisms are composed of DNA, the genes of viruses can be RNA or DNA. Both DNA and RNA therefore represent viable targets in genetic engineering and medicine.

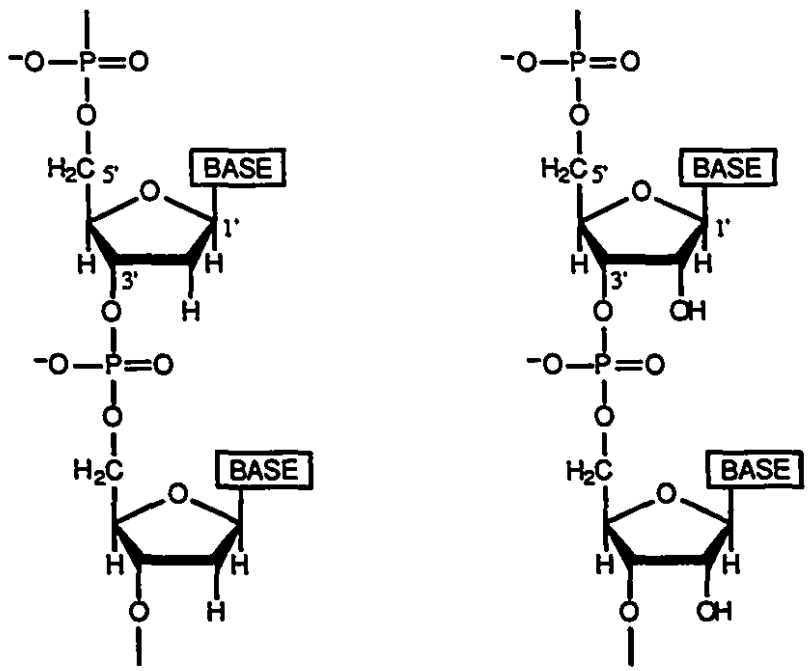

DNA **RNA**

Figure 1.1 Structures of DNA and RNA

DNA is a polymer of deoxyribonucleotide units (figure 1.1). A nucleotide consists of a base, a C5-carbohydrate (a deoxyribose) and a phosphate group. The sequence of the polymer defined by the four bases, Adenine (A), Guanine (G), Cytosine (C), and Thymine (T) contains the genetic information of the organism. The 3'-hydroxyl of the sugar is linked by a phosphodiester bridge to the 5'-hydroxyl of the adjacent sugar. It is the integrity of this phosphate linkage that imparts such remarkable stability to the DNA polymer. Indeed, it has been estimated that the half-life at neutral pH and 25 °C for the hydroxide catalyzed hydrolysis of the phosphodiester bond in DNA is 10^{-16} s^{-1} or 200 million years.[1]

The three dimensional structure of DNA consists of two complementary chains coiled in a double helical structure which places the bases on the inside of the helix and the sugar phosphate backbone on the outside. Hydrogen bonds between the bases hold the chains together in the normal "Watson-Crick" fashion.

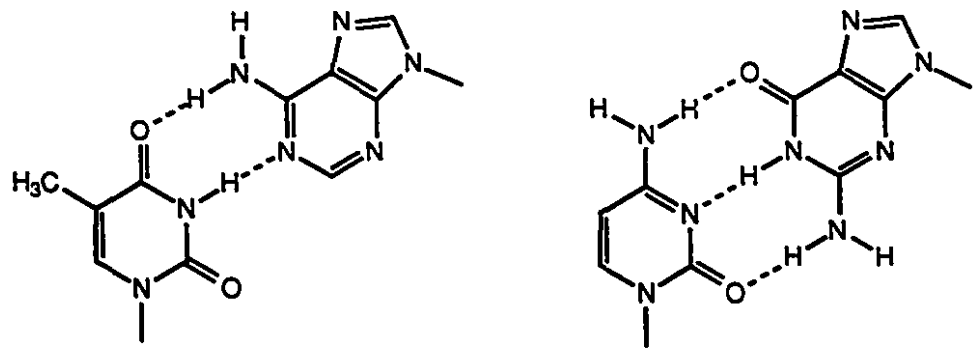

Figure 1.2 Models of adenine-thymine and guanine-cytosine base pairs

RNA is a polymer of ribonucleotide units. Uracil (U) is present as a base and Thymine (T) is not observed. Unlike DNA, the C5-carbohydrate is a ribose unit which contains a 2'-OH (figure 1.1). It is estimated that RNA is 10^7 times more reactive than DNA towards cleavage of the phosphate diester linkage. This extra reactivity can be attributed to the presence of the deprotonated 2'-OH which acts as the nucleophile in the first step of the RNA cleavage. Unlike DNA, the cleavage of RNA proceeds in two steps

with transesterification first occurring to form a cyclic phosphate which hydrolyzes further to a phosphate monoester. (figure 1.3).

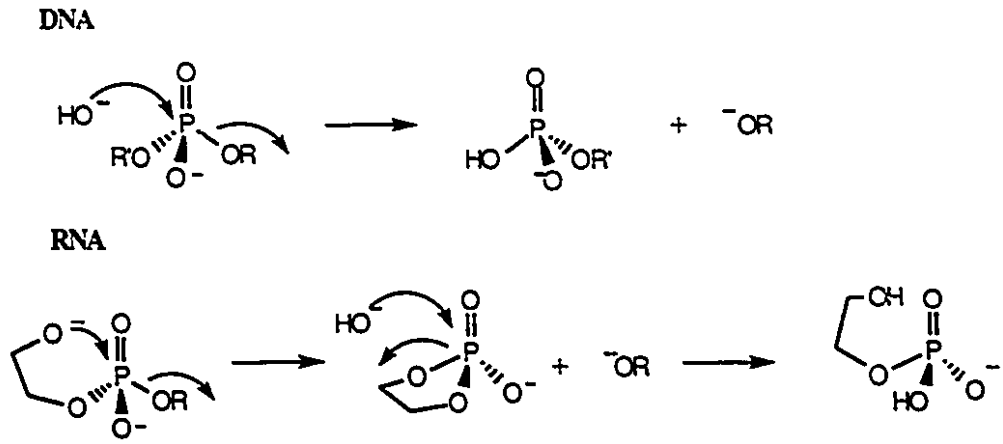

Figure 1.3 Difference in the cleavage mechanism of DNA and RNA

It is estimated that nucleases accelerate the hydrolysis reaction of phosphate diesters by up to 10^{16} fold.[2,3] Metals play an important role in many of these enzymes. The ability to mimic the rate accelerations obtained by these enzymes would lead to molecular tools for DNA and RNA manipulation. To do this, it is important to understand the mechanisms by which phosphate diesters are cleaved. First, the general mechanism for substitution at phosphorous will be discussed. Secondly, the general mechanisms by which nucleases and ribozymes are believed to hydrolyze DNA and RNA will be reviewed. A general overview of the contributions and advancements towards the design of artificial nucleases will follow.

2 Phosphate Diester Hydrolysis

2.1 General Mechanism

Nucleophilic substitution at a phosphate diester phosphorous occurs by an associative mechanism $S_N2(P)$. Inversion of configuration occurs at phosphorous by a direct in-line substitution mechanism. Retention of configuration is observed when the

nucleophile attacks adjacent to the leaving group and pseudorotation occurs once. The pseudo rotation is required by the principle of microscopic reversibility to expel the leaving group from the apical position (since the nucleophile attacks at an apical position - figure 1.4).

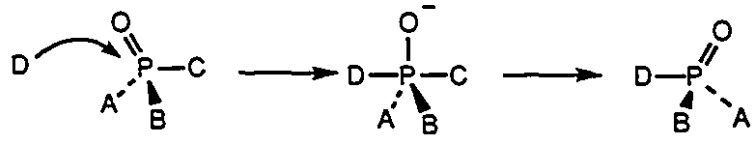

Direct in line mechanism - inversion of configuration

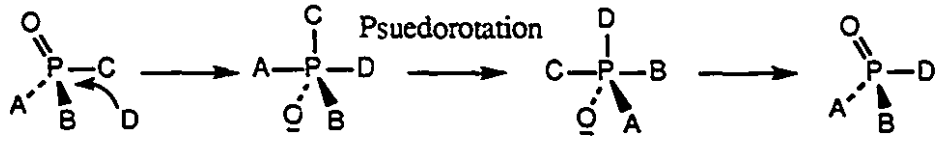

Adjacent attack - retention of configuration

Figure 1.4 Stereochemistry of nucleophilic substitution at phosphorous

The general mechanism proceeds by guidelines outlined by Westheimer.[4,5]

1) Attack of the nucleophile on the tetrahedral phosphorous results in a pentacoordinate trigonal bipyramidal (TBP) species which may be an intermediate.
2) If the TBP species is an intermediate ligand reorganization is possible. Pseudorotation occurs in a defined manner. Pseudo rotation exchanges two equatorial ligands for two apical ligands. The original trigonal bipyramidal intermediate can therefore pseudorotate to three other isomers.
3) Nucleophiles will attack from an apical position and in accordance with the extended principle of microscopic reversibility the leaving group will leave from the apical position.

4) i) if phosphorous is contained in a four or five-membered ring, the ring will prefer to be apical/equatorial
   ii) more-electronegative ligands prefer equatorial positions
   iii) p-donor ligands prefer equatorial positions ; ligands with low-lying p-acceptor orbitals preferentially occupy equatorial positions. Due to cross conjugation with the aromatic ring and the oxygen lone pair, the phenoxy ligand possesses a high apicophilicity. The cross-conjugation reduces the O(p)-P(d) orbital interaction and thus the equatorial preference of the ligand.
   iv) steric effects are minimized when bulky substituents occupy equatorial positions

The above guidelines were developed based on the reactivity of phosphorous contained in a five-membered ring. Some of the original guidelines now require modification and review. Pseudorotation , apicophilicity and Westheimer's rules may be applied to predict the stereochemistry of substitution at acyclic phosphorous,[6] however a number of exceptions to these rules have been found, for example, in five membered rings containing P-S[7] or P-N[8,9] bonds. A new term apical potentiality has been defined. Unlike apicophilicity, apical potentiality is dependent on the nucleophile, the solvent, and other conditions of reaction. This term has little predictive value and is simply descriptive.

The pK_a of a phosphate diester occurs between one and two. Therefore, under neutral conditions, the diester exists in its anionic form. Repulsion between the attacking nucleophile and the anion is at least partially responsible for the unreactive nature of phosphate diesters towards hydrolysis.[10] The pH-rate profiles[11] of some diaryl phosphate esters are shown in figure 1.5. For the more reactive phosphate diesters, A, B and C, a pH independent region exists between pH 3 and 7. Qualitatively, at lower and higher pH, the observed hydrolysis of phosphate diesters is due to acid and base catalyzed reaction. For the more unreactive phosphate diesters, D and E, the pH independent region is very small and close to the minimum of the pH-rate curve. The minimum is observed near pH 4.

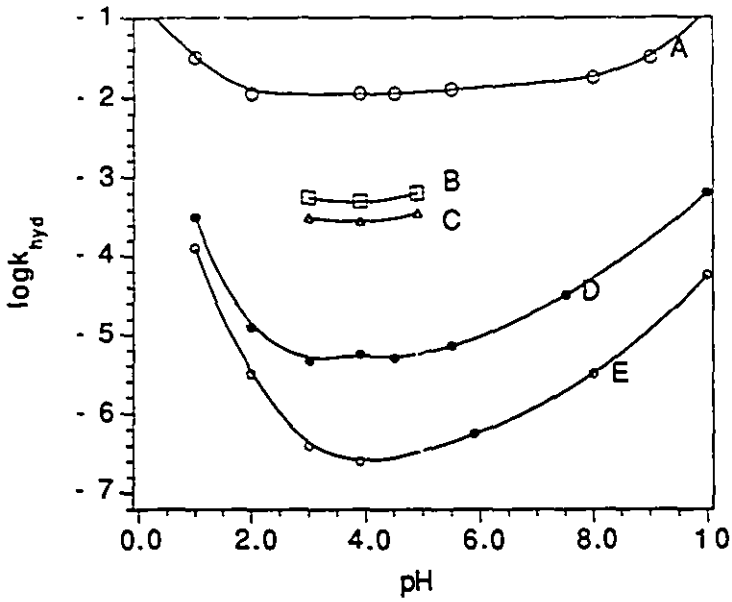

Figure 1.5 pH rate profiles[11] for the observed hydrolysis at 100 °C and ionic strength 1.0 of A bis-2,4-dinitrophenyl phosphate; B bis-4-acetyl-2-nitrophenyl phosphate; C bis-4-chloro-2-nitrophenyi phosphate; D bis-4-nitrophenyl phosphate, and E bis-3-nitrophenyl phosphate

The hydrolysis reactions of phosphate diesters are complicated by P-O vs. C-O bond cleavage. In strong alkaline solution, the most unreactive diesters such as dimethyl phosphate and dibenzyl phosphate react largely via carbon-oxygen cleavage, the rest proceeding via nucleophilic attack at phosphorous.[12] Phosphorous-oxygen bond cleavage dominates under neutral or weakly basic conditions. For reactive esters such as bis (2,4-dinitrophenyl) phosphate the hydrolysis reactions proceed largely via phosphorus-oxygen bond cleavage.[13]

2.2 Phosphate Diesters With Internal Nucleophiles

The reaction of phosphate diesters containing an internal nucleophile constitute a special case of phosphate diester cleavage. As discussed earlier the 10^7 rate difference between the cleavage reaction of RNA and DNA is attributed to the presence of the internal nucleophile in RNA. This discussion will be limited to phosphate diesters with alkoxyl nucleophiles.

In a study of the hydrolysis reactions of some RNA models, Brown and Usher [14] have shown that for a series of 2-hydroxypropyl phosphate esters two modes of breakdown exist (figure 1.6); one is transesterification with the expulsion of OR and production of cyclic phosphate; the other is epoxide formation leading to displacement of $ROPO_3^{2-}$ (figure 1.6).

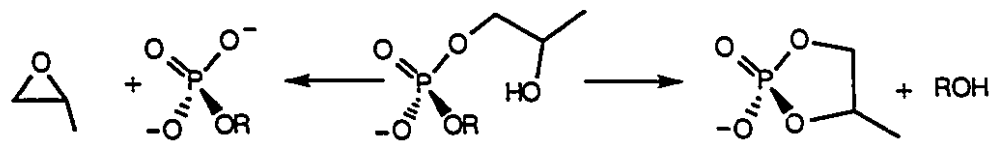

Figure 1.6 Cleavage of 2-hydroxypropyl phosphate esters

The ratio of the epoxide route to the cyclic phosphate route is dependent on the basicity of the OR leaving group. The results for the series of 2-hydroxypropyl phosphates is tabulated in table 1.1. In general there is negligible epoxide formation for the esters containing good leaving groups and larger amounts for esters with poor leaving groups. The rate of the epoxide route is similar for most esters but increased amount of percentage total product due to the epoxide route is observed due to differences in the rates of the cyclic phosphate route. In the alkyl ester case, there is negligible cyclic phosphate accumulation since the cyclic phosphate formation is much slower than subsequent ring opening. In the case of esters with good leaving groups, the formation of the cyclic phosphate is faster than the subsequent cleavage, and thus the cyclic phosphate is observed.

Table 1.1 Selected data from Brown and Usher.[14] Hydrolysis of 2-hydroxypropyl phosphate esters at 80 °C, in aqueous NaOH. a: extrapolated from data at 25 and 35 °C

leaving group	Rate of ROH formation $(10^6k)M^{-1}s^{-1}$	Mole (%) of product	Rate of $ROPO_3H_2$ $(10^6k)M^{-1}s^{-1}$	Mole (%)
p-Nitrophenol[a]	$260x10^4$	100	-	-
Phenol[a]	$740x10^2$	100	-	-
Methanol	127	93	9.8	7
Cyclohexanol	0.55	16	3.0	84

Figure 1.7 shows the pH dependence of the phenyl ester of 4-hydroxy tetrahydrofuran 3-phosphate.[15] The pH dependence of phosphate diesters with internal nucleophiles is similar to that of 'normal' phosphate diesters. A pH independent region between 4 and 6 is observed.

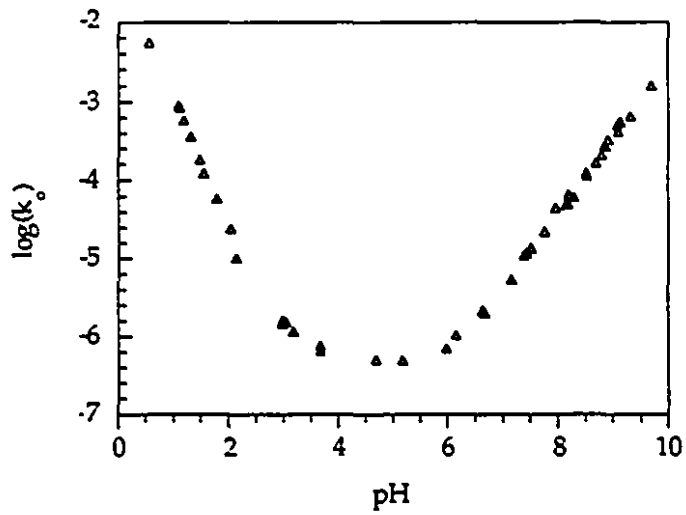

Figure 1.7 pH rate profile[15] for phenyl-4-hydroxy tetrahydrofuran-3-phosphate at 50 °C and 0.1 KCl. k_o in s^{-1}.

3 DNA and RNA Model Compounds

3.1 DNA Model Compounds

Since the half-life of DNA is about 200 million years even an impressive rate acceleration of 10^8 fold would translate to a half-life of 2 years. Thus most studies related to the mechanism and catalysis of DNA are carried out on models of DNA which possess reactivities that allow their measurements on a practical time scale.

A very good linear free energy relationship (figure 1.8) exists between the second order rate constant for the base catalyzed hydrolysis and the pK_a of the leaving group for a wide range of phosphodiesters.[1] A β value of -0.76 was obtained for a range of leaving groups spanning 12 orders of magnitude in pK_a and including both aryl and alkyl groups. The observed linear free energy relationship suggests that all the diesters, regardless of leaving group, hydrolyze by the same base catalyzed mechanism and chemically justifies the use of model compounds.

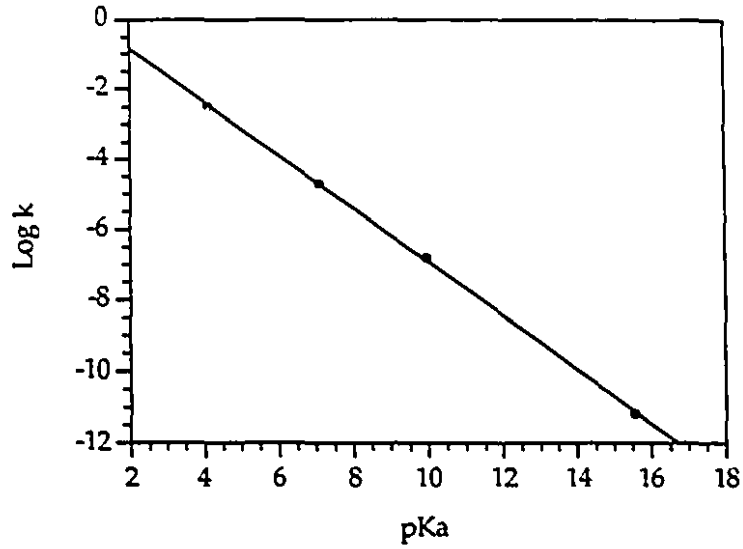

Figure 1.8 Linear free energy relationship between the second order rate constant for the base hydrolysis of phosphate diesters[1] at 25 °C

3.2 RNA Model Compounds

For diesters with internal alkoxyl nucleophiles, linear free energy relationships have also been demonstrated between the second order rate constant of the base catalyzed cleavage and the pK_a of the leaving group alcohol (figure 1.9 plotted with the data from figure 1.8). The β value for a series 2-hydroxypropyl phosphate esters[14] was determined to be -0.56. In a related study [16] a series of aryl uridine-3'-phosphates was determined to have a β value of -0.54. The similar β values for these two series of compounds also suggest that, like DNA and its models, the mechanism for the base catalyzed transesterification of RNA proceeds by one mechanism regardless of leaving group. The parallel linear free energy lines for the different RNA analogues also indicate that the mechanism is constant regardless of the nature of the second OR group in the phosphate diester.

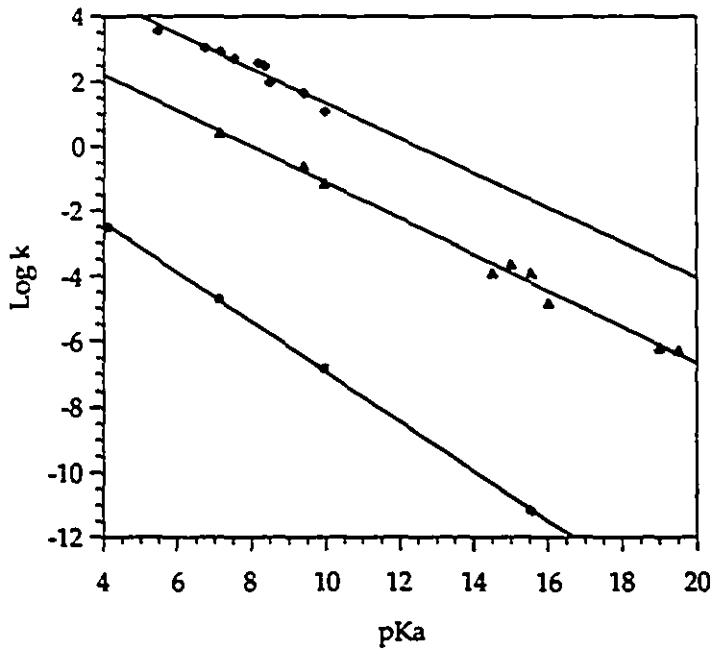

Figure 1.9 Linear free energy relationship between the second order rate constant ($M^{-1}s^{-1}$) for the • base hydrolysis of phosphate diesters[1] at 25 °C and the base catalyzed cleavage of RNA model compounds (♦ aryl uridine-3'-phosphates[16] at 25 °C ▲ 2-hydroxypropyl phosphate esters[14]) at 80 °C and pK_a of leaving group

The rate constants for the hydroxide catalyzed cleavage[16] and relative reactivities of some commonly used RNA model compounds (figure 1.10) with the same phenol leaving group is tabulated in table 1.2 for I-IV. The effective molarity and the basicity of the alkoxide nucleophile is responsible for the order of reactivities observed. Larger effective molarities are observed when the attacking hydroxyl is held rigidly in close proximity to the phosphate as in II, III and IV.

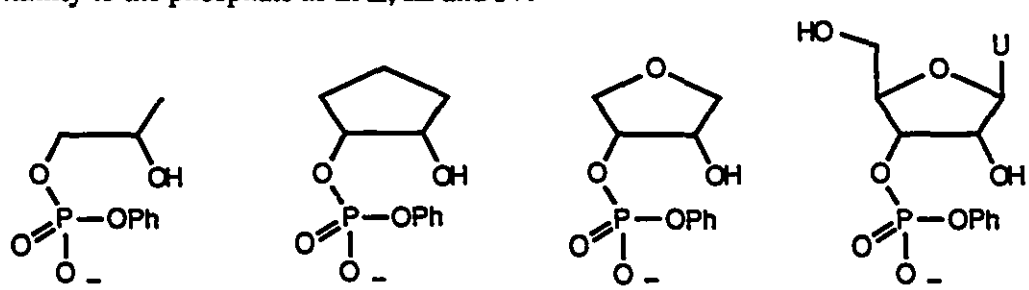

I II III IV

Figure 1.10 RNA analogues

Table 1.2 Data from Davis[16] *et al.* k is the rate constant for the hydroxide catalyzed cleavage of I-IV at 25 °C.

	$k\ (M^{-1}s^{-1})$	Rel Rates
I	0.98×10^{-3}	1
II	0.03	30.6
III	2.17	2214
IV	12	12245

The effective molarities for some of these compounds have been measured (table 1.3). This value compares the rate of the intramolecular unimolecular reaction to the rate of the intermolecular reaction of the appropriate diester and is a measure of the efficiency of the intramolecular catalysis.[17] Effective molarities as large as 3×10^7 M occur for these systems. Even with this intramolecular assistance RNA or even RNA models are cleaved only slowly at neutral pH in the absence of any enzyme or catalyst. The half-life of uridyl (3'-5') uridine (UpU) at pH 7 is 3500 days or 10 years at 25 °C (see chapter 2). Clearly, the acceleration of RNA hydrolysis reactions to rates suitable for RNA manipulation is also a significant challenge.

Table 1.3 Effective Molarities of RNA Analogues

	Effective Molarity (M)
I	2.5×10^4
III	3×10^7

4 Nucleases and Ribozymes

Nucleases are enzymes (proteins) capable of degrading DNA and RNA. Those that are specific to RNA are ribonucleases and those specific to DNA are deoxyribonucleases. The exonucleases cleave only the last nucleotide of the DNA chain. Endonucleases are those nucleases which cleave the phosphodiester backbone to yield a 3'-hydroxyl and a 5'-phosphoryl end via hydrolytic cleavage. The class of enzymes which recognize specific sequences of DNA four to eight base pairs long are termed restriction enzymes. The biological role of the nucleases is the degradation of foreign DNA in the organism.[18]

In 1981 a significant discovery was made. RNA can catalyze its own splicing.[19] Further, it is now realized that RNA is a true enzyme since it can catalyze the cleavage or ligation of external RNA[20,21] or even DNA.[22] These discoveries have altered the notion that all biological catalyst are proteins. Three general mechanisms of RNA and DNA hydrolysis are believed to occur in most nucleases and ribozymes.[23] The majority of these catalysts rely on metals for their function.

4.1 Proposed Mechanisms of Activity

Pancreatic ribonuclease A hydrolyzes RNA to yield a 3'-PO_4 and 5'-OH proceeding through a cyclic phosphate intermediate. One lysine and two histidine residues are required for activity (figure 1.11). In the cyclization step, His-12 acts as a general base catalyst and His-119 acts as a general acid by protonating the leaving group. In the hydrolysis step, the roles of the histidine residues are reversed and His 119 now acts as a general base to activate water for nucleophilic attack. It is believed that the role of Lys-41 is to interact with the phosphate and stabilize the pentacoordinate intermediate. The essential feature of the first general mechanism is the formation of the cyclic phosphate intermediate.

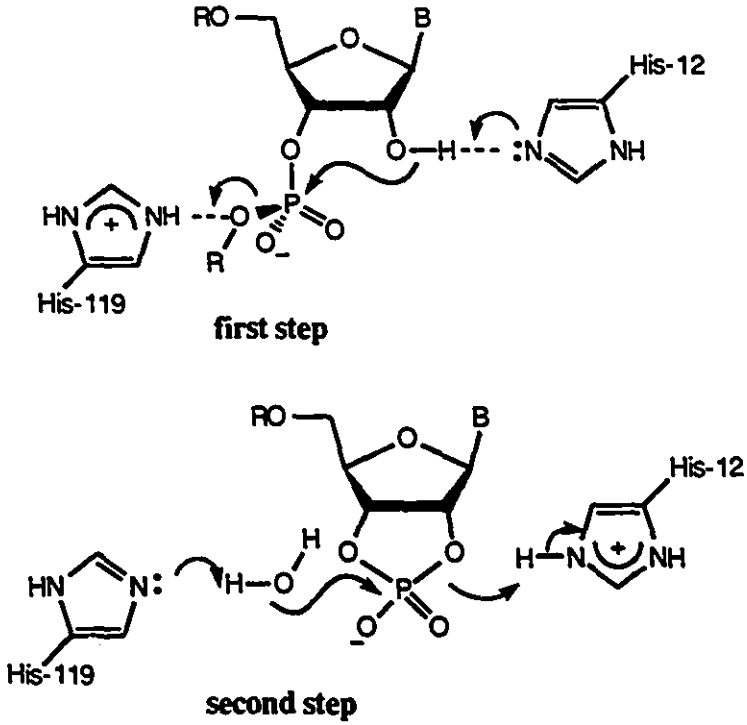

Figure 1.11 Generally accepted mechanism[24] for pancreatic ribonuclease A.

The 2',3'-cyclic phosphate intermediate is also observed in RNA cleavage by the hammerhead, hairpin, hepatitis delta , Neurospora and tRNA ribozymes.[25] The products of the enzymatic reactions are 3'-PO_4 and 5'-OH fragments. Catalysis is due to a divalent metal activation of the phosphoryl group to nucleophilic attack, which is represented by M^{2+} in figure 1.12. Other catalytic roles for divalent metal ions, represented by M in the figure, have not been eliminated and a two metal catalytic system can not be ruled out. It is the internal nucleophilic attack, common to both RNase A and the ribozyme mechanism, that results in the common 2'-3'-cyclic phosphate intermediate.

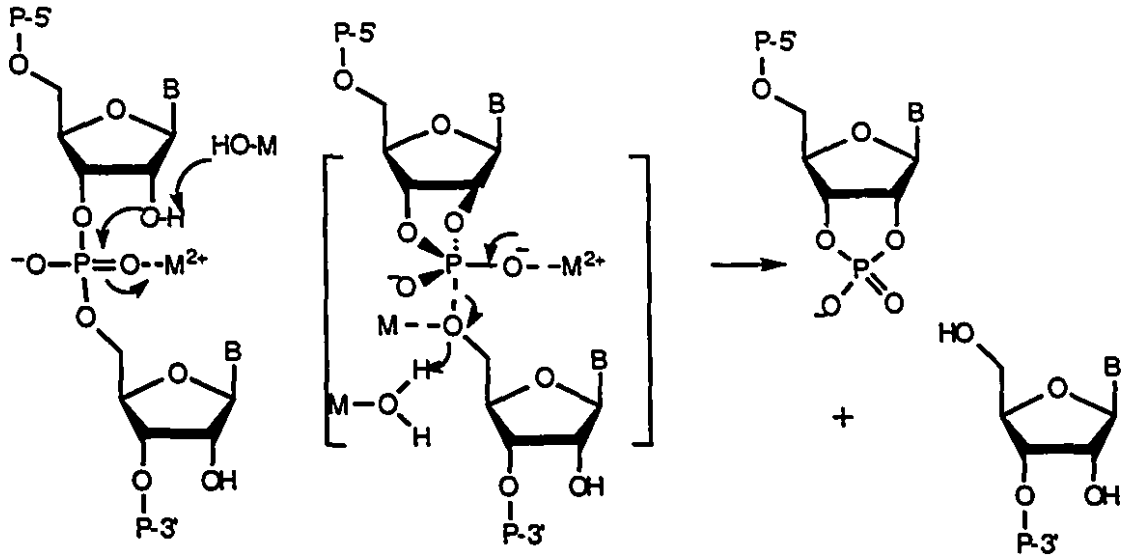

Figure 1.12 RNA cleavage in hammerhead, hairpin, and tRNA ribozyme

Bovine Pancreatic DNase I, a non specific endonuclease, belongs to a second mechanistic category of nucleases. Catalysis is believed to require one metal, a water molecule, a histidine, and glutamate residue. The histidine residue activates the water molecule by acting as a general base. The catalytic triad defined by the water, histidine and glutamate residues is shown below in figure 1.13.[18]

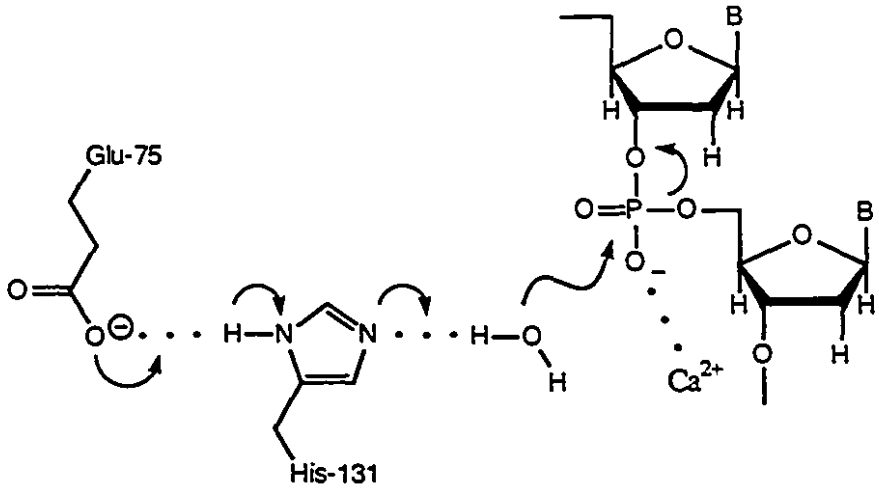

Figure 1.13 Catalytic triad of Bovine Pancreatic DNase I[18]

A third general mechanism requires the presence of di- or tri-nuclear metal centers. These RNA and DNA hydrolysis reactions yield 5'-PO_4 and 3'-OH fragments. The X-ray structures of wild type 3'-5'-exonuclease DNA polymerase I (*E.Coli*) and the protein co-crystallized with a bound single stranded DNA substrate, and bound deoxynucleoside monophosphate product have been determined.[26] Both the wild-type and the product bound protein show the metals 3.9 Å apart. The mechanism proposed (figure 1.14) involves double Lewis activation by the two metals on the phosphoryl oxygen. M_a also activates a water molecule toward nucleophilic attack, M_b assists in the departure of the leaving group. The activity of the enzyme is supported by Mg^{2+}, Mn^{2+}, and Zn^{2+} although Zn^{2+} is believed to be the only metal used in the wild-type.

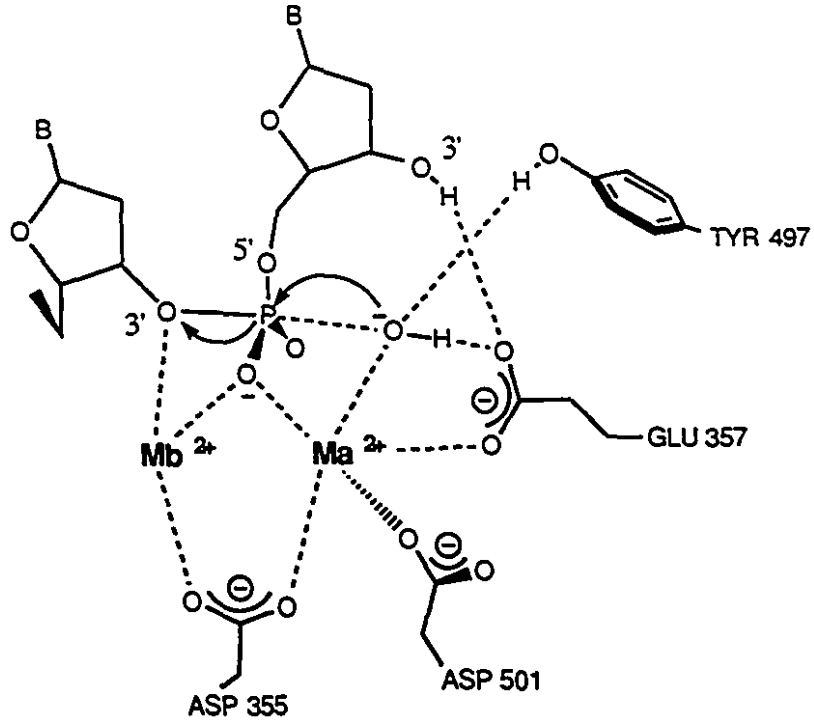

Figure 1.14 Proposed mechanism[26] for 3'-5'-exonuclease DNA polymerase I (*E. Coli*)

A similar general two-metal mechanism has been proposed for RNA hydrolysis by catalytic RNA or ribozymes.[23] Figure 1.15 shows the first step of the two step reaction involved in group II Introns. In this ribozyme a 2'-OH from a distinct residue acts as the nucleophile and thus a cyclic phosphate intermediate is never formed. One metal M_a activates the 2'-OH of the adenosine residue for nucleophilic attack as well as activating of the phosphoryl bond to the attack. The second metal ion M_b also acts as a Lewis acid and facilitates the loss of the leaving group. In the second step, not shown, the role of the two metal ions are reversed and the M_b activates the newly created 3'-OH which attacks at a distinct site and M_a assists in the departure of the guanosine leaving group. This mechanism would apply to group I and II intron ribozymes as well as ribonuclease P.

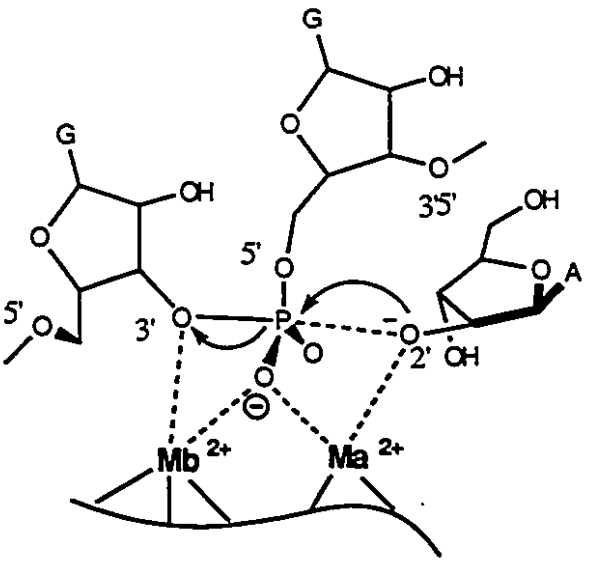

Figure 1.15 Mechanism for group II splicing. The first of the two step reaction involved.

Recently, the crystal structure of RNase H from HIV-1 reverse transcriptase has been determined.[27] Two divalent metals bind in the active site. In the crystal structure the two Mn^{2+} ions are approximately 4 Å apart. A mechanism similar to that of 3'-5'-exonuclease of DNA polymerase has been suggested.[28]

Interestingly, the same structural-functional motif is believed to occur in other related enzymes such as alkaline phosphatase, and phospholipase C.[29] Alkaline Phospholipase is a phosphomonoesterase which contains two Zn^{2+} and one Mg^{2+} ion in the active site. Recently, the X-ray crystal structure of the native enzyme and the enzyme complexed to an inorganic phosphate inhibitor has been published.[30] The two Zn^{2+} ions are also about 4 Å apart while the Mg^{2+} ion is 4.9 Å from Zn2 and 7.1 Å form Zn1. The exact role of the Mg^{2+} ion has not been determined but it does not appear to interact directly with the substrate.

5 Artificial Restriction Enzymes

Although more than ninety natural restriction enzymes have been purified and characterized, there is a still a need for the development of artificial restriction enzymes. Today, restriction enzymes play a major role in molecular genetics and medical science.

They are used as tools for the analysis of chromosome structure, sequencing of long DNA fragments, isolation of genes, and creation of smaller DNA molecules for cloning (recombinant DNA technology).

In recombinant DNA technology,[31] small fragments of DNA are created using restriction enzymes and if necessary, ligated to other small fragments. This segment of DNA can be integrated into a plasmid. A bacterial culture is then used to clone and amplify the segment of DNA. Bacteria containing natural or unnatural DNA fragments can produce pharmaceutical quantities of valuable proteins. Insulin and growth hormones are produced using this technology.

The molecular mechanisms of many diseases have been elucidated and the diagnosis of genetic disorders, infectious diseases and cancers is becoming feasible with the use of DNA probes. An increasing number of stretches of DNA coding for genetic diseases or conditions are being discovered. Clinical trials for a genetic cure of Cystic Fibrosis are already underway. In Cystic Fibrosis, a defect in a protein leads to the accumulation of mucus in the lungs. A normal gene could be inserted into the cell, thereby inducing the manufacturing of the correct protein.

In natural DNA, domains that contain segments recognized by natural restriction enzymes are methylated to protect the DNA from scission. An artificial restriction enzyme could in theory recognize any sequence of DNA and cleave at any predetermined site. A versatile restriction enzyme would be an important tool in these biological applications.

6 Catalyzed Cleavage of Phosphate Diesters

6.1 Oxidative Cleavage

Oxidative systems which cleave DNA and RNA by free-radical and oxidative pathways are efficient catalysts at neutral pH and physiological temperatures. Because of the mechanism which can involve diffusable or non-diffusable hydroxyl radicals as well as other radical species, the products of oxidative cleavage are irreversibly severed. Thus for any practical applications in gene therapy or DNA manipulation these catalysts are not ideal. In a hydrolytic system, the ligated fragments could in theory be re-ligated. In fact, Dervan *et al.* have already demonstrated that by using a guiding sequence to form a triple helix, the cleaved strand of a duplex DNA could be chemically re-ligated.[32]

Catalysis by 1,10-phenanthroline-Copper, Ferrous-EDTA, metal chelating tripeptides, metalloporphorins, and octahedral rhodium complexes have all been

demonstrated to cleave DNA by oxidative pathways.[33,34] The 2:1 tetrahedral complex formed by 1,10-phenanthroline and copper binds reversibly to the minor groove of DNA, then undergoes a one electron oxidation by hydrogen peroxide (figure 1.16).

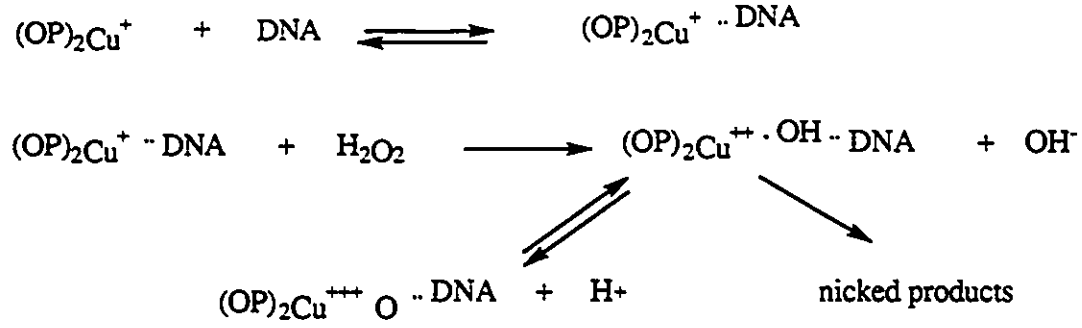

Figure 1.16 1,10-phenanthroline-Copper interaction with DNA

A reactive intermediate involving an hydroxyl radical which is coordinated to the copper(II) is known to occur. This species attacks the C-1 hydrogen (figure 1.17) of the deoxyribose which leads to a series of products. Among the stable products characterized are 3' and 5' phosphorylated ends, free bases and 5-methylene-2(5H)-furanone. RNA cleavage has also been observed with this system.

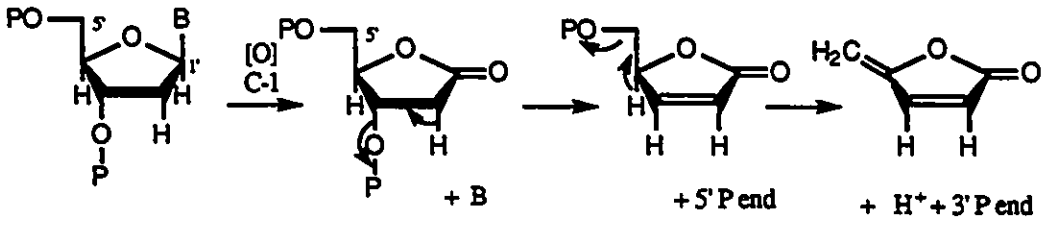

Figure 1.17 Scission of DNA by $(OP)_2Cu^+$

Ferrous-EDTA is able to cleave DNA but does not form a complex in its scission reaction. The mechanism of ferrous-EDTA is thought to involve diffusable hydroxyl radicals generated from the reduction of hydrogen peroxide. This reduction produces a hydroxyl anion and a hydroxyl radical and results in the oxidation of the metal. A

reductant is then required, to allow the reaction to cycle. The reduction can be accomplished by superoxide (O^{2-}), ascorbic acid or dithiothreitol. Attachment of Fe(II)-EDTA to an intercalator methidium allows single stranded and some double stranded cleavage of DNA to occur.[35] Fe(II)-EDTA[36,37] has also been attached to oligonucleotides which can bind a complimentary oligonucleotide strand by triple helix formation and mediate its cleavage.

A different approach to the oxidative cleavage of DNA or RNA is the use of metal chelating tripeptides such as Glycyl-Glycyl-Histidine (GGH) with copper or nickel. In the case of Cu(II) the reaction mechanism is believe to produce diffusable hydroxyl radicals while with Ni(II) a metal-bound oxidizing equivalent is believed to be formed. By attaching the amino terminus of the DNA binding domain of Hin recombinase to the tripeptide[38] Mack and Dervan were able to exploit the oxidizing potential of this system. The protein binds to specific sites and cleaves the DNA in the presence of copper, hydrogen peroxide and ascorbate, or nickel and monoperoxyphthalic acid. Since the metal binds to the terminal amine functionality of the tripeptide unit, the incorporation of the G G H unit is limited to ligation to the amino terminus of other polypeptide structures. A recent redesign (figure 1.18) allows the metal to be placed in the interior of a short peptide chain and therefore can to be incorporated into any site of a polypeptide chain.[39]

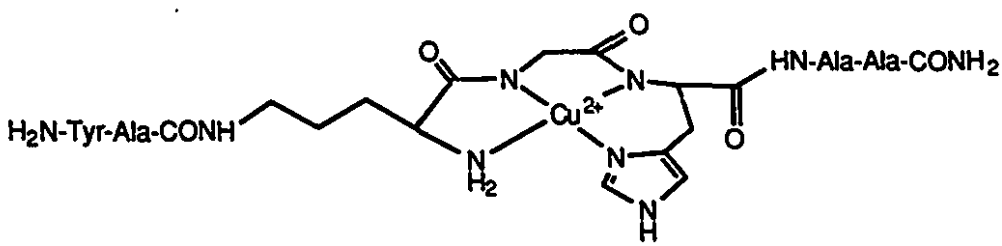

Figure 1.18 Design of modified metal chelating tripeptides

Octahedral complexes of rhodium and ruthenium are interesting in that they possess chirality and thus each enantiomer can discriminate between right and left handed helix. The rhodium complexes of 1,10 - phenanthroline target DNA and RNA upon photoactivation. A light dependent atom abstraction at the C-3H position is postulated and does not involve diffusable intermediates.[40] Octahedral complexes of ruthenium are believed to cleave RNA and DNA by a different mechanism since following the generation of a singlet oxygen, the attack occurs at the base and only if pipiridine is present will the phosphodiester be cleaved.[41]

The last oxidative catalysts which will be discussed are the tetracoordinate nickel(II) complexes which have interesting reactivity for DNA[42] in the presence of monopersultate HSO_5^-. In single stranded regions of DNA, specific recognition of guanine residues was observed. For in-vivo applications, complexes that rely on physiologically available O_2 should be more useful than those that rely on hydroperoxides or peroxy acids. Burrows *et al.* have reported[43] the complete nicking of super coiled plasmid DNA pBR322 after 45 minutes at room temperature with nickel complexes that react in the presence of O_2 to form a nickel(III) superoxido structure. The advantage of this system is that these oxidative catalysts will cause scission under physiological condition using only O_2. Additional reagents, or light is not required for the reaction.

It has been known for some years that lanthanide gels promote the hydrolysis of phosphate esters,[44] but the exact mechanism was not known. Recently, a cooperative effect between peroxide and lanthanum(III) ion has been shown[45] to be effective in the net hydrolysis of BNPP. The pseudo-first order rate constant for the hydrolysis is 4.8 x 10^{-3} s^{-1} (a half-life of 144 s) at pH 7, 2 mM La, 20 mM H_2O_2 and 25 °C. The mechanism proposed (figure 1.19) involves a lanthanum peroxide dimer which can bind the phosphate diester. Oxidative cleavage of the phosphate diester bond results in a peroxyphosphate which in the presence of peroxide reduces to phosphate. Rapid hydrolysis of dApdA with Ce(III) and molecular oxygen was also observed.[46] This type of oxidative catalyst is an improvement over those already discussed in that the ligated fragments are products of the hydrolysis reaction and no nucleotide is destroyed while the extreme reactivity of the oxidative catalyst is maintained. Thus far a ligand system which does not substantially reduce the reactivity of the system has not been found.

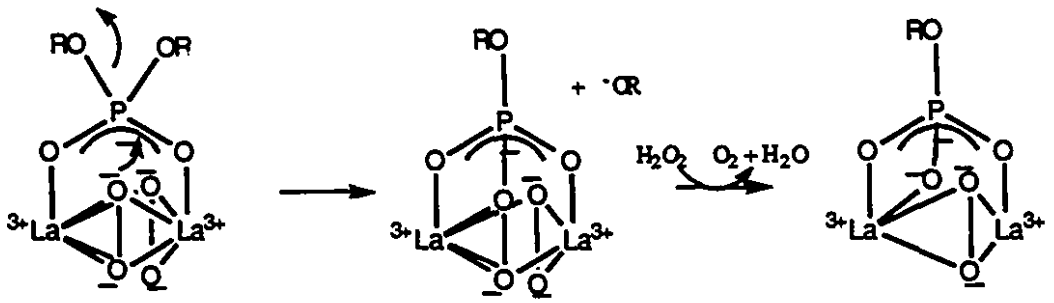

Figure 1.19 Proposed mechanism of cleavage by Lanthanum / peroxide systems

Que Jr. has reported rapid double stranded cleavage of super coiled plasmid DNA by a dinuclear iron complex[47] in the presence of hydrogen peroxide or oxygen and a reductant (dithiothreitol or ascorbate). The linearized DNA can be religated with a DNA ligase indicating that the products of the reaction are hydrolytic. This appears to be another example of net hydrolytic cleavage under oxidative conditions as was observed in the cerium / oxygen and lanthanum / peroxide systems. 10 μM of catalyst yielded 69 % nicked plasmid and 31% linearized DNA. At 50 μM concentration of catalyst the linearized plasmid in degraded even further. The advantage of this system (as in the cerium and lanthanum systems) is that it has the reactivity of an oxidative catalyst, but results in hydrolytic products. Further, the catalysts is a metal complex (and not a metal salt) which allows the possibility of attachment to a DNA or RNA recognition agent and therefore sequence specific hydrolysis.

At present oxidative cleavage reagents are used as reagents for foot printing, analysis of secondary structures of oligonucleotides as well as affinity labeling. Although the reactions are extremely fast at physiological temperature and pH, the involvement of such reactive and potentially damaging species eliminates their potential use in in vivo applications.

6.2 Catalysis by Non-Metal Systems

There have been several studies reporting catalysis of the hydrolysis of phosphate diesters by non-metal systems. Two recent studies (figure 1.20) attempt to mimic the arginine residues of staphylococcal nuclease (SN), which hydrolyses DNA 10^{16}-fold faster than the background rate. One study uses a Bis(acylguanidinium) receptor model A[48] to hydrolyze HPNP and the other uses aminoimidazoline groups B[49] separated by a rigid spacer group to accelerate the hydrolysis of mRNA. The maximum rate acceleration was calculated to be 10^3 using the Michealis Menton treatment for A, although the highest rate acceleration achieved was 700-fold at 30 mM in acetonitrile solvent. B gave a 20 fold acceleration at 37 °C and pH 7.05 for 0.5 μM of receptor. This receptor was found to require imidazole; negligible hydrolysis was detected with imidazole or receptor alone. Hamilton *et al.* proposes (figure 1.20 A) that the rate acceleration is achieved by the stabilization of the trigonal-bipyramidal intermediate via four hydrogen bonds, with simultaneous charge neutralization, in addition to facilitation of proton transfer from the receptor to the leaving group. Anslyn proposes that the receptor functions to enhance the nucleophilic attack in the fashion shown in figure 1.20 B.

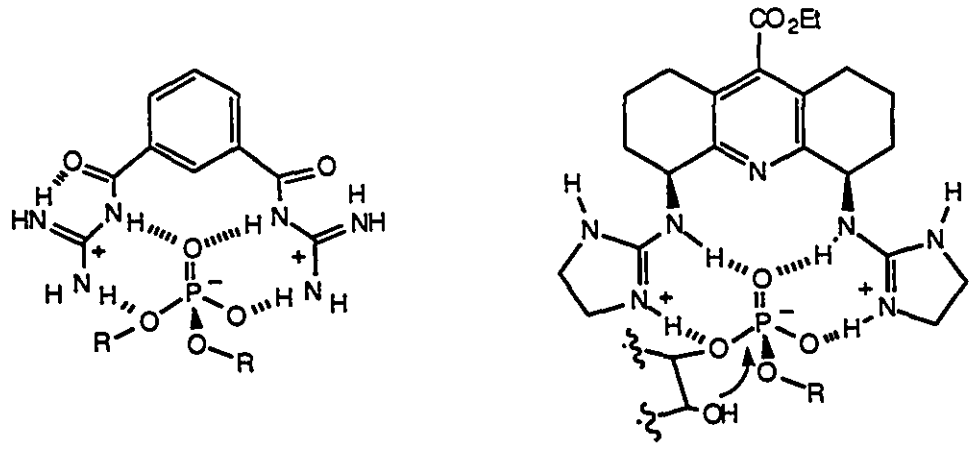

A B

Figure 1.20 Models of staphylococcal nuclease

Breslow *et al.*[50] have used imidazole to catalyze the hydrolysis of ApA, UpU and other RNA analogs. The mechanism postulated involves general acid catalysis to produce a phosphorane intermediate which can either react further by general base catalysis to the 2'3 cyclic phosphate or isomers with no involvement of buffer to form the 2'-adenosine phosphate observed. Recently, this mechanism has been called into question.[51,52] The rate accelerations achieved by these methods are low. At 10 mM pH 7 imidazole buffer, only a 2.3 fold rate acceleration[53] was observed for UpU hydrolysis at 80 °C. Much better rate accelerations (10^3 fold) were achieved when Zn^{2+} (1 mM) was added to the buffer. Zn^{2+} alone provided a 32 fold rate enhancement. For the RNA analogue, HPNP, zinc (0.5 mM) alone accelerated the reaction 150 fold, while in the presence of 12 mM buffer 850 fold rate acceleration was observed.[53] The HPNP hydrolysis reactions where followed at pH 7 and 37 °C.

In general, the rate enhancements achieved by these non-metal catalytic systems are modest. These studies, however, contribute significantly to the understanding of electrostatic or buffer catalysis in the enzyme mechanism.

7 Metal Assisted Hydrolytic Cleavage

A number of mechanisms exist by which metals can facilitate the hydrolysis of phosphate esters.

1) coordination to the phosphoryl oxygen bond polarizes the ester to nucleophilic attack (Lewis acid activation)
2) electrophilic catalysis stabilizing the negative charge at the transition state
3) activation of water at physiological pH thus providing a source of nucleophilic hydroxyl groups under these conditions (Metal hydroxide)
4) binding and assisting leaving group departure

In addition to these modes of catalysis, the metal can assist in bringing the reacting species together, thereby effectively providing intramolecular catalysis and lowering the entropy of activation of the reaction. The challenge in the design of a functional hydrolytic enzyme model is the incorporation of these modes of catalysis into a small inorganic complex.

7.1 Mononuclear Complexes

Although the literature is replete with examples of metal complex catalyzed hydrolysis of phosphate monoesters and triesters, carboxylic amides and esters, there are very few reports of metal catalyzed phosphate diester hydrolysis. Sargeson,[54,55] has demonstrated the use of an intramolecular metal bound hydroxide ion in the complexes shown in figure 1.21 A and 1.21 B. In these complexes the phosphate diesters are bound to iridium(III) through one oxygen. The rate enhancement observed are about 10^5 for 1.21 A and 10^6 fold for 1.21 B compared to the corresponding unbound diesters, ethyl *p*-nitrophenyl phosphate (ENPP) and bis(*p*-nitrophenyl) phosphate (BNPP). Interestingly, the metal ion itself can produce a large effect in the rate enhancement observed. A 10^3 fold increase in rate was observed when cobalt(III) was substituted for iridium(III). The decreased rate for the iridium complexes has been attributed to the longer metal-oxygen bond distance in the iridium complexes due to the larger metal and its effect on the O-M-O angle. Thus iridium imposes a greater strain on the formation of the four membered ring intermediate and diminishes the catalytic activity. The difference in degree of electrophilic activation can be discounted since these effects have been shown to be insignificant between iridium and cobalt.[56]

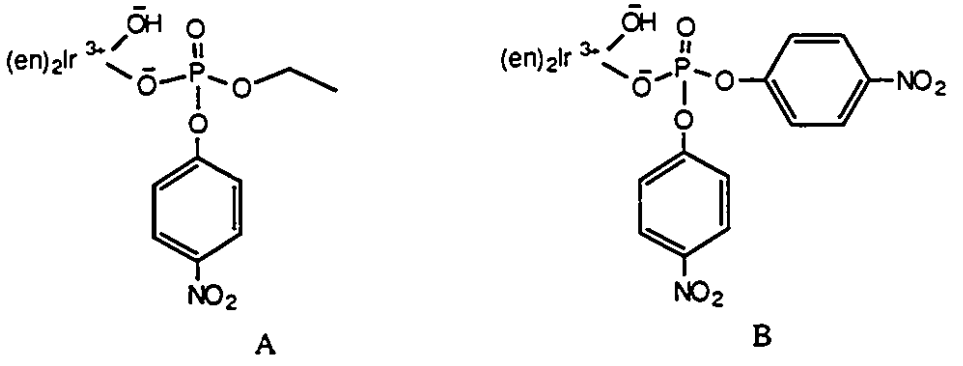

Figure 1.21 Intramolecular metal hydroxide attack

Sargeson has also shown that Lewis acid activation of a divalent metal ion at a phosphate center is modest and contributes at most a 10^2-10^3 fold rate enhancement for the hydrolysis reaction. When ethyl *p*-nitrophenyl phosphate was synthesized coordinated to pentaamminecobalt(III) a real measure of the Lewis Acid activation could not be made.[57] It was found that the coordinated diester released *p*-nitrophenol between 10^8-10^{10} times faster than the uncoordinated diester. The origin of the reactivity however was a result of both the Lewis acid effect as well as the attack of coordinated amido ion (figure 1.22 A). An estimated value for Lewis acid activation is arrived at therefore from comparing the rate accelerations of the complexes in figure 1.22 B and 1.22 C. Complex 1.22 B is about 100 fold faster than complex 1.22 C.

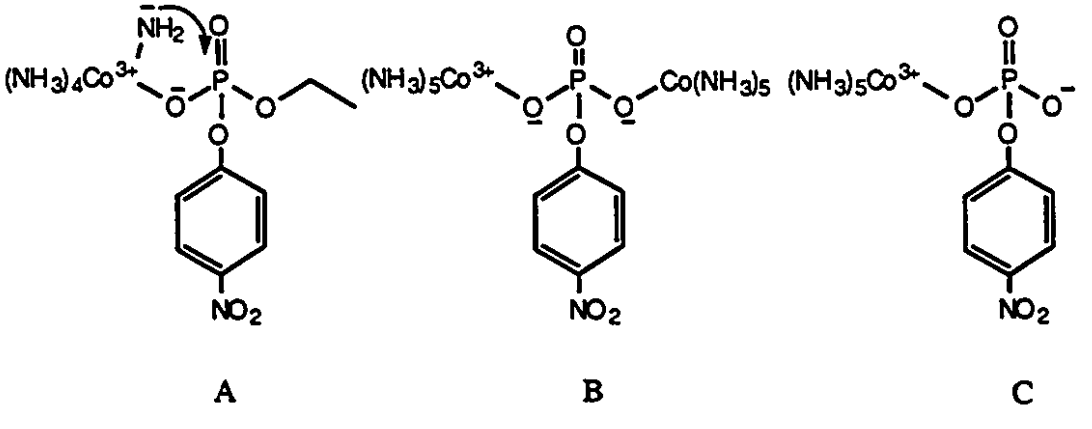

Figure 1.22 Measurement of Lewis acid activation

The *cis*-diaqua complexes of tetrammine Co(III) complexes[1,58,59] (figure 1.23) have been the most successful in accelerating the hydrolysis of activated and unactivated phosphate diesters. Indeed, the hydrolysis rate of BNPP bound to the trpn complex is 10^{10} fold greater than the hydroxide rate at neutral pH[1] and 50 °C. The proposed mechanism involves monodentate binding of the diester to the hydroxy - aqua form of the catalyst followed by rate determining intramolecular metal hydroxide attack on the coordinated diester and formation of a four-membered ring. The reactivity of the cobalt complexes is sensitive to the tetrammine ligand structure. A stucture reactivity study showed that for a series of cobalt complexes were the aqua ligands are constrained in a cis position the reactivity of the cobalt complex is related to its ability to stabilize the four-membered ring in the cobalt phosphate complex. This can be understood in terms of the ability of the ligand to expand the N-Co-N angle opposite the O-Co-O of the four-membered ring. Evidence for this comes from the X-ray structures of the tren and trpn cobalt carbonato complexes, in which it can be seen that the N-Co-N angle[60] in the trpn complex is free to expand to 100° while the tren complex N-Co-N angle[61] is held at 87°. Further evidence is the observation that acetate chelates to $[(trpn)Co(H_2O)(OH)]^{2+}$ (1.23 A) forming a four-membered ring acetato complex but $[(tren)Co(H_2O)(OH)]^{2+}$ (1.23 C) only binds acetate in a monodentate fashion. The large rate accelerations achieved with these *cis*-diaqua cobalt systems is accounted for by a combination of Lewis acid activation and metal hydroxide attack.

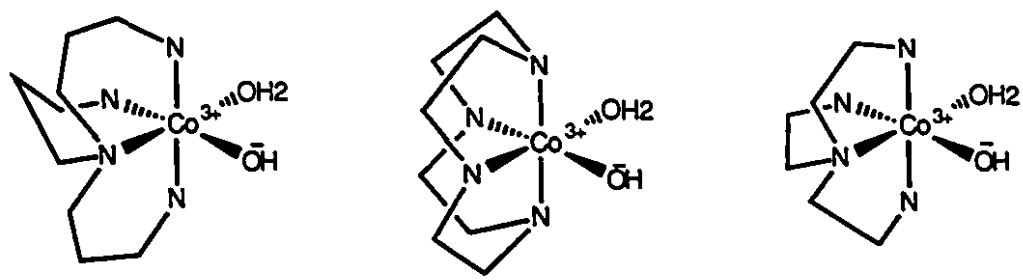

Figure 1.23 Active species of *cis*-diaqua tetrammine cobalt(III) complexes, A $[(trpn)Co(H_2O)(OH)]^{2+}$, B $[(cyclen)Co(H_2O)(OH)]^{2+}$, C $[(tren)Co(H_2O)(OH)]^{2+}$

Catalysis of dimethyl phosphate[59] (DMP) at 60 °C and near neutral pH (pD 6.3) has been demonstrated with $[(cyclen)Co(H_2O)(OH)]^{2+}$. The cobalt bound dimethyl

phosphate has a lifetime of 40 days under these conditions. DMP is more unreactive than DNA since the 3' or 5' OH groups of nucleosides are more acidic than that of methanol. This catalysis represents a 10^{10} fold rate acceleration over the water rate of dimethyl phosphate. Thus it can be seen that the tetrammine cobalt(III) system is efficient in the catalysis of both activated and unactivated phosphate diesters.

The cobalt(III) tetrammine system, is a well-defined substitutionally inert system, which allows detailed study of the catalytic mechanism. It is ultimately important, however, to develop a catalytic system where the metal is labile in order to have efficient turnover and thus true catalysis. Unfortunately, the lability of the metal complicates the experimental system since numerous complexes can exist in rapid equilibrium and this results in problems in assigning the exact complex responsible for catalysis. The *cis*-diaqua copper complexes $[(bpy)Cu(H_2O)(OH)]^{+}$[62] and $(DPA)Cu(H_2O)(OH)]^{+}$[63] also accelerate the cleavage reaction of phosphate diesters such as BNPP. A first order rate constant (k_{cat}) for the decomposition of the coordinated diester (figure 1.24) of 5.6×10^{-4} s^{-1} was observed which translates to a rate enhancement for the bound phosphate diester of 6300 as calculated by Trogler from a control uncatalyzed rate. In both catalysts, diammine ligands leave two coordination sites open for water to assist in the catalysis. A mechanism similar to that proposed for the cobalt complex promoted hydrolysis of phosphate diesters has been postulated.[62,63] Recently, a *cis*-diaqua copper complex with a triammine ligand[64] (TACN) has also been observed to hydrolyze BNPP. A rate enhancement of about 10^3 was also observed in this system.

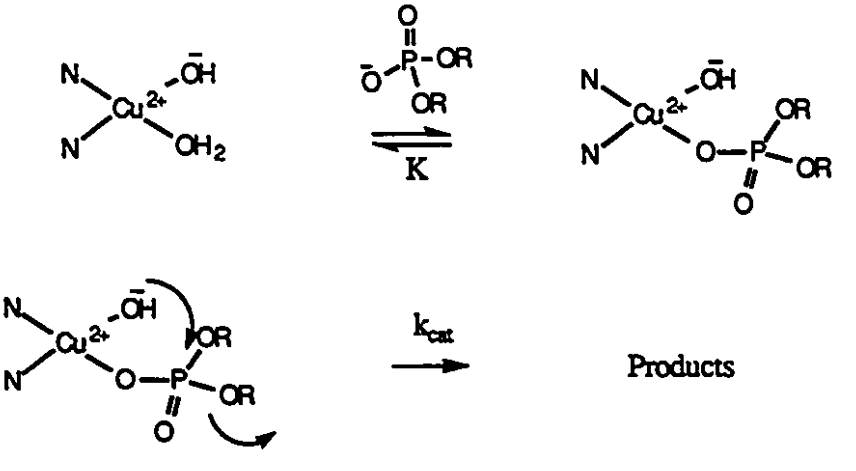

Figure 1.24 Proposed mechanism for *cis*-diaqua copper(II) complexes

Bashkin and Stern have shown that a simple copper complex, $Cu(TER)^{2+}$ (TER = 2,2',6'2''-terpyridine), promotes the transesterification of RNA.[65] At pH 7.1 the observed rate constant (0.06 mM poly (A) and 0.06 mM $Cu(TER)^{2+}$ was 6.1×10^{-2} hr^{-1}. The half-life for the hydrolysis at 37°C is therefore 11.4 hrs. A general acid and general base catalyzed mechanism had been originally proposed for this system, in which the metal bound water acts as the general acid or base (as shown in figure 1.25) however, the reaction was found to be only first order[66] in catalyst. $[Cu(TER)^{2+}]$ also promotes the hydrolysis of the resulting 2':3'-cyclic phosphate.[67] A Lewis acid / general base mechanism has been proposed for this system. The attachment of this catalyst to a modified DNA oligomer[68] led to the first example of sequence specific hydrolytic cleavage of RNA producing 18-25 % cleavage after 72 hrs at 45 °C.

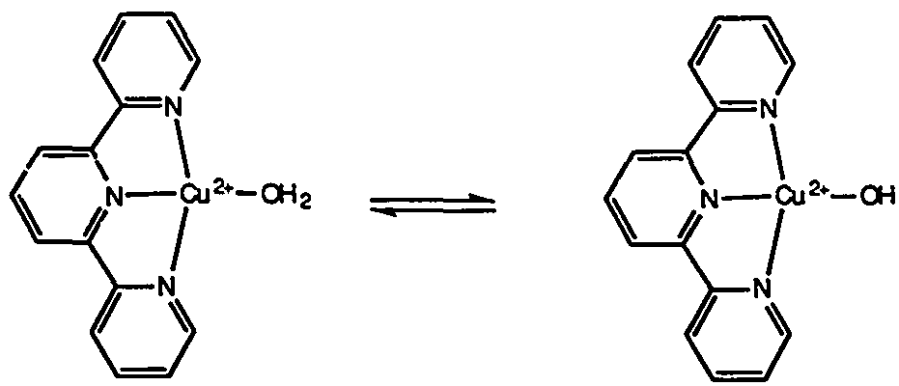

Acid Base

Figure 1.25 General acid and general base proposed in catalysis of RNA

Very few ligands which bind lanthanide ions tightly while retaining the intrinsic reactivity of the metal are known. One advancement in this area is the reported[69] hydrolysis of poly (A) fragments as well as ApUp by Ln^{3+} macrocyclic complexes (figure 1.26 A). The pseudo first order rate constant for the cleavage of ApUp by 490 µL $Eu(L)^{3+}$ is 0.14 hr^{-1} at 37°C and pH 7.0. Studies to improve the stability of the lanthanide macrocyclic complexes and control the metal release from the macrocylcle are needed to improve the reactivity of the complex. In the last year several groups[68,70-72] have been succesful in achieving sequence specific cleavage of RNA by attaching different lanthanide complexes to binding domains which recognize RNA. Site-Specific

cleavage of an RNA oligomer was observed[71] when a Eu(III) pentadentate texaphyrin ligand (shown in figure 1.26 B) was attached to a DNA oligomer. After a 24 hr incubation at 37 °C, 30 % cleavage was observed. The most succesful,[72] reports 88 % cleavage of a synthetic 29-mer oligoribonucleotide at 37 °C within a 16 hr incubation period.

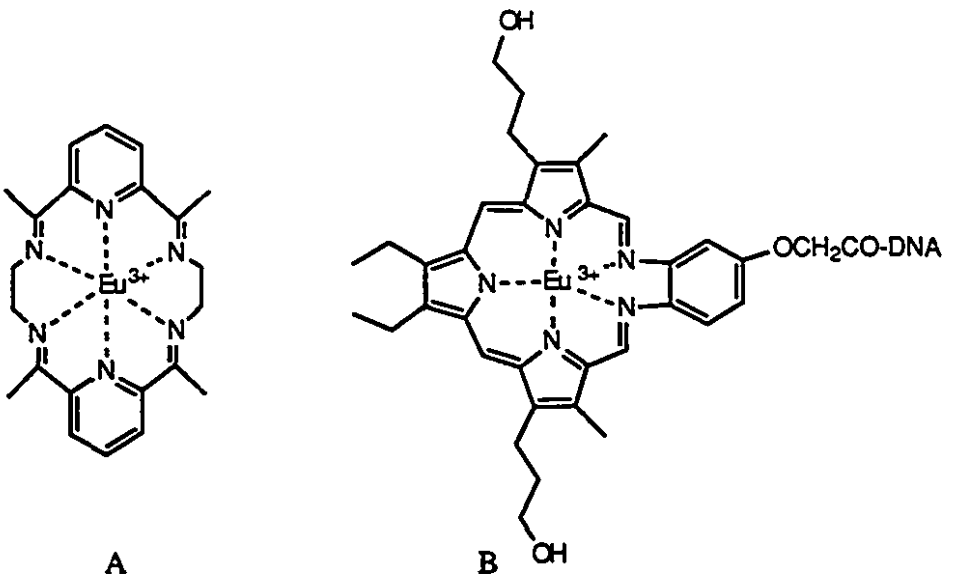

Figure 1.26

7.2 Dinuclear Complexes

Very few reports of catalysis by two metal systems on the hydrolysis of phosphate diesters are available although many examples of enzymes and ribozymes that rely on the catalytic power of two metals are known. The correctly designed dinuclear complex should offer even larger rate accelerations over that already achieved by single metal systems.

Recently, in this lab,[73] it was found that 1:1 copper and zinc complexes of the ligand neocuproine are extremely reactive towards the hydrolysis of ApA and poly (A). The half-life of [Cu(neo) $^{2+}$] (10 mM) catalyzed hydrolysis of ApA is 3 mins at pH 7 and 25°C. This is over 100 fold faster than any previously reported metal (transition or lanthanide) catalyst for the cleavage of RNA. Only a first order dependence on [Cu(neo) $^{2+}$] is observed but the proposed mechanism shown in figure 1.27 A involves a chelated phosphate and hence two contacts with the phosphate. For [Zn(neo)$^{2+}$] second order kinetics in Zn complex are observed.[74] The zinc complex has a half-life of 4.4 hrs at 50

°C, pH 7.4 and 1 mM complex for ApA hydrolysis. The mechanism in this case is believed to involve the formation of a hydroxy bridged dimer (figure 1.27 B) which can bind the RNA providing double Lewis acid activation and facilitating nucleophilic attack of the nucleophile.

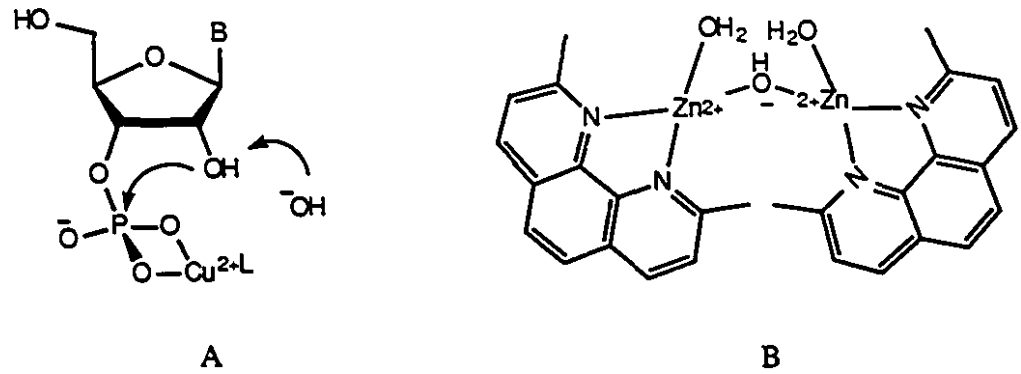

A B

Figure 1.27 A [Cu(neo)$^{2+}$] mechanism involves chelation followed by intramolecular hydroxy attack by deprotonated alkoxyl B [Zn(neo)$^{2+}$]: active catalytic species

Modest rate enhancements were achieved when two [(cyclen)Co(OH2)2] moieties were bridged by an anthracene spacer[75] (figure 1.28). The greatest rate enhancement achieved was 10 fold over the rate of free Co(III) cyclen for the hydrolysis of BNPP.

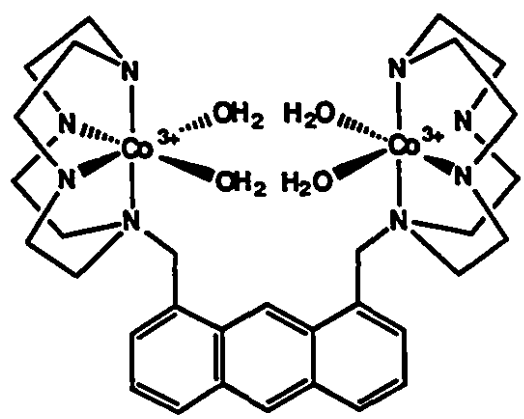

Figure 1.28 Dinuclear catalyst for the hydrolysis of BNPP. Modest rate enhancements were observed over the corresponding mononuclear complex

Plan of Study

The study of enzyme structure and reactivity is revealing that in biology, enzymes and ribozymes take advantage of di and tri nuclear metal systems. Among these are included 3'-5'-exonuclease and HIV reverse transcriptase from RNase H. The goal of our research is to examine the potential of dinuclear catalysts for the hydrolysis of phosphate diesters and develop a first generation of catalysts in which we can asses some basic mechanistic questions. A dinuclear complex offers new possibilities in the design of hydrolytic catalysts and new ways to improve on the large rate accelerations already achieved by small inorganic complexes.

We have focused on a dinuclear complex design in which the two metals are positioned favourably to bridge the phosphate diester. This catalyst design is directed at the cleavage of RNA and its analogues since the rate enhancement from this interaction is expected to supplement the catalysis available to these diesters from their internal nucleophiles. We wished to synthesize a dinuclear complex capable of interacting with a phosphate diester in the expected manner and of promoting the cleavage of RNA and its analogues.

We wished to synthesize a complex in which a phosphate diester was bridged between two cobalt atoms to asses the rate acceleration available for the hydrolysis a phosphate diester from a double Lewis acid mechanism. This substitutionally inert system would allow us to examine the mechanism of double Lewis acid catalysis in greater detail.

Chapter 2: Copper(II) Complex Promoted Cleavage of HPNP

1 Introduction

There have been several investigations to determine the stability of RNA. An accurate determination of the background rate is important in assessing and comparing the reactivity of catalysts. In this study the RNA model compound used is 2-hydroxypropyl phosphate HPNP (figure 2.1). In the following discussion the background rates for RNA cleavage will be compared with the background rates for HPNP cleavage.

The rate of hydrolysis of UpU and ApA have been measured by Lonnberg *et al.*[76] and are tabulated in table 2.1 for the cleavage of the ionized (2'-OH) species at 60 °C. The second order rate constant can be calculated at 60 °C from these values, pK_w (13.02) and the pK_a of the 2'-OH (12.55 and 12.24 for UpU and ApA respectively) at 60 °C. The calculated second order rate constants at 60 °C are therefore 0.020 and 0.034 $M^{-1}s^{-1}$ respectively. At pH 7 and 60 °C the rate constants are 1.9×10^{-8} s^{-1} and 3.3×10^{-8} s^{-1} corresponding to a half-life of 1 and 0.68 years. At 25 °C (using a 2.6 fold temperature correction per 10 °C as shown experimentally by Usher[15]) and pH 7 the rates are therefore 6.7×10^{-10} and 1.2×10^{-9} s^{-1} corresponding to a half-life of 32 and 18 years for UpU and ApA respectively.

Williams *et al.*[16] have studied the hydrolysis of a series of aryl uridine-3'-phosphates. They report a second order rate constant for the base catalyzed hydrolysis reaction of 12 $M^{-1}s^{-1}$ at 25 °C for the phenyl ester. An estimate for the half-life of UpU can be obtained in the following way. The leaving group pK_a of phenyl uridine 3'-phosphate is 9.95 and the leaving group pK_a in UpU is estimated to be 15. Since a linear free energy relationship ($\beta = 0.54$) exists for the leaving group with respect to the base catalyzed hydrolysis, we can calculate the second order rate constant for UpU to be 2.25×10^{-2} $M^{-1}s^{-1}$. At pH 7 this corresponds to a half-life for the hydrolysis at 25 °C of about

3500 days or 10 years. Lonnberg's experimental data at 60 °C and the extrapolated value from Williams' LFE relationship agree quite reasonably.

Another available figure can be obtained from Breslow's studies[77] of imidazole catalyzed hydrolysis of polyU. At 80 °C and pH 7.23, a rate constant of about 3.7×10^{-4} hr^{-1} for the rate at zero buffer concentration can be calculated from the tabulated data. This represents a half-life of 78 days at 80 °C. Breslow[53] has also reported a half-life for UpU hydrolysis of 1.7 years at pH 7 and 80 °C. Komiyama[78] reports that the pH rate profile between 8 and 13 of ApA is a straight line with a slope of 1. From these data he reports that at pD 6 the rate constant for the hydrolysis reaction is 3×10^{-10} min^{-1} at 50 °C. This is a half-life for the reaction of over 4000 years. At pH 7 and 50 °C this would correspond to 1.9×10^{-8} min^{-1} or 70 years. The experimental data are summarized in table 2.1.

Table 2.1 Table of reported values for the hydrolysis of polyU, UpU and ApA

substrate	conditions	rate constants	half-life
UpU[76]	60 °C	6.92×10^{-3} s^{-1} (0.020 $M^{-1}s^{-1}$)	
ApA[76]	60 °C	5.68×10^{-3} s^{-1} (0.034 $M^{-1}s^{-1}$)	
polyU[77]	80 °C pH 7.23	3.7×10^{-4} hr^{-1}	0.21 years
*UpU[16]	25 °C pH 7.0	8.1×10^{-6} hr^{-1}	10 years
UpU[53]	80 °C pH 7.0	4.6×10^{-5} hr^{-1}	1.7 years
ApA[78]	50 °C pD 6.0	1.8×10^{-8} hr^{-1}	70 years

* Extrapolated value from the LFE of a series of aryl uridine-3'-phosphates

In table 2.2 are listed the data at pH 7 and 25°C extrapolated from the experimental data for temperature (2.6 fold per 10 °C) and pH (hydroxide catalyzed[76] throughout the pH range). Under these conditions the reported background rates for RNA hydrolysis range between 7 to 325 years. The data taken from Breslow's work is obtained from a single experimental value while the data from Lonnberg and Williams is obtained from a series of experimental points. The experimental data suggests that a reasonable value for the cleavage of RNA is between 7 to 40 years.

Table 2.2 Background rates and half-lives for RNA hydrolysis at 25°C and pH 7

substrate	k (s^{-1})	half-life
UpU	6.7×10^{-10}	38 years
ApA	1.2×10^{-9}	18 years
UpU	2.25×10^{-9}	10 years
polyU[77]		40 years
UpU[53]		325 years
ApA[78]		7 years

As described in the introduction there are a wide range of model compounds for RNA. HPNP has been widely used as an RNA analogue. HPNP has a much better leaving group (pK_a 7.14) than RNA (pK_a 15), and should react 10^4-10^5 times faster than RNA (β value of -0.56). However, the nucleophile in HPNP is not held rigidly in a favourable position to attack the phosphorous as in UpU or RNA. In this respect, HPNP should be about 10^4 less reactive than UpU or ApA for its cleavage reaction.[16] This analysis suggests that HPNP may react up to 10 times faster than RNA.

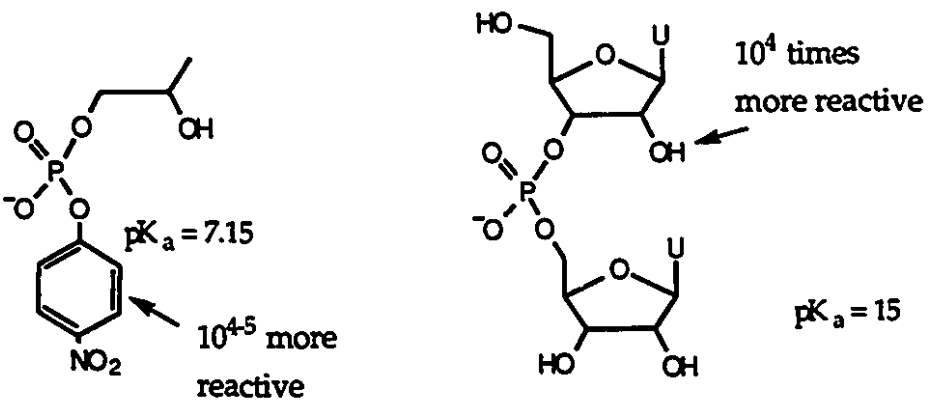

HPNP UpU

Figure 2.1 HPNP and UpU

Two reported values for HPNP cleavage are 5.82×10^{-5} hr^{-1} at pH 7, 25°C[16] and 1.15×10^{-4} hr^{-1} at 37°C and pH 7.[53] These are listed below in table 2.3 along with their

corresponding half-lives. If we compare these half-lives with those obtained for RNA (table 2.2) at pH 7 and 25°C we find that these values confirm that HPNP is about 10 times more reactive than RNA.

Table 2.3 Literature values for HPNP cleavage

k_O at pH 7	half-life
$5.82 \times 10^{-5} hr^{-1}$ (25°C)	496 days (1.4 years)
$1.15 \times 10^{-4} hr^{-1}$ (37°C)	251 days (0.69 years)

The available data for the cleavage of HPNP by metal and metal complexes is listed below in table 2.4.

Table 2.4 Literature values for the metal catalyzed cleavage of HPNP at pH 7 and 37°C.

complex	rate constant (hr^{-1})	half-life (hrs)
*ZnW[79] (0.5 mM)	7.4 x 10-4	937
*Zntacd[79] (0.5 mM)	4.64×10^{-2}	15
Zn^{2+} (0.5 mM) and *2MeIm (8 mM)[53]	1.74×10^{-1}	4
*La(tcmc)[80] 1mM, pH 7.4	5.8×10^{-2}	12

* W is 2,12-dimethyl-3,7,11,17-tetraazabicyclo[11.3.1]-heptadeca-1(17),2,11,13,15-pentaene or Wooley's ligand, tacd is 1,5,9-triazacyclododecane, MeIm is 2-methylimidazole, and tcmc is 1,4,7,10-tetrazacyclododecane-1,4,7,10 -tetramethylamide

As part of our investigation of the catalysis by a dinuclear copper(II) complex (chapter 3) for the cleavage reaction of HPNP we have studied the catalysis of the transesterification reaction of HPNP by a series of mononuclear copper(II) complexes. The complexes shown below in figure 2.2, Cu(N3) and Cu(N3OH) were extremely reactive in promoting the cleavage reaction of HPNP.

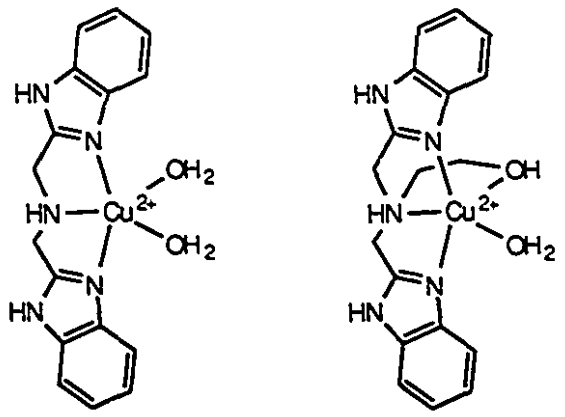

Cu(N3) Cu(N3OH)

Figure 2.2 Structure of diaquo-[(bis(benzimidazol-2-ylmethyl)amine)copper(II)] and diaquo-[(bis(benzimidazol-2-ylmethyl)aminehydroxyethylamine)copper(II)] generated from the dichloro complexes Cu(N3) and Cu(N3OH) respectively

2 Results

The acid dissociation constants for the copper complexes (figure 2.3) used in this study are listed in table 2.5. In all cases the neutral dichloro copper complex is isolated and upon dissolution in water the corresponding diaqua complexes are generated.

Table 2.5

Complex (5 mM)	pK_a
Cu(N3)	6.80
Cu(N3OH)	6.70
Cu(DPA)	6.90
Cu(TER)	8.10
Cu(DIEN)	9.20

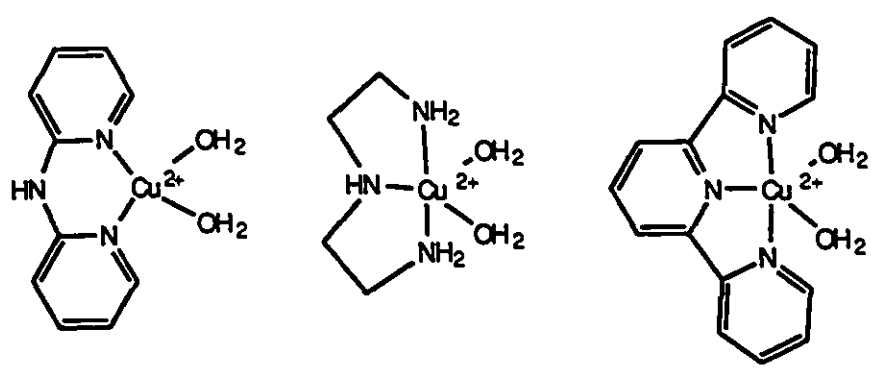

Cu(DPA) Cu(DIEN) Cu(TER)

Figure 2.3 Structure of $[(2,2'\text{-dipyridylamine})Cu(OH_2)_2]^{2+}$ Cu(DPA), $[(\text{diethylenetriamine})Cu(OH_2)_2]^{2+}$ Cu(DIEN), and $[(2,2'\text{-}6,6'\text{-terpyridine})Cu(OH_2)_2]^{2+}$ Cu(TER).

The kinetic experiments were followed by monitoring the increase in visible absorbance at 400 nm due to the release of *p*-nitrophenolate ion. In a typical kinetic experiment , 5 μL of a stock 10 mM solution of HPNP in water was added to 1 mL of copper(II) complex solution at 25 °C. For complexes Cu(N3), Cu(N3OH) the observed

rate constants were obtained by fitting the first three half-lives of the reaction to a first-order kinetics equation. For Cu(DPA), Cu(TER) or Cu(DIEN) initial rates method were used under low concentration or pH conditions.

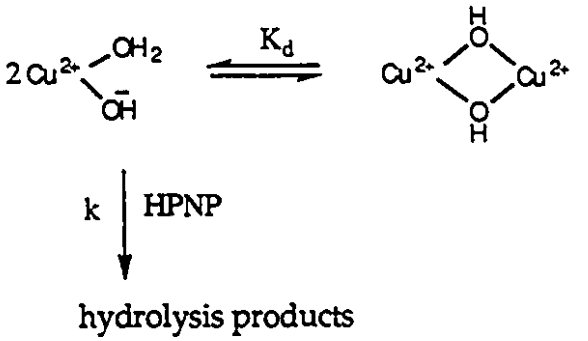

$$k_o = k\left(\frac{-1+\sqrt{1+8K_d[Cu]_T}}{4K_d}\right) \quad (2.4)$$

Figure 2.4 Kinetic Scheme and equation 2.4

The dependence on concentration of Cu(DPA), Cu(TER) and Cu(DIEN) for the complex promoted transesterification of HPNP are shown below in figures 2.5 to 2.8. Figure 2.5 shows the concentration dependence of the observed pseudo first order rate constant of Cu(DPA) fit to equation 2.4 derived from the scheme in figure 2.4 where K_d is the dimerization constant of the complex.[81] The derivation of equation 2.4 and the assumptions made are found in appendix 5.2.

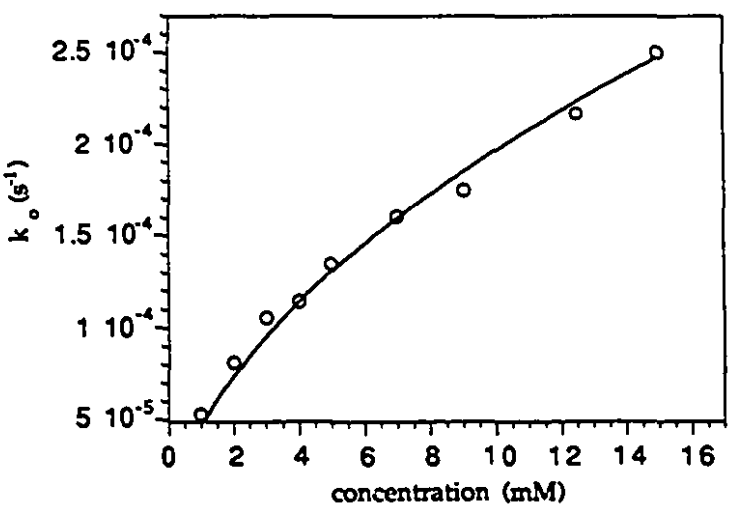

Figure 2.5 Concentration dependence of Cu(DPA) for the transesterification of HPNP at 25°C and pH 8.01 where K_d is 570 ± 260 M^{-1} fit to equation 2.4 with k = 7.7 x 10^{-2} ± 1.1 x 10^{-6} and R = 0.994.

At low concentrations of Cu(DPA) a first order dependence is observed for the observed rate constant which decreases below one at higher concentrations. This is consistent with the dimerization of the active aqua-hydroxy catalyst to the inactive di-hydroxy bridged dimer shown in figure 2.4. The concentration dependence for the cleavage of HPNP of Cu(TER) and Cu(DIEN) are shown below in figure 2.6 fit to a straight line. The dependence is linear throughout the observed concentration range.

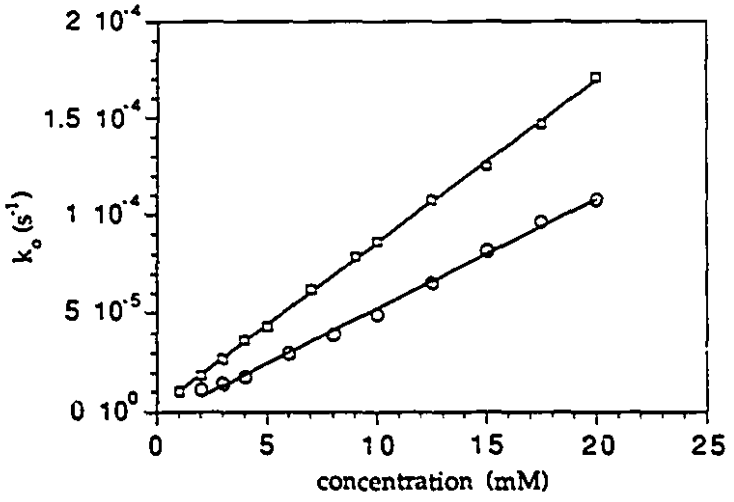

Figure 2.6 Concentration dependence of Cu(TER) (open squares) and Cu(DIEN) (open circles) at 25°C for the cleavage of HPNP at pH 9.28 and pH 9.80 respectively

Unlike Cu(DPA) where the reactivity of the catalyst levels off with increasing concentration, or Cu(TER) where the reactivity increases linearly, the reactivity of Cu(N3) increases with a second order dependence on catalyst concentration. The concentration dependence of Cu(N3) for the transesterification of HPNP at pH 6.75 is shown fit to equation 2.7 which gave the best fit to the data. k' is the contribution to the observed rate from the undimerized Cu(N3) complex. Also shown in figure 2.7 is a log plot of the data in which the slope of the line is 2.24 ± 0.05. The second order dependence on catalyst concentration suggests that two molecules of the catalyst make up the active catalytic species in the transesterification reaction. This is an interesting result since the dependence on the catalyst concentration for the cleavage of RNA or RNA analogues have so far proven to be first order. Since this work was published, two zinc complexes have also been found to exhibit the same concentration dependence.[74]

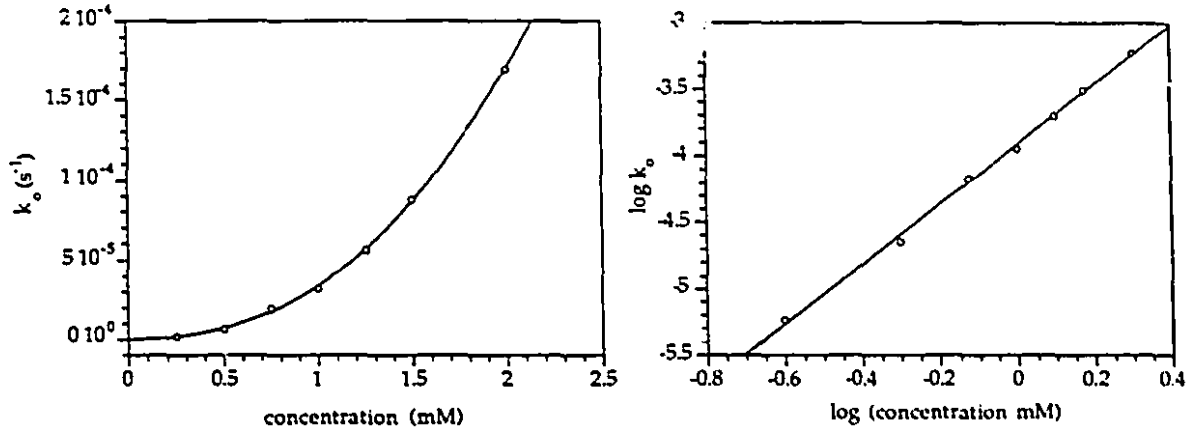

$$k_o = k'[Cu(N3)] + kK[Cu(N3)]^n \qquad (2.7)$$

Figure 2.7 concentration dependence of Cu(N3) vs. observed rate constant for the transesterification of HPNP at pH 6.75 and 25°C fit to equation 2.7 with k'= 1.31 x 10^{-3} ± 4.4 x 10^{-3}, kK = 32.4 ± 4.32, n = 2.36 ± 0.12 and R = 0.999. Log of concentration of Cu(N3) and k_o for the transesterification reaction of HPNP fit to a linear equation with slope = 2.24 ± 0.05 and R = 0.999

We can compare the log data in figure 2.7 to the log data for the concentration dependence of Cu(DPA), Cu(TER) and Cu(DIEN) shown in figure 2.8. For Cu(DPA) the slope of the log plot is 0.54 ± 0.02 as expected due to the dimerization. The slope of the log plots for Cu(TER) and Cu(DIEN) are 0.94 ± 0.03 and 1.03 ± 0.01 respectively. It is clear that Cu(N3) is catalyzing the transesterification of HPNP by a mechanism more complicated than 'normal' copper complexes.

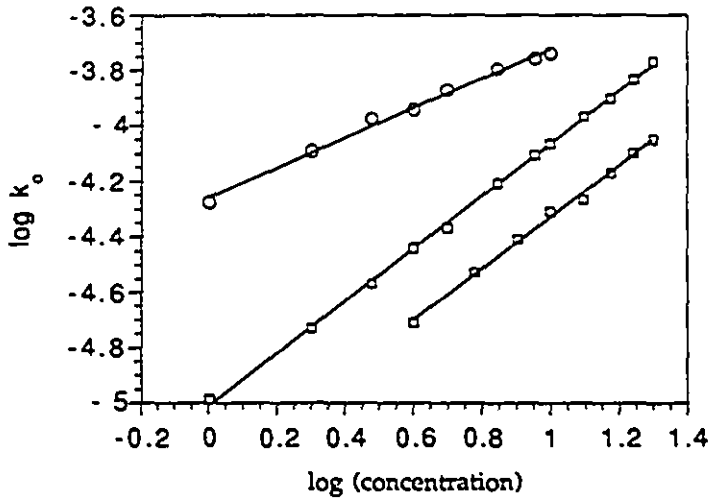

Figure 2.8 Log plot of concentration of Cu(DPA) ,Cu(TER) and Cu(DIEN) vs. observed rate constant for the transesterification of HPNP

In the following section, the effect of pH on the observed rate constant for these four complexes will be examined. For Cu(DPA), Cu(TER), and Cu(DIEN) the observed rate constant depends on the aqua-hydroxy form of the complex (equation 2.9).

$$k_0 = k[Cu(H_2O)(OH)] \qquad (2.9)$$

Figure 2.9

Expressions (equation 2.10.1 and 2.10.2) for the dependence of k_O on pH are derived in appendix 5.2. Equation 2.10.1 assumes no dimerization to the inactive di-hydroxy bridged dimer with the reaction proceeding by the aqua-hydroxy form (k) of the catalyst. Figure 2.11 shows the pH rate profile for the cleavage of HPNP promoted by Cu(TER), fit to equation 2.10.1.

$$k_o = \left(\frac{kK_a}{K_a + [H^+]}\right)[Cu_T] \qquad (2.10.1)$$

$$k_o = k\frac{-\left(\frac{K_a + [H^+]}{K_a}\right) + \sqrt{\left(\frac{K_a + [H^+]}{K_a}\right)^2 + 8K_d[Cu]_T}}{4K_d} \qquad (2.10.2)$$

Figure 2.10

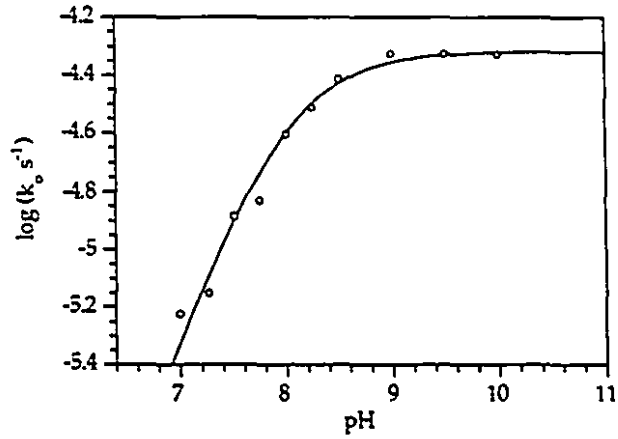

Figure 2.11 pH rate profile for the cleavage of HPNP with 5 mM Cu(TER) at 25°C and [buffer] = 0.1 M fit to equation 2.10.1 with $k = 9.6 \times 10^{-3} \pm 6.4 \times 10^{-4}$, $K_a = 1.09 \times 10^{-8} \pm 1.4 \times 10^{-9}$, R = 0.996.

The pH rate data for Cu (DIEN) and Cu(DPA) promoted cleavage of HPNP are shown in figures 2.12 and 2.13 fit to equation 2.10.1 and 2.10.2 respectively. Equation 2.10.2 takes into account the dimerization of the catalyst to an inactive dimer with K_d = 570. The data obtained for the pH rate profile (k and K_a) fits are tabulated below in table 2.6.

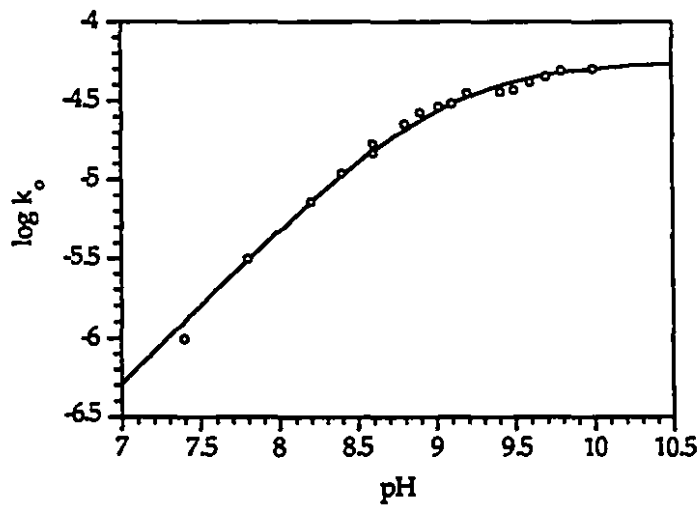

Figure 2.12 pH rate profile for the cleavage of HPNP with 5 mM Cu(DIEN) at 25°C and [buffer] = 0.1 M fit to equation 2.10.1 with $k = 1.1 \times 10^{-2} \pm 5.1 \times 10^{-4}$ and $K_a = 9.26 \times 10^{-10} \pm 7.3 \times 10^{-11}$ R = 0.996.

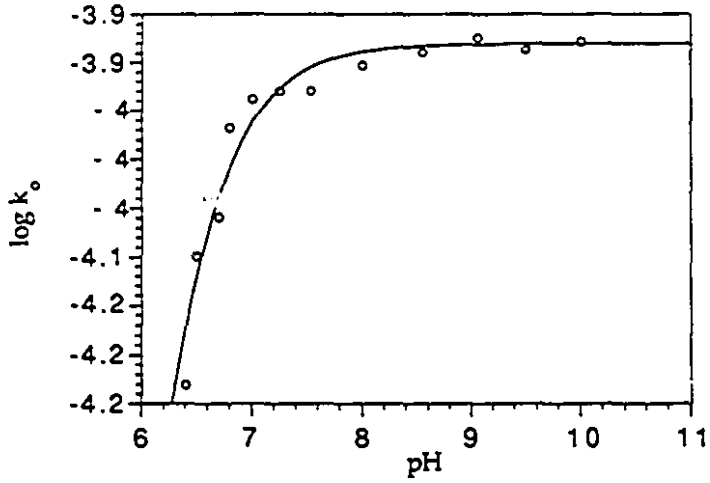

Figure 2.13 pH rate profile for the hydrolysis reaction of HPNP with 5 mM Cu(DPA) at 25°C and [buffer] = 0.1 M fit to equation 2.10.2 with $k = 7.7 \times 10^{-2} \pm 2.0 \times 10^{-3}$, $K_a = 1.03 \times 10^{-7} \pm 1.0 \times 10^{-8}$ and R = 0.977.

Table 2.6 Summary of data from the pH rate profile fits

complex	$k(M^{-1}s^{-1})$	K_a	pK_a
Cu(TER)	9.6×10^{-3} $\pm 6.4 \times 10^{-4}$	1.09×10^{-8} $\pm 1.4 \times 10^{-9}$	7.96
Cu(DIEN)	1.1×10^{-2} $\pm 5.1 \times 10^{-4}$	9.26×10^{-10} $\pm 7.3 \times 10^{-11}$	9.03
Cu(DPA)	7.7×10^{-2} $\pm 2.0 \times 10^{-3}$	1.03×10^{-7} $\pm 1.0 \times 10^{-8}$	6.99

The pH rate profile of Cu(N3) is shown below in figure 2.14. The reactivity of the catalyst levels off near the pKa, however, solutions at pH's higher than seven become cloudy. The leveling off is therefore more abrupt than expected and may reflect the precipitation of the catalytically active species. Unlike the other copper complexes, Cu(N3) increases with a second order dependence on hydroxide. Figure 2.14 B shows the data from 2.14 A fit to a slope of 2 (R = 0.997).

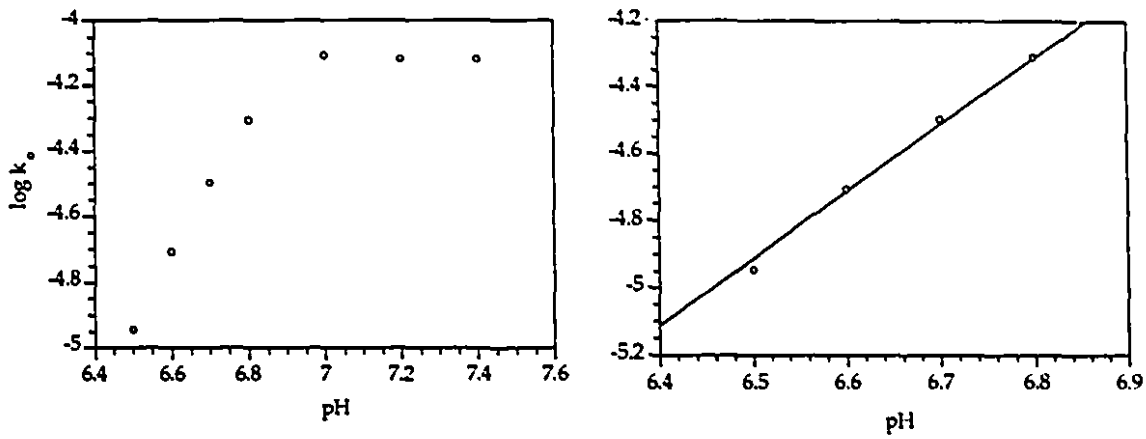

Figure 2.14 pH rate profile for Cu(N3) at 1mM complex concentration and 25°C

Cu(N3OH) was also found to be an extremely reactive catalyst for the cleavage of HPNP. At pH 7 and 2 mM catalyst the observed rate constant is 5.23×10^{-3} s^{-1} (a half-life of 2.2 mins). The poor stability of the complex does not allow a detailed kinetic analysis. The product analysis, which will be discussed below, suggests that neither the alkoxide arm nor a metal bound alkoxide is acting as a nucleophile.

The products of the cleavage reaction of HPNP with Cu(N3) and Cu(N3OH) are *p*-nitrophenolate and the cyclic 1,2-propylene phosphate as determined by ^{1}H and ^{31}P NMR. Figure 2.15 A shows the ^{1}H NMR of the starting material HPNP. Figure 2.15 B is a genuine sample of HPNP and the transesterification products *p*-nitrophenolate and cyclic 1,2-propylene phosphate. Figure 2.15 C is the mixture of starting material and products from the reaction catalyzed by Cu(N3OH). After 20 mins at pD 7 a 2 mM solution of Cu(N3OH) and 2 mM HPNP was quenched with a pD 7.40 EDTA solution. The ^{1}H NMR of the quenched reaction mixture is shown in figure 2.15 C. The ^{31}P NMR of the reaction mixture contains only the signals corresponding to free HPNP (-7.9 ppm) and the cyclic phosphate product (15 ppm).

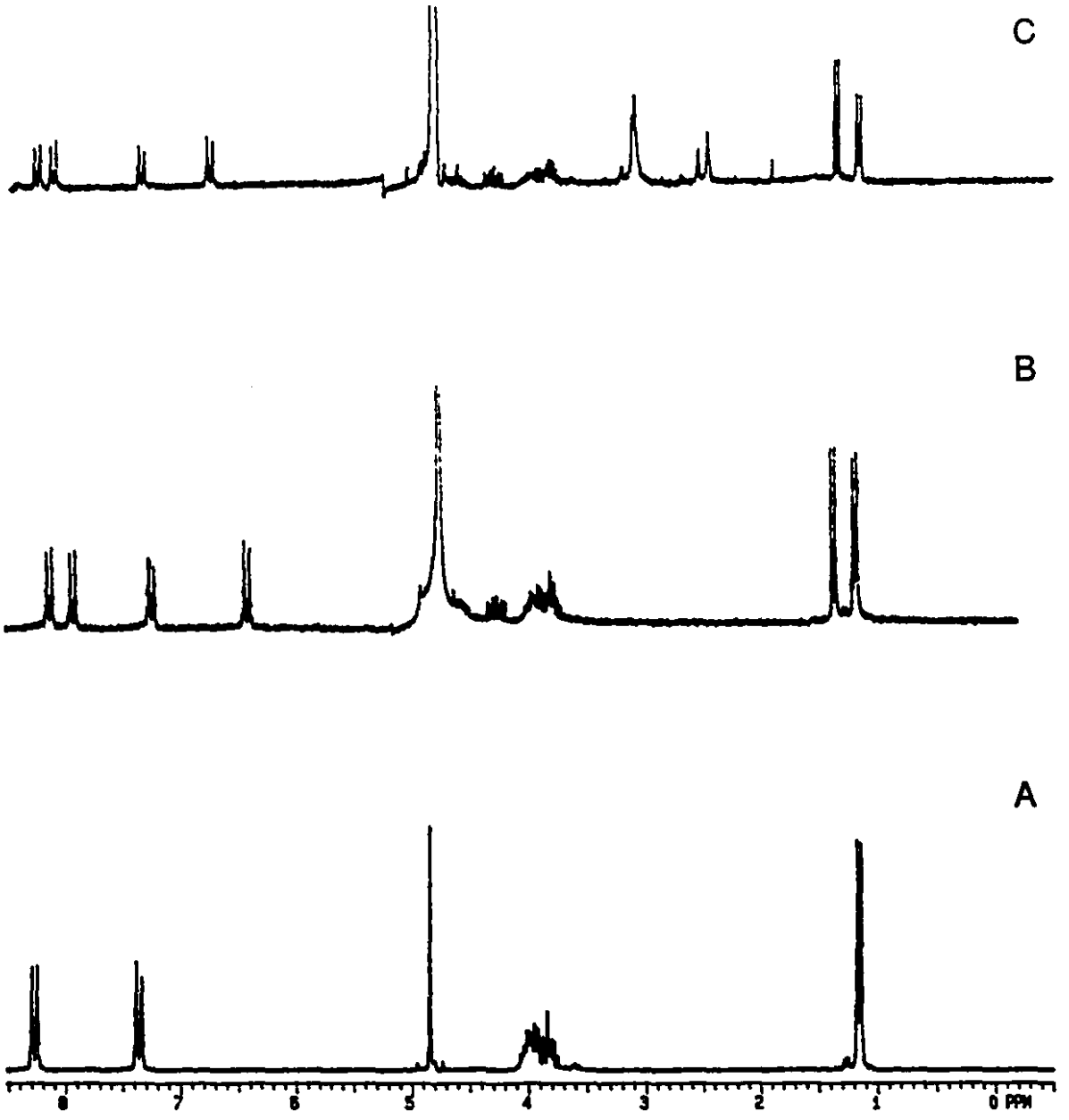

Figure 2.15 ^{1}H NMR at 200 MHz of A: HPNP in D_2O B: HPNP and transesterification products, cyclic 1,2-propylene phosphate and *p*-nitrophenoxide in D_2O. C: mixture of HPNP and products from the reaction of Cu(N3OH) quenched with a pD 7.40 EDTA solution

The most consistent results for Cu(N3) were obtained in 20 mM HEPES buffer at pH's 6.75 or lower and concentrations of 1mM or below. The data for the pH rate profiles and concentration profiles of Cu(N3) was therefore collected under these conditions. To compare the reactivity of the complexes in this study, we compare the observed rate constants of 2 mM Cu(DPA), Cu(TER) and Cu(DIEN) at their pH independent region with the data at pH 7 and 2 mM for Cu(N3) and Cu(N3OH).

Table 2.7

Complex	k_o at 2 mM 25°C (s^{-1})	$t_{1/2}$(mins)
Cu(DPA)	8.14×10^{-5}	142
Cu(TER)	1.86×10^{-5}	621
Cu(DIEN) (4 mM)	1.95×10^{-5}	592
Cu(N3)	5.8×10^{-4}	20
Cu(N3OH)	5.23×10^{-3}	2.2

At 2 mM and pH 7, Cu(N3) cleaves HPNP with a half life of 20 mins at 25 °C. The half life for the reaction catalyzed by Cu(N3OH) is 2.2 mins under the same conditions. Due to solubility limitations we are forced to compare Cu(N3) and Cu(N3OH) at 2 mM or less. We expect that the reactivity of Cu(N3) would continue to increase with a second order dependence until the saturation concentration of the active dimerized complex is formed. Further increase in the concentration of catalyst would result in a linear dependence on concentration.

In order to gain some insight into the mechanism a crystal structure of the complex interacting with an unreactive phosphate diester (DMP) was sought. It was expected that DMP would more easily displace a perchlorate ion than a chloride ion from the copper, thus the corresponding diperchlorate copper(II) complex of Cu(N3) was synthesized. When Cu(N3)(ClO_4)2 was combined with one equivalent of sodium dimethyl phosphate, a light blue precipitate formed. From this powder we obtained single crystals suitable for X-ray defraction after recrystalization at an acetone/hexane interface. The ORTEP of Cu(N3DMP) is shown below in figure 2.16 with relevent bond distances and angles listed in table 2.8 and 2.9.

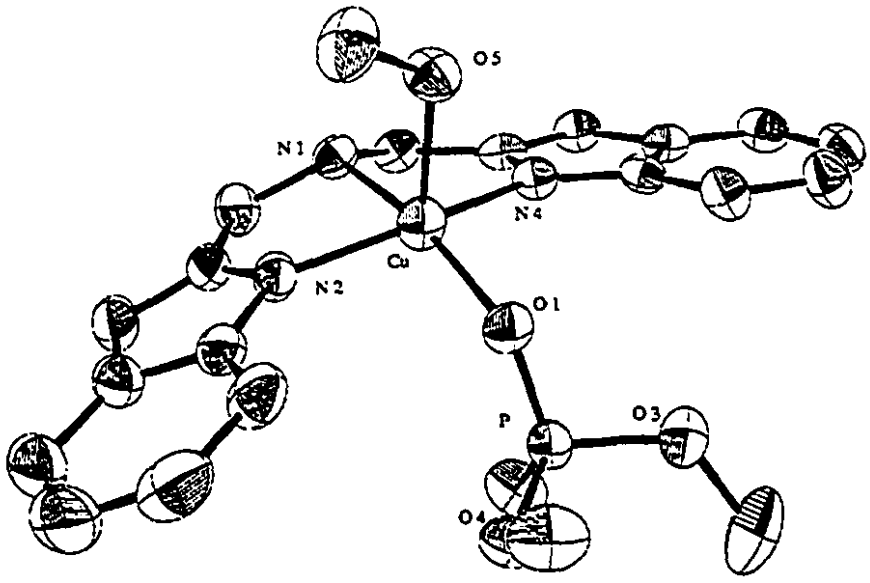

Figure 2.16 ORTEP view of Cu(N3DMP)

The DMP was not observed to bridge two Cu(N3) units as was expected. The geometry about the copper cation is best described as distorted square pyramidal with O(5) occupying the apical position and N(2), N(1), N(4) and O(1) forming the base of the pyramid. Copper(II) can adopt 4, 5, and 6 coordinate geometries either in solution or in the solid state. At least in the solid state, Cu(N3) can adopt the five coordinate geometry required to form the active catalytic species proposed. To what extent the structure reveals the solution behavior of the complex is a debatable point. In the next section will be discussed several published X-ray structures of copper and other metal compounds which indirectly provide support for the structure of the active species.

Table 2.8 Crystallographic Data for dimethylphosphato-methanol-[(bis(benzimidazol-2-ylmethyl)-amine)copper(II)] perchlorate

molecular formula	$C_{19}H_{25}N_5O_9PClCu$	Z	2
molecular weight, g mol^{-1}	597.40	ρcalc g/cm^3	1.643
crystal system	triclinic	μ, mm^{-1}	3.47
space group	$P\bar{1}$	*F*(000)	614
a (Å)	7.2573 (11)	data collected	3337
b (Å)	12.7707 (17)	unique data	3045
c (Å)	13.3686 (20)	data with $I > 2.5\sigma(I)$	2808
α (°)	85.213 (12)	*R*	0.047
β (°)	80.009 (12)	R_w	0.063
γ (°)	82.413 (12)	R_{int}	0.016
V ($Å^3$)	1207.2 (3)	goodness of fit	4.62

Table 2.9 Selected Bond Distances (Å) and Angles (°) and estimated standard deviations of the last significant figure in parenthesis for dimethylphosphato-methanol-[(bis(benzimidazol-2-ylmethyl)-amine)copper(II)] perchlorate

Bond Distances

Cu - O(1)	1.970 (3)	Cu - N(1)	2.101 (4)
Cu - O(5)	2.241 (4)	Cu - N(2)	1.966 (4)
Cu - N(4)	1.960 (4)		

Bond Angles

O (1) - Cu - O (5)	95.70 (14)	O (5) - Cu - N (2)	98.14 (16)
O (1) - Cu - N (1)	164.95 (16)	O (5) - Cu - N (4)	95.42 (15)
O (1) - Cu - N (2)	96.17 (16)	N (1) - Cu - N (2)	81.39 (17)
O (1) - Cu - N (4)	97.76 (15)	N (1) - Cu - N (4)	81.25 (16)
O (5) - Cu - N (1)	99.34 (15)	N (2) - Cu - N (4)	159.46 (17)

3 Discussion

Cu(N3) and Cu(N3OH) are among the fastest catalysts for promoting the transesterification reaction of HPNP. The reactivity of Cu(N3) is only 6.6 times slower than the parent dinuclear complex LCu_2 (Chapter 3). The reactivity of Cu(N3OH) is comparable to that of LCu_2. In table 2.10 are the results of the present study in comparison with previously published results. In general, the reactivities of Cu(DPA), Cu(DIEN), and Cu(TER) also compare favourably to the previously published results.

Table 2.10

complex	concentration(mM) Temp (°C) and pH	rate constant (hr^{-1})	half-life (hrs)
ZnW	0.5, 37, 7.0	7.4×10^{-4}	937
Zntacd	0.5,37,7.0	4.64×10^{-2}	15
Zn^{2+} and 2MeIm (8 mM)	5,37,7.0	1.74×10^{-1}	4
La(tcmc)	1,37,7.4	5.8×10^{-2}	12
$Cu(NO_3)_2$[82]	1,37,6.85	1.44×10^{-1}	4.8
Cu(DPA)	2, 25, 8.0	2.93×10^{-1}	2.4
Cu(TER)	2, 25, 9.3	6.70×10^{-2}	10.4
Cu(DIEN)	2, 25, 9.8	7.02×10^{-2}	9.9
Cu(N3)	2, 25, 7.0	2.08	0.33
Cu(N3OH)	2, 25,7.0	18.83	0.04

We had expected that the reactivity of Cu(N3) and Cu(N3OH) should be negligible compared to that of the parent dinuclear complex LCu_2. The dinuclear complexes in figure 2.17 A and 2.17 B were found to be reactive for the cleavage of HPNP and hydrolysis of DMF respectively. The corresponding mononuclear catalyst ('half' the dinuclear catalyst) catalyzed the same reaction significantly slower than the parent dinuclear complex.

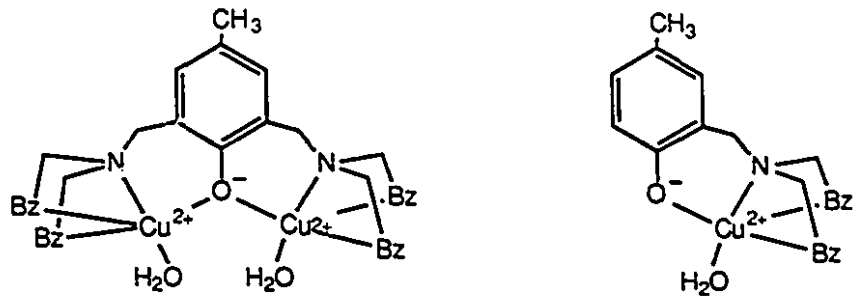

2.17 A

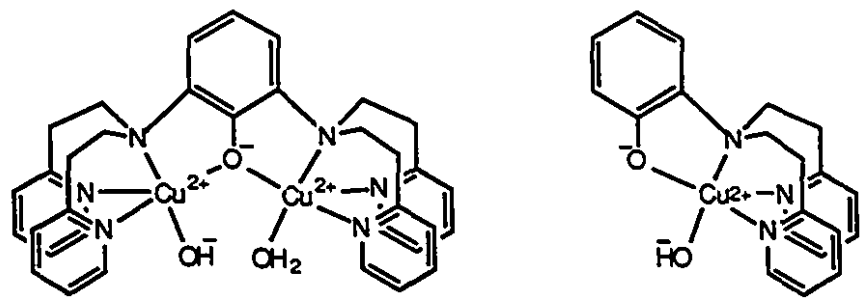

2.17 B

Figure 2.17 Two dinuclear systems A: for the transesterification of HPNP[83] and B: hydrolysis of DMF.[84] In both cases the mononuclear catalyst is significantly slower in promoting their corresponding reactions. Bz represents a pendant benzimidazole group.

The 1:1 complexes of copper and various ammine ligands have a varying range of reactivity for catalyzing phosphate diester hydrolysis. Cu(DPA) is known to hydrolyze BNPP quite rapidly with a half-life of 1.5 hrs at 50 °C at 1 mM complex.[63] The concentration dependence of *cis*-diaqua copper(II) complexes for the hydrolysis of phosphate diesters has been studied.[62,63] A first order dependence on concentration is observed at low complex concentrations. The dependence on concentration decreases at higher concentrations until the reactivity reaches a plateau. This is consistent with the known dimerization behavior of these complexes.[85] The side equilibrium introduced by the dimerization lowers the rate of the hydrolysis reaction by decreasing the concentration of the reactive hydroxy-aqua species. Copper complexes of triammine ligands are, in general, expected to exhibit a linear dependence over a larger concentration range than

complexes with diammine ligands for the hydrolysis reaction. The dimerization constants, K_d, for these complexes are generally smaller. The observed behaviour of Cu(DPA), Cu(DIEN), and Cu(TER) for the cleavage of HPNP is consistent with the known behaviour of 'normal' copper complexes.

As we have shown, unlike other copper complexes in which the reactivity levels off or increases linearly with increasing concentration, Cu(N3) exhibits a second order dependence on the catalyst concentration. Several mechanisms can be proposed to explain the observed products, and the concentration dependence of Cu(N3).

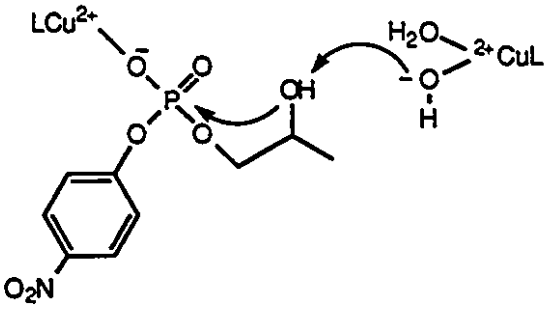

Figure 2.18 A possible mechanism for the cleavage of HPNP by Cu(N3)

One reasonable mechanism is shown in figure 2.18. One copper complex can provide Lewis activation upon coordination of the phosphate while a second can act as a general base to deprotonate the hydroxyl group for intramolecular attack. This mechanism, however, should exhibit first order dependence on hydroxide and hence is rejected.

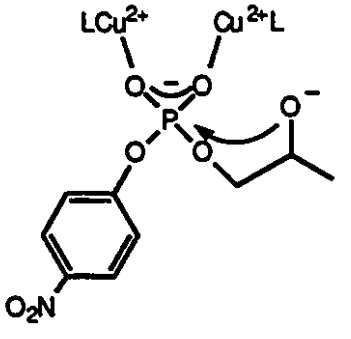

Figure 2.19 A possible mechanism for the cleavage of HPNP by CuN3

Two distinct copper complexes can coordinate the phosphate diester followed by intramolecular hydroxide attack. This can occur if two distinct equivalents of the complex

bind two of the oxygens of the phosphate (as shown in figure 2.19) or if there is a preequilibrium formation of a dinuclear complex (shown in figure 2.20). We expect that the third order process necessary in figure 2.19 would be less likely than the preequilibrium formation of the dinuclear copper complex in figure 2.20. The hydroxide dependence of the mechanism in figure 2.19 should also only be first order in hydroxide and thus this mechanism cannot be operating. It has been proposed[73,74] that certain copper complexes hydrolyze RNA via chelation of the phosphate followed by base catalysis on the attacking hydroxyl. This chelation/base catalyzed mechanism also requires a first order dependence in hydroxide and can not be operating in the cleavage reaction of HPNP with Cu(N3).

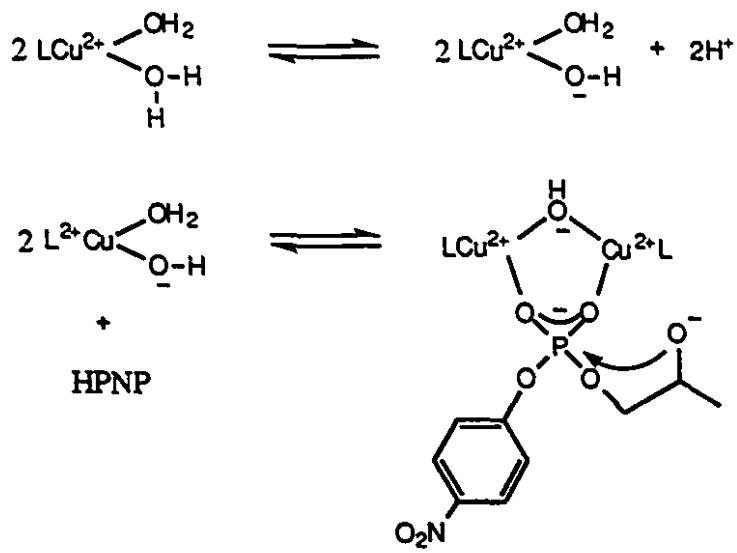

Figure 2.20 pre-equilibrium formation of active dimerized complex with double Lewis acid activation and internal nucleophilic attack on the coordinated phosphate diester. Proposed mechanism for the catalysis of the transesterification reaction of HPNP by Cu(N3).

In figure 2.20, there is a pre-equilibrium formation of a dimerized complex which can subsequently bind the phosphate diester in a bridging fashion. Intramolecular attack of the deprotonated alkoxyl occurs to give the cyclic 1,2-propylene phosphate and the *p*-nitrophenolate anion products.

Isolation of the proposed dimerized complex was not possible. There is, however, precedent in the inorganic literature for the spontaneous formation of hydroxy or oxy bridging dimers in solution. When the mononuclear iron(III) complex of the ligand N,N'-bis(2-pyridylmethyl)ethane-1,2-diamine (bispicen) is dissolved in water in the presence of

potassium iodide a μ-oxo dimer is formed.[86] In the presence of sodium acetate and sodium carbonate, the corresponding (μ-oxo)(μ-acetato) dimer is formed. The spontaneous assembly in solution of μ-oxo bridging dimers with a second bridging phosphato or phosphinato group in iron complexes has also been observed.[87] In figure 2.21 A is shown the structure of a dinuclear copper complex with a bridging hydroxy ligand and a second bridging carbonato ligand.[88] This complex precipitates from methanol when 2,2'-bipyridine, formic acid and $Cu(BF_4)_2$ are combined in the presence of triethylamine and has been characterized by X-ray crystallography.

The crystal structure obtained of dimethyl phosphate bound to Cu(N3) does not show DMP bridging two equivalents of Cu(N3). However, the complex obtained when bis(2-(1-methylimidazolyl) methyl)amine (B-MINA) is combined in methanol with copper(II)acetate in the presence of sodium perchlorate is polymeric with acetate bridging the copper complexes.[89] B-MINA is structurally similar to the ligand N3 of this study. The crystal structure of this complex (figure 2.21 B) has been reported and is structurally similar to the X-ray structure we have obtained of Cu(N3). The geometry about the copper is also square pyramidal with the acetate binding the fourth basal position where our phosphate diester binds. In this structure, however, acetate does bridge two different metal ions. The apex of the square pyramid in this case is occupied by a second acetate ligand.

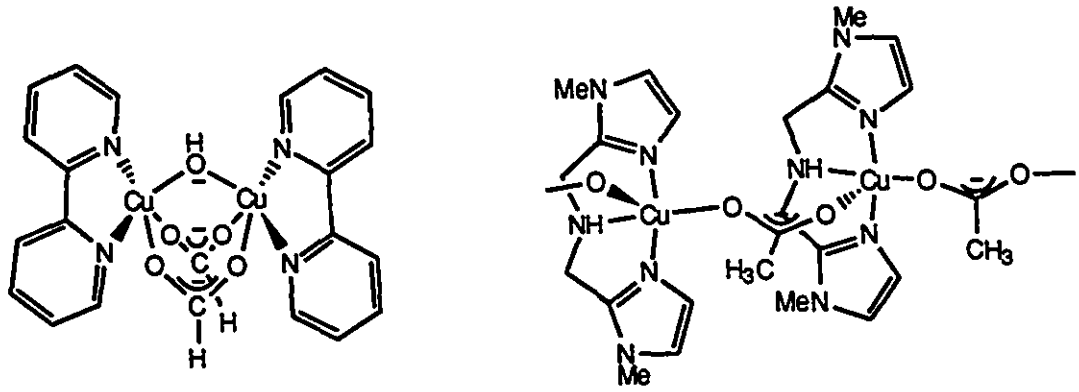

A B

Figure 2.21 Chemical precedence for the reactive species in the proposed cleavage mechanism of HPNP by Cu(N3)

In conclusion, it has been shown that Cu(N3) and Cu(N3OH) are the most effective mononuclear copper(II) catalysts for promoting HPNP cleavage. A dinuclear mechanism is proposed for this cleavage reaction promoted by Cu(N3). In chapter 3 the reactivity of Cu(N3) and Cu(N3OH) will be compared to the reactivity of their parent dinuclear complex.

4 Experimental

General

Instrumentation

^{1}H NMR were recorded on a Varian XL 200 spectrometer. ^{13}C NMR were recorded on a Varian XL 300 (75.4 MHz) or Gemini 200 (50.3 MHz). ^{31}P NMR were recorded on a Varian XL 300 (75.4 MHz) or a Unity 500-FT (202.3 MHz). For ^{1}H NMR, tetramethyl silane (TMS,$CDCL_3$) and 3-trimethylsilyl-1-propanesulfonic acid (DSS,D_2O) were used as internal standards. Data is reported in parts per million (ppm) downfield with respect to these standards. The proton signals of DMSO (δ 2.49) and methanol (δ 3.3) were used as reference values in these solvents. For ^{13}C NMR, $CDCl_3$ (77.0 ppm) or 1,4-dioxane (67.7 ppm in D_2O) were used as reference values. 10% trimethylphosphate in D_2O was used as an external reference for ^{31}P NMR.

A Hewlett-Packard 8452A diode array spectrophotometer equipped with an RMS lauda thermostat water bath was used for UV-Vis kinetic experiments.

Titration of metal complexes were performed on a Radiometer PHM63 pH meter equipped with a Radiometer RTS822 automatic titrator and an RMS Lauda thermostat water bath.

X-ray diffraction Studies: The intensity data was collected on a Rigaku AFC6S diffractometer. The structure of $tacn_2Co_2(OH)_2DMP$ (chapter 4) was solved by Dr. Anne-Marie Lebuis, all other structures were solved by Dr. Rosemary Hynes.

Mass spectral data: Mass spectra were obtained on a Kratos MS25RFA mass spectrometer with an ion source temperature of 200°C.

Elemental Analysis: Elemental analyses were performed by Guelph Chemical Laboratories Ltd., Guelph, Ontario.

Curve fitting: Linear and non-linear curve fits were generated by the least squares method using Kaleidagraph data analysis version 3.0.1. from Abelbeck Software.

Kinetics

Rate constants were obtained by fitting the first three half-lives of the reaction to a first-order kinetic equation. In some cases, initial rate methods were used. The slope of

the first 3 - 5 % of the reaction was divided by the extinction coefficient (ε = 18 700 for *p*-nitrophenoxide) and the concentration of substrate (5×10^{-5} M). Where necessary a correction was made for the concentration of *p*-nitrophenoxide present at a given pH. Experiments were run in triplicate and were reproducible to within 5% error.

Chemicals

2,2'-Dipyridylamine, and 2,2':2',2"-terpyridine and diethylenetriamine were purchased from Aldrich and used without further purification. HPNP was synthesized by Phillip Hurst according to literature procedure.[14]

CAUTION! While none of the present perchlorate complexes proved to be shock sensitive, care is recommended in handling these complexes

Bis(benzimidazol-2-ylmethyl)amine (N3)

N3 was synthesized by a modified literature procedure.[90] (8.12 g, 0.075 mol) of 1,2-diaminobenzene was ground to a fine powder and ground together with (5 g, 0.038 mol) of iminodiacetic acid. These were heated to 170-180 °C until no further steam was detected. After cooling the resulting glass was dissolved in concentrated hydrochloric acid which upon standing formed a blue solid. This was collected by vacuum filtration and washed with acetone. The recovered precipitate was dissolved in approx. 300 mL of water and dilute ammonium hydroxide added dropwise until a new blue-pink precipitate formed. The precipitate was collected and recrystallized twice from acetone. Finally the precipitate was dissolved in methanol and stirred for 2-3 hrs at room temperature in the presence of decolourising carbon. After filtering over a celite bed and concentrating the filtrate an off-white ppt (2.7 g, 26 %) was obtained. ^{1}H NMR (CD_3OD, 200 MHz): δ 4.10 (4H, s), 7.21 (4H, m), 7.53 (4H, m) ^{13}C NMR (CD_3OD, 75.4 MHz): δ 47.39, 115.67, 123.52, 139.38, 155.01

dichloro-[(bis(benzimidazol-2-ylmethyl)amine)copper(II)]·CH_3OH Cu(N3)

To a stirred solution (0.06 g, 0.35 mmol) of $CuCl_2.2H_2O$ in 5 ml of ethanol was added dropwise a solution (0.1g, 0.36 mmol) of N3 in 5 mL of ethanol. The green precipitate which forms after 3-5 mins was filtered after stirring for 1hr and washed with cold methanol. 0.12g of a light green powder was isolated (77.4 %).

X-ray structure of dichloro-[(bis(benzimidazol-2-ylmethyl)amine)copper(II)]·CH_3OH: Crystals suitable for X-ray crystallography were obtained by slow recrystalization from methanol. In a 2 dram vial approx. 10 mg of the complex was dissolved in the minimum amount of methanol (0.3 mL). A layer of paraffin with a single pin hole was used to cover the vial. After a few days the blue crystals were removed from the supernatant liquid. Crystal system: orthorhombic, space group: Pbca with a = 14.020 (4) Å, b = 14.380(3) Å, c = 18.268(4) Å, V = 3683.0(15) $Å^3$, Z = 8. R = 0.048, R_w = 0.044, GoF = 1.96. Additional X-ray data is appended.

diperchloro-[(bis(benzimidazol-2-ylmethyl)amine)copper(II)]·$2H_2O$ $Cu(N3)(ClO_4)_2$

To a stirred solution of (0.40 g, 1.08 mmol) of $Cu(ClO_4)_2·H_2O$ in 2-3 ml methanol was added dropwise a solution of N3 (0.30 g, 1.08 mmol) in 5-7 mL methanol. After stirring for 1 hr, the solution was left standing for 12 hrs. The blue crystals which appeared were filtered, washed with cold methanol and dried under vacuum for 8 hrs. 0.41 g of a dull blue precipitate was isolated (66 %). Analysis calculated for $C_{16}H_{19}N_5O_{10}CuCl_2$: C, 33.38, H. 3.32, N, 12.16 Found : C, 33.39 H, 3.07, N, 12.10

dimethylphosphato-methanol-[(bis(benzimidazol-2-ylmethyl)amine)copper(II)] perchlorate·$2H_2O$ Cu(N3)DMP

To a stirred solution of (0.28 g, 0.519 mmol) of $CuN3(ClO_4)_2$ in 5 mL methanol was added dropwise a solution of (0.077 g, 0.519 mmol) sodium dimethylphosphate (DMP) in 5 mL methanol. A blue precipitate appears after 5-10 mins. After stirring for one hour, the blue precipitate was washed with cold methanol, filtered and dried under vacuum for 6 hrs. 0.17 g of a blue precipitate was isolated (58 %). A blue block crystal was isolated from an acetone-hexane interface for x-ray crystallographic analysis. Crystal data is tabulated in abbreviated form in the results section. Supporting crystallographic data is found in the appended material. Analysis calculated for C19H25N5O9CuClP : C, 38.20, H, 4.21, N 11.72. Found : C, 38.32 H, 4.08 N, 11.85

Bis(benzimidazol-2ylmethyl)hydroxyethylamine (N3OH)

The two reagents, (2.0g, 0.01mol) of N-(2-hydroxyethyl)iminodiacetic acid and (2.44g, 0.023 mol) of 1,2-diaminobenzene were ground into a fine powder with a mortar and pestle. These were heated to 170-180 °C for 1 hr until no further steam was detected.

After cooling to room temperature, 100 mL of concentrated hydrochloric acid was added to dissolve the resulting dark glass. A blue precipitate forms after approx. 5 mins of sonication. This precipitate was filtered and washed with acetone and immediately dissolved in approx. 100 mL of water. The solution was basified by the slow addition of concentrated ammonium hydroxide. The pink-white precipitate which forms was collected and recrystallized from hot acetone to yield 2.1g of an off-white precipitate (58%). ^{1}H NMR (CD_3OD, 200 MHz): δ 2.76 (2H, t, J = 5.5 Hz), 3.66 (2H, t, J = 5.5 Hz), 4.06 (4H, s), 7.22 (4H, m), 7.54 (4H, m) ^{13}C NMR (CD_3OD, 75.4 MHz): δ 53.73, 57.68, 60.41, 115.73, 123.71, 139.27, 154.04 MS, EI, 350 °C, (m/z, rel. int., assignment): 321 ($M^{+\cdot}$, 0.06), 189(27), 160(51.7), 132(100), 131(58.8), 119(20.4)

chloro-[(bis(benzimidazol-2ylmethyl)hydroxyethylamine)copper(II)] chloride·3(H_2O) Cu(N3OH)

To a stirred solution (0.106 g, 0.622 mmol) of $CuCl_2.2H_2O$ in 5 ml of ethanol was added dropwise a solution (0.201 g, 0.625 mmol) of N3OH in 5 mL of ethanol. The green precipitate which forms after 5-10 mins was filtered after stirring for 1hr and washed with cold methanol. 0.144 g of a light green powder was isolated (48 %). Analysis calculated for $C_{18}H_{25}N_5CuCl_2$: C, 42.40 H, 4.94 N, 13.73 Found: C, 41.35 H, 3.72, N, 13.36

X-ray crystal structure of chloro-[(bis(benzimidazol-2ylmethyl)hydroxyethylamine)copper(II)] chloride·3(H_2O): A blue oblong crystal was isolated by slow recrystalization from methanol. Crystal system: monoclinic, space group: A2/a, a = 14.324(4) Å, b = 17.158(5) Å, c = 18.712(5) Å, β = 109.305 (18) V = 4340.3(19) $Å^3$, pcalc = 1.564 g/cm^3, Z = 8. R = 0.059, R_W = 0.069, GoF = 3.59 Additional X-ray data is appended.

dichloro-[(2,2'-dipyridylamine)copper(II)] Cu(DPA)

To a stirred solution of (4.98 g, 0.03 mol) of $CuCl_2.2H_2O$ in approx. 30 mL of methanol was added 35 mL (5 g, 0.03 mol) of 2,2'-dipyridylamine in methanol. A dark green (8.6 g, 96 %) precipitate forms which is filtered off washed with cold methanol and ether. Analysis calculated for $C_{10}H_9N_3CuCl_2$: C, 39.30 H, 2.97 N, 13.75 Found : C, 39.48 H, 2.88 N, 13.64

dichloro-[(diethylenetriamine)copper(II)] Cu(DIEN)

To a stirred solution of (2.5 g, 0.015 mol) of $CuCl_2.2H_2O$ in approx. 10 mL of methanol is added approx. 10 mL of a diethylenetriamine (2.5 g, 0.015 mol) in methanol. The blue precipitate (2.35 g, 67 %) which forms after 5 - 10 mins is filtered off, washed with cold methanol and ether. Analysis calculated for $C_4H_{13}N_3CuCl_2$: C, 20.22 H, 5.51 N, 17.68 Found : C, 20.34 H, 5.77 N, 17.50

dichloro-[(2,2':2',2"-terpyridine)copper(II)] Cu(TER)

To a stirred solution (1.46 g, 8.6 mmol) of $CuCl_2.2H_2O$ in approx. 10 mL methanol was added 10 mL (2 g, 8.6 mmol) of 2,2'-6',2"- terpyridine. The bright green precipitate (3 g, 95 %) which forms after 5-10 mins was filtered off and washed with cold methanol and ether. Analysis calculated for $C_{15}H_{11}N_3CuCl_2$: C, 48.99 H, 3.01 N, 11.43 Found : C, 48.77 H, 2.97 N, 11.30

5 Appendix

5.1 Tables of Data

Table 2.1 Data from figure 2.5. Concentration dependence of Cu(DPA) at 25°C and pH 8.01 in 0.1 M EPPS buffer

Concentration (mM)	$k_O \times 10^5$ (s^{-1})
1.0	5.30
2.0	8.15
3.0	10.5
4.0	11.5
5.0	13.5
7.0	16.0
9.0	17.5
12.5	21.5
15.0	25.0

Table 2.2 Data from figure 2.6. Concentration dependence of Cu(TER) at 25 °C and pH 9.28 in 0.1 M CHES buffer

concentration (mM)	$k_O \times 10^5$ (s^{-1})
1.0	1.00
2.0	1.85
3.0	2.70
4.0	3.60
5.0	4.30
7.0	6.20
9.0	7.85
10.0	8.60
12.5	10.5
15.0	12.5
17.5	14.5
20.0	17.0

Table 2.3 Data from figure 2.6. Concentration dependence of Cu(DIEN) at 25 °C and pH 9.80 in 0.1 M CHES buffer

concentration (mM)	$k_O \times 10^5$ (s^{-1})
4.0	1.95
6.0	3.00
8.0	3.90
10.0	4.10
12.5	5.40
15.0	6.75
17.5	8.00
20.0	8.90

Table 2.4 Data from figure 2.7. Concentration dependence of Cu(N3) at pH 6.75 and 25°C at 20 mM HEPES buffer.

Concentration (mM)	log (k_O s^{-1})
2.00	-3.25
1.50	-3.50
1.25	-3.70
1.00	-3.95
0.75	-4.20
0.50	-4.65
0.25	-5.25

Table 2.5 Data from figure 2.11. pH-rate profile data for the transesterification of HPNP at 25 °C, [Cu(TER)] = 5 mM, [HPNP] = $5x10^{-5}$ M in 0.1 M buffer. CHES buffer between pH 10.00 - pH 8.60, EPPS buffer between pH 8.50 - pH 7.80, HEPES buffer between pH 7.75 and pH 7.00

pH	$k_O \times 10^5$ (s^{-1})
10.00	4.70
9.50	4.70
9.05	4.70
8.50	3.90
8.25	3.10
8.00	2.50
7.75	1.50
7.51	1.30
7.27	0.80
7.00	0.60
6.58	0.42

Table 2.6 Data from figure 2.12. pH rate profile data for the transesterification of HPNP at 25°C, [Cu(DIEN)] = 5 mM,[HPNP] = $5x10^{-5}$ M and [Buffer] = 0.1 M. CHES between pH 8.80 and pH 10.00, EPPS between pH 8.60 and 7.80, HEPES at pH 7.40

pH	$k_O \times 10^5$ (s^{-1})
10.00	5.02
9.80	4.90
9.70	4.50
9.60	4.10
9.50	3.70
9.41	3.60
9.20	3.50
9.10	3.00
9.02	2.90
8.91	2.70
8.80	2.25
8.62	1.70
8.60	1.50
8.40	1.10
8.20	0.70
7.80	0.30
7.40	0.10

Table 2.7 Data from figure 2.13. pH-rate profile data for the transesterification of HPNP at 25 °C, [Cu(DPA)] = 5 mM, [HPNP] = $5x10^{-5}$M [Buffer] = 0.1 M. HEPES buffer between pH 7.75 and pH 6.90, MES buffer between pH 6.80 and 6.00

pH	$k_o \times 10^4$ (s^{-1})
10.00	1.30
9.50	1.30
9.05	1.35
8.55	1.30
8.00	1.25
7.75	1.30
7.53	1.18
7.25	1.20
7.00	1.15
6.70	8.70
6.60	9.10
6.50	8.00×10^{-1}
6.40	5.90×10^{-1}

Table 2.8 Data from figure 2.14. pH-rate profile data for the transesterification of HPNP at 25°C, [Cu(N3)] = 1 mM, [HPNP] = $5x10^{-5}$ M

pH	$k_o \times 10^5$ (s^{-1})
6.51	1.15
6.60	1.95
6.70	3.20
6.80	4.95
7.02	7.85
7.20	7.65
7.40	7.60

5.2 Derivations

Derivation of equation 2.4

The observed rate constant for the hydrolysis is:

$$k_o = k[Cu(H_2O)(OH)] \tag{1.1}$$

The acid dissociation constant for the coordinated water molecule is :

$$K_a = \frac{[Cu(H_2O)(OH)][H^+]}{[Cu(H_2O)_2]} \tag{1.2}$$

The dimerization constant is:

$$K_d = \frac{[Cu_2(OH)_2]}{[Cu(H_2O)]^2} \tag{1.3}$$

The total complex concentration is defined as:

$$[Cu]_T = [Cu(H_2O)_2] + [Cu(H_2O)(OH)] + 2[Cu_2(OH)_2] \tag{1.4}$$

Substituting equation 1.2 and 1.3 into 1.4 we obtain:

$$2K_d[Cu(H_2O)(OH)]^2 + \left(\frac{[H^+]}{K_a} + 1\right)[Cu(H_2O)(OH)] - [Cu]_T = 0 \tag{1.5}$$

We can solve for [Cu(H2O)(OH)] by solving the quadratic equation 1.5 to give:

$$[Cu(H_2O)(OH)] = \frac{-\left(\frac{[H^+]}{K_a} + 1\right) + \sqrt{\left(\frac{[H^+]}{K_a} + 1\right)^2 + 8K_d[Cu]_T}}{4K_d} \tag{1.6}$$

An expression for k_O can be obtained by substituting equation 1.6 into 1.1:

$$k_o = (k)\frac{-\left(\frac{[H^+]}{K_a}+1\right)+\sqrt{\left(\frac{[H^+]}{K_a}+1\right)^2+8K_d[Cu]_T}}{4K_d} \qquad (1.7)$$

If the reaction is followed at a pH greater than the pK_a of the complex, 1.7 reduces to equation 1.8:

$$k_o = (k)\frac{-1+\sqrt{1+8K_d[Cu]_T}}{4K_d} \qquad (1.8)$$

Derivation of equation 2.10.1

The observed rate constant and the acid dissociation constant is defined as in 1.1 and 1.2

The total concentration of copper in solution is given by:

$$[Cu]_T = [Cu(H_2O)(OH)] + [Cu(H_2O)_2] \qquad (2.1)$$

Substituting equation 1.2 into equation 2.1 and rearranging one obtains:

$$[Cu]_T = [Cu(H_2O)_2]\left(\frac{K_a + [H^+]}{[H^+]}\right) \qquad (2.2)$$

Therefore:

$$[Cu(H_2O)_2] = \left(\frac{[H^+]}{K_a + [H^+]}\right)[Cu]_T \qquad (2.3)$$

Substituting equation 1.2 into 1.1 one obtains:

$$k_o = \frac{kK_a}{[H^+]}[Cu(H_2O)_2] \qquad (2.4)$$

Upon substitution of 2.3 into 2.4 one obtains equation 2.10.1:

$$k_o = \left(\frac{kK_a}{K_a + [H^+]}\right)[Cu]_T \qquad (2.5)$$

Equation 2.10.2

Equation 1.6 can be simplified to give:

$$[Cu(H_2O)(OH)] = \frac{-\left(\frac{K_a + [H^+]}{K_a}\right) + \sqrt{\left(\frac{K_a + [H^+]}{K_a}\right)^2 + 8K_d[Cu]_T}}{4K_d} \qquad (3.1)$$

An expression for k_O can be obtained be substituting equation 3.1 into 1.1:

$$k_o = k\frac{-\left(\frac{K_a + [H^+]}{K_a}\right) + \sqrt{\left(\frac{K_a + [H^+]}{K_a}\right)^2 + 8K_d[Cu]_T}}{4K_d}$$

Chapter 3: Dinuclear Copper(II) Complex Promoted Cleavage of HPNP

1 Introduction

The *cis*-diaqua cobalt(III) complexes of trpn, and cyclen are among the fastest known catalysts for the hydrolysis of phosphate diesters.[58,59] Rate accelerations of up to 10^{10} are observed with these catalysts. These catalyst designs have provided substantial mechanistic insight into the role of metal ions in phosphate diester hydrolysis. Increasingly, the study of enzyme structure and reactivity is revealing that in biology, enzymes and ribozymes take advantage of di or tri nuclear metal systems. Among these are included 3'-5'-exonuclease and HIV reverse transcriptase form RNase H. A dinuclear catalyst offers new possibilities in the design of hydrolytic catalysts for phosphate diesters and new ways to improve on the large rate accelerations already achieved by small inorganic catalysts.

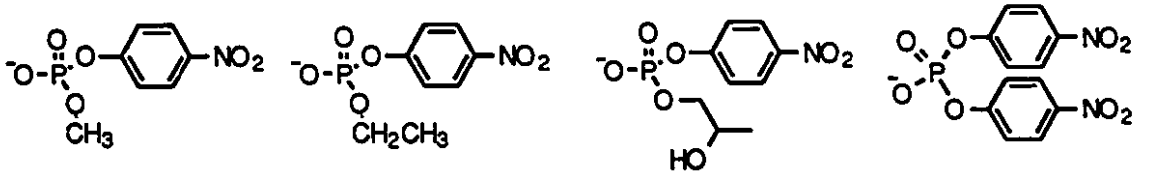

Figure 3.1 methyl *p*-nitrophenyl phosphate MPNP, ethyl *p*-nitrophenyl phosphate EPNP, hydroxypropyl *p*-nitrophenyl phosphate HPNP, bis(*p*-nitrophenyl) phosphate BNPP

The substrates used in this study as models for DNA and RNA are MPNP and HPNP respectively. The background rates and previous work on accelerating the transesterification of HPNP is discussed in chapter 2. A few studies have assessed the background hydrolysis of MPNP. One reported value[91] is 1.9×10^{-7} s^{-1} measured at pH 13 and 45°C. This corresponds to a 42 day half-life under these conditions. The background rate[14] for HPNP cleavage at pH 13 is 1.68×10^{-2} s^{-1} and 25 °C. Thus the difference in reactivity between these two substrates is 8.8×10^{4} without correction for the temperature difference (table 3.1). We can directly compare the rates at 25 °C by comparing the literature values for EPNP. At 25°C the reported second order rate constant for EPNP[92] hydrolysis is 3.3×10^{-7} M^{-1} s^{-1}. The difference in reactivity between EPNP and MPNP should be negligible since the difference between a methoxy or ethoxy substituent on phosphorous should correspond to a small effect on the hydrolysis reaction. These figures are tabulated in table 3.1. MPNP cleaves significantly slower than HPNP since the cleavage reaction of HPNP proceeds by intramolecular alkoxide attack.

Table 3.1 Second order rate constants for the background hydrolysis of some phosphate diesters

	k ($M^{-1}s^{-1}$)	relative rates
MPNP	1.9×10^{-6} (45°C)	5
HPNP	0.168 (25°C)	5×10^{5}
EPNP	3.3×10^{-7} (25°C)	1
BNPP[93]	2.0×10^{-5} (25°C)	60

MPNP is an ideal model substrate for DNA. Unlike BNPP no complications arise from the hydrolysis of the monoester product releasing a second equivalent of *p*-nitrophenol. Although the background hydrolysis rates of MPNP and EPNP differed by a negligible amount, the background rates of MPNP and BNPP are significantly different (table 3.1). Substitution of a *p*-nitrophenol ($pK_a = 7.15$) group for a methyl group (pKa = 15.6) retards the rate by about sixty fold.

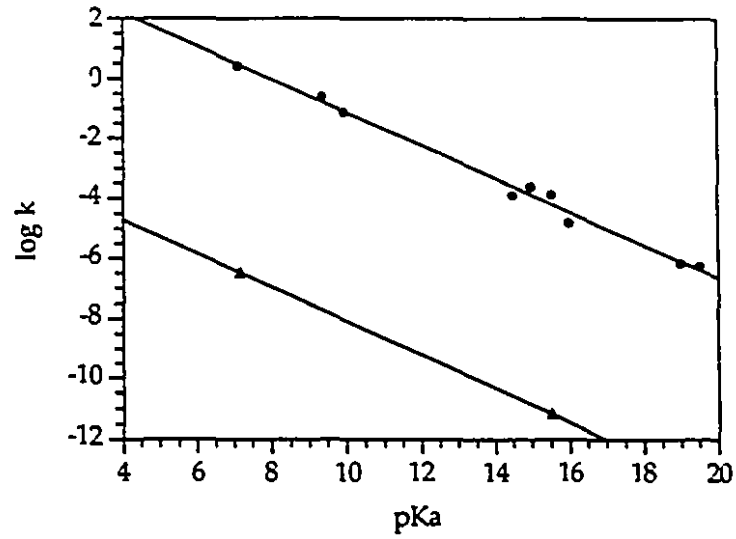

Figure 3.2 Linear free energy relationship between the second order rate constant ($M^{-1}s^{-1}$) for ▼: the hydroxide catalyzed reaction of EPNP, and DMP ($k = 6.8 \times 10^{-12}$ $M^{-1}s^{-1}$) and the pK_a of the leaving group ●: the hydroxide catalyzed cleavage of 2-hydroxypropyl phosphate esters and the pK_a of the leaving group

When the background hydroxide rates at 25°C for EPNP, DMP[94] are plotted a linear free energy relationship is observed with a slope of -0.56. The previously published[1] free energy relationship for the series, BDNPP, BNPP, DPP and DMP resulted in a line of slope -0.76 as we saw in figure 1.4. This relationship, however, does not factor out the electronic effect of the 'non-leaving' OR group. The 'non-leaving' group of DNA is better represented in the new series plotted in figure 3.2. As a consequence of this new LFE relationship a corrected value for the half-life of DNA can be calculated which takes into account the nature of the second OR group of DNA. Assuming a pK_a of 13-15 for the leaving group of DNA, the corrected rate constant for the hydroxide catalyzed hydrolysis of DNA is 10^{-16} to 10^{-18} s^{-1} at 25 °C and pH 7. Relatively, the corrected half-life differs by a small amount, however it is important to determine a true value for the background rate in order to determine the true efficiencies of catalysts and of distinct modes of catalysis. It is also important to distinguish between the mechanism of DNA hydrolysis where the leaving group is the 3'-OH ($\sim pK_a = 13$) or 5'-OH ($\sim pK_a = 15$). Also plotted above is the LFE relationship between a series of 2-hydroxypropyl esters[14] (recall that the slope for the LFE correlation for the hydroxide catalyzed cleavage and the leaving group

pK_a of several RNA analogues have a β value of about -0.56). The β value for both the DNA and RNA analogues are the same as expected since both correlate nucleophilic attack at phosphorous.

The goal of our research has been to examine the potential of dinuclear catalysts and develop a first generation of dinuclear complexes. Complexes which were designed to chelate[73] phosphate diesters have proven extremely succesful for the cleavage of RNA. We have focused on a dinuclear design which positions two metals at a distance which allows the phosphate diester to bridge them. In this new design it might be possible to assess the potential of a double Lewis acid mechanism in accelerating the cleavage reaction of phosphate diesters. We are also interested in probing the question of whether there is any favourable gain in reactivity if two metals are positioned at distinct oxygens of a phosphate diester rather than at the same oxygen. The rationalization for this catalyst design is expanded on in the introduction of chapter 4.

There have been many examples of dinuclear complexes that bridge acetates, formates, azide and in dinuclear iron complexes a few examples of bridging phosphates are known. At the time of this work, a dinuclear copper complex with a bridging phosphate diester was also characterized. This will be further elaborated on, in context with this work, in the discussion.

A survey of the intermetal distance of a wide range of dinuclear copper complexes and molecular mechanics indicated that LCu_2 (figure 3.3 B) would have a metal-metal distance suitable to support a bridging phosphate diester. The crystal structure of the complexes shown in figure 3.3 A with bridging acetate and azide ligands have been reported[95] and the copper - copper distances found are 3.459 and 3.615 Å respectively.

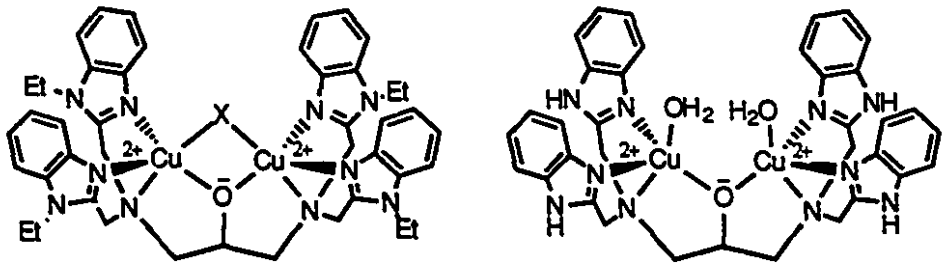

A x = OAc, N_3 B LCu_2

Figure 3.3 A : Published[95] dinuclear copper(II) structure with bridging acetate and azide ligands. B: Structure of diaquo-[(N,N,N',N'-tetrakis(2-benzimidazolyl)-2-hydroxy-1,3-diaminopropane)dicopper(II)] trichloride generated from the dissolution of LCu_2

2 Results

It was possible to isolate the dinuclear complex LCu_2 with a bridging dimethyl phosphate ligand. LCu_2DMP has been characterized by X-ray crystallography. The ORTEP of LCu_2DMP is shown below and relevant bond distances and bond angles are listed in table 3.2 and 3.3. In the structure of LCu_2DMP , the two copper atoms are separated by 3.569(2) Å. This distance forces the O(2) - P - O(3) angle to expand to 120.01(24) ° instead of the unstrained 109.5° expected for the tetrahedral geometry about phosphorous. The size of the O-P-O angle may be relevant in determining the amount of rate acceleration achieved by the dinuclear metal complex as will be elaborated in the discussion.

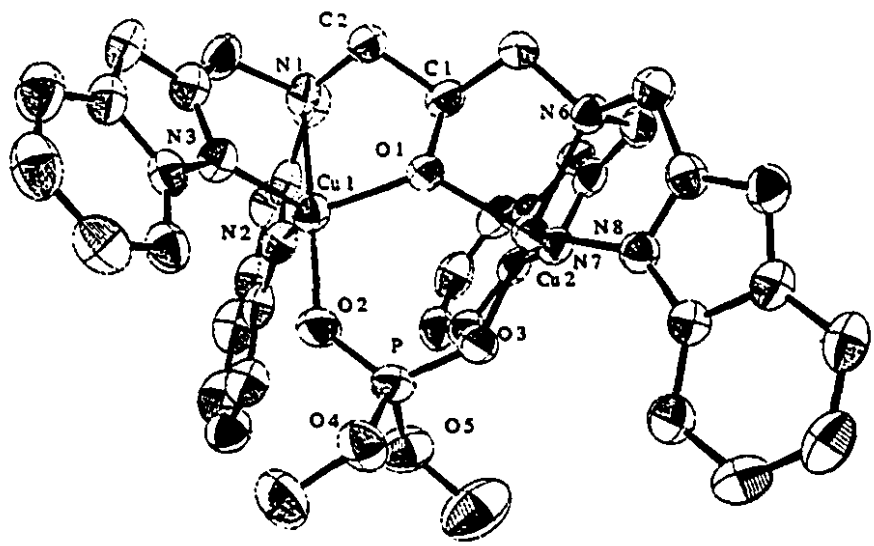

Figure 3.4 ORTEP view of LCu_2DMP

In the solid state structure of LCu_2DMP two oxygens of dimethyl phosphate are coordinated to the two copper atoms. The heptadentate ligand places the two copper atoms in distinct environments. The asymmetric unit contains the complex cation, two perchlorates, one acetone and one water molecule of solvation. The coordination about Cu(1) is distorted square pyramidal with N(3) in the axial position. The geometry about Cu(2) is also square pyramidal with N(7) in the axial position. The Cu(2)-N(7) is significantly longer 2.342(4) than the other Cu-N bonds which vary between 1.967(4) to 2.099(5). The bis(benzimidazolylmethyl)amine fragments of the heptadentate ligands form a pseudo facial arrangement about the copper atoms.

Table 3.2 Crystallographic Data for μ-dimethylphosphato-[(N,N,N',N'-tetrakis(2-benzimidazolyl)-2-hydroxy-1,3-diaminopropane)dicopper(II)] diperchlorate·(H_2O)

molecular formula	$C_{40}H_{47}N_{10}O_{15}PCl_2Cu_2$	Z	2
molecular weight, g mol^{-1}	1136.84	pcalc g/cm^3	1.574
crystal system	triclinic	μ, cm^{-1}	1.11
space group	$P\bar{1}$	F (000)	1168
a (Å)	13.250 (3)	data collected	6624
b (Å)	13.891(5)	unique data	6289
c (Å)	15.575 (3)	data with $I > 2.5\sigma(I)$	4649
α(°)	92.18 (3)	R	0.049
β (°)	114.883 (15)	R_w	0.050
γ	109.452 (24)	R_{int}	0.010
V(Å^3)	2398.4 (11)	goodness of fit	2.22

Table 3.3 Selected Bond Distances (Å) and Angles (°) with estimated standard deviations of the last significant figure in parenthesis for μ-dimethylphosphato-[(N,N,N',N'-tetrakis(2-benzimidazolyl)-2-hydroxy-1,3-diaminopropane)dicopper(II)] diperchlorate·(H_2O)

Bond Distances			
Cu (1) - O (1)	1.991 (4)	Cu (2) - O(1)	1.934 (4)
Cu (1) - O (2)	1.935 (4)	Cu (2) - O(3)	1.941 (4)
Cu (1) - N(1)	2.099 (5)	Cu (2) - N(6)	2.091 (4)
Cu (1) - N(2)	2.011 (5)	Cu (2) - N(7)	2.342 (4)
Cu (1) - N(3)	2.096 (5)	Cu (2) - N(8)	1.967 (4)
Cu (1) - Cu (2)	3.569(2)		
Bond Angles			
O (1) - Cu (1) - O(2)	97.49 (16)	O (1) - Cu (2) - O (3)	97.48 (16)
O (1) - Cu (1) - N(1)	83.49 (17)	O (1) - Cu (2) - N (6)	85.15 (16)
O (1) - Cu (1) - N (2)	127.24 (18)	O (1) - Cu (2) - N (7)	87.55 (16)
O (1) - Cu (1) - N (3)	108.55 (17)	O (1) - Cu (2) - N (8)	153.10 (18)
O (2) - Cu (1) - N (1)	178.75 (18)	O (3) - Cu (2) - N (6)	175.68 (17)
O (2) - Cu (1) - N (2)	97.50 (19)	O (3) - Cu (2) - N (7)	103.30 (17)
O (2) - Cu(1) - N (3)	99.59 (19)	O (3) - Cu (2) - N (8)	94.70 (17)
N (1) - Cu(1) - N (2)	81.27 (19)	N (6) - Cu (2) - N (7)	80.18 (17)
N (1) - Cu(1) - N (3)	80.82 (18)	N (6) - Cu (2) - N (8)	81.51 (18)
N (2) - Cu(1) - N (3)	118.22 (19)	N (7) - Cu (2) - N (8)	112.82 (18)
O (2) - P - O (3)	120.01 (24)		

The cleavage reaction of HPNP was followed by monitoring the increase in visible absorbance at 400 nm due to the release of *p*-nitrophenolate ion at pH 7 and 25 °C. The observed rate constants were obtained by fitting the first three half-lives of the reaction to a first-order equation. The pseudo-first order rate constant for complex LCu_2 (2 mM) promoted cleavage of HPNP at pH 7.00 is 3.9×10^{-3} s^{-1}. The half-life for the transesterification is about 3 minutes and thus represents one of the fastest catalysis of the cleavage reaction of HPNP. The products of the transesterification reaction as in chapter two are *p*-nitrophenoxide and the cyclic 1,2-propylene phosphate shown in figure 3.5.

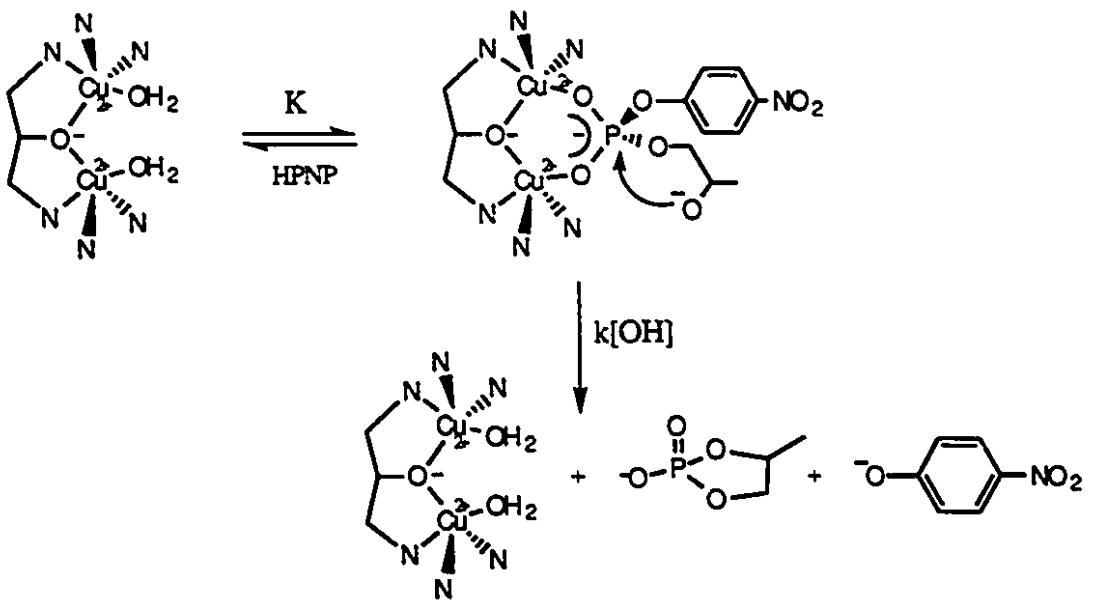

Figure 3.5 Proposed mechanism for the cleavage reaction of HPNP by LCu_2 and the products *p*-nitrophenoxide and cyclic 1,2-propylene phosphate

The products were identified in solution by ^1H NMR and ^{31}P NMR. The ^{31}P NMR is shown in figure 3.6. The starting material HPNP has a characteristic ^{31}P NMR shift at -7.9 ppm under these conditions. The only product peak observed after quenching the reaction with a pD 7.30 ethylenediamine solution is the peak observed at about 15 ppm. A peak at 15 ppm is characteristic of the cyclic 1,2-propylene phosphate product shown in figure 3.6. Since the ethylenediamine binds the copper there is no ambiguity in the ^{31}P NMR signals. The ^{31}P NMR of alkyl phosphate diesters appear near 0 ppm relative to TMP. The effect of *p*-nitrophenol on the phosphorous signal is a 7 ppm upfield shift. The

cyclic ethylene phosphate signal is characteristically observed 15 ppm downfield from non cyclic phosphate signals.

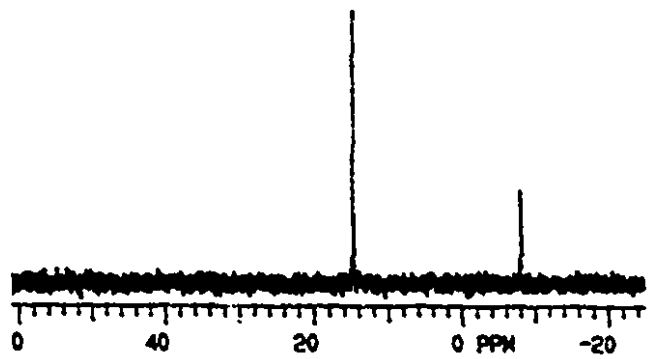

Figure 3.6 ^{31}P NMR of the products of LCu_2 catalyzed transesterification of HPNP with $[LCu_2]$ = 2 mM, [HPNP] = 2 mM. Reaction quenched after 40 mins at pD 7.30 with a pD 7.30 ethylenediamine solution.

Figure 3.5 represents the proposed mechanistic scheme for the catalysis by LCu_2. The first step is binding of HPNP to the dinuclear complex followed by attack of the hydroxyl group of the HPNP on the phosphorus centre with loss of the *p*-nitrophenolate group. The benzimidazoles are omitted for clarity. The observed rate constant obeys the equation shown in figure 3.7. This equation is derived in appendix 5.2.

$$k_o = \frac{kK[LCu_2][OH]}{1+K[LCu_2]} \qquad (3.7)$$

Figure 3.7 Expression for the observed pseudo first order rate constant (k_o)

A titration of a 2 mM solution of LCu_2 showed two pK_a values at 6.00 and 7.30 which we have assigned as a ligand pK_a and a bound water pK_a respectively. For copper(II) the pK_a values for metal bound waters fall in the range of 7 to 8. The first pK_a we have assigned to the benzimidazole NH. It is unlikely that the first pK_a is due to the protonated alkoxide since the pK_a of the alkoxide bound to two metals is expected to be much lower than 6.

The equilibrium constant for coordination of a phosphate diester, the first step in the mechanism, can be determined by a competitive inhibition study. When the hydrolysis of BDNPP is followed at pH 5.82 in the presence of increasing concentrations of dimethyl phosphate the dimethyl phosphate acts as a competitive inhibitor and binds reversibly to the dinuclear complex retarding the rate of the hydrolysis reaction. An additional equilibrium must be considered and the mechanistic scheme is shown in figure 3.8.

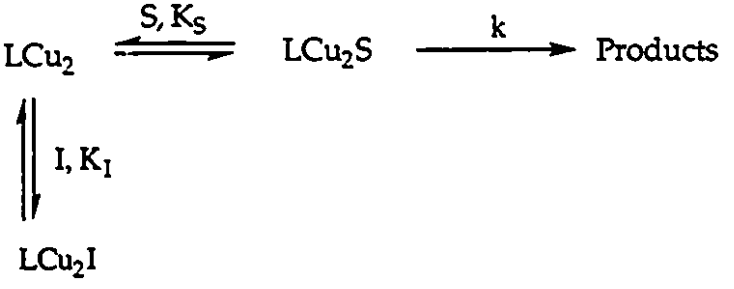

Figure 3.8 Reaction of substrate (S) in the presence of an inhibitor (I)

A plot of 1/ rate versus inhibitor concentration can be fit to equation 3.10. The equilibrium constant for binding of LCu_2 to DMP is determined by dividing the slope of the line by the intercept and is calculated to be $21 \pm 2\ M^{-1}$. The data for figure 3.9 is tabulated in appendix 5.1. As will be discussed in chapter 4 the equilibrium constant for binding to a dinuclear cobalt(III) complex is much larger than this value.

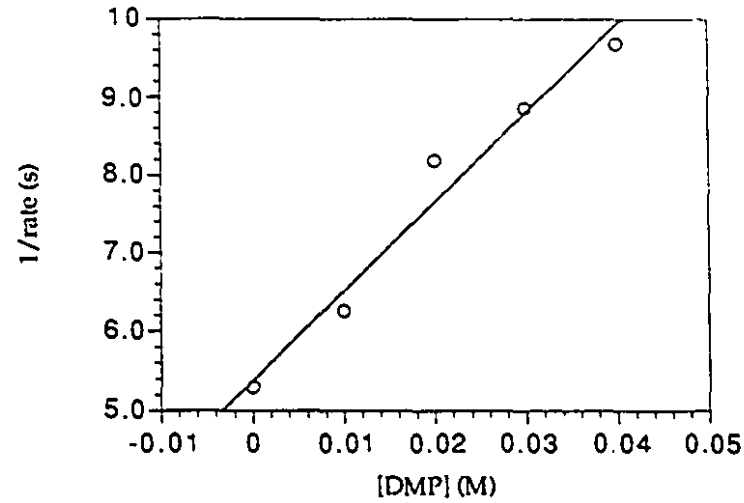

Figure 3.9 Hydrolysis of 5 x 10^{-5} M BDNPP in the presence of DMP at pH 5.82 fit to the equation 3.10 with slope = 1.26 x10^{6} ±1.3 x 10^{5}, intercept = 5.97 x 10^{4} ± 3.20 x 10^{3} and R = 0.984.

$$\frac{1}{\text{rate}} = \frac{1}{k[LCu_2]_t[S]} + \frac{K_I[I]}{k[LCu_2]_t[S]} \qquad (3.10)$$

$$\text{slope} = \frac{K_I}{k[LCu_2][S]}$$

$$\text{Intercept} = \frac{1}{k[LCu_2][S]}$$

Figure 3.10 Equation 3.10 and expressions for the slope and intercept for a plot of 1/rate versus inhibitor concentration

The second order rate constant for the background hydroxide catalyzed cleavage reaction of HPNP at 25°C is 0.168 M^{-1} s^{-1}. Using equation 3.7, the measured observed pseudo first order rate constant and the equilibrium constant for binding determined we can calculate a value for k (k is defined in figure 3.5). The unimolecular rate constant (k) for the copper bound HPNP is therefore 0.097s^{-1} at pH 7 and 25°C and the second order rate constant is 9.7 x 10^{5} $M^{-1}s^{-1}$. Comparing this second order rate constant to tha. of the

background rate we calculate a rate acceleration of 6×10^6 for the copper bound HPNP. Listed is table 3.4 are the observed rate constants for LCu_2 with the values found in chapter 2 for Cu(N3) and Cu(N3OH) and the background HPNP rate at pH 7 and 25 °C.

Table 3.4

Complex	k_O (s^{-1})	Relative rates
none	1.68×10^{-8}	1
LCu_2	3.9×10^{-3}	2.3×10^5
Cu(N3)	5.8×10^{-4}	3.5×10^4
Cu(N3OH)	5.23×10^{-3}	3.1×10^5

Cis-diaqua cobalt(III) complexes have been shown to efficiently hydrolyze phosphate esters including 3',5'-c-AMP[96] and RNA.[78] $[(cyclen)Co(H_2O)(OH)]^{2+}$ is among the most reactive cobalt(III) complexes for hydrolyzing a variety of substrates. LCu_2 however is about 20 times more reactive in cleaving HPNP than complex $[(cyclen)Co(H_2O)(OH)]^{2+}$. In contrast, the relative reactivity is reversed for the hydrolysis of MPNP. The observed rate constants for $[(cyclen)Co(H_2O)(OH)]^{2+}$ and LCu_2 the hydrolysis of HPNP and MPNP are tabulated in table 3.5 along with the relative reactivities in parenthesis.

Table 3.5

	MPNP	HPNP
$[(cyclen)Co(H_2O)(OH)]^{2+}$	2.5×10^{-4} s^{-1} (23)	2.0×10^{-4} s^{-1} (18)
LCu_2	1.1×10^{-5} s^{-1} (1)	3.9×10^{-3} s^{-1} (355)

Despite the large reactivity difference between MPNP and HPNP (10^5) $[(cyclen)Co(H_2O)(OH)]^{2+}$ hydrolysis both diesters at comparable rates. $[(cyclen)Co(H_2O)OH)]^{2+}$ hydrolyzes phosphate diesters by a joint Lewis acid/ metal hydroxide mechanism. The comparable rates of MPNP and HPNP suggests that the

metal-hydroxide of $[(cyclen)Co(H_2O)(OH)]^{2+}$ is more effective than the internal nucleophile of HPNP. In contrast, LCu_2 hydrolyzes HPNP 355 times faster than MPNP. The dinuclear complex is observed to be more efficient for the substrate which possesses its own internal nucleophile. This reversal of reactivity for the two complexes depending on the substrate is kinetic evidence for the involvement of a double lewis acid mechanism. The rate acceleration observed for the catalysis (6×10^6 over the background rate) is larger than the upper limit of 10^3 expected for the rate acceleration of one metal acting as a Lewis acid.

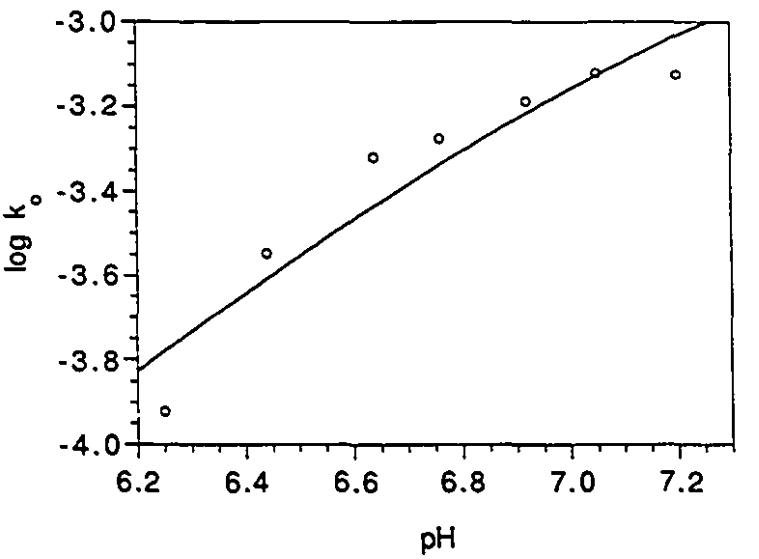

Figure 3.11 pH rate profile for the cleavage of HPNP at 0.5 mM LCu_2 at 25 °C fit to equation 3.12 with fixed values $k = 9.7 \times 10^5\ M^{-1}\ s^{-1}$, $K = 21\ M^{-1}$. K_a from the fit is $4.6 \times 10^{-8} \pm 1.4 \times 10^{-8}$ and R = 950. Data for figure 3.11 is tabulated in appendix 5.1

$$k_o = \frac{kK_a[LCu_2]_T[OH]}{\left(1+\frac{K_a}{[H^+]}\right)+K_a[LCu_2]_T} \quad (3.12)$$

Figure 3.12

As shown above the pH rate profile of LCu_2 the reactivity of the catalyst levels off as the first pKa of the metal bound waters is reached. This is consistent with the diaqua form of the catalyst as shown in figure 3.5 as the active catalytic species.

3 Discussion

A dinuclear copper(II) complex has been shown to be reactive for the cleavage of HPNP. The cleavage of HPNP coordinated to this complex occurs 6 x 10^6 times faster than the background cleavage reaction of free HPNP. In our lab,[83] the complex shown in figure 3.12 B has also been found to be active for catalyzing the cleavage of HPNP with reactivity comparable to LCu_2.

We have proposed a mechanism for the complex promoted reaction which involves coordination of the diester to LCu_2. Double Lewis acid activation and subsequent nucleophilic attack of the internal alkoxyl nucleophile results in the cleavage of HPNP and the formation of the *p*-nitrophenoxide and cyclic 1,2-propylene phosphate products.

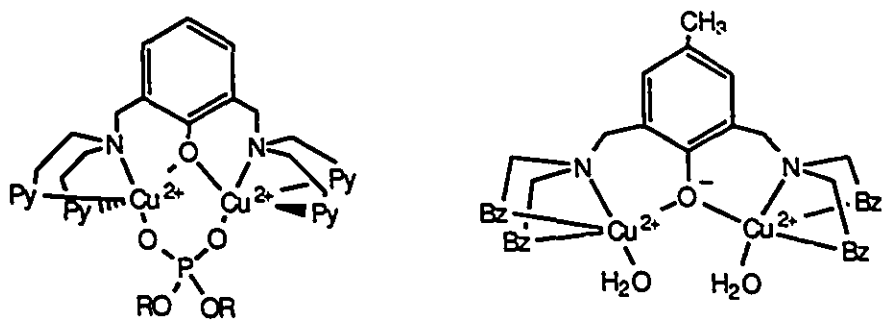

A B

Figure 3.12

An unreactive phosphate diester (DMP) has been shown to bridge the coppers of LCu_2 in the manner proposed in the cleavage reaction mechanism. This novel complex has been characterized by X-ray crystallography. At the time of this study a similar complex (figure 3.12 A) was reported by Karlin[97] *et al.* In this system a phosphate diester (BNPP) was also observed to bridge two copper atoms.

We have been interested in probing whether a catalyst designed to place the two metals at distinct oxygens of a phosphate diester will be more efficient than one in which the two metals interact at the same oxygen. In phosphate diester hydrolysis, the reaction

proceeds with a developing negative charge at the phosphoryl oxygen. A second metal positioned at this developing charge should be more efficient than placing both metals at the same oxygen.

The rate acceleration in this dinuclear complex has been calculated at 6×10^6. This is the rate acceleration that occurs from double Lewis acid activation at two distinct oxygens of HPNP. The ceiling value (10^3) for single Lewis acid contribution is calculated for the effect of Co(III) on a phosphate ester. The amount of activation available from the single Lewis acid contribution from Cu(II) should be less than this value since Cu(II) is a worse Lewis acid. The rate acceleration observed of 6×10^6 does suggest that the Lewis acid effect of the second metal is larger than the first. However, the ideal system to answer this question would be a substitionally inert Co(III) dinuclear system in which a phosphate diester is synthesized bridged to the complex. The breakdown of this complex would provide a direct measurement of the rate enhancement possible for a double Lewis acid catalyst of this design.

The O - P - O angle in the crystal structure of LCu_2DMP is 120.01 (24)°. This angle is significantly larger than the 'normal' size of the angle in a uncoordinated phosphate diester and it is close the ideal angle expected for the transition state (TBP) of the proposed mechanism (figure 3.13). We propose that the rate acceleration from this catalyst design may be tunable and will depend on the metal - metal distance of the dinuclear catalyst.

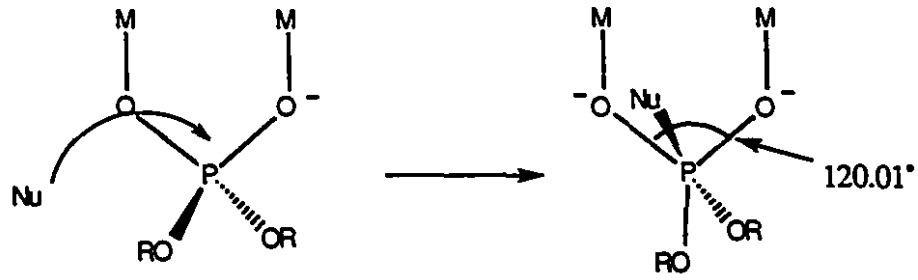

Figure 3.13

In chapter two, two mononuclear complexes were shown to cleave HPNP with reactivities (k_O) comparable to that of the dinuclear complex LCu_2. One, Cu(N3) has been shown to proceed via a mechanism involving a dimerized complex. The products observed for the catalysis of the transesterification reaction of HPNP by Cu(N3OH) are the same as for Cu(N3) which suggests that an alkoxide or metal alkoxide from the complex is

not involved in the reaction. Cu(N3OH) may be proceeding via a similar binuclear mechanism.

Due to solubility limitations, the concentration dependence for Cu(N3) could only be followed up to 2 mM. Even at this concentration the observed concentration dependence is still second order in catalyst. Therefore, the saturation concentration of active dimer is not reached at these concentrations (A linear dependence on catalyst should be observed when the saturation concentration of active dimer is reached).

In the cleavage of RNA or RNA analogues the rate acceleration available from a double Lewis acid mechanism occurs in excess of the 10^5 enhancement (or greater for RNA and other analogues) available from the contribution of the internal nucleophile. This type of catalyst design is best suited, therefore, for the cleavage of phosphate diesters with internal nucleophiles such as RNA and its analogues. Phosphate diesters without internal nucleophiles should proceed only slowly (approximately 6×10^6) over the background rate. For the hydrolysis of these phosphate diesters the combination of an efficient nucleophile with the rate acceleration available from a double Lewis acid mechanism is required to effect rapid hydrolysis. In chapter 4, a dinuclear cobalt(III) complex which is able to deliver both double Lewis acid activation and an efficient nucleophile for the hydrolysis of a phosphate diester will be investigated.

4 Experimental

Chemicals

N,N,N',N'-tetrakis(2-benzimidazolyl)-2-hydroxy-1,3-di-aminopropane (L) were synthesized according to literature procedure.[95]

dichloro-[(N,N,N',N'-tetrakis(2-benzimidazolyl)-2-hydroxy-1,3-di-aminopropane)dicopper(II)] chloride (LCu_2)

To a solution of (0.056 g, 0.328 mmol) $CuCl_2 \cdot 2H_2O$ in ethanol was added dropwise with magnetic stirring one half an equivalent of the septadendate binucleating ligand (0.1 g, 0.165 mmol) dissolved in the minimum amount of ethanol. The resulting green precipitate (0.114 g, 82 %) was collected and washed with cold ethanol and ether.

diperchloro-[(N,N,N',N'-tetrakis(2-benzimidazolyl)-2-hydroxy-1,3-di-aminopropane)dicopper(II)] perchlorate ($LCu_2(ClO_4)_2$)

To a solution of (0.12 g, 0.33 mmol) $Cu(ClO_4)_2.6H_2O \cdot 2H_2O$ in iso-propanol was added dropwise with magnetic stirring one half an equivalent of the septadendate binucleating ligand (0.10 g, 0.165 mmol) dissolved in the minimum amount of iso-propanol. The resulting blue precipitate (0.146 g, 73 %) was collected and washed with cold ethanol and ether.

μ-dimethylphosphato-[(N,N,N',N'-tetrakis(2-benzimidazolyl)-2-hydroxy-1,3-di-aminopropane)dicopper(II)] diperchlorate·H_2O (LCu_2DMP)

To (0.1 g, $8x10^{-5}$ mol) of $[(L)Cu(II)_2(ClO_4)_2]$ dissolved in 1 mL of ethanol was added (0.011 g, $8x10^{-5}$ mol) of sodium dimethyl phosphate dissolved in 2 mL of ethanol. A precipitate begins to form immediately. The solution was left stirring for 1 h at room temperature before the light green precipitate (0.05 g, 60 %) was filtered, washed with cold ether and collected. Crystals suitable for X-ray diffraction were grown at an acetone-hexane interface. The green powder was dissolved in acetone and the resulting solution placed inside an NMR tube. A layer of hexane was carefully placed on the acetone layer. The NMR tube was capped and after 3 days green-blue diamond crystals were collected. Crystal data is tabulated in abbreviated form in the results section. Supporting crystallographic data is found in the appended material.

5 Appendix

5.1 Tables of Data

Table 3.1 Data for figure 3.9

Concentration (mM)	1/rate
0	5.90×10^4
10	6.95×10^4
20	9.10×10^4
30	9.80×10^4
40	1.10×10^5

Table 3.2 Data for figure 3.11.

pH	k_o	log k_o
6.25	1.2×10^{-4}	-3.90
6.44	2.8×10^{-4}	-3.55
6.64	4.8×10^{-4}	-3.30
6.76	5.3×10^{-4}	-3.30
6.92	6.5×10^{-4}	-3.20
7.05	7.6×10^{-4}	-3.10
7.20	7.5×10^{-4}	-3.10

5.2 Derivation of Equations

Derivation of equation 3.7

The rate of formation of product is given by:

$$\frac{dP}{dT} = k_o[S]_T \qquad (1.1)$$

The equilibrium for binding is defined by:

$$K = \frac{[LCu_2S]}{[LCu_2][S]} \qquad (1.2)$$

The total substrate concentration is:

$$[S]_T = [S] + [LCu_2S] \qquad (1.3)$$

The rate of product formation is also given by:

$$\frac{dP}{dt} = k[LCu_2S][OH] \qquad (1.4)$$

Substituting equation 1.2 into 1.4 we obtain the following equation:

$$\frac{dP}{dt} = kK[LCu_2][S][OH] \qquad (1.5)$$

substitution of equation 1.3 into 1.5 yields::

$$\frac{dP}{dt} = \frac{kK[LCu_2][S]_T[OH]}{1 + K[LCu_2]} \qquad (1.6)$$

From equation 1.1 and 1.6 an expression for k_o can be obtained:

$$k_o = \frac{kK[LCu_2][OH]}{1 + K[LCu_2]} \qquad (1.7)$$

Derivation of equation 3.9

The rate of product formation is given by:

$$\frac{dP}{dt} = k[LCu_2][S] \qquad (2.1)$$

The total complex concentration is given by 2.2 assuming negligible concentration of bound substrate:

$$[LCu_2]_T = [LCu_2I] + [LCu_2] \qquad (2.2)$$

The equilibrium for inhibitor binding is given by :

$$K_i = \frac{[LCu_2I]}{[LCu_2][I]} \qquad (2.3)$$

Substituting equation 2.3 into 2.2 we obtain the following equation:

$$[LCu_2]_T = K_i[LCu_2][I] + [LCu_2] \qquad (2.4)$$

Upon rearrangement we obtain an expression for LCu2:

$$[LCu_2] = \frac{[LCu_2]_T}{(1 + K_i[I])} \qquad (2.5)$$

The rate can therefore can be expressed by the following equation:

$$\frac{dP}{dt} = \frac{k[LCu_2]_T[S]}{1 + K_i[I]} \qquad (2.6)$$

An expression for 1/rate can be obtained by taking the reciprocal to give equation 3.9

Derivation of equation 3.12

$$LCu_2 \underset{}{\overset{K_a}{\rightleftharpoons}} LCu_2(OH)$$

The acid dissociation constants are defined as:

$$K_a = \frac{[LCu_2(OH)][H^+]}{[HLCu_2]} \qquad (3.1)$$

The total copper complex concentration is:

$$[LCu_2]_T = [LCu_2] + [LCu_2(OH)] \qquad (3.3)$$

The observed rate constant is defined by:

$$k_o = \frac{kK_a[LCu_2]}{1 + K_a[LCu_2]}[OH] \qquad (3.4)$$

An expression for LCu_2 can be obtained by substituting equation 3.1 and 3.2 into equation 3.3:

$$[LCu_2] = \frac{[LCu_2]_T}{1 + \frac{K_a}{[H^+]}} \qquad (3.5)$$

Substituting equation 3.5 into equation 3.4 and rearranging:

$$k_o = \frac{kK_a[LCu_2]_T[OH]}{\left(1 + \frac{K_a}{[H^+]}\right) + K_a[LCu_2]_T} \qquad (3.6)$$

Chapter 4: Reactivity of a Phosphate Diester Bridged to Cobalt(III)

1 Introduction

It has long been known that cobalt(III) complexes of tetraamine ligands and facial triammine ligands dimerize into di and tri-hydroxy bridged dimers, respectively, under basic pH conditions.[98] In the design of hydrolytic metal catalysts this usually represents an unfavorable side equilibrium and the formation of an inactive dimer. Complexes like Co(bamp)(H_2O)3, where the nitrogens of the ligand force the coordination to be meridinal, can exist in the triaqua (and different protonation) state regardless of pH and can be titrated giving three sequential pKa's. Co(tacn)(H_2O)3 which has a facial coordination of the ligand to cobalt (figure 4.1), can not be titrated due to the condensation to polynuclear species.

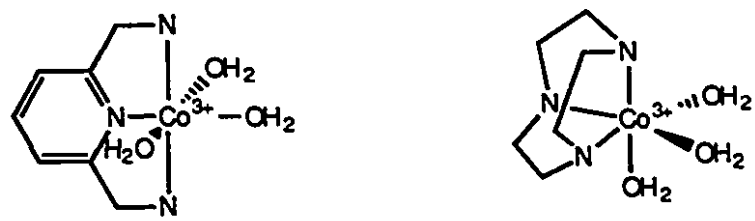

Co(bamp)(H_2O)3 Co(tacn)(H_2O)3

Figure 4.1 Meridinal coordination in Co(bamp)(OH_2)3 and facial coordination in Co(tacn)(OH_2)3

In the case of tri-hydroxy bridged cobalt (III) dimers $(N_3)_2Co_2(OH)_3$, the acid catalyzed first hydroxy bridge cleavage has been well studied.[98-100] The tri-hydroxy bridged dimers of tacn[101], tris(ammine)[102], 1,3,5-triazacyclohexane[98](tach) and diethylenetriamine[103] have been isolated. Figure 4.2 shows the mechanism of hydroxy-bridge cleavage. The first of the three hydroxy bridges opens easily due to the octahedral geometric requirements of the cobalt which greatly strains one of the three bridges. This is followed by isomerization of the resulting *cis*-diaqua dimer complex (*cis*-$(N_3)_2Co_2(OH)_2(OH_2)_2$) to the more stable trans isomer (*trans*-$(N_3)_2Co_2(OH)_2(OH_2)_2$).

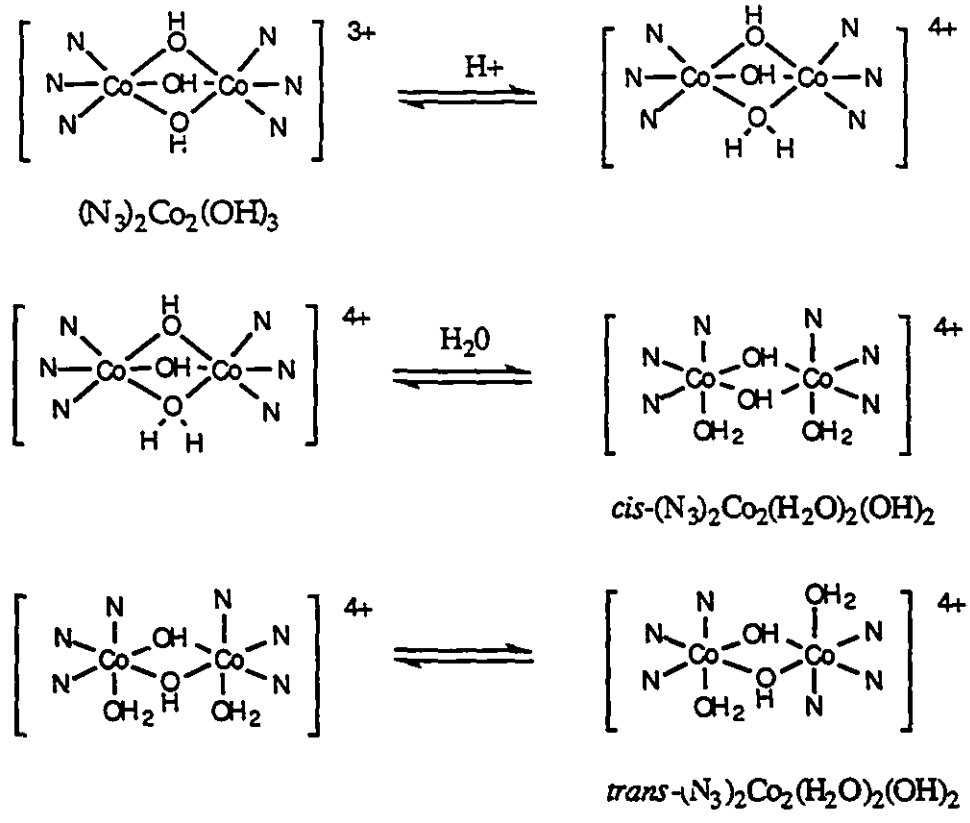

Figure 4.2 Mechanism of hydroxy-bridge cleavage in tri-hydroxy bridged cobalt(III) dimers

For $tacn_2Co_2(OH)_3$ a mechanism involving a fast protonation step and a rate determining cis-trans isomerization step is known to occur. The *trans*-$tacn_2Co_2(H_2O)_2(OH)_2$ complex can be isolated and is stable in acidic solution. A crystal structure of the thermodynamically stable trans isomer has been reported.[98] Under neutral to basic conditions the *trans*-diaqua dimer reforms the tri-hydroxy bridged

dimer tacn2Co2(OH)3. In strong acid the second and third bridges of tacn2Co2(OH)3 are also broken to form the mononuclear complex tacnCo(OH2)3. In strong base the trihydroxy bridged dimer is cleaved to form two equivalents of tacnCo(OH)3.

Werner and others have shown that under conditions where the first hydroxy bridge is cleaved in the presence of acetate or formate, the *cis*-diaqua cobalt dimers (*cis*-(N3)2Co2(H2O)2(OH)2) are trapped.[104-106] Crystal structures of these bridging acetato and chloroacetato dinuclear cobalt species have not been reported.

Sargeson has shown that single Lewis acid activation for phosphate diester hydrolysis provides about 10^3 fold rate acceleration.[107] Joint Lewis acid and metal hydroxide can provide up to 10^{10} fold rate acceleration.[1,58] Intramolecular metal hydroxide is therefore responsible for up to 10^7 fold rate enhancement. What would two metals contribute to the rate acceleration of a phosphate diester? It is reasonable to assume that two metals bound to one oxygen would provide not more than 10^6 fold rate enhancement. Should we expect 10^6 or more rate enhancement when the two metals are coordinated to two different oxygens of the phosphate diester? We propose that for phosphate diesters, positioning metals at two different oxygens (either chelation of one metal or bridging between two metals as shown in figure 4.3) will result in more than just twice the rate acceleration for one metal. In phosphate diester hydrolysis the reaction proceeds to the transition state developing a negative charge at one of the phosphoryl oxygens. We expect that placing a metal at this developing charge would stabilize the transition state for this reaction. This extra stabilization is not present when one metal is interacting at only one oxygen since the negative charge in the transition state will occur away from the metal (figure 4.3).

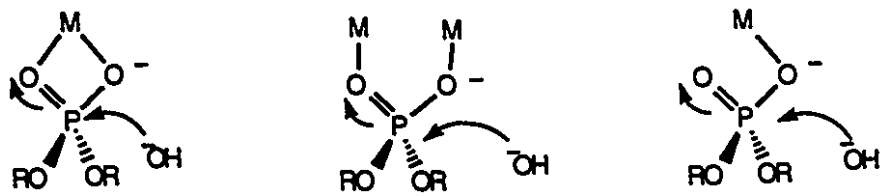

Figure 4.3 Interaction of one metal or two with two oxygens of a phosphate diester

In our lab we have investigated the feasibility of chelating phosphate esters[108,109,110] to cobalt(III) complexes. Although a chelated phosphate monoester has now been isolated, binding studies indicate that the likelihood of isolating a chelated phosphate diester is small. A dinuclear system placing the phosphate diester in a bridging fashion could serve the same purpose as a chelated phosphate diester.

We wished to investigate the possibility of inorganic phosphate and phosphate esters bridging the two cobalt atoms of *cis*-$(N3)_2Co_2(H_2O)_2(OH)_2$ in the same way that acetates and chloroacetates bind. We chose the well studied triazacyclononane system since the macrocyclic system would provide the maximum stability of all the characterized species.

If a bridging phosphate diester could be isolated this would provide an ideal system to assess the role of two metals bound at distinct oxygens of a phosphate diester in its hydrolysis reaction.

2 Results

1,4,9-triazacyclononane was synthesized by literature methods.[111-113] The tri-hydroxybridged triazacyclonane cobalt(III) dimer was synthesized with slight modification of literature methods. The reaction scheme is shown below in figure 4.4.[98,101]

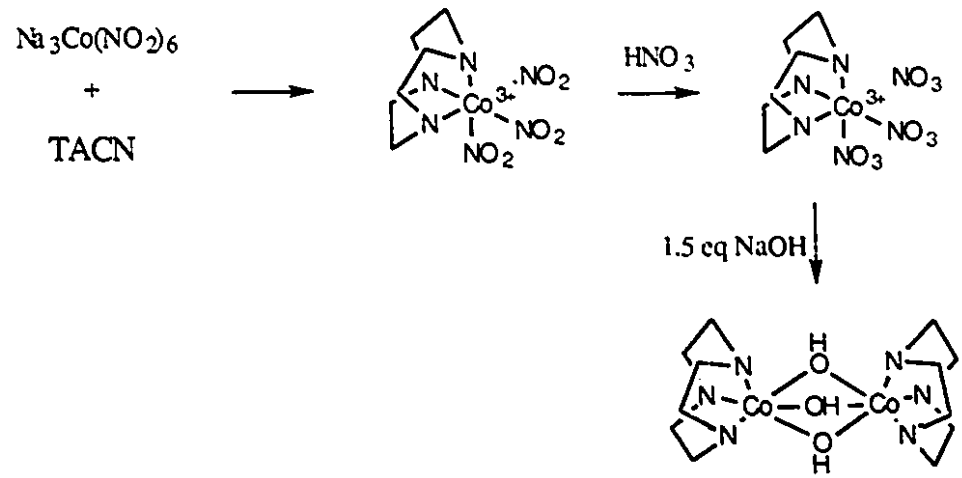

Figure 4.4 Reaction scheme for the synthesis of tacn2Co2(OH)3

As described in the introduction, one of the three hydroxy bridges in the dimer is strained due to the octahedral geometry's about the cobalt atoms. Under acidic conditions this bridge is known to open. Under acidic conditions therefore, in the presence of bridging ligands, the *cis*-diaqua form of the dimer may be trapped. Acetate is known to bridge in this way, and we proposed that inorganic phosphate and even phosphate diesters may bind in this fashion (figure 4.5).

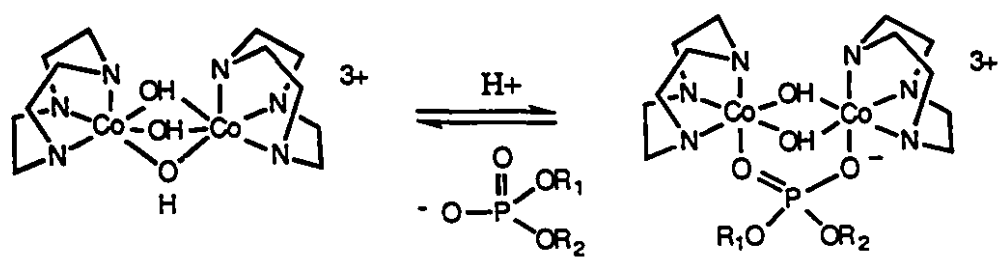

Figure 4.5 Trapping of *cis*-diaqua cobalt dimer under acidic conditions

Figure 4.6 A-C shows the binding of dimethyl phosphate (A), methyl phosphate (B) and inorganic phosphate (C) to *cis*-tacn$_2$Co$_2$(H$_2$O)$_2$(OH)$_2$ as observed by ^{31}P NMR. The unbound species is observed near zero ppm with respect to trimethyl phosphate. Phosphate which is singly coordinated to the cobalt complex should be observed near 7 ppm. This had been observed for the mono dentate binding of dimethyl phosphate to Co (trpn).[1] The only peaks observed in the binding experiments appear 14 ppm downfield relative to the free species. We propose this peak to be the complex formed when phosphate bridges trapping the *cis*-diaqua form of the dimer as shown in figure 4.5 Interestingly, under these conditions no monodentate binding to cobalt is observed for the phosphate esters. The spectra in figure 4.6 corresponds to 40, 47 , and 52 % of bridging phosphate complex for DMP, MMP and inorganic phosphate respectively. Binding of acetate (figure 4.7) under the same conditions shows one peak for free acetate (^{13}C labeled at carbonyl carbon) and a peak 12 ppm downfield for the bridging acetate species.

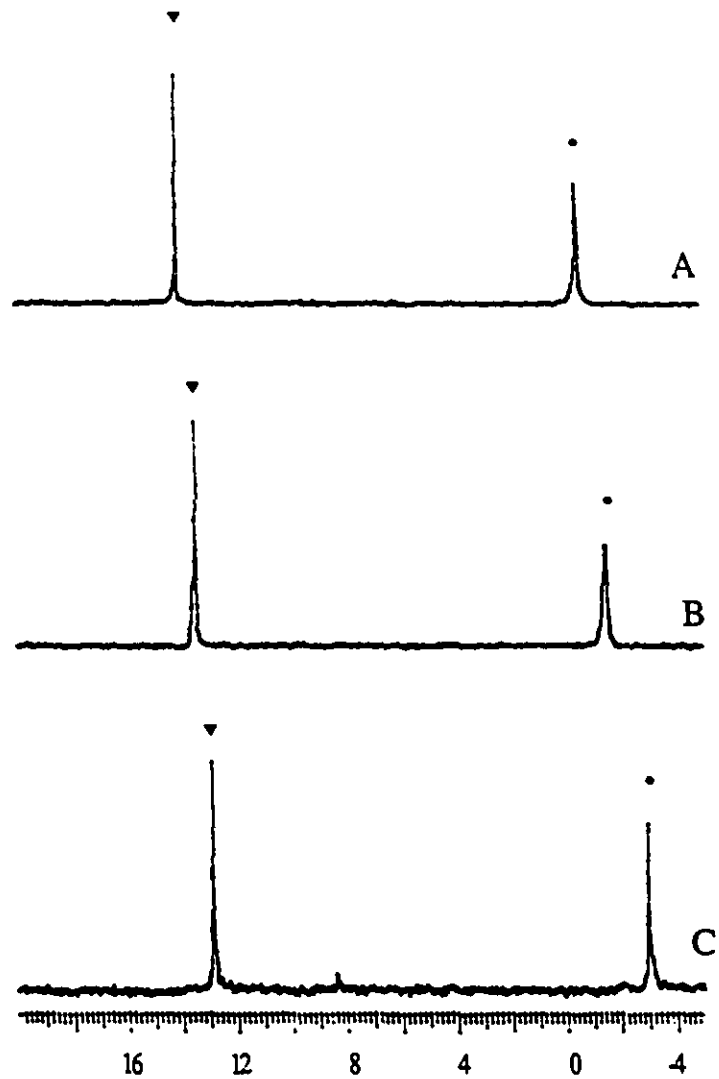

Figure 4. 6 A - C: ^{31}P NMR spectra of 50 mM $tacn_2Co_2OH_3$ in 500 mM $HClO_4$ and A: 50 mM dimethyl phosphate B: 50 mM of methyl phosphate. C: 50 mM of inorganic phosphate after 40 min at room temperature. Only free (•) and bridging(▼) phosphate is observed. Referenced to an external 10% TMP solution in D_2O.

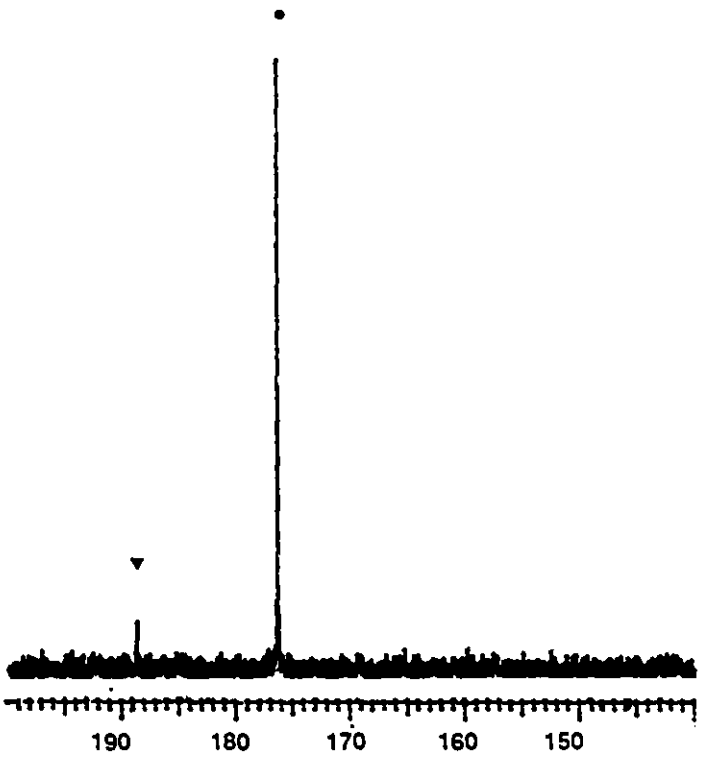

Figure 4.7 ^{13}C NMR spectra of 50 mM $tacn_2Co_2OH_3$ and 50 mM $CH_3C^*(O)ONa$ in 500 mM $HClO_4$ after 40 min at room temperature. Only free(•) and bridging (▼) acetate is observed.

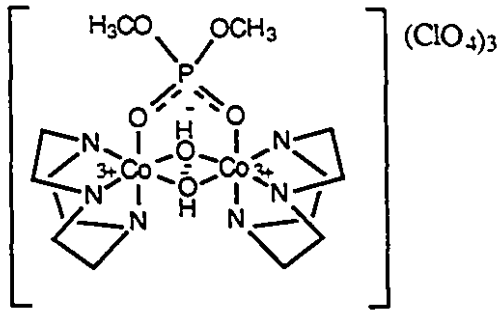

Figure 4.8 Structure of tacn2Co2(OH)2DMP

To confirm the identity of the peaks near 14 ppm as the bridging phosphate species, we have synthesized and characterized the novel compound tacn2Co2(OH)2DMP (figure 4.8). Supporting elemental analysis data is found in the experimental section. The ^{1}H, ^{13}C, and ^{31}P spectra of tacn2Co2(OH)2DMP are shown in figure 4.9 and are consistent with the proposed structure. X-ray quality crystals were obtained after recrystalization from water. Figure 4.10 shows the ORTEP diagram of tacn2Co2(OH)2DMP. Tables of crystal data as well as selected bond distances and angles are given below and supporting crystallographic data is appended. Tacn2Co2(OH)2DMP represents the first crystallographic evidence of the proposed bridging species in these dinuclear cobalt systems, and the trapping of the proposed *cis*-diaqua dimer species in the bridge cleavage reactions of N3Co2(OH)3. It is also the first example of a phosphate diester bridging two substitutionally inert metals.

The complex crystallizes as the monohydrate with two of the three perchlorate counterions disordered. The O-CH3 groups on the phosphate are also disordered with occupancies refined to 0.58 and 0.42. The distance found between the two cobalt atoms is 2.903 (2) Å and the O1-P-O2 angle of the bridged phosphate is 117.4 (4)° instead of the theoretical 109.5 ° expected about phosphorous. The geometry about the cobalt(III) atoms are essentially octahedral. The angle defined by N1 - Co - O2 is less than 180 °C and is forced to 172.6 (3)° by the bridging phosphate. The difference between the structure of LCu2DMP and that of tacn2Co(OH)2DMP will be elaborated in the following discussion section.

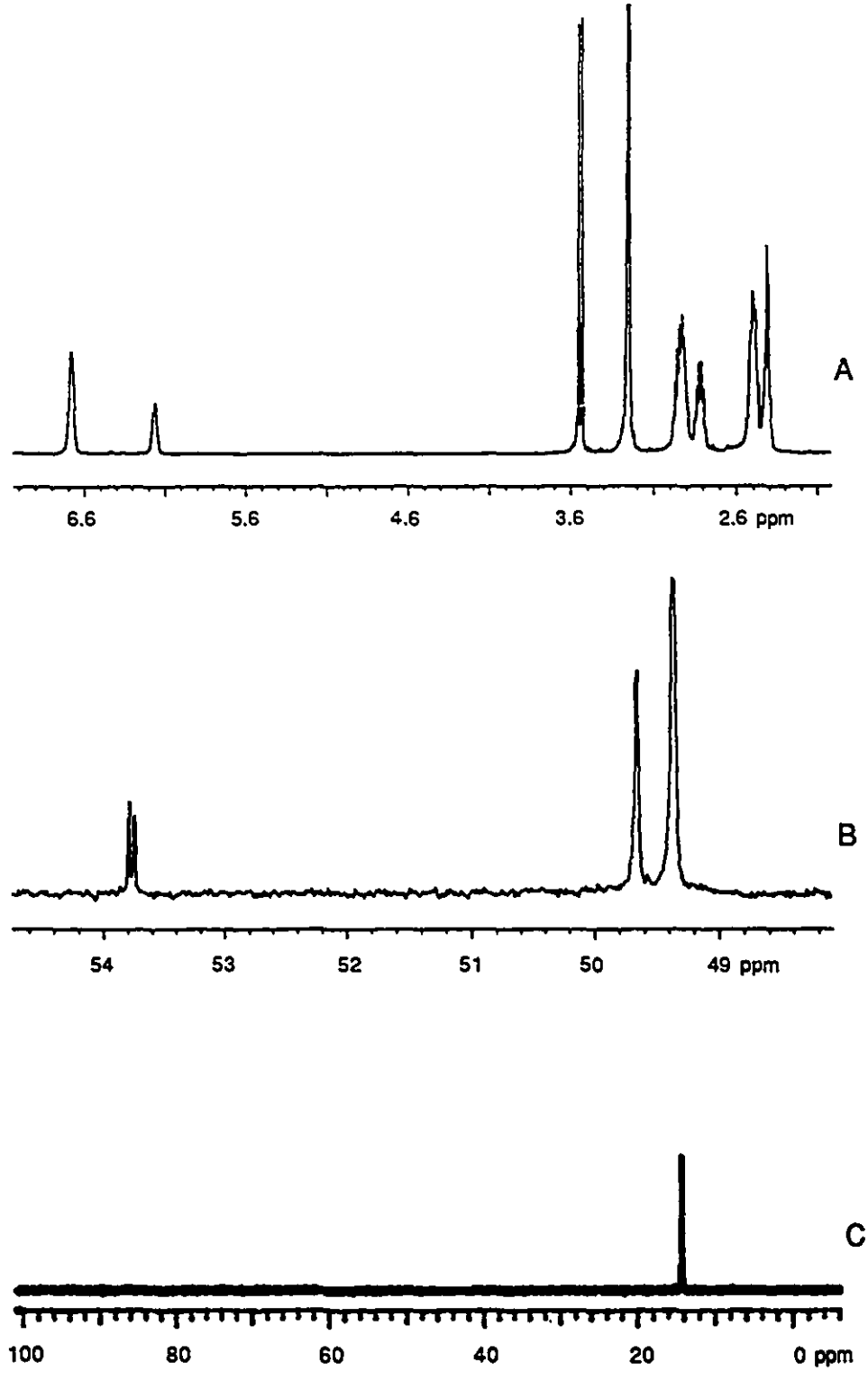

Figure 4.9 ^{1}H at 500 MHz, ^{13}C NMR at 125.7 MHz in DMSO. ^{31}P NMR at 121.4 MHz of $tacn_2Co_2(OH)_2DMP$

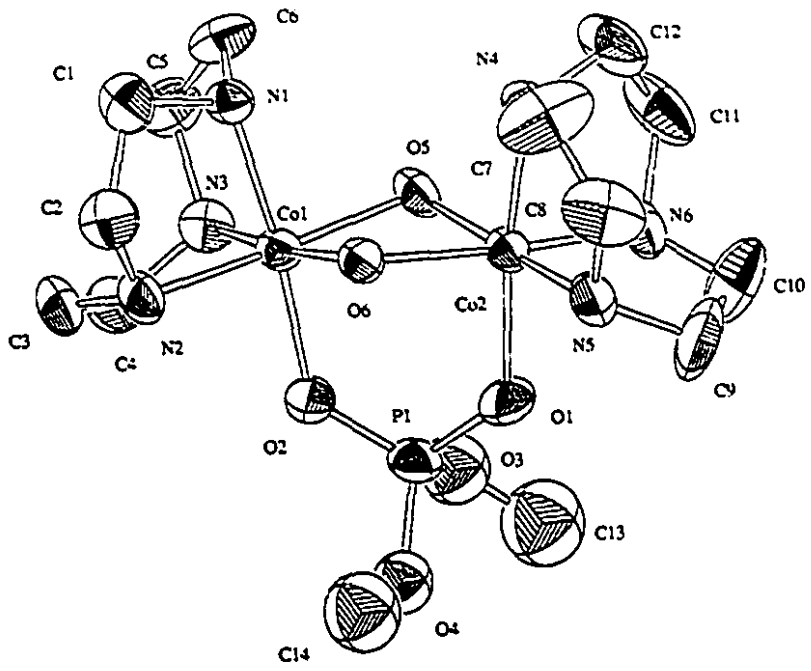

Figure 4. 10 ORTEP view of $tacn_2Co_2(OH)_2DMP$

The bridging phosphate diester complexes were obtained by combining the phosphate diester (25 mM) and the trihydroxy bridged cobalt dimer (25 mM) in 1M perchloric acid solution. The bridging complexes could also be obtained by first isolating the *trans*-diaqua cobalt dimer and then combining in an approximately 50 mM solution with an equimolar amount of phosphate diester.

Table 4.1 Crystallographic Data for μ-(dimethylphosphato)-di-μ-hydroxy-bis[(1,4,7-triazacylononane)cobalt(III)] triperchlorate·H_2O

molecular formula	$C_{14}H_{40}N_6O_{19}PCl_3Co_2$	ρcalc g/cm^3	1.742
molecular weight, g mol^{-1}	851.70	μ (Mo Kα), cm^{-1}	13.98
crystal dimensions, mm	0.50 x 0.37 x 0.20	*F*(000)	1752
crystal system	monoclinic	data collected	11987
space group	$P2_1/c$ (#14)	unique data	6043
a (Å)	13.084 (3)	data with $I > 2.5\sigma(I)$	2547
b (Å)	11.222 (3)	*R*	0.057
c (Å)	22.784 (5)	R_w	0.068
β (deg)	103.87(2)	R_{int}	0.106
V	3248 (1)	goodness of fit	1.77
Z	4		

Table 4. 2 Selected Bond Distances (Å) and Angles (°) and estimated standard deviations in the last significant figure in parenthesis for μ-(dimethylphosphato)-di-μ-hydroxy-bis[(1,4,7-triazacylononane)cobalt(III)] triperchlorate·H_2O

Bond Distances

Co (1) - Co (2)	2.903 (2)	Co (1) - O (5)	1.914 (6)
Co (1) - O (2)	1.935 (6)	Co (1) - O (6)	1.927 (6)
Co (1) - N (1)	1.918 (7)	Co (1) - N (2)	1.930 (8)
Co (1) - N (3)	1.924 (9)		

Bond Angles

O (2) - Co (1) - O (5)	95.0 (3)	O (2) - Co (1) - O (6)	94.1 (3)
O (2) - Co (1) - N (1)	172.6 (3)	O (2) - Co (1) - N (2)	88.6 (3)
O (2) - Co (1) - N (3)	89.2 (3)	O (2) - P (1) - O (1)	117.4 (4)

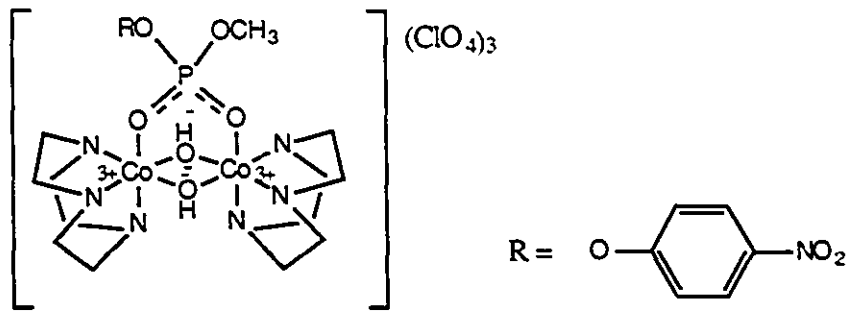

Figure 4.11 Structure of tacn2Co2(OH)2MPNP

Tacn2Co2(OH)2MPNP (figure 4.11) was synthesized to determine the effect of two cobalt(III) atoms on the hydrolysis reaction of phosphate diesters. Hydrolysis of tacn2Co2(OH)2MPNP was monitored by UV-vis methods. The log plot for over four half-lives of a typical kinetic run is shown below in figure 4.12.

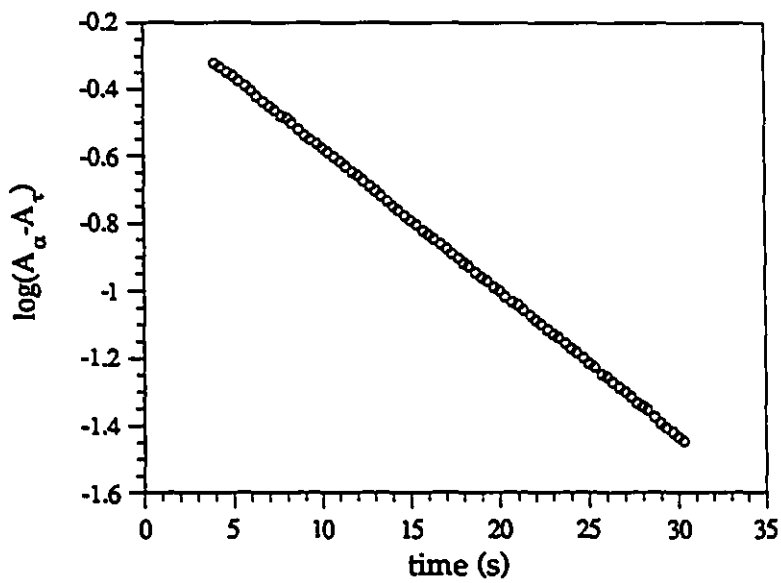

Figure 4.12 Typical kinetics for the hydrolysis of tacn2Co2OH2MPNP over four half-lives at pH 8 and 25°C.

The half-life of methyl *p*-nitrophenol phosphate bound to the dinuclear complex is an amazing 6 seconds at pH 8 and 25 °C. The rate constants were obtained by fitting the first three half-lives of the reaction according to a first-order kinetics equation. The pH-

rate profile for the hydrolysis reactions is shown below (figure 4.13) fit to a linear equation with a slope of one (R= 0.996).

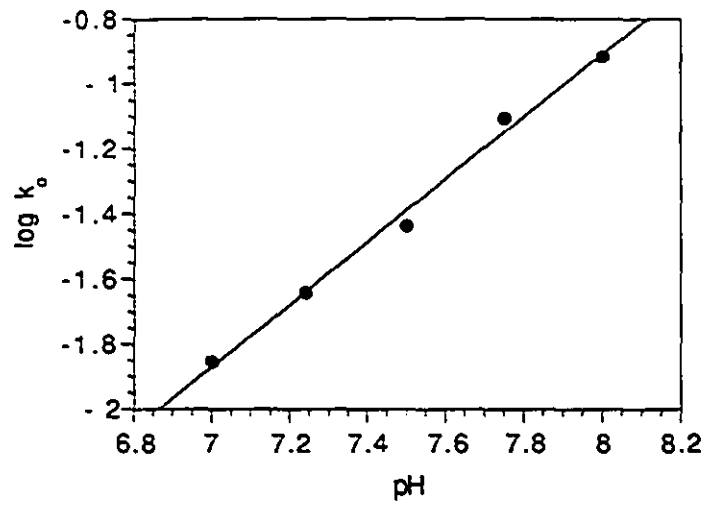

Figure 4.13 pH rate profile for the hydrolysis of 5 x 10^{-5}M tacn2Co2OH2MPNP at 25°C with 5 x 10^{-3} M HEPES buffer. Data are tabulated in appendix 5.1

The rate constant for the hydroxide catalyzed reaction of MPNP has been measured at 45°C. MPNP is hydrolyzed with a second order rate constant[91] of 1.9 x 10^{-6} $M^{-1}s^{-1}$. This corresponds to a half-life of 10^5 years at pH 7 and a first order rate constant of 1.9 x 10^{-13} s^{-1} at this pH. At 45°C and pH 7, the first order rate constant for the hydrolysis of the phosphate diester bond in tacn2Co2OH2MPNP is 1.1 x 10^{-1} s^{-1}. This is a remarkable rate acceleration of 6 x 10^{11} for the hydrolysis of the bound phosphate diester over that of the uncoordinated diester. This represents the greatest rate acceleration reported to date for the hydrolysis of phosphate diesters with cobalt(III) complexes.

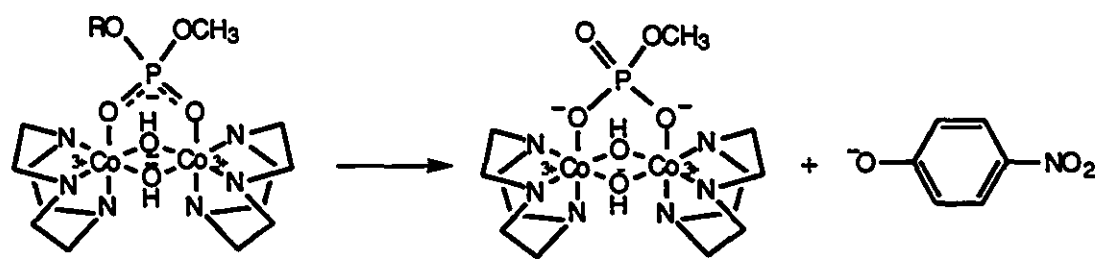

Figure 4.14 Hydrolysis reaction of tacn2Co2OH2MPNP and products of the reaction

The products of the reaction have been identified as the bridging methyl phosphate tacn2Co2OH2MMP and *p*-nitrophenolate figure 4.14. Figure 4.15 shows the ^{31}P NMR

of starting material A and product B. The product of the reaction has a characteristic ^{31}P peak at 14.97 ppm. No dissociated MPNP (-7 ppm) was detected under the hydrolysis conditions. C is the coupled spectrum of B consistent with the proposed methyl phosphate product. The same product is observed when the reaction is kept at a constant pH by buffer or when one equivalent of hydroxide is added to the starting compound tacn2Co2OH2MPNP. The ^{1}H NMR of the compound obtained by adding one equivalent of hydroxide is also consistent with the bridging methyl phosphate species proposed. Tacn2Co2OH2MMP was characterized in solution by ^{1}H, ^{13}C, and ^{31}P NMR.

The product obtained by mixing a genuine sample of methyl phosphate and the trihydroxy bridged cobalt dimer under acidic conditions has the same characteristic ^{31}P NMR signal when placed in a pD 8.4 buffer solution to the product formed for the reaction of tacn2Co2OH2MPNP.

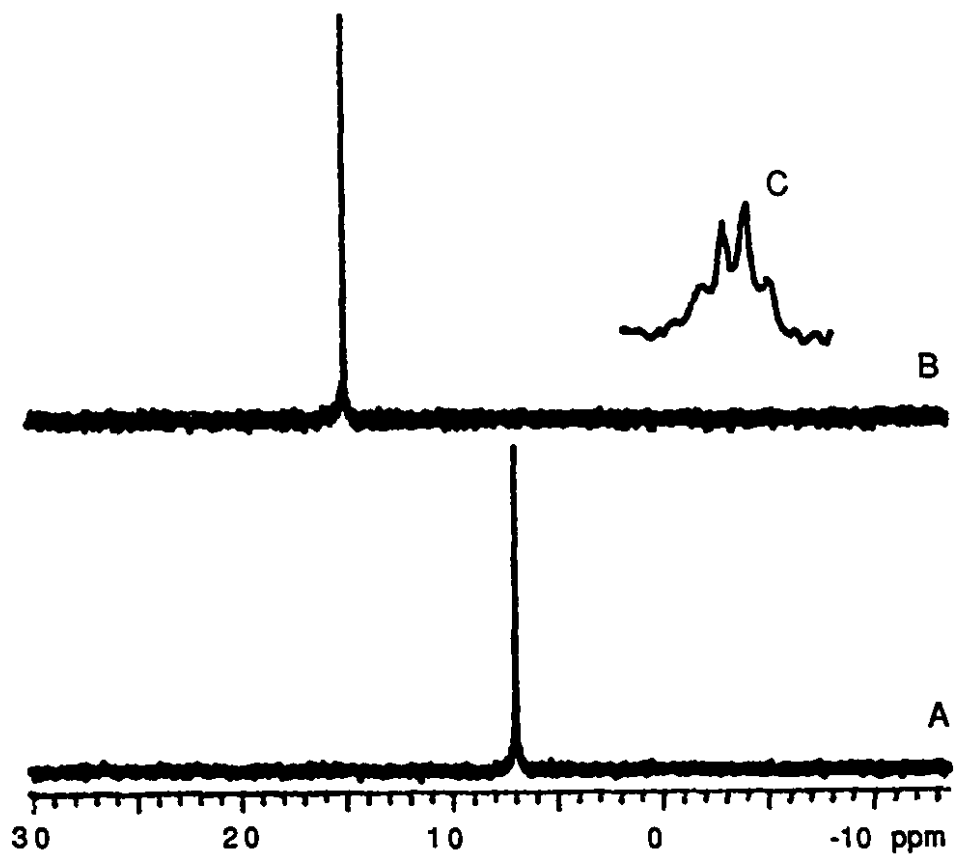

Figure 4.15 ^{31}P NMR of A: the starting material tacn2Co2OH2MPNP (5 mM) and B: the reaction product tacn2Co2OH2MMP (5 mM) and C: P - H coupled spectrum of B, A-C at pD 8.4, 50 mM HEPES buffer.

Initially we proposed that the reaction should proceed via double Lewis acid activation and external nucleophiiic hydroxide attack (figure 4.16). We expected that two cobalt(III) atoms would give significantly over $10^3 \times 10^3$. The observed rate acceleration of 6×10^{11} would indicate that the second metal acting as a Lewis acid would provide in excess of eight orders of magnitude rate acceleration.

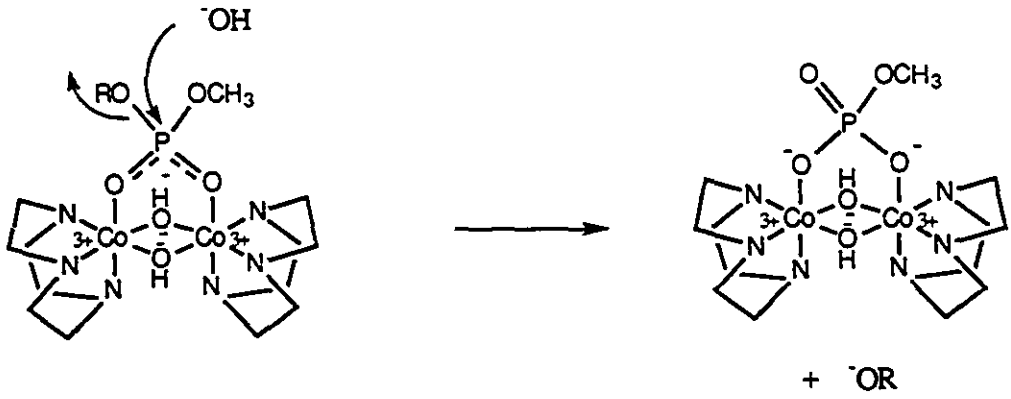

Figure 4.16 Scheme of the expected mechanism for the hydrolysis reaction of tacn2Co2(OH)2MPNP

When the reaction was monitored under identical conditions but in the presence of strong nucleophiles such as hydrogen peroxide anion, hydroxylamine, or fluoride (which are known to be highly reactive for cleaving uncoordinated phosphate diesters) no increase in rate of reaction was observed. The lack of rate acceleration by strong external nucleophiles suggests that an efficient internal nucleophiie is likely to be involved in the mechanism. We therefore proposed that the hydroxy bridges might be involved in the catalysis.

For tacn2Co2(OH)2MPNP the hydrolysis reaction is much faster than the dissociation of MPNP from the complex. DMP is expected to be about 5×10^4 times more stable than MPNP towards based catalyzed hydrolysis. When tacn2Co2(OH)2DMP is brought up to neutral or basic pH no hydrolysis is observed. Instead, only dissociation of dimethyl phosphate is seen.

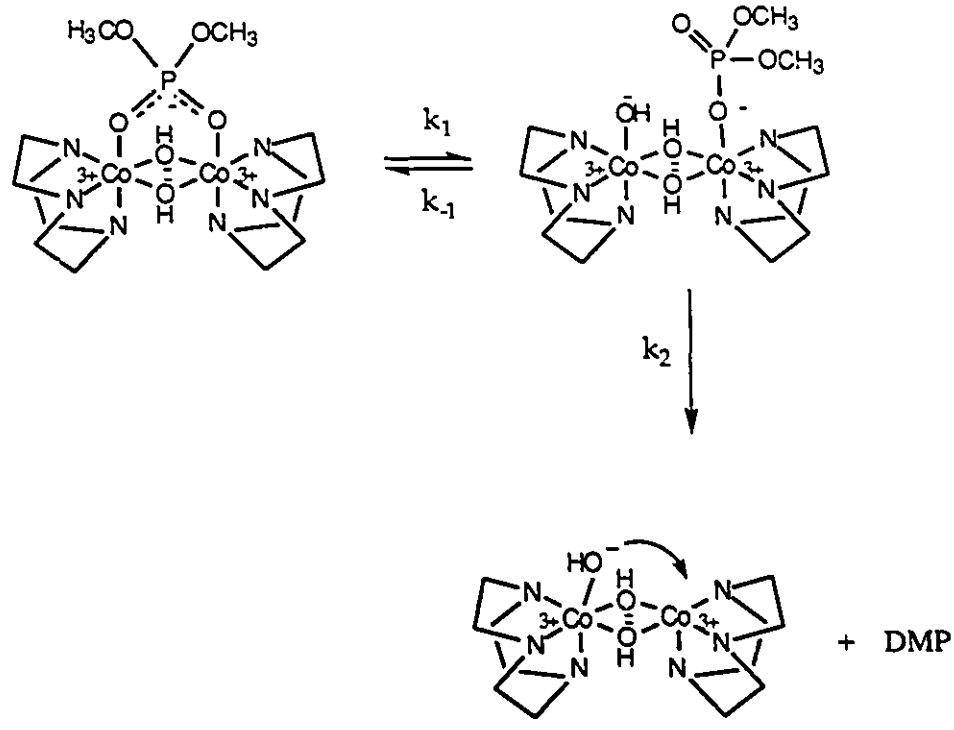

Figure 4.17 Mechanism of dissociation of DMP from tacn2Co2(OH)2DMP under basic conditions

It was possible to determine the rate of dissociation of dimethyl phosphate by following the rate of tacn2Co2(OH)3 formation (λ=512) at pH's ranging from 8-11. The rate constant for the hydroxide catalyzed elimination of dimethylphosphate from tacn2Co2(OH)2DMP is 2.0×10^1 $M^{-1}s^{-1}$. In the dissociation reaction (figure 4.17), under basic conditions the rate determining step for the dissociation is k_1. This is true since for the intermediate shown, hydroxide is a poorer leaving group than dimethylphosphate and $k_2 > k_{-1}$. The pH rate profile for the dissociation is shown below fit to a line with a slope of one. The rate of dissociation of methyl *p*-nitrophenol phosphate could not be measured because of the hydrolysis reaction.

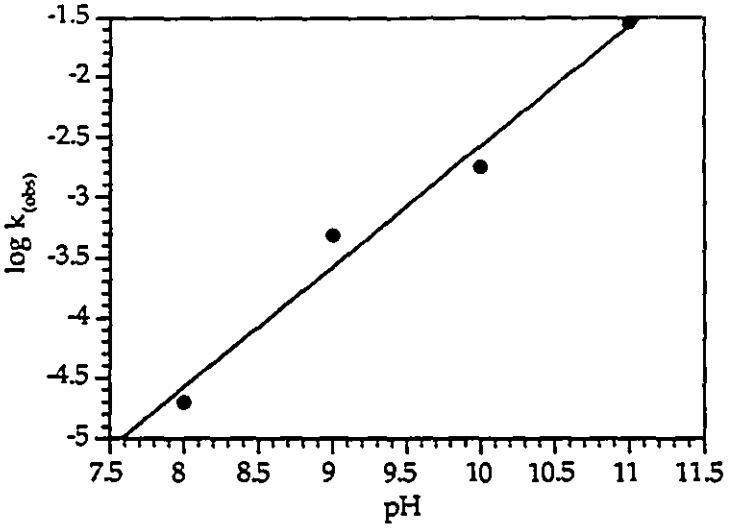

Figure 14.18 pH rate profile for the hydroxide catalyzed dissociation of DMP from tacn2Co2(OH)2DMP. [tacn2Co2(OH)2DMP] = 2.5 x 10^{-3} M [buffer] = 100 mM at 25 °C. Data is tabulated in appendix 5.1

For *trans*-tacn2Co2(H_2O)2(OH)2 it was possible to determine the equilibrium constant for binding of dimethyl phosphate. Only the overall binding to the trans-diaqua-di-hydroxyl cobalt tacn dimer can be measured due to the *cis*-trans isomerization equilibrium. The *cis-trans* isomerization equilibrium constant is not known but favours the trans isomer (K>>1). To determine the equilibrium constant, tacn2Co2(OH)2DMP was dissolved at an initial concentration of 5 mM at pH 2.5, kept at 25 °C and monitored over time until equilibrium was reached. Figure 4.19 shows the dissociation of DMP from tacn2Co2(OH)2DMP showing 0, 13 , and 35 %, for 0, 9, and 24 hrs respectively. Figure 4.20 shows a time plot of the dissociation of dimethyl phosphate. Here again under these conditions no monodentate phosphate diester is observed. Only the peaks due to bridging (14.3 ppm) and free (-0.3 ppm) DMP are observed throughout.

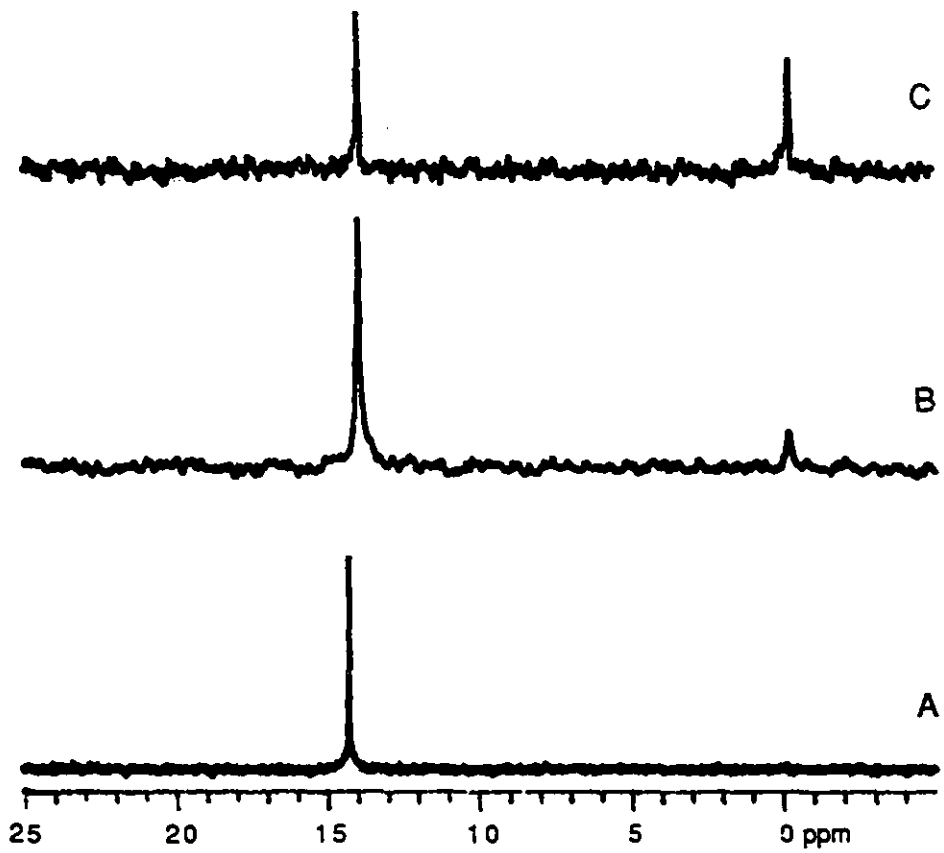

Figure 4.19 ^{31}P NMR of $tacn_2Co(OH)_2DMP$ at pH 2.5 and 25°C at A: 0 hours B: 9 hours and C: 24 hrs

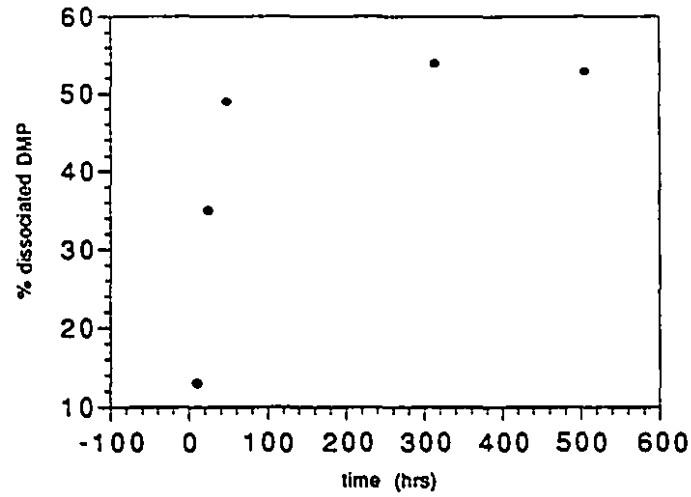

Figure 4.20 Time plot for the dissociation of dimethyl phosphate from ^{31}P NMR data shown in figure 4.19. Data is tabulated in appendix 5.1

The final spectrum in the dissociation experiment acquired after three weeks corresponds to 53.44 % dissociated DMP and therefore the equilibrium constant for binding of dimethyl phosphate to the trans diaqua cobalt dimer is calculated to be about 330 M^{-1}.

Two ^{18}O labelling experiments were performed in order to confirm or reject the involvement of the bridging hydroxide groups in the hydrolysis reaction. In the first experiment tacn2Co2(OH)2MPNP was synthesized with 50% ^{18}O incorporated into the bridging hydroxides. The hydrolysis reaction was allowed to proceed and the products were analyzed. In the second labelling experiment, normal unlabelled tacn2Co2(OH)2MPNP was allowed to react in 50% labelled solvent. The results of these experiments were analyzed by ^{31}P NMR and are shown in figure 4.21. It is known that the effect of ^{18}O adjacent to phosphorous of a phosphate is a 0.02 ppm upfield shift of the phosphorous NMR signal.[114] Since the experiments are done under 50% labelling conditions, two peaks are expected when the label is incorporated into the product. Only one peak is expected when no label is incorporated. The product analysis of this labelling study shows that incorporation into the methylphosphate of the product occurs when the ^{18}O label originates in the hydroxy bridge. Two clear and distinct peaks are observed with a difference in shift of 0.021 ppm when the products of the hydrolysis of tacn2Co2($^{16/18}$OH)2MPNP were analyzed (figure 4.21). When the label originates in the solvent (50% ^{18}O labelled $H_2{}^{18}O/D_2O$) only one peak was observed corresponding to the unlabelled bridging methylphosphate product.

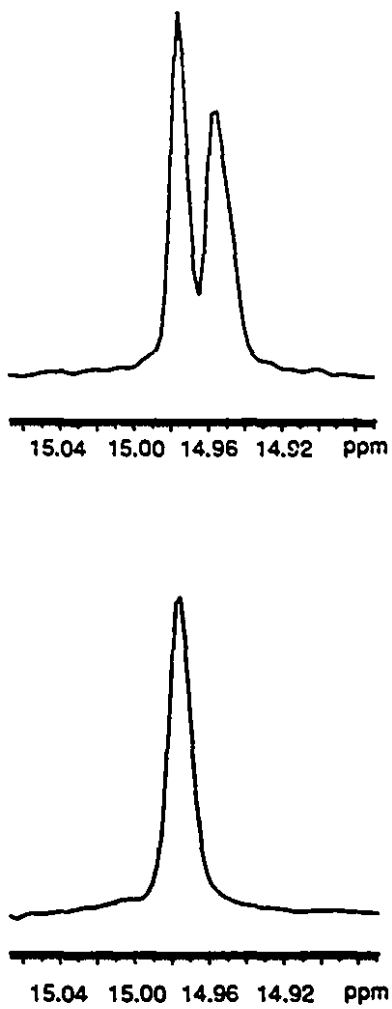

Figure 4.21 ^{31}P NMR (202.3 MHz) reaction products of Top: 10 mM tacn2Co2($^{16/18}$OH)2MPNP in 100 mM pD 8.53 HEPES buffer and Bottom: tacn2Co2(OH)2MPNP in 100 mM pD 8.53 HEPES buffer in $H_2{}^{18}O$/D2O

3 Discussion

Several mechanism are possible for the hydrolysis reaction of tacn2Co2(OH)2MPNP. Mechanism one (figure 4.16) involves attack of external hydroxide and Lewis acid activation by two metals. This mechanism would be first order in hydroxide and result in bridging methyl phosphate; however, under the same pH conditions but in the presence of nucleophiles which are known to be more reactive than hydroxide no further rate enhancement was observed. This suggests that hydrolysis is proceeding without involving external nucleophiles. The results of the labeling experiments which will be discussed later also argue against mechanism one.

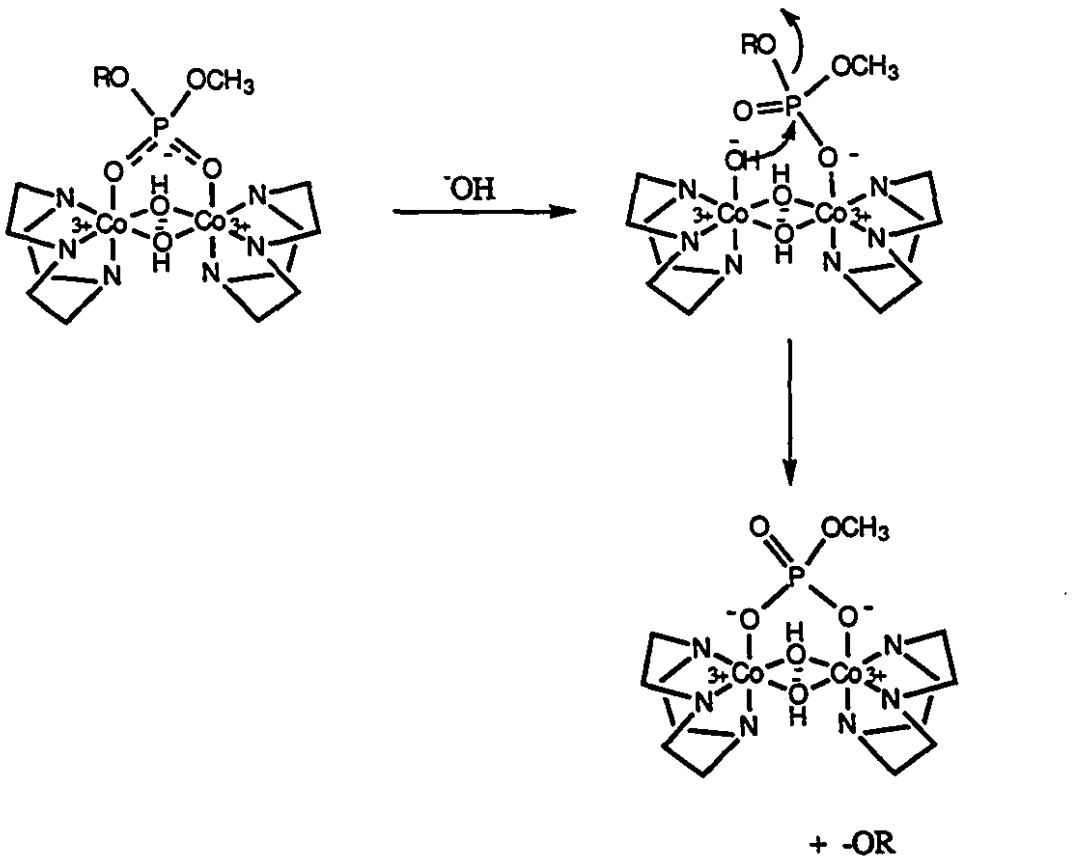

Figure 4.22 Mechanism two involving dissociation of the phosphate diester followed by intramolecular M-OH attack leading to the observed product.

A second reasonable mechanism is that in figure 4.22. This mechanism involves displacement by hydroxide with subsequent metal hydroxide attack on the resulting monodentate phosphate diester. This type of mechanism has already been observed by Sargeson [107] in the system shown in figure 4.23. In this case, methyl phosphate first dissociates via base hydrolysis and is followed by nucleophilic attack of a metal hydroxide on the remaining metal. An overall rate acceleration of about 10^8 over the uncoordinated phosphate monoester is observed. The mechanism observed in Sargeson's system can not be operating in tacn2Co2(OH)2MPNP. We have found that the rate of dissociation of dimethyl phosphate from tacn2Co2(OH)2DMP is 2.0 x 10 $M^{-1}s^{-1}$. This is about 10^4 slower than the observed rate of hydrolysis of the phosphate diester bond in tacn2Co2(OH)2MPNP. The dissociation rate of MPNP should not be significantly faster than that of DMP dissociation. The rate determining step in the dissociation mechanism is the first step of mechanism two. Since the measured rate of dissociation is about 10^4 times slower than the observed hydrolysis rate, mechanism two cannot be operating.

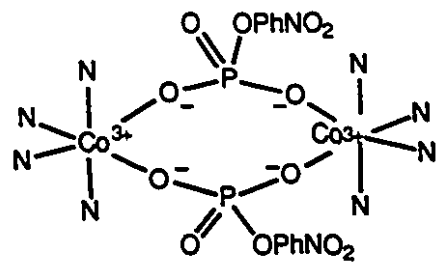

Figure 4.23 Hydrolysis of *p*-nitrophenol phosphate in Sargeson *et al.* proceeds by mechanism two and results in 10^8 fold rate acceleration compared to the hydrolysis of uncoordinated *p*-nitrophenolphosphate

A third reasonable mechanism is shown below in figure 4.24. Since efficient nucleophiles do not further accelerate the hydrolysis reaction, an efficient internal nucleophile must be operating. In this mechanism a deprotonated bridging hydroxide attacks the phosphorous of the phosphate diester. The pK_a of the hydroxy bridge in tacn2Co2(OH)3 has been measured [103] at 14. The pK_a in tacn2Co2(OH)2DMP or tacn2Co2(OH)2MPNP is not expected to vary significantly. The pH rate profile is consistent with the deprotonated hydroxide bridge being involved in the reaction. At this point two possibilities exist; solvent can attack phosphorous to displace the bridging oxide leaving group or one of the two Co - O bonds will break as shown in figure 4.25.

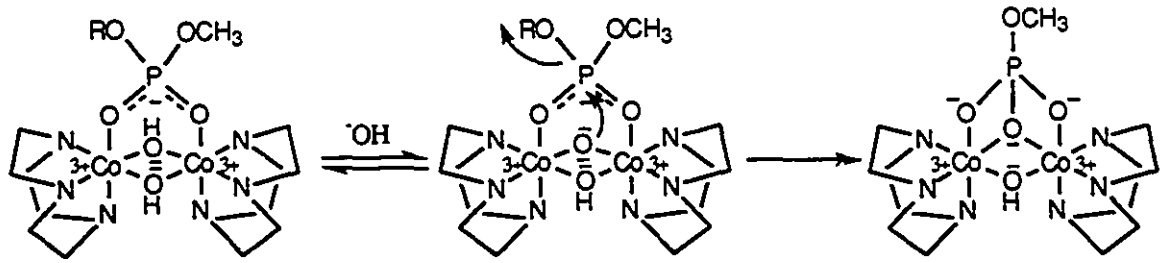

Figure 4.24 Mechanism three involving attack of a bridging oxo species and loss of *p*-nitrophenol

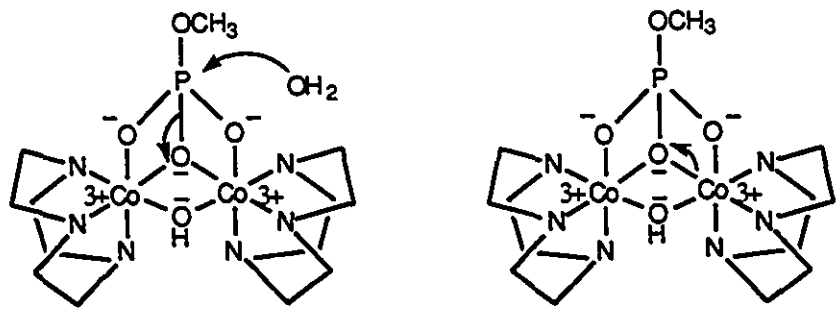

A B

Figure 4.25 Breakdown of proposed intermediate A: solvent attack at phosphorous or B: cleavage of Co - O bond shown.

The two labelling studies eliminate mechanism one and two. Mechanism one and two should result in an incorporation of the label into the phosphate of the product when the label is placed in the solvent. This is true since in mechanism one external hydroxide acts as the nucleophile in the reaction and in mechanism two the nucleophile is a metal hydroxide which is generated from the solvent after dissociation of the diester. ^{18}O was not incorporated into the phosphate when the label was placed in the solvent but was incorporated when it originated in the bridging hydroxide ligands. In mechanism three it is the bridging oxide ligand which is the nucleophile in the hydrolysis reaction and therefore the label is expected to be incorporated into the product if it proceeds by this mechanism. The ^{18}O experiments indicate that it is the bridging oxide which acts as the nucleophile to cleave the phosphate diester. Furthermore, we can distinguish between the diverging pathways which may occur in mechanism three. The label remains in the product, thus it cannot be the solvent water which displaces the bridging oxide by attacking the phosphorous, but instead the Co - O bonds of the doubly coordinated bridging oxide must cleave to generate the observed bridging methyl phosphate complex.

The phosphate diester bond in tacn2Co2(OH)2MPNP cleaves by a novel mechanism which involves double Lewis acid activation and nucleophilic oxide attack which provides a remarkable 6×10^{11} rate enhancement over the background hydrolysis reaction of MPNP.

Interestingly, bridging of a phosphate diester ($K=330\ M^{-1}$) in this dinuclear cobalt(III) system is more favourable than monodentate coordination of a phosphate diester to mononuclear cobalt(III) complexes which have binding constants of about $4\ M^{-1}$. The second metal appears to be providing a cooperative effect for the binding of the diester.

In this system it was not possible to determine the contribution of the rate enhancement which is available from a double Lewis acid activation of a phosphate diester bridging two cobalt atoms. However, in chapter 3, it was possible to calculate a factor of 6×10^6 for this effect in LCu2. If we extrapolate this value to the dinuclear cobalt system, we can assign a tentative value of about 10^5 for the importance of a bridging oxide nucleophile in promoting the cleavage reaction of phosphate diesters.

If we compare the structure of LCu2DMP and tacn2Co2(OH)2DMP we find that in tacn2Co2(OH)2DMP the metal-metal distance 2.903 (2)° is significantly shorter than in LCu2DMP 3.569 (2)°. The O - P - O is also significantly smaller 117. 4 (4)° vs 120.01 (24)°. From the geometric requirements of the double Lewis acid mechanism alone (discussion chapter 3), the dinuclear cobalt system should not be able to offer as effective a rate enhancement. However, in the dinuclear cobalt system, the net charge per metal is greater than in LCu2 (2 vs. 1.5). It may therefore be reasonable to estimate in this dinuclear cobalt catalyst, a rate enhancement contribution of 6×10^6 for the double Lewis acid effect. A rate acceleration of this magnitude is not enough to bring the half-life of DNA to a reasonable value at 25 °C and near neutral pH; however, as we have shown this type of mechanism can be combined with others to achieve more practical rate enhancements for DNA cleavage. In our dinuclear cobalt system, for example, a reactive internal nucleophile is also involved in the catalysis.

In conclusion, we have examined the potential of dinuclear catalysts which are designed to deliver double Lewis activation when the phosphate diester is bridged between the two metals. A rate enhancement of 6×10^6 was observed for this mechanism in a dinuclear copper complex. We have proposed a novel mechanism for the cleavage of a phosphate diester by a mononuclear copper complex which involves the formation of a dimer and a similar double Lewis acid mechanism. Lastly, we have observed and given evidence for the involvement of a nucleophilic bridging oxide in the hydrolysis of a phosphate diester.

4 Experimental

^{18}O labelling experiments were analyzed by ^{31}P NMR on a Varian Unity-500 FT spectrometer.
TACN[111,112], DMP[74] were synthesized according to literature procedures. MPNP was synthesized by literature procedure[115] and isolated as the sodium salt. MMP was purchased from Sigma.

Trinitro-[(1,4,7-triazacyclononane)cobalt(III)]

(0.25 g, 0.002 mol) of tacn was dissolved in 1-2 mL of water. This was added dropwise to a solution of (0.78 g, 0.002 mol) $Na_3Co(NO_2)_6$ in 2 mL of water. A yellow precipitate forms instantly. After stirring at room temperature for 3-4 hrs , the precipitate (0.51 g, 79%) was filtered, washed with copious amounts of water and collected. Analysis calculated for $C_6H_{15}N_6O_6Co$: Calc: C, 22.10 N, 25.77 H, 4.64 Found : C, 22.67 N, 25.78 H, 4.78

Trinitrato-[(1,4,7-triazacyclononane)cobalt(III)]

The trinitro complex (0.21 g, $6x10^{-4}$ mol) was dissolved in concentrated HNO_3 (approx. 2 mL) and allowed to stir at room temperature until the evolution of red-brown gas subsided. The red solution was evaporated to dryness; the resulting film is triturated with ethanol and washed with ether to yield a purple solid which was collected by filtration (0.21g, 88%). ^1H NMR (D_2O, 200 MHz): δ 2.65-2.85 (12H, m), 3.05-3.30(12H, m) ^{13}C NMR (D_20, 50.3 MHz) δ 52.44 52.31 51.99 Analysis calculated for $C_6H_{15}N_6O_9Co$: C, 19.26 H, 4.04 N, 22.46 Found: C, 19.41 H, 4.20 N, 22.07

Tri-μ-hydroxo-bis[(1,4,7-triazacyclononane)cobalt(III)] trinitrate $tacn_2Co_2(OH)_3$

(0.100g, $2.7x10^{-3}$ mol) of trinitrato-(1,4,7-triazacyclononane)cobalt(III) was dissolved in 1.5 equivalents (0.4 mL, $4x10^{-3}$ mol) of a 1M NaOH solution. The mixture was warmed to 35 $^{\circ}$C for 2 hrs and left stirring at room temperature for 12 hrs. Over time, the purple solution becomes ruby red in colour. The resulting solution was evaporated to dryness and the resulting red film triturated with ether (with some

sonication) to yield a light red powder. The procedure results in a product containing 16 % of $NaNO_3$ by weight which was not purified further. ^1H NMR (D_2O, 200 MHz): δ 2.60-2.80 (12H, m) 3.10-3.30 (12H. m) ^{13}C NMR (D_2O, 50.3 MHz): δ 50.85

diaquo-di-μ-hydroxo-bis[(1,4,7-triazacyclononane)cobalt(III)] tetraperchlorate
$tacn_2Co_2(OH)_2(H_2O)_2$

(0.05 g, 0.08 mmol) of tri-μ-hydroxo-bis[(1,4,7-triazacyclononane)-dicobalt(III)] trinitrate was dissolved in 0.63 mL of 1 M $HClO_4$. After a few minutes, a purple precipitate forms. The solution is allowed to stand for 3-4 h and then filtered to collect the (0.04g, 69 %) purple precipitate. ^1H NMR (1M $HClO_4$, D_2O, 200 MHz): δ 2.6-2.9 (br m, 6H), 3.1-3.4 (br m, 6H), 6.8 (br s) 6.9 (br s) ^{13}C NMR (1M $HClO_4$, 50.3 MHz): δ 51.77, 52.04

μ-dimethylphosphato-di-μ-hydroxy-bis[(1,4,7-triazacyclononane)cobalt(III)] triperchlorate· H_2O $tacn_2Co_2(OH)_2DMP$

To (15 mg, 0.10 mmol) of sodium dimethyl phosphate dissolved in 3-4 mL of 1M $HClO_4$ acid were added all at once in powder form (65 mg, 0.09 mmol) of tri-μ-hydroxo-bis[(1,4,7-triazacyclononane)-dicobalt(III)]trinitrate. The solution was stirred with occasional heating for 1-1.5 hours. The solution was left standing without further heating for 12 hours. To the resulting purple solution was added 1-2 mL of a 1 M $NaClO_4$ solution. After 30 min when no precipitate had formed the solution was rotovapped until a precipitate was observed . A further 1mL of solvent was removed. 14 mg (18.8%) of a purple precipitate was obtained. ^1H NMR (D_2O, 200 MHz): δ 2.7 (12H, br m), 3.25 (12H, br m), 3.72 (6H, d, J_{P-H} = 10.9 Hz, CH_3), 6.7 (br s, NH) ^{31}P NMR (D_2O, 121.4 MHz): δ 14.3 ^{13}C NMR (DMSO, 500 MHz): δ 49.37, 49.66, 53.74, 53.79
Analysis calculated for $C_{14}H_{40}N_6O_{19}PCo_2Cl_3$: C, 19.74 H, 4.73 N, 9.88 Found : C, 19.75 H, 4.73 N, 9.88

X-ray structure of μ-dimethylphosphato-di-μ-hydroxy-bis[(1,4,7-triazacyclononane) cobalt(III)] triperchlorate. Red block crystals were isolated by recrystalization from water. Graphite-monochromated Mo-Kα (Å) radiation was used. Abbreviated tables of crystal data can be found in the results section of chapter 4. Supporting crystal data is tabulated in the appended material.

μ-(methyl-*p*-nitro-phenylphosphato)-di-μ-hydroxy-bis[(1,4,7-triazacyclononane)cobalt(III)] triperchlorate $tacn_2Co_2(OH)_2MPNP$

To (26 mg, 0.1 mmol) of methyl *p*-nitrophenyl phosphate in 3-4 mL of 1M $HClO_4$ was added (65 mg,0.09 mmol) of tri-μ-hydroxo-bis[(1,4,7-triazacyclononane)-dicobalt(III)]trinitrate. The solution was stirred at room temperature for approximately one hour. 2 mL of 1M $NaClO_4$ was added. A purple precipitate forms immediately. After one hour the precipitate was collected by filtration and washed with ethanol. 30 mg (35.8 %) of product was obtained. ^1H NMR (D_2O, 200 MHz): δ 2.7 (12H, br m), 3.25 (12H, br m), 3.76 (3H, d, J_{P-H} = 11.4 Hz, CH_3), 6.7 (br s, NH) 6.8 (br s, NH), 7.41 (2H,d,9.1 Hz), 8.31 (2H, d, J = 9.1 Hz) ^{31}P NMR (D_2O, 121.4 MHz): δ 7.0 ^{13}C NMR (DMSO, 500 MHz) 49.25, 49.44, 49.60, 49.63, 49.70, 50.05, 54.67, 54.72, 121.12, 121.16, 125.79, 143.99, 155.67
Analysis calculated for $C_{19}H_{39}N_7O_{20}PCo_2Cl_3$: C, 24.26 H, 4.18 N, 10.42 Found : C, 23.99 H, 4.32 N, 10.18

Synthesis of $tacn_2Co_2(^{16/18}OH)_2MPNP$

(0.015g, 0.04 mmol) of trinitrato-(1,4,7-triazacyclononane)cobalt(III) was dissolved in 60 μL of 1M NaOH in 50 % $H_2{}^{18}O/H_2{}^{16}O$. The $tacn_2Co_2(^{18}OH)_3$ was not isolated. After 2-3 hrs at room temperature 250 μL of a 2 M $HClO_4$ solution in 50 % $H_2{}^{18}O/H_2{}^{16}O$ was added. A purple precipitate forms over 30 - 40 mins which was centrifuged, washed with ethanol, centrifuged again, washed with ether and centrifuged a final time to collect 0.0065 g of $tacn_2Co_2(^{18}O/^{16}OH)_2(H_2{}^{18}O/^{16}O)_2$. Two equivalents (0.0039 g mM) of MPNP were combined with 0.0065 g of $tacn_2Co_2(^{18}O/^{16}OH)_2(H_2{}^{18}O/^{16}O)_2$ in 0.15 mL of D_2O. After 2-3 hrs after no precipitate formed, approx. 1 ml of ethanol/ether was added and the resulting solution was refrigerated for 12 hrs. A purple precipitate was obtained after decanting the solution and washing the remaining solid with ether. After drying under vacuum for several hours 4 mg (11 % overall) of $tacn_2Co_2(^{16/18}OH)_2MPNP$ was obtained.

μ-methylphosphato-μ-di-hydroxy-bis[(1,4,7-triazacyclononane)cobalt(III)] triperchlorate $tacn_2Co_2(OH)_2MMP$

One equivalent of sodium hydroxide was added to a 10 mM solution of $tacn_2Co_2(OH)_2MPNP$. ^1H NMR (D_2O, 200 MHz): δ 2.65 (12 H,m), 3.20 (12 H,m) 3.53 (3 H, d, J_{P-H} =10.2) ^{31}P NMR (D_2O, 202.3 MHz): δ 14.97 ^{13}C NMR (D_2O, MHz): δ 49.88, 50.58, 50.95, 51.17

^{18}O labeling experiments

The labeled complex (0.004g, 10 mmol) was dissolved in 0.4 mL of 100 mM HEPES (pH meter = 8.13, pD = 8.53) buffer in D_2O.

A 100 mM HEPES buffer solution was prepared by combining 0.2 mL of a 200 mM HEPES buffer solution at pD = 8.53 with 0.2 mL of $H_2{}^{18}O$. $Tacn_2Co_2(OH)_2MPNP$ (0.004g, 10 mmol) was dissolved in 0.4 mL of this solution.

5 Appendices

5.1 Tables of Data

Table 4.1 Data from figure 4.13. pH-rate profile data for the hydrolysis of 5×10^{-5} M tacn2Co2OH2MPNP at 25 °C in 5×10^{-3} M HEPES buffer. k_o in s^{-1}.

pH	log k_o
7.01	-1.85
7.24	-1.65
7.50	-1.45
7.75	-1.10
8.00	-0.92

Table 4.2 Data from figure 4.18. pH rate profile for the dissociation of DMP from 2.5×10^{-3} M tacn2Co2OH2DMP in 0.1M buffer. CAPS buffer at 11, CHES buffer at 10 and 9, HEPES buffer at 8.

pH	log k_o
8.00	-4.70
9.00	-3.30
10.00	-2.75
11.00	-1.55

Table 4.3 Data from figure 4.20. Dissociation of DMP at 25°C and 5.0 mM tacn2Co2OH2DMP at pH 2.5

time (hrs)	% dissociated DMP
9	13
24	35
48	49
312	54
504	53

Contributions to Knowledge

Cu(N3) and Cu(N3OH) have been shown to be the most effective mononuclear copper (II) catalysts for promoting HPNP cleavage. The second order kinetics and pH rate profile have been explained through a proposed mechanism in which a dimerized complex provides double Lewis acid activation and facilitates attack of the internal nucleophile of HPNP. This is the first example of a dinuclear system for the cleavage of HPNP.

A dinuclear copper(II) complex LCu_2 has been shown to promote the rapid cleavage of HPNP. The proposed mechanism involves binding of the phosphate diester to the complex, double Lewis acid activiation and facilitation of the internal nucleophilic attack on HPNP. LCu_2 is as effective for promoting the cleavage reaction of HPNP as the mononuclear catalyst Cu(N3OH). A value for the rate enhancement expected by a double Lewis acid mechanism for the cleavage reaction of phosphate diesters has been reported.

The synthesis of two novel dinuclear cobalt(III) complexes have been described. These complexes were designed to investigate the effect of two cobalt(III) atoms bound at two distinct oxygens of a phosphate diester on its hydrolysis reaction. The ^{18}O labeling experiments, pH rate profile and identified reaction products have been explained through the proposed mechanism. This mechanism involves double Lewis activation of the phosphate diester and nucleophilic attack of a bridging oxide . The breakdown of the intermediate formed by this nucleophilic attack involves Co - O bond cleavage. The involvement of a oxide bridge as a nucleophile in facilitating the hydrolysis of phosphate diesters has not been previously reported. The equilibrium constant for the binding of DMP to *trans*-$tacn_2Co_2(OH)_2(H2O)_2$ was found to be 330 M^{-1}

The following papers have been published as a result of this research:

Wahnon, Daphne; Lebuis, Anne-Marie; Chin, Jik "Hydrolysis of a Phosphate Diester Doubly Coordinated to a Dinuclear Cobalt(III) Complex: A Novel Mechanism Involving a Nucleophilc Bridging Oxide" *Angew. Chem.* (*in press*)

Young, Mary Jane; Wahnon, Daphne; Hynes, Rosemary C.; Chin, Jik "Metal-Alkoxide Activation in Phosphate Diester Transesterification" *J. Am. Chem. Soc* (*in press*)

Wahnon, Daphne; Hynes, Rosemary C.; Chin, Jik "Dramatic Ligand effect in Copper(II) Complex Promoted Transesterification of a Phosphate Diester" *J. Chem. Soc., Chem. Commun.*, **1994**, 1441

References

1) Chin, J.; Banaszczyk, M.; Jubian, V.; Zou, X. *J. Am. Chem. Soc.* **1989**, *111*, 186-190.

2) Acquist, J.; Warshel, A. *Biochem.* **1989**, *28*, 4680.

3) Weber, D. J.; Meeker, A. K.; Mildvan, A. S. *Biochem.* **1991**, *30*, 6103.

4) Westheimer, F. H. *Acc. Chem. Res.* **1968**, *1*, 70-78.

5) Thatcher, G.; Kluger, R. In *Advances in Physical Organic Chemistry*; Thatcher, G.; Kluger, R., Ed.; Academic Press, 1990; Vol. 25, pp 99-265.

6) Hall, C.; Inch, T.; Peacock, G.; Pottage, C.; Williams, N. *J. Chem. Soc. Perkin Trans. 1* **1984**, 669.

7) Gay, D.; Hamer, N. *J. Chem. Soc. Perkin Trans. 2* **1972**, 1972.

8) Brown, C.; Boudreau, J.; Hewitson, B.; Hudson, R. *J. Chem. Soc., Chem. Commun.* **1975**, 504.

9) Brown, C.; Boudreau, J.; Hewitson, B.; Hudson, R. *J. Chem. Soc. Perkin Trans. 2* **1976**, 888.

10) Westheimer, F. H. *Science* **1987**, *235*, 1173-1178.

11) Kirby, A. J.; Younas, M. *J. Chem. Soc. (B)* **1970**, 510-513.

12) Cox, J. R.; Ramsay, O. B. *Chem. Rev.* **1963**, *64*, 317-351.

13) Bunton, C. A.; Farber, S. J. *J. Org. Chem.* **1969**, *34*, 767-772.

14) Brown, D. M.; Usher, D. A. *J. Chem. Soc.* **1965**, 6558-6564.

15) Usher, D. A.; Richardson Jr., D. I.; Oakenfull, D. G. *J. Am. Chem. Soc.* **1970**, *92*, 4699-4712.

16) Davis, A. M.; Hall, A. D.; Williams, A. *J. Am. Chem. Soc.* **1988**, *110*, 5105-5108.

17) Kirby, A. J. *Advances in Physical Organic Chemistry* **1980**, *17*, 183-278.

18) Stryer, L. *Biochemistry*; Third ed.; W H Freeman and Company: New York, 1988 p 1064.

19) Cech, T.; Zuag, A.; Grabowski, P. *Cell* **1981**, *27*, 487-496.

20) Zuag, A.; Been, M.; Cech, R. *Nature* **1986**, *324*, 429-433.

21) Zuag, A.; Cech, T. *Science* **1986**, 470-475.

22) Herschlag, D.; Cech, T. *Nature* **1990**, *344*, 405.

23) Steitz, T. A.; Steitz, J. A. *Proc. Natl. Acad. Sci. USA* **1993**, *90*, 6498-6502.

24) Fersht, A. *Enzyme Structure and Mechanism*; 2 nd ed.; W.H. Freeman and Company: New York, 1985 p 475.

25) Pyle, A. *Science* **1993**, *261*, 709-714.

26) Beese, L. S.; Steitz, T. A. *EMBO J.* **1991**, *10*, 25-33.

27) Davies II, J. F.; Hostomska, Z.; Hostomsky, Z.; Jordon, S. R.; Matthews, D. A. *Science* **1991**, *252*, 88-94.
28) Yang, W.; Hendrickson, W. A.; Crouch, R. J.; Satpw, Y. *Science* **1990**, *249*, 1398.
29) Vallee, B. L.; Auld, D. S. *Biochem.* **1993**, *32*, 6493.
30) Kim, E. K.; Wyckoff, H. W. *J. Mol. Biol.* **1990**, *218*, 449-463.
31) Martin Jr., D. W.; Mayes, P. A.; Rodwell, V. W.; Granner, D. K. *Harper's Review of Biochemistry*; 20 ed.; Lange Medical Publications: Los Altos, 1985 p680.
32) Luebke, K. J.; Dervan, P. B. *J. Am. Chem. Soc.* **1991**, *113*, 7447-7448.
33) Sigman, D. S.; Mazumder, A.; Perrin, D. M. *Chem. Rev.* **1993**, *93*, 2296-2316.
34) Sigman, D. S.; Bruice, T. W.; Mazumder, A.; Sutton, C. L. *Acc. Chem. Res.* **1993**, *26*, 98-104.
35) Hertzberg, R. P.; Dervan, P. B. *J. Am. Chem. Soc.* **1982**, *104*, 313-315.
36) Beal, P. A.; Dervan, P. B. *J. Am. Chem. Soc.* **1992**, *114*, 4976-4982.
37) Strobel, S.; Dervan, P. *Nature* **1991**, *350*, 172.
38) Mack, D. P.; Dervan, P. *J. Am. Chem. Soc.* **1990**, *112*, 4604-4606.
39) Shullenberger, D. F.; Eason, P. D.; Long, E. C. *J. Am. Chem. Soc.* **1993**, *115*, 11038-11039.
40) Sitlani, A.; Kong, E. C.; Pyle, A. M.; Barton, J. K. *J. Am. Chem. Soc.* **1992**, *114*, 2303-2312.
41) Mei, H. Y.; Barton, J. K. *Proc. Natl. Acad. Sci. USA* **1988**, *85*, 1339-1343.
42) Chen, X.; Rokita, S.; Burrows, C. *J. Am. Chem. Soc.* **1991**, *113*, 5884-5886.
43) Cheng, C.; Rokita, S.; Burrows, C. *Angew. Chem. Int. Ed. Engl.* **1993**, *32*, 277-278.
44) Butcher, W.; Westheimer, F. *J. Am. Chem. Soc.* **1955**, *77*, 2420-2424.
45) Takasaki, B. K.; Chin, J. *J. Am. Chem. Soc.* **1993**, *115*, 9337-9338.
46)Takasaki, B. K.; Chin, J. *J. Am. Chem. Soc.* **1994**, *116*, 1121-1122.
47) Schnaith, L. M. T.; Hanson, R. S.; Que Jr., L. *Proc. Natl. Acad. Sci. USA* **1994**, *91*, 569-573.
48) Jubian, V.; Dixon, R. P.; Hamilton, A. D. *J. Am. Chem. Soc.* **1992**, *114*, 1120-1121.
49) Smith, J.; Ariga, K.; Anslyn, E. V. *J. Am. Chem. Soc.* **1993**, *115*, 362-364.
50) Anslyn, E.; Breslow, R. *J. Am. Chem. Soc.* **1989**, *111*, 4473-4482.
51) Kirby, A. J.; Marriott, R. E. *J. Am. Chem. Soc.* **1995**, *117*, 833-834.
52) Perrin, C. L. *J. Org. Chem.* **1995**, *60*, 1239-1243.
53) Breslow, R.; Huang, D.; Anslyn, E. *Proc. Natl. Acad. Sci. USA* **1989**, *86*, 1746-1750.
54) Hendry, P.; Sargeson, A. M. *Progress in Inorganic Chemistry* **1990**, *38*, 201-259.
55) Hendry, P.; Sargeson, A. M. *J. Am. Chem. Soc.* **1989**, *111*, 2521-2527.
56) Hendry, P.; Sargeson, A. *Aust. J. Chem.* **1986**, *39*, 1177.

57) Hendry, P.; Sargeson, A. M. *Inorg. Chem.* **1990**, *29*, 92-97.
58) Chin, J.; Banaszczyk, M.; Jubian, V. *J. Chem. Soc., Chem. Commun.* **1988**, *11*, 735-736.
59) Kim, J. H.; Chin, J. *J. Am. Chem. Soc.* **1992**, *114*, 9792-9795.
60) Drouin, M. Ph. D. Thesis, McGill University, 1989.
61) Schlemper, E. O.; Sen Gupta, P. K.; Dasgupta, T. P. *Acta Cryst.* **1983**, *C39*, 1012.
62) Morrow, J. R.; Trogler, W. C. *Inorg. Chem.* **1988**, *27*, 3387-3394.
63) Jubian, V. Ph.D. Thesis, McGill University, 1991.
64) Burstyn, J. N.; Deal, K. A. *Inorg. Chem.* **1993**, *32*, 3585-3586.
65) Stern, M. K.; Bashkin, J. K.; Sall, E. D. *J. Am. Chem. Soc.* **1990**, *112*, 5357-5359.
66) Bashkin, J. K.; Jenkins, L. A. *Comments Inorg. Chem.* **1994**, *16*, 77-93.
67) Bashkin, J. K.; Jenkins, L. A. *J. Chem. Soc., Dalton Trans.* **1993**, 3631-3632.
68) Bashkin, J.; Frolova, E.; Sampath, U. *J. Am. Chem. Soc.* **1994**, *116*, 5981-5982.
69) Morrow, J. R.; Buttrey, L. A.; Shelton, V. M.; Berbacl, K. A. *J. Am. Chem. Soc.* **1992**, *114*, 1903-1905.
70) Matsumura, K.; Endo, M.; Komiyama, M. *J. Chem. Soc., Chem. Commun.* **1994**, 2019-2020.
71) Magda, D.; Miller, R. A.; Sessler, J. L.; Iverson, B. L. *J. Am. Chem. Soc.* **1994**, *116*, 7439-7440.
72) Hall, J.; Husken, D.; Pieles, U.; Moser, H.; Haner, R. *Chemistry and Biology* **1994**, *1*, 185-190.
73) Linkletter, B.; Chin, J. *Angew. Chem. Int. Ed. Engl.* **1995**, *34*, 472-474.
74) Linkletter, B. Ph.D. Thesis, McGill University, 1995.
75) Vance, D. H.; Czarnik, A. W. *J. Am. Chem. Soc.* **1993**, *113*, 12165-12166.
76) Jarvinen, P.; Oivanen, M.; Lonnberg, H. *J. Org. Chem.* **1991**, *56*, 5396-5401.
77) Breslow, R.; Labelle, M. *J. Am. Chem. Soc.* **1986**, *108*, 2655-4001.
78) Matsumoto, Y.; Komiyama, M. *J. Chem. Soc., Chem. Commun.* **1990**, 1050-1051.
79) Breslow, R.; Berger, D.; Huang, D.-L. *J. Am. Chem. Soc.* **1990**, *112*, 3686-3687.
80) Amin, S.; Morrow, J. R.; Lake, C. H.; Churchill, M. R. *Angew. Chem. Int. Ed. Engl.* **1994**, *33*, 773-775.
81) Wahnon, D.; Hynes, R.; Chin, J. *Chem. Soc., Chem. Commun.* **1994**, 1441-1442.
82) Morrow, J. R.; Buttrey, L. A.; Berback, K. A. *Inorg. Chem.* **1992**, *31*, 16-20.
83) Wall, M.; Hynes, R. C.; Chin, J. *Angew. Chem. Int. Ed. Engl.* **1993**, *32*, 1633-1635.
84) Murthy, N. N.; Mahroof-Tahir, M.; Karlin, K. D. *J. Am. Chem. Soc.* **1993**, *115*, 10404-10405.

85) Courtney, R. C.; Gustafson, R. L.; Jr. S. C.; Martell, A. E. *J. Am. Chem. Soc.* **1959**, *81*, 519-524.

86) Arulsamy, N.; Hodgson, D. J.; Glerup, J. *Inorg. Chim. Acta* **1993**, *209*, 61-69.

87) Turowski, P. N.; Armstrong, W. H.; Roth, M. E.; Lippard, S. J. *J. Am. Chem. Soc.* **1990**, *112*, 681-690.

88) Tokii, T.; Nagamatsu, M.; Hamada, H.; Nakashima, M. *Chem. Lett.* **1992**, 1091-1094.

89) Oberhausen, K. J.; Richardson, J. F.; Buchanan, R. M. *Polyhedron* **1989**, *8*, 659-668.

90) Berends, H. P.; Stephan, D. W. *Inorg. Chim. Acta* **1984**, *93*, 173-178.

91) Hengge, A. C.; Cleland, W. W. *J. Org. Chem.* **1991**, *56*, 1972-1974.

92) Hendry, P.; Sargeson, A. m. *Inorg. Chem.* **1990**, *29*, 97-104.

93) Menger, F. M.; Gan, L. H.; Johnson, E.; Durst, D. H. *J. Am. Chem. Soc.* **1987**, *109*, 2800-2803.

94) Guthrie, J. P. *J. Am. Chem. Soc.* **1977**, *99*, 3991-4000.

95) McKee, V.; Zvagulis, M.; Dagdigian, J. V.; Patch, M. G.; Reed, C. A. *J. Am. Chem. Soc.* **1984**, *106*, 4765-4772.

96) Chin, J.; Zou, X. *Can. J. Chem.* **1987**, *65*, 1882-1884.

97) Mahroof-Tahir, M.; Karlin, K. D.; Chen, Q.; Zubieta, J. *Inorg. Chim. Acta* **1993**, *207*, 135-138.

98) Schwarzenbach, G.; Boesch, J.; Egli, H. *J. Inorg. Nucl. Chem.* **1971**, *33*, 2141-2156.

99) Jentsch, W.; Schmidt, W.; Sykes, A. G.; Wieghardt, K. *Inorg. Chem.* **1977**, *16*, 1935-1937.

100) Edwards, J. D.; Wieghardt, K.; Sykes, A. G. *J. Chem. Soc., Dalton Trans.* **1974**, 2198-2204.

101) Wieghardt, K.; Schmidt, W.; Nuber, B.; Weiss, J. *Chemische Berichte* **1979**, *112*, 2220-2230.

102) Baur, W. H.; Wieghardt, K. *J. Chem. Soc., Dalton Trans.* **1973**, 2669-2674.

103) Kahler, H. C.; Geier, G. *Helv. Chim. Acta* **1974**, *57*, 802-822.

104) Siebert, V. H.; Tremmel, G. *Zietschrift fur anorganische und algemeine Chemie* **1972**, *390*, 292-302.

105) Wieghardt, K. *Zietschrift fur anorganische und algemeine Chemie* **1972**, *391*, 142.

106) Wieghardt, K. *J. Chem. Soc., Dalton Trans.* **1973**, 2548.

107) Jones, D. R.; Lindoy, L. F.; Sargeson, A. M. *J. Am. Chem. Soc.* **1984**, *106*, 7807-7819.

108) Connolly, J. A.; Banaszczk, M.; Hynes, R. C.; Chin, J. *Inorg. Chem.* **1994**, *33*, 667.

109) Chin, J.; Jubian, V. *J. Chem. Soc., Chem. Commun.* **1989**, *13*, 839-41.

110) Connolly, J. A.; Kim, J. H.; Banaszczyk, M.; Drouin, M.; Chin, J. *Inorg. Chem.* **1995**, *34*, 1094-1099.

111) Briellmann, M.; Kaderli, S.; Meyer, C. J.; Zuberbuhler, A. D. *Helv. Chim. Acta* **1987**, *70*, 680-689.

112) Richman, J. E.; Atkins, T. J. *J. Am. Chem. Soc.* **1974**, *96*, 2268-2270.

113) *Organic Synthesis*; John Wiley and sons, 1978; Vol. 58, pp 86-97.

114) Cohn, M.; Hu, A. *Proc. Natl. Acad. Sci. USA* **1978**, *75*, 200-203.

115) Ba-Saif, S. A.; Davis, A. M.; Williams, A. *J. Org. Chem.* **1989**, *54*, 5483-5486.

Appendix 1: X-ray Supplemental Material for dimethylphosphato-methanol-[(bis(benzimidazol-2-ylmethyl)amine)copper(II)] perchlorate·$2H_2O$

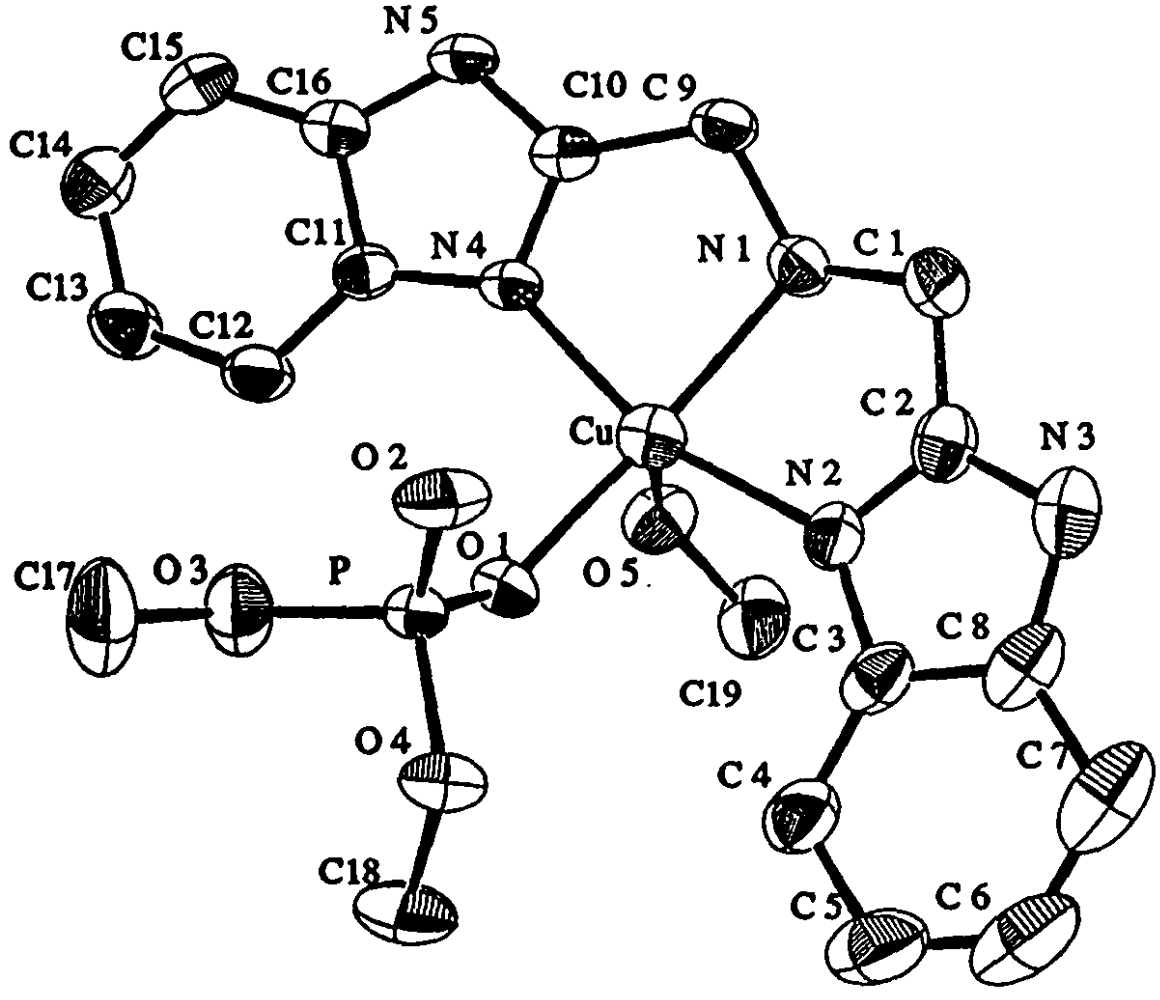
N5
C15
C16
C10
C9
C14
C11
N4
N1
C1
C13
C12
C2
Cu
N3
O2
N2
O1
O5
C17
O3
P
C3
C8
C19
O4
C4
C7
C18
C5
C6

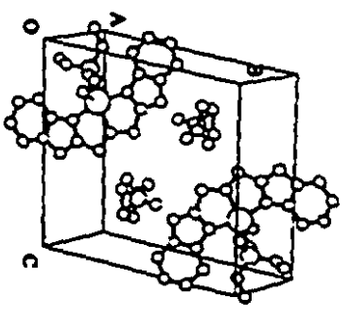
O
A
C

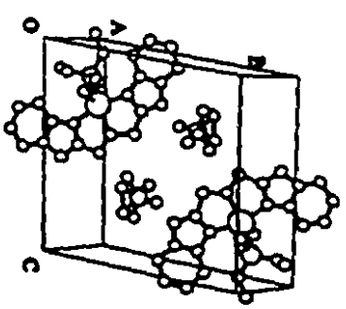
O
A
B
C

DAPH7A - DAPHNE/CHIN - MAY21/93

Space Group and Cell Dimensions Triclinic, P -1
7.2573(11) b 12.7707(17) c 13.3686(20)
alpha 85.213(12) beta 80.009(12) gamma 82.413(12)
Volume 1207.2(3)A**3

Empirical formula : Cu C19 H25 N5 O9 P Cl

Cell dimensions were obtained from 25 reflections with 2Theta angle in the range 70.00 - 90.00 degrees.

Crystal dimensions : 0.40 X 0.23 X 0.20 mm

FW = 597.40 Z = 2 F(000) = 614

Dcalc 1.643Mg.m-3, mu 3.47mm-1, lambda 1.54056A, 2Theta(max) 109.9

The intensity data were collected on a Rigaku diffractometer, controlled by TEXRAY software, using the theta/2theta scan mode.
The h,k,l ranges used during structure solution and refinement are :--
Hmin,max -7 7; Kmin,max 0 13; Lmin,max -14 14
No. of reflections measured 3337
No. of unique reflections 3045
No. of reflections with Inet > 2.5sigma(Inet) 2808
Absorption corrections were made from 4 psi scans.
The minimum and maximum transmission factors are 0.375657 and 0.524973.

The last least squares cycle was calculated with
64 atoms, 353 parameters and 2808 out of 3045 reflections.
Weights based on counting-statistics were used.
The weight modifier K in KFo**2 is 0.000050

The residuals are as follows :--
For significant reflections, RF 0.047, Rw 0.063 GoF 4.62
For all reflections, RF 0.051, Rw 0.063.
where RF = Sum(Fo-Fc)/Sum(Fo),
Rw = Sqrt[Sum(w(Fo-Fc)**2)/Sum(wFo**2)] and
GoF = Sqrt[Sum(w(Fo-Fc)**2)/(No. of reflns - No. of params.)]
The maximum shift/sigma ratio was 0.168.

In the last D-map, the deepest hole was -0.640e/A**3,
and the highest peak 0.320e/A**3.

Secondary ext. coeff. = 0.19(3)

Standard intensities remained constant throughout collection (average deviation 0.4%) Merging R was 1.6% for 292 pairs of symmetry related reflections. Structure was solved by direct methods; hydrogens on N, O were located in a difference map but not refined. Other hydrogens were included in calculated positions. Structure was refined by full-matrix least-squares with all non-hydrogens anisotropic. The perchlorate anion has two orientations, differing by a rotation about the CL01-Cl bond. All computing done using the NRCVAX system of crystallographic software.

The following references are relevant to the NRCVAX System.

1. Full System Reference :
   NRCVAX, Gabe, E.J., Le Page, Y., Charland,.J.-P., Lee, F.l. and White, P.S. (1989) J. Appl. Cryst., 22, 384-387.

2. Scattering Factors from Int. Tab. Vol. 4 :
   International Tables for X-ray Crystallography, Vol. IV, (1974) Kynoch Press, Birmingham, England.

3. ORTEP Plotting :
   Johnson, C.K., (1976) ORTEP - A Fortran Thermal Ellipsoid Plot Program, Tehnical Report ORNL-5138, Oak Ridge Tennessee.

4. Extinction Treatment :
   Larson, A.C., (1970) p.293, Crystallographic Computing, Munksgaard, Copenhagen.

Table 2. Atomic Parameters x,y,z and Beq
E.S.Ds. refer to the last digit printed.

	x	y	z	Beq
Cu	0.35586(10)	0.16619(5)	0.28076(5)	3.29(4)
P	0.69800(19)	0.01628(10)	0.16843(10)	2.35(6)
O 1	0.5030 (5)	0.0711 (3)	0.17940(24)	2.75(16)
O 2	0.8194 (5)	0.0343 (3)	0.2423 (3)	3.64(19)
O 3	0.6725 (6)	-0.1046 (3)	0.1680 (3)	4.18(20)
O 4	0.8116 (5)	0.0447 (3)	0.05975(24)	3.09(17)
O 5	0.0848 (5)	0.1763 (3)	0.2198 (3)	3.52(17)
N 1	0.2671 (6)	0.2651 (3)	0.4023 (3)	2.66(18)
N 2	0.4432 (6)	0.2977 (3)	0.2131 (3)	2.78(20)
N 3	0.5475 (7)	0.4488 (4)	0.2307 (4)	3.79(24)
N 4	0.2916 (6)	0.0579 (3)	0.3895 (3)	2.43(19)
N 5	0.2282 (6)	0.0120 (3)	0.5540 (3)	2.63(20)
C 1	0.3723 (8)	0.3586 (4)	0.3870 (4)	3.2 (3)
C 2	0.4522 (7)	0.3689 (4)	0.2761 (4)	3.03(25)
C 3	0.5408 (8)	0.3312 (4)	0.1196 (4)	3.3 (3)
C 4	0.5746 (9)	0.2857 (5)	0.0262 (4)	4.1 (3)
C 5	0.6856 (10)	0.3391 (6)	-0.0534 (5)	5.4 (3)
C 6	0.7571 (10)	0.4312 (6)	-0.0400 (6)	5.7 (4)
C 7	0.7218 (9)	0.4775 (5)	0.0507 (6)	5.3 (4)
C 8	0.6087 (8)	0.4250 (5)	0.1314 (5)	3.9 (3)
C 9	0.2708 (7)	0.2043 (4)	0.5014 (4)	2.79(23)
C10	0.2617 (7)	0.0911 (4)	0.4828 (4)	2.49(24)
C11	0.2770 (7)	-0.0499 (4)	0.4002 (4)	2.39(23)
C12	0.2912 (8)	-0.1241 (4)	0.3270 (4)	3.2 (3)
C13	0.2657 (9)	-0.2264 (5)	0.3635 (4)	3.8 (3)
C14	0.2272 (8)	-0.2555 (4)	0.4669 (4)	3.5 (3)
C15	0.2113 (8)	-0.1833 (4)	0.5394 (4)	3.2 (3)
C16	0.2362 (7)	-0.0793 (4)	0.5041 (4)	2.63(25)
C17	0.8301 (12)	-0.1850 (5)	0.1672 (6)	6.7 (4)
C18	0.7476 (8)	0.0219 (5)	-0.0314 (4)	4.1 (3)
C19	0.0320 (10)	0.2539 (5)	0.1459 (5)	4.8 (3)
CL	0.89632(24)	0.53141(11)	0.34005(11)	3.65(8)
CLO1	0.9455 (8)	0.4228 (4)	0.3392 (4)	7.2 (3)
CLO2	0.7037 (22)	0.5374 (11)	0.3939 (11)	8.0 (8)
CLO3	0.8669 (22)	0.5663 (8)	0.2395 (9)	7.3 (6)
CLO4	1.001 (3)	0.5877 (15)	0.3768 (11)	8.4 (10)
CLO2'	1.021 (5)	0.5727 (18)	0.2613 (19)	15.2 (18)
CLO3'	0.727 (4)	0.5840 (15)	0.3435 (24)	9.8 (20)
CLO4'	0.977 (4)	0.5687 (19)	0.4272 (13)	6.3 (10)

Beq is the mean of the principal axes of the thermal ellipsoid.
Perchlorate oxygens CLO2, CLO3 and CLO4 have two orientations (flagged CLOx') at 60 and 40% occupancies.

Table 3. Bond Distances in Angstroms

Cu-O(1)	1.970(3)	N(4)-C(10)	1.324(6)
Cu-O(5)	2.241(4)	N(4)-C(11)	1.388(6)
Cu-N(1)	2.101(4)	N(5)-C(10)	1.345(6)
Cu-N(2)	1.966(4)	N(5)-C(16)	1.381(7)
Cu-N(4)	1.960(4)	C(1)-C(2)	1.497(8)
P-O(1)	1.483(4)	C(3)-C(4)	1.390(8)
P-O(2)	1.483(4)	C(3)-C(8)	1.384(9)
P-O(3)	1.580(4)	C(4)-C(5)	1.404(9)
P-O(4)	1.580(4)	C(5)-C(6)	1.382(13)
O(3)-C(17)	1.431(8)	C(6)-C(7)	1.363(13)
O(4)-C(18)	1.441(6)	C(7)-C(8)	1.416(9)
O(5)-C(19)	1.404(7)	C(9)-C(10)	1.499(7)
N(1)-C(1)	1.482(7)	C(11)-C(12)	1.400(7)
N(1)-C(9)	1.482(6)	C(11)-C(16)	1.400(7)
N(2)-C(2)	1.305(7)	C(12)-C(13)	1.380(8)
N(2)-C(3)	1.390(7)	C(13)-C(14)	1.391(8)
N(3)-C(2)	1.351(7)	C(14)-C(15)	1.374(8)
N(3)-C(8)	1.372(8)	C(15)-C(16)	1.395(7)
Cl-CLO1	1.386(5)		
Cl-CLO2	1.453(14)		
Cl-CLO3	1.423(9)		
Cl-CLO4	1.291(17)		
Cl-CLO2'	1.383(16)		
Cl-CLO3'	1.31(3)		
Cl-CLO4'	1.528(22)		

Table 4. Bond Angles in Degrees

O(1)-Cu-O(5)	95.70(14)	C(10)-N(5)-C(16)	107.5(4)
O(1)-Cu-N(1)	164.95(16)	N(1)-C(1)-C(2)	106.8(4)
O(1)-Cu-N(2)	96.17(16)	N(2)-C(2)-N(3)	112.5(5)
O(1)-Cu-N(4)	97.76(15)	N(2)-C(2)-C(1)	122.6(5)
O(5)-Cu-N(1)	99.34(15)	N(3)-C(2)-C(1)	124.8(5)
O(5)-Cu-N(2)	98.14(16)	N(2)-C(3)-C(4)	130.5(5)
O(5)-Cu-N(4)	95.42(15)	N(2)-C(3)-C(8)	108.1(5)
N(1)-Cu-N(2)	81.39(17)	C(4)-C(3)-C(8)	121.4(5)
N(1)-Cu-N(4)	81.25(16)	C(3)-C(4)-C(5)	115.9(6)
N(2)-Cu-N(4)	159.46(17)	C(4)-C(5)-C(6)	122.2(6)
O(1)-P-O(2)	118.88(21)	C(5)-C(6)-C(7)	122.4(6)
O(1)-P-O(3)	104.13(21)	C(6)-C(7)-C(8)	116.0(7)
O(1)-P-O(4)	110.49(20)	N(3)-C(8)-C(3)	106.6(5)
O(2)-P-O(3)	111.80(23)	N(3)-C(8)-C(7)	131.2(6)
O(2)-P-O(4)	105.76(20)	C(3)-C(8)-C(7)	122.1(6)
O(3)-P-O(4)	105.06(21)	N(1)-C(9)-C(10)	106.5(4)
Cu-O(1)-P	132.38(21)	N(4)-C(10)-N(5)	112.1(4)
P-O(3)-C(17)	121.0(4)	N(4)-C(10)-C(9)	121.4(4)
P-O(4)-C(18)	120.9(3)	N(5)-C(10)-C(9)	126.5(4)
Cu-O(5)-C(19)	123.5(4)	N(4)-C(11)-C(12)	130.8(4)
Cu-N(1)-C(1)	110.5(3)	N(4)-C(11)-C(16)	108.3(4)
Cu-N(1)-C(9)	111.1(3)	C(12)-C(11)-C(16)	120.9(5)
C(1)-N(1)-C(9)	115.1(4)	C(11)-C(12)-C(13)	116.3(5)
Cu-N(2)-C(2)	113.7(3)	C(12)-C(13)-C(14)	122.6(5)
Cu-N(2)-C(3)	138.1(4)	C(13)-C(14)-C(15)	121.7(5)
C(2)-N(2)-C(3)	106.1(4)	C(14)-C(15)-C(16)	116.6(5)
C(2)-N(3)-C(8)	106.6(5)	N(5)-C(16)-C(11)	105.9(4)
Cu-N(4)-C(10)	114.9(3)	N(5)-C(16)-C(15)	132.2(5)
Cu-N(4)-C(11)	138.7(3)	C(11)-C(16)-C(15)	121.9(5)
C(10)-N(4)-C(11)	106.2(4)		

CLO1-Cl-CLO2	101.2(6)
CLO1-Cl-CLO3	106.1(6)
CLO1-Cl-CLO4	118.9(9)
CLO1-Cl-CLO2'	104.6(10)
CLO1-Cl-CLO3'	127.7(8)
CLO1-Cl-CLO4'	106.9(9)
CLO2-Cl-CLO3	101.2(9)
CLO2-Cl-CLO4	113.7(10)
CLO3-Cl-CLO4	113.6(8)
CLO2'-Cl-CLO3'	110.6(18)
CLO2'-Cl-CLO4'	97.1(18)
CLO3'-Cl-CLO4'	105.8(16)

Table S-2. Hydrogen Atom Parameters

	x	y	z	Biso
HO5	-0.004	0.113	0.234	4.3
HN1	0.138	0.294	0.394	3.4
HN3	0.572	0.508	0.263	3.2
HN5	0.211	0.019	0.623	3.2
H 1A	0.278	0.429	0.409	4.1
H 1B	0.482	0.348	0.434	4.1
H 4	0.516	0.215	0.016	4.6
H 5	0.716	0.308	-0.128	5.7
H 6	0.844	0.470	-0.102	6.1
H 7	0.774	0.550	0.062	6.0
H 9A	0.398	0.213	0.530	3.6
H 9B	0.150	0.232	0.556	3.6
H12	0.321	-0.101	0.247	4.0
H13	0.278	-0.286	0.309	4.6
H14	0.209	-0.337	0.491	4.3
H15	0.181	-0.206	0.620	4.0
H17A	0.930	-0.172	0.099	7.4
H17B	0.902	-0.182	0.231	7.4
H17C	0.788	-0.263	0.165	7.4
H18A	0.742	-0.062	-0.033	4.9
H18B	0.608	0.063	-0.035	4.9
H18C	0.843	0.046	-0.098	4.9
H19A	-0.119	0.264	0.149	5.8
H19B	0.096	0.228	0.072	5.8
H19C	0.077	0.330	0.153	5.8

Hydrogens on N, O were located in a difference map but not refined. Other hydrogens were included in calculated positions assuming C-H of 1.08Å and Biso(H) from Uiso(H) = Ueq(C) + 0.01.

Table S-3. Anisotropic u(i,j) values *100.
E.S.Ds. refer to the last digit printed

	u11	u22	u33	u12	u13	u23
Cu	4.87(5)	3.99(5)	3.56(5)	-0.58(3)	-0.39(3)	-0.35(3)
P	3.59(8)	2.97(8)	2.33(7)	-0.49(6)	-0.22(6)	-0.26(6)
O 1	4.01(22)	3.59(20)	2.70(19)	-0.29(17)	0.01(16)	-0.76(16)
O 2	5.19(25)	6.4 (3)	2.55(20)	-1.61(21)	-1.00(18)	0.14(18)
O 3	5.5 (3)	3.35(22)	6.7 (3)	-0.48(20)	0.01(22)	-0.47(19)
O 4	3.70(22)	5.44(24)	2.62(19)	-0.90(18)	-0.23(17)	-0.52(17)
O 5	4.10(23)	5.09(24)	4.53(23)	-0.94(19)	-1.75(19)	0.45(19)
N 1	3.5 (3)	3.40(25)	3.16(24)	-0.06(21)	-0.52(20)	-0.68(19)
N 2	4.0 (3)	2.76(24)	3.6 (3)	-0.24(21)	-0.28(22)	0.06(21)
N 3	4.7 (3)	3.4 (3)	6.4 (3)	-0.96(24)	-1.3 (3)	0.11(24)
N 4	3.47(25)	3.5 (3)	2.16(23)	-0.45(20)	-0.08(19)	-0.28(19)
N 5	3.6 (3)	4.3 (3)	2.00(22)	-0.31(21)	-0.15(19)	-0.22(20)
C 1	5.0 (4)	3.5 (3)	4.1 (3)	-0.9 (3)	-1.3 (3)	-0.6 (3)
C 2	3.4 (3)	3.2 (3)	4.9 (3)	-0.3 (3)	-1.1 (3)	0.2 (3)
C 3	3.7 (3)	3.7 (3)	4.5 (4)	0.4 (3)	-0.2 (3)	1.1 (3)
C 4	5.9 (4)	4.3 (4)	4.5 (4)	0.7 (3)	-0.2 (3)	0.9 (3)
C 5	7.1 (5)	7.0 (5)	4.6 (4)	2.3 (4)	0.7 (4)	1.6 (4)
C 6	6.1 (5)	7.5 (5)	6.8 (5)	0.0 (4)	0.4 (4)	3.5 (4)
C 7	4.7 (4)	5.8 (4)	9.1 (6)	-0.8 (3)	-1.3 (4)	3.2 (4)
C 8	3.8 (3)	4.3 (4)	6.2 (4)	-0.5 (3)	-0.8 (3)	1.7 (3)
C 9	3.8 (3)	4.0 (3)	2.6 (3)	0.0 (3)	-0.45(24)	-0.59(24)
C10	2.5 (3)	4.2 (3)	2.7 (3)	-0.09(24)	-0.40(23)	-0.21(25)
C11	2.8 (3)	3.6 (3)	2.6 (3)	-0.64(24)	-0.15(23)	0.05(23)
C12	4.8 (4)	4.2 (3)	3.0 (3)	-1.4 (3)	-0.1 (3)	-0.4 (3)
C13	5.8 (4)	4.4 (4)	4.4 (4)	-2.0 (3)	-0.3 (3)	-1.0 (3)
C14	4.1 (3)	4.2 (3)	5.0 (4)	-1.5 (3)	-0.7 (3)	0.6 (3)
C15	3.7 (3)	4.9 (4)	3.5 (3)	-0.9 (3)	-0.6 (3)	1.0 (3)
C16	2.7 (3)	4.1 (3)	3.2 (3)	-0.3 (3)	-0.56(24)	-0.4 (3)
C17	10.8 (7)	3.9 (4)	10.2 (6)	1.8 (4)	-2.3 (5)	-0.7 (4)
C18	5.0 (4)	7.9 (5)	2.7 (3)	-0.5 (3)	-1.0 (3)	-1.1 (3)
C19	7.2 (5)	4.9 (4)	6.8 (4)	0.0 (3)	-4.1 (4)	0.2 (3)
CL	5.87(11)	3.14(8)	4.78(9)	-0.32(8)	-0.72(8)	-0.41(7)
CLO1	12.4 (5)	4.4 (3)	11.8 (4)	0.4 (3)	-5.9 (4)	-1.4 (3)
CLO2	6.4 (7)	14.2 (14)	10.0 (10)	-3.1 (10)	2.9 (7)	-7.7 (9)
CLO3	14.4 (11)	7.4 (6)	6.8 (7)	-4.9 (8)	-3.6 (8)	4.0 (5)
CLO4	13.1 (12)	9.4 (9)	12.2 (15)	-5.6 (8)	-6.2 (14)	-0.2 (11)
CLO2'	24.4 (30)	15.3 (19)	12.8 (20)	-6.5 (21)	14.2 (21)	-1.0 (15)
CLO3'	9.4 (17)	4.5 (10)	24.6 (38)	-2.5 (10)	-4.1 (22)	-2.8 (13)
CLO4'	11.9 (15)	7.8 (14)	5.5 (11)	0.6 (12)	-4.1 (12)	-3.9 (10)

Anisotropic Temperature Factors are of the form
Temp=-2*Pi*Pi*(h*h*u11*astar*astar+---+2*h*k*u12*astar*bstar+---)

Appendix 2: X-ray Supplemental Material for dichloro-[(bis(benzimidazol-2-ylmethyl)amine)copper(II)]·CH_3OH

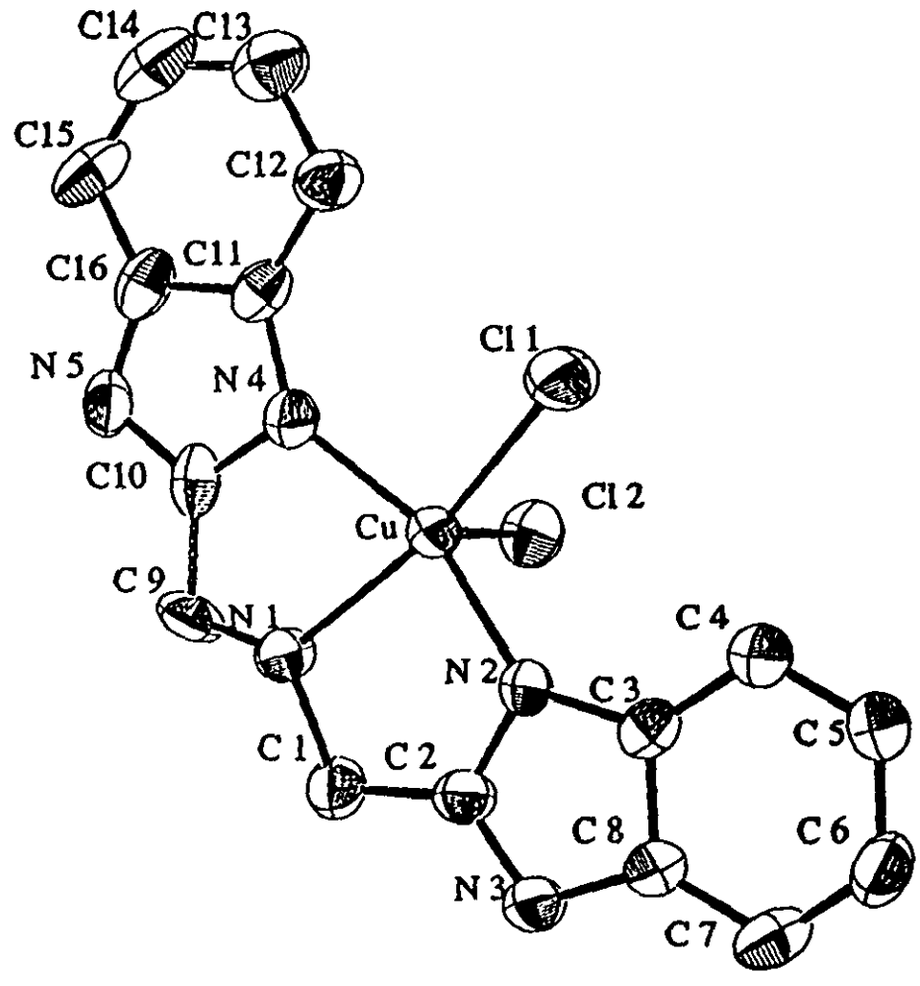
C14
C13
C15
C12
C16
C11
N5
N4
Cl1
C10
Cl2
Cu
C9
N1
C4
N2
C3
C5
C1
C2
C8
C6
N3
C7

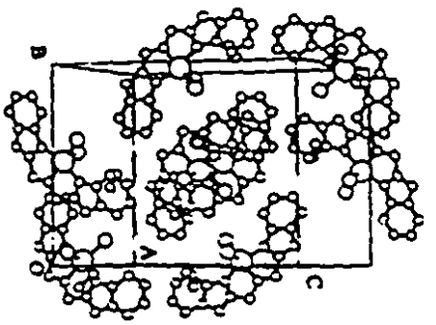

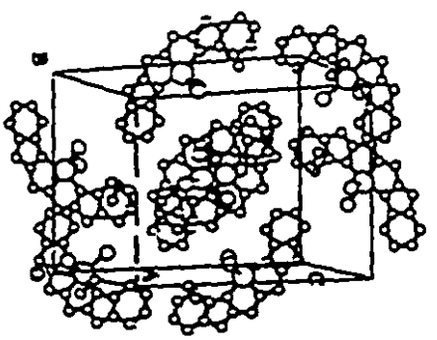

DAPH7 - DAPHNE - JUN4/93

Space Group and Cell Dimensions Orthorhombic P bca
14.020(4) b 14.380(3) c 18.268(4)
Volume 3683.0(15)A**3

Empirical formula : Cu C17 H18 N5 O Cl2

Cell dimensions were obtained from 25 reflections with 2Theta angle in the range 30.00 - 35.00 degrees.

Crystal dimensions : 0.30 X 0.30 X 0.30 mm

FW = 442.81 Z = 8 F(000) = 1808

Dcalc 1.597Mg.m-3, mu 1.50mm-1, lambda 0.70930A, 2Theta(max) 45.0

The intensity data were collected on a Rigaku diffractometer, controlled by TEXRAY software, using the theta/2theta scan mode.
The h,k,l ranges used during structure solution and refinement are :--
Hmin,max 0 15; Kmin,max 0 15; Lmin,max 0 19
No. of reflections measured 2626
No. of unique reflections 2398
No. of reflections with Inet > 0.0sigma(Inet) 1458
No correction was made for absorption

The last least squares cycle was calculated with
44 atoms, 235 parameters and 1458 out of 2398 reflections.
Weights based on counting-statistics were used.
The weight modifier K in KFo**2 is 0.000050

The residuals are as follows :--
For significant reflections, RF 0.048, Rw 0.044 GoF 1.96
For all reflections, RF 0.104, Rw 0.046.
where RF = Sum(Fo-Fc)/Sum(Fo),
Rw = Sqrt[Sum(w(Fo-Fc)**2)/Sum(wFo**2)] and
GoF = Sqrt[Sum(w(Fo-Fc)**2)/(No. of reflns - No. of params.)]
The maximum shift/sigma ratio was 0.037.

In the last D-map, the deepest hole was -0.430e/A**3,
and the highest peak 0.400e/A**3.

Standard intensities remained constant over the course of collection (average decrease 0.31%). Merging R was 1.9% for 258 pairs of symmetry-related pairs. Structure was solved by direct methods; hydrogens were located in a difference map then idealized. Structure was refined by full-matrix, least-squares with all non-hydrogens anisotropic. N(1) is disordered across two sites at 50% occupancy each. The solvent methanol is hydrogen bonded to N(3). All computing done using the NRCVAX system of crystallographic software.

The following references are relevant to the NRCVAX System.

1. Full System Reference :
NRCVAX, Gabe, E.J., Le Page, Y., Charland, J.-P., Lee, F.L. and White, P.S. (1989) J. Appl. Cryst., 22, 384-387.

2. Scattering Factors from Int. Tab. Vol. 4 :
International Tables for X-ray Crystallography, Vol. IV, (1974) Kynoch Press, Birmingham, England.

3. ORTEP Plotting :
Johnson, C.K., (1976) ORTEP - A Fortran Thermal Ellipsoid Plot Program, Tehnical Report ORNL-5138, Oak Ridge Tennessee.

Table 2. Atomic Parameters x,y,z and Beq
E.S.Ds. refer to the last digit printed.

	x	y	z	Beq
Cu	0.36199(6)	0.02403(5)	0.99739(5)	3.06(4)
Cl 1	0.41910(18)	0.12650(14)	1.08093(11)	5.09(11)
Cl 2	0.18245(14)	0.06999(13)	0.99556(13)	4.44(10)
N 1	0.3125 (13)	-0.0735 (13)	0.9192 (11)	4.2 (10)
N 1'	0.3748 (12)	-0.0835 (15)	0.9265 (12)	3.9 (9)
N 2	0.3924 (4)	0.0940 (4)	0.9073 (3)	3.0 (3)
N 3	0.3914 (4)	0.0978 (4)	0.7849 (3)	3.4 (3)
N 4	0.3444 (4)	-0.0836 (4)	1.0640 (3)	3.2 (3)
N 5	0.3064 (4)	-0.2331 (4)	1.0757 (3)	3.8 (3)
C 1	0.3462 (5)	-0.0532 (4)	0.8482 (4)	3.4 (4)
C 2	0.3779 (5)	0.0463 (5)	0.8453 (4)	3.1 (3)
C 3	0.4172 (5)	0.1839 (5)	0.8845 (4)	2.9 (3)
C 4	0.4395 (6)	0.2636 (5)	0.9256 (4)	3.9 (4)
C 5	0.4577 (6)	0.3441 (5)	0.8868 (4)	4.1 (4)
C 6	0.4563 (6)	0.3455 (5)	0.8102 (4)	4.4 (4)
C 7	0.4343 (6)	0.2692 (5)	0.7699 (4)	4.2 (4)
C 8	0.4154 (6)	0.1871 (5)	0.8077 (4)	3.2 (4)
C 9	0.3206 (6)	-0.1672 (5)	0.9482 (4)	3.8 (4)
C10	0.3231 (6)	-0.1615 (5)	1.0294 (4)	3.3 (4)
C11	0.3421 (5)	-0.1050 (5)	1.1384 (4)	3.4 (4)
C12	0.3581 (6)	-0.0507 (5)	1.2005 (4)	3.8 (4)
C13	0.3506 (6)	-0.0936 (6)	1.2677 (5)	4.8 (5)
C14	0.3262 (6)	-0.1863 (6)	1.2737 (5)	5.5 (5)
C15	0.3094 (6)	-0.2419 (6)	1.2139 (4)	5.0 (5)
C16	0.3180 (5)	-0.1996 (5)	1.1456 (4)	3.7 (4)
O	0.1073 (4)	0.9629 (3)	0.1393 (3)	4.9 (3)
C17	0.0587 (7)	0.8959 (5)	0.0960 (4)	5.8 (5)

Beq is the mean of the principal axes of the thermal ellipsoid.

Table 3. Bond Distances in Angstroms

Cu-Cl(1)	2.2674(21)	C(1)-C(2)	1.500(9)
Cu-Cl(2)	2.6027(22)	C(3)-C(4)	1.405(10)
Cu-N(1)	2.119(19)	C(3)-C(8)	1.404(10)
Cu-N(1')	2.024(22)	C(4)-C(5)	1.381(10)
Cu-N(2)	1.975(5)	C(5)-C(6)	1.399(11)
Cu-N(4)	1.984(6)	C(6)-C(7)	1.357(11)
N(1)-C(1)	1.412(23)	C(7)-C(8)	1.394(10)
N(1)-C(9)	1.451(21)	C(9)-C(10)	1.486(10)
N(1')-C(1)	1.549(22)	C(11)-C(12)	1.396(11)
N(1')-C(9)	1.477(22)	C(11)-C(16)	1.407(10)
N(2)-C(2)	1.338(9)	C(12)-C(13)	1.379(11)
N(2)-C(3)	1.402(9)	C(13)-C(14)	1.381(13)
N(3)-C(2)	1.343(9)	C(14)-C(15)	1.373(13)
N(3)-C(8)	1.390(9)	C(15)-C(16)	1.395(11)
N(4)-C(10)	1.321(9)	O-C(17)	1.421(10)
N(4)-C(11)	1.393(9)		
N(5)-C(10)	1.352(9)		
N(5)-C(16)	1.374(10)		

Table 4. Bond Angles in Degrees

Cl(1)-Cu-Cl(2)	100.67(9)	N(2)-C(3)-C(4)	130.5(6)
Cl(1)-Cu-N(1)	178.4(5)	N(2)-C(3)-C(8)	108.7(6)
Cl(1)-Cu-N(1')	153.6(5)	C(4)-C(3)-C(8)	120.7(6)
Cl(1)-Cu-N(2)	98.86(17)	C(3)-C(4)-C(5)	116.8(6)
Cl(1)-Cu-N(4)	97.92(18)	C(4)-C(5)-C(6)	121.5(7)
Cl(2)-Cu-N(1)	80.9(5)	C(5)-C(6)-C(7)	122.3(6)
Cl(2)-Cu-N(1')	105.7(5)	C(6)-C(7)-C(8)	117.3(6)
Cl(2)-Cu-N(2)	93.93(18)	N(3)-C(8)-C(3)	105.9(6)
Cl(2)-Cu-N(4)	94.93(19)	N(3)-C(8)-C(7)	132.8(6)
N(1)-Cu-N(2)	81.1(6)	C(3)-C(8)-C(7)	121.3(6)
N(1)-Cu-N(4)	81.7(6)	N(1')-C(9)-C(10)	102.2(10)
N(1')-Cu-N(2)	80.6(6)	N(1)-C(9)-C(10)	108.4(9)
N(1')-Cu-N(4)	78.9(6)	N(4)-C(10)-N(5)	112.7(7)
N(2)-Cu-N(4)	159.22(23)	N(4)-C(10)-C(9)	121.9(6)
Cu-N(1)-C(1)	111.9(11)	N(5)-C(10)-C(9)	125.4(7)
Cu-N(1)-C(9)	110.0(11)	N(4)-C(11)-C(12)	131.7(6)
C(1)-N(1)-C(9)	120.1(14)	N(4)-C(11)-C(16)	108.1(7)
Cu-N(1')-C(1)	110.7(11)	C(11)-C(12)-C(13)	117.5(7)
Cu-N(1')-C(9)	113.9(13)	C(12)-C(13)-C(14)	121.4(8)
C(1)-N(1')-C(9)	110.1(12)	C(13)-C(14)-C(15)	122.9(7)
Cu-N(2)-C(2)	114.3(4)	C(14)-C(15)-C(16)	116.3(7)
Cu-N(2)-C(3)	140.3(5)	N(5)-C(16)-C(11)	106.3(6)
C(2)-N(2)-C(3)	105.0(5)	N(5)-C(16)-C(15)	132.0(7)
C(2)-N(3)-C(8)	107.2(5)	C(11)-C(16)-C(15)	121.8(8)
Cu-N(4)-C(10)	113.4(5)		
Cu-N(4)-C(11)	140.7(5)		
C(10)-N(4)-C(11)	105.9(6)		
C(10)-N(5)-C(16)	107.1(6)		
N(1)-C(1)-C(2)	109.2(9)		
N(1')-C(1)-C(2)	102.9(9)		
N(2)-C(2)-N(3)	113.1(6)		
N(2)-C(2)-C(1)	120.3(6)		
N(3)-C(2)-C(1)	126.6(6)		

Table S-2. Normalized Hydrogen Atom Positions

	x	y	z	Biso
HN3	0.384	0.074	0.728	4.3
HN5	0.288	-0.304	1.059	4.8
H 1A	0.276	-0.062	0.826	4.4
H 1B	0.404	-0.099	0.831	4.4
H 4	0.439	0.257	0.984	4.9
H 5	0.480	0.404	0.919	4.8
H 6	0.465	0.416	0.791	5.3
H 7	0.436	0.269	0.711	5.0
H 9A	0.343	-0.229	0.918	4.7
H 9B	0.243	-0.165	0.941	4.7
H12	0.381	0.021	1.194	4.8
H13	0.360	-0.047	1.314	5.7
H14	0.328	-0.220	1.327	6.1
H15	0.268	-0.304	1.222	6.1
HO	0.154	1.005	0.104	5.8
H17A	0.012	0.850	0.125	6.9
H17B	0.071	0.911	0.039	6.9
H17C	0.119	0.848	0.104	6.9

Hydrogen atom positions adjusted so that C/N-H = 1.08A. Biso(H) is from Uiso(H) = Ueq(C/N) + 0.1.

Table S-3. Anisotropic u(i,j) values *100.
E.S.D's. refer to the last digit printed

	u11	u22	u33	u12	u13	u23
Cu	5.35(6)	3.14(5)	3.15(5)	-0.37(5)	0.19(6)	-0.12(5)
Cl 1	9.98(20)	5.00(12)	4.36(12)	-2.49(14)	-1.59(15)	-0.10(11)
Cl 2	5.47(13)	5.21(12)	6.21(13)	-0.20(11)	-0.10(15)	0.41(12)
N 1	12.3 (19)	1.5 (8)	2.0 (9)	-2.2 (13)	-0.6 (13)	-0.2 (7)
N 1'	8.3 (16)	2.9 (9)	3.4 (10)	-2.6 (11)	-1.0 (12)	-0.1 (7)
N 2	5.0 (5)	2.8 (3)	3.6 (4)	-0.6 (3)	0.2 (3)	0.1 (3)
N 3	5.5 (5)	4.1 (4)	3.5 (4)	-0.8 (3)	0.3 (4)	0.0 (3)
N 4	4.8 (5)	3.3 (4)	4.0 (4)	-0.3 (4)	-0.2 (4)	0.1 (3)
N 5	5.9 (5)	3.3 (4)	5.4 (4)	1.1 (4)	0.6 (4)	0.4 (4)
C 1	5.0 (5)	3.8 (4)	4.1 (5)	0.0 (4)	-1.0 (5)	0.0 (4)
C 2	4.3 (5)	4.6 (5)	3.1 (4)	0.3 (4)	0.3 (4)	0.0 (4)
C 3	3.1 (5)	4.1 (5)	3.9 (5)	0.1 (4)	0.3 (4)	0.7 (4)
C 4	6.5 (6)	4.1 (5)	4.3 (5)	-0.6 (5)	0.1 (5)	0.0 (4)
C 5	6.9 (6)	3.7 (5)	4.8 (5)	-0.5 (5)	-0.2 (5)	-0.3 (4)
C 6	7.0 (7)	3.7 (5)	5.9 (6)	-0.6 (5)	-0.4 (5)	1.2 (4)
C 7	5.7 (6)	6.2 (6)	4.0 (5)	-1.1 (5)	0.1 (4)	1.6 (5)
C 8	4.3 (5)	4.2 (5)	3.6 (5)	0.0 (4)	-0.1 (4)	0.3 (4)
C 9	6.3 (7)	4.9 (5)	3.4 (5)	-0.6 (5)	-0.1 (5)	-1.6 (4)
C10	3.5 (5)	2.7 (4)	6.5 (6)	-0.1 (4)	-0.2 (4)	0.3 (4)
C11	3.6 (5)	4.6 (5)	4.6 (5)	0.5 (4)	-0.2 (5)	1.2 (4)
C12	5.3 (6)	5.2 (5)	3.9 (5)	0.2 (5)	0.6 (5)	0.5 (4)
C13	5.7 (6)	7.1 (6)	5.3 (6)	0.8 (5)	0.3 (5)	0.8 (5)
C14	6.4 (7)	8.6 (8)	5.7 (6)	1.0 (6)	0.4 (6)	3.7 (6)
C15	6.8 (6)	6.7 (6)	5.5 (6)	-0.9 (6)	-0.6 (5)	3.3 (5)
C16	2.9 (5)	4.6 (5)	6.5 (6)	0.5 (4)	-0.2 (5)	1.6 (5)
O	8.1 (4)	6.2 (4)	4.2 (3)	-0.6 (3)	0.3 (3)	0.9 (3)
C17	11.4 (9)	6.1 (6)	4.6 (6)	-2.1 (6)	-0.2 (6)	0.3 (5)

Anisotropic Temperature Factors are of the form
Temp=-2*Pi*Pi*(h*h*u11*astar*astar+---+2*h*k*u12*astar*bstar+---)

Appendix 3: X-ray Supplemental Material for chloro-[(bis(benzimidazol-2ylmethyl)hydroxyethylamine)copper(II)] chloride·3(H_2O)

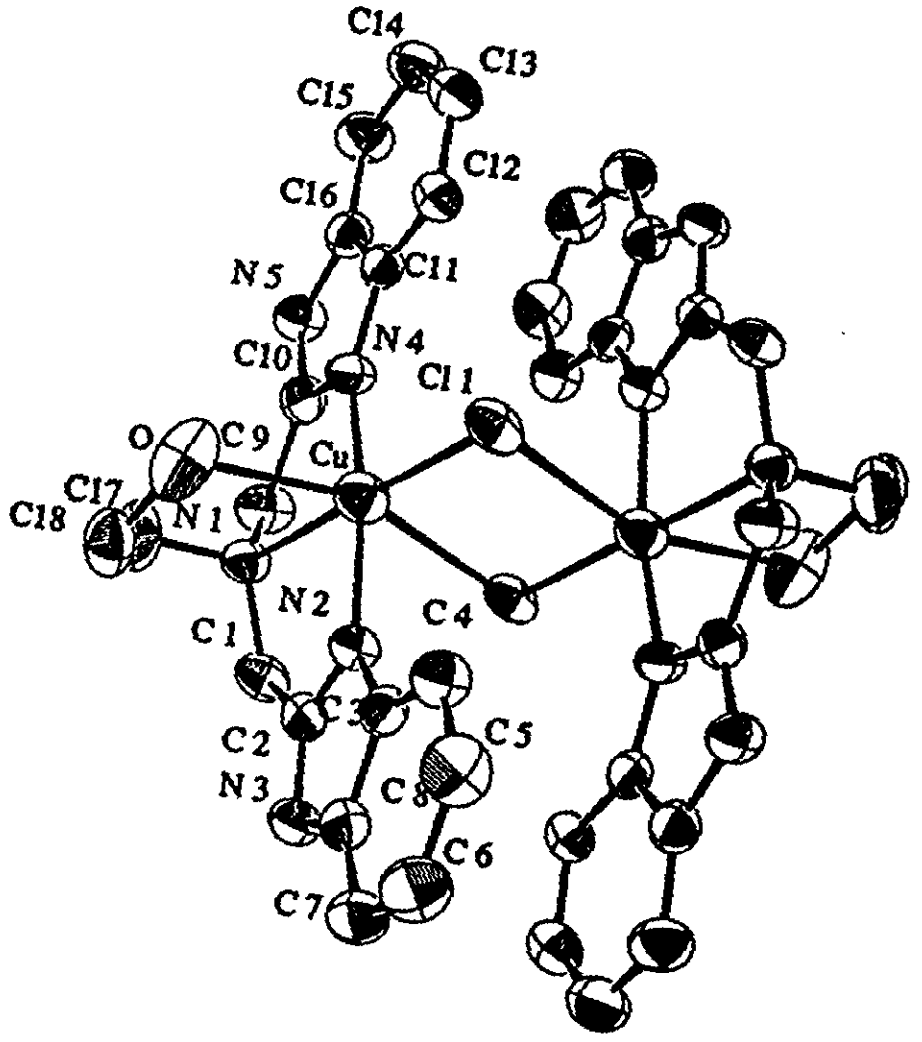
C14
C13
C15
C12
C16
C11
N5
N4
C10
Cl1
O
C9
Cu
C17
C18
N1
N2
C4
C1
C3
C5
C2
N3
C8
C6
C7

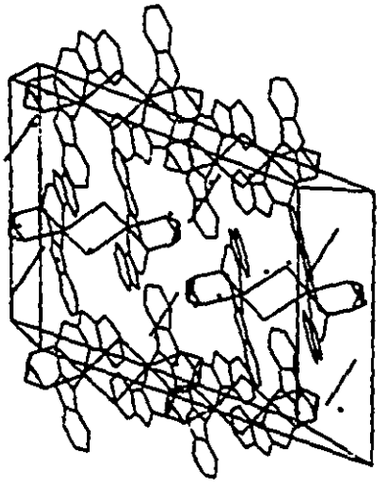

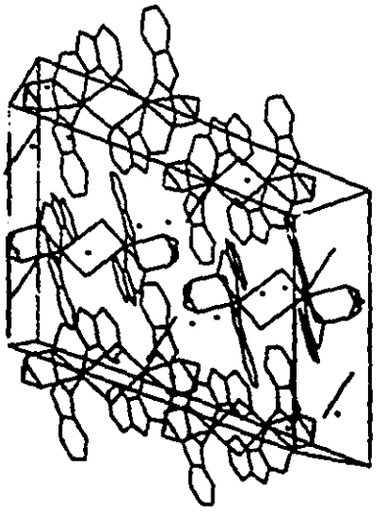

DAPH8 - DAPHNE/CHIN - MAY 93

Space Group and Cell Dimensions Monoclinic, A 2/a
a 14.324(4) b 17.158(5) c 18.712(5)
beta 109.305(18)
Volume 4340.3(19)A**3

Empirical formula : Cu C18 H25 N5 O4 Cl2

Cell dimensions were obtained from 25 reflections with 2Theta angle in the range 90.00 - 100.00 degrees.

Crystal dimensions : 0.40 X 0.20 X 0.20 mm

FW = 509.88 Z = 8 F(000) = 2104

Dcalc 1.561Mg.m-3, mu 4.02mm-1, lambda 1.54056A, 2Theta(max) 110.0

The intensity data were collected on a Rigaku diffractometer, using the theta/2theta scan mode.
The h,k,l ranges used during structure solution and refinement are :--
Hmin,max -15 14; Kmin,max 0 18; Lmin,max 0 19

No. of reflections measured	2879
No. of unique reflections	2745
No. of reflections with Inet > 2.5sigma(Inet)	2382

Absorption corrections were made.
The minimum and maximum transmission factors are 0.454485 and 0.519666.

The last least squares cycle was calculated with 52 atoms, 280 parameters and 2379 out of 2742 reflections.
Weights based on counting statistics were used.

The residuals are as follows :--
For significant reflections, RF 0.059, Rw 0.069 GoF 3.59
For all reflections, RF 0.067, Rw 0.073.
where RF = Sum(Fo-Fc)/Sum(Fo),
Rw = Sqrt[Sum(w(Fo-Fc)**2)/Sum(wFo**2)] and
GoF = Sqrt[Sum(w(Fo-Fc)**2)/(No. of reflns - No. of params.)]
The maximum shift/sigma ratio was 0.003.

In the last D-map, the deepest hole was -0.680e/A**3, and the highest peak 0.840e/A**3.

Standard intensities monitored throughout data collection showed an average decrease of 0.6%. Merging R was 2.1% for 134 pairs of symmetry-related reflections. Structure was solved by direct methods; hydrogens were calculated. Hydrogens on the solvent water molecules were omitted. Structure was refined by full-matrix least-squares with all non-hydrogens anisotropic. C(18) is disordered in two positions with occupancies of 0.35 and 0.65. There are three water molecules per copper. The structure exists as a loosely associated dimer arranged about an inversion centre with asymmetric Cl bridges. The copper of one moiety interacts with the Cl of the other with a Cu-Cl distance of 3.1849(24)A. The OH is also coordinated to the metal through a long Cu-O bond of 2.509(6)A. All computing done using the NRCVAX system of crystallographic software.

The following references are relevant to the NRCVAX System.

1. Full System Reference :
NRCVAX, Gabe, E.J., Le Page, Y., Charland, J.-P., Lee, F.L. and White, P.S. (1989) J. Appl. Cryst., 22, 384-387.

2. Scattering Factors from Int. Tab. Vol. 4 :
International Tables for X-ray Crystallography, Vol. IV, (1974) Kynoch Press, Birmingham, England.

3. ORTEP Plotting :
Johnson, C.K., (1976) ORTEP - A Fortran Thermal Ellipsoid Plot Program, Tehnical Report ORNL-5138, Oak Ridge Tennessee.

Table 2. Atomic Parameters x,y,z and Beq
E.S.Ds. refer to the last digit printed.

	x	y	z	Beq
Cu	0.94620(7)	0.22742(6)	0.14970(6)	3.49(5)
Cl 1	0.88323(15)	0.17367(11)	0.23257(11)	3.28(9)
Cl 2	0.8599 (3)	0.61598(20)	0.04851(19)	8.14(19)
O	0.8510 (5)	0.1611 (4)	0.0279 (3)	5.4 (3)
N 1	1.0075 (4)	0.2794 (3)	0.0727 (3)	2.9 (3)
N 2	1.0487 (4)	0.1506 (3)	0.1574 (3)	2.6 (3)
N 3	1.1832 (4)	0.1177 (4)	0.1308 (3)	3.1 (3)
N 4	0.8694 (4)	0.3240 (3)	0.1315 (3)	2.7 (3)
N 5	0.8522 (5)	0.4455 (3)	0.0877 (4)	3.2 (3)
C 1	1.1117 (5)	0.2530 (4)	0.0941 (4)	3.2 (4)
C 2	1.1164 (5)	0.1736 (4)	0.1281 (4)	2.8 (3)
C 3	1.0724 (5)	0.0733 (4)	0.1812 (4)	2.9 (3)
C 4	1.0260 (6)	0.0199 (5)	0.2142 (4)	3.5 (4)
C 5	1.0674 (7)	-0.0531 (5)	0.2289 (5)	4.5 (5)
C 6	1.1526 (7)	-0.0730 (5)	0.2128 (5)	4.6 (5)
C 7	1.1994 (6)	-0.0216 (5)	0.1797 (5)	3.9 (4)
C 8	1.1575 (6)	0.0527 (4)	0.1646 (4)	3.1 (4)
C 9	0.9980 (6)	0.3653 (5)	0.0797 (5)	3.8 (4)
C10	0.9051 (5)	0.3792 (4)	0.0984 (4)	3.0 (3)
C11	0.7872 (5)	0.3565 (4)	0.1441 (4)	2.6 (3)
C12	0.7207 (5)	0.3258 (4)	0.1764 (4)	3.0 (3)
C13	0.6443 (6)	0.3729 (5)	0.1788 (5)	3.7 (4)
C14	0.6329 (6)	0.4484 (5)	0.1495 (5)	4.3 (4)
C15	0.6976 (6)	0.4801 (5)	0.1180 (5)	4.1 (4)
C16	0.7751 (5)	0.4325 (4)	0.1161 (4)	3.1 (4)
C17	0.9509 (7)	0.2546 (7)	-0.0052 (5)	5.8 (6)
C18	0.9211 (13)	0.1820 (9)	-0.0189 (7)	4.7 (8)
C18'	0.8499 (18)	0.2174 (14)	-0.0230 (12)	3.5 (11)
OW1	0.9148 (6)	0.7406 (4)	0.1718 (4)	6.7 (4)
OW2	1.3392 (5)	0.1413 (4)	0.0650 (4)	5.9 (4)
OW3	0.4108 (8)	0.9971 (6)	0.0242 (5)	10.8 (7)

Beq is the mean of the principal axes of the thermal ellipsoid.

Table 3. Bond Distances in Angstroms

Cu-Cl(1)	2.2346(20)	N(5)-C(16)	1.393(9)
Cu-Cl(1)a	3.1849(24)	C(1)-C(2)	1.496(10)
Cu-O	2.509(6)	C(3)-C(4)	1.390(11)
Cu-N(1)	2.116(6)	C(3)-C(8)	1.399(10)
Cu-N(2)	1.942(6)	C(4)-C(5)	1.375(11)
Cu-N(4)	1.956(6)	C(5)-C(6)	1.394(13)
Cl(1)-Cua	3.1849(24)	C(6)-C(7)	1.373(13)
O-C(18)	1.576(18)	C(7)-C(8)	1.397(11)
O-C(18')	1.352(23)	C(9)-C(10)	1.503(10)
N(1)-C(1)	1.482(9)	C(11)-C(12)	1.390(10)
N(1)-C(9)	1.491(10)	C(11)-C(16)	1.395(10)
N(1)-C(17)	1.477(11)	C(12)-C(13)	1.372(11)
N(2)-C(2)	1.322(9)	C(13)-C(14)	1.396(12)
N(2)-C(3)	1.406(9)	C(14)-C(15)	1.364(12)
N(3)-C(2)	1.342(9)	C(15)-C(16)	1.389(11)
N(3)-C(8)	1.391(10)	C(17)-C(18)	1.315(19)
N(4)-C(10)	1.323(9)	C(17)-C(18')	1.514(25)
N(4)-C(11)	1.393(9)		
N(5)-C(10)	1.344(10)		

Table 4. Bond Angles in Degrees

Cl(1)-Cu-Cl(1)a	97.65(7)	N(2)-C(2)-C(1)	120.7(6)
Cl(1)-Cu-O	102.75(15)	N(3)-C(2)-C(1)	126.8(6)
Cl(1)-Cu-N(1)	179.05(18)	N(2)-C(3)-C(4)	131.5(7)
Cl(1)-Cu-N(2)	97.90(17)	N(2)-C(3)-C(8)	107.7(6)
Cl(1)-Cu-N(4)	97.95(17)	C(4)-C(3)-C(8)	120.8(7)
Cl(1)a-Cu-O	158.80(15)	C(3)-C(4)-C(5)	116.8(7)
Cl(1)a-Cu-N(1)	81.40(17)	C(4)-C(5)-C(6)	122.1(8)
Cl(1)a-Cu-N(2)	85.53(18)	C(5)-C(6)-C(7)	122.2(7)
Cl(1)a-Cu-N(4)	85.84(18)	C(6)-C(7)-C(8)	115.9(7)
O-Cu-N(1)	78.20(21)	N(3)-C(8)-C(3)	105.2(6)
O-Cu-N(2)	86.00(23)	N(3)-C(8)-C(7)	131.6(7)
O-Cu-N(4)	96.91(23)	C(3)-C(8)-C(7)	122.2(7)
N(1)-Cu-N(2)	82.09(23)	N(1)-C(9)-C(10)	106.9(6)
N(1)-Cu-N(4)	81.96(23)	N(4)-C(10)-N(5)	113.0(6)
N(2)-Cu-N(4)	162.82(23)	N(4)-C(10)-C(9)	120.3(6)
Cu-Cl(1)-Cua	82.35(7)	N(5)-C(10)-C(9)	126.7(6)
Cu-O-C(18)	98.5(6)	N(4)-C(11)-C(12)	131.5(6)
Cu-O-C(18')	101.1(10)	N(4)-C(11)-C(16)	108.5(6)
C(18)-O-C(18')	46.2(12)	C(12)-C(11)-C(16)	120.0(7)
Cu-N(1)-C(1)	107.1(4)	C(11)-C(12)-C(13)	117.4(7)
Cu-N(1)-C(9)	106.7(4)	C(12)-C(13)-C(14)	121.6(7)
Cu-N(1)-C(17)	109.6(5)	C(13)-C(14)-C(15)	122.2(7)
C(1)-N(1)-C(9)	113.0(6)	C(14)-C(15)-C(16)	116.1(7)
C(1)-N(1)-C(17)	110.8(6)	N(5)-C(16)-C(11)	106.1(6)
C(9)-N(1)-C(17)	109.5(7)	N(5)-C(16)-C(15)	131.1(7)
Cu-N(2)-C(2)	114.1(5)	C(11)-C(16)-C(15)	122.7(7)
Cu-N(2)-C(3)	139.6(5)	N(1)-C(17)-C(18)	120.2(10)
C(2)-N(2)-C(3)	106.2(6)	O-C(18)-C(17)	109.4(10)
C(2)-N(3)-C(8)	107.4(6)	O-C(18')-C(17)	111.0(16)
Cu-N(4)-C(10)	114.0(5)		
Cu-N(4)-C(11)	140.2(5)		
C(10)-N(4)-C(11)	105.8(6)		
C(10)-N(5)-C(16)	106.6(6)		
N(1)-C(1)-C(2)	107.1(6)		
N(2)-C(2)-N(3)	112.5(6)		

Atoms flagged 'a' are symmetry equivalents.

Cl(1)a	1.11677	0.32633	0.26743	2.000-x	0.500-y	0.500-z
Cua	1.05380	0.27258	0.35030	2.000-x	0.500-y	0.500-z

Table S-2. Calculated Hydrogen Atom Parameters

	x	y	z	Biso
HO	0.813	0.108	0.034	5.6
HN3	1.244	0.123	0.107	3.4
HN5	0.879	0.504	0.077	3.5
H 1A	1.133	0.250	0.044	3.9
H 1B	1.159	0.292	0.134	3.9
H 4	0.962	0.035	0.228	4.3
H 5	1.033	-0.096	0.254	5.3
H 6	1.182	-0.131	0.226	5.2
H 7	1.264	-0.037	0.167	4.7
H 9A	1.060	0.388	0.123	4.8
H 9B	0.991	0.393	0.026	4.8
H12	0.728	0.268	0.199	3.7
H13	0.592	0.351	0.205	4.4
H14	0.688	0.537	0.095	5.0
H15	0.572	0.482	0.152	5.3
H17A	0.995	0.267	-0.040	6.8
H17B	0.885	0.291	-0.024	6.8
H18A	0.880	0.174	-0.078	5.2
H18B	0.983	0.143	-0.002	5.2
H18'A	0.832	0.191	-0.078	4.2
H18'B	0.798	0.261	-0.022	4.2

Hydrogen positions calculated assuming C-H distance of 1.08A. Biso(H) is from Uiso(H) = Ueq(C) + 0.01.

Table S-3. Anisotropic u(i,j) values *100.
E.S.Ds. refer to the last digit printed

	u11	u22	u33	u12	u13	u23
Cu	4.63(6)	4.18(6)	5.00(6)	0.27(5)	2.33(5)	0.65(5)
Cl 1	5.04(12)	3.38(11)	5.25(12)	-0.01(9)	3.34(10)	0.85(9)
Cl 2	11.3 (3)	9.54(23)	10.24(24)	-1.69(20)	3.73(20)	1.54(19)
O	7.2 (4)	5.4 (4)	6.3 (4)	-2.7 (3)	-0.1 (3)	1.4 (3)
N 1	3.4 (3)	3.8 (4)	4.0 (4)	0.1 (3)	1.7 (3)	0.8 (3)
N 2	3.5 (3)	2.6 (3)	4.0 (4)	0.0 (3)	1.6 (3)	0.3 (3)
N 3	3.7 (4)	4.2 (4)	4.5 (4)	0.4 (3)	2.0 (3)	0.2 (3)
N 4	3.1 (3)	3.4 (4)	4.2 (4)	0.5 (3)	1.7 (3)	0.9 (3)
N 5	4.3 (4)	3.3 (4)	5.1 (4)	1.0 (3)	2.1 (3)	1.6 (3)
C 1	4.0 (4)	3.6 (4)	5.2 (5)	-0.2 (3)	2.6 (4)	0.1 (4)
C 2	3.7 (4)	3.7 (4)	3.3 (4)	0.4 (4)	1.3 (3)	0.1 (3)
C 3	3.5 (4)	3.8 (5)	3.2 (4)	0.4 (4)	0.6 (3)	-0.1 (4)
C 4	4.8 (5)	3.8 (5)	5.0 (5)	0.1 (4)	1.9 (4)	0.6 (4)
C 5	7.4 (6)	3.4 (5)	6.6 (6)	0.3 (5)	2.9 (5)	1.4 (4)
C 6	6.9 (6)	3.8 (5)	6.7 (6)	1.6 (5)	2.3 (5)	0.9 (5)
C 7	5.3 (5)	4.4 (5)	5.4 (5)	1.6 (4)	2.0 (4)	0.3 (4)
C 8	4.1 (5)	4.1 (5)	3.7 (4)	0.4 (4)	1.2 (4)	-0.1 (4)
C 9	4.7 (5)	4.3 (5)	6.3 (6)	1.0 (4)	2.9 (4)	2.4 (4)
C10	3.7 (4)	4.3 (5)	3.6 (4)	0.0 (4)	1.5 (4)	0.8 (4)
C11	3.4 (4)	3.4 (4)	3.0 (4)	0.4 (3)	0.8 (3)	0.0 (3)
C12	4.0 (4)	3.9 (4)	3.9 (4)	-0.2 (4)	1.7 (4)	-0.1 (4)
C13	4.5 (5)	5.2 (5)	5.0 (5)	0.0 (4)	2.4 (4)	-0.3 (4)
C14	5.2 (6)	5.7 (6)	6.2 (6)	1.2 (4)	2.8 (5)	0.2 (5)
C15	5.5 (5)	4.3 (5)	6.2 (6)	1.9 (4)	2.4 (5)	0.8 (4)
C16	3.9 (5)	4.2 (5)	3.8 (4)	0.1 (4)	1.2 (4)	0.4 (4)
C17	5.8 (6)	12.9 (10)	3.6 (5)	-2.5 (6)	1.7 (4)	0.1 (6)
C18	8.0 (11)	5.0 (9)	4.1 (8)	0.9 (9)	1.2 (8)	-0.6 (7)
C18'	4.7 (14)	4.5 (15)	3.8 (13)	-0.8 (13)	1.2 (11)	0.3 (12)
OW1	11.8 (6)	5.0 (4)	7.4 (5)	2.0 (4)	1.7 (4)	-0.2 (3)
OW2	6.4 (4)	10.2 (5)	7.3 (4)	-0.9 (4)	4.4 (4)	-1.6 (4)
OW3	19.0 (10)	10.7 (7)	10.3 (7)	2.3 (7)	3.2 (7)	2.9 (6)

Anisotropic Temperature Factors are of the form
Temp=-2*Pi*Pi*(h*h*u11*astar*astar+---+2*h*k*u12*astar*bstar+---)

Appendix 4: X-ray Supplemental Material for μ-dimethylphosphato-[(N,N,N',N'-tetrakis(2-benzimidazolyl)-2-hydroxy-1,3-di-aminopropane)dicopper(II)] diperchlorate·H_2O

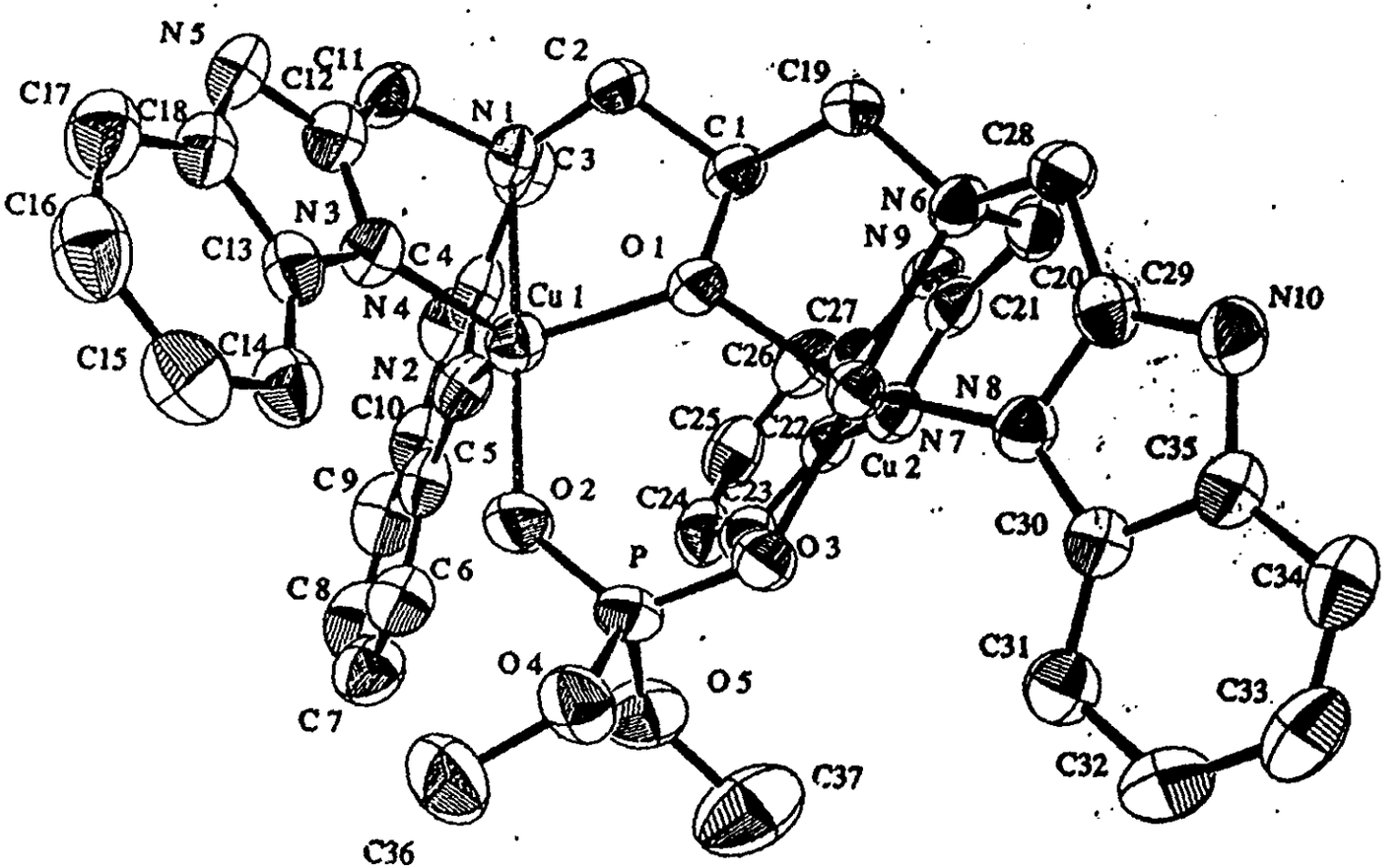
N5
C11
C12
C2
C19
C17
C18
N1
C1
C28
C3
C16
N3
N6
C13
C4
O1
N9
C20
C29
N10
Cu 1
N4
C27
C21
C15
C14
C26
N2
N8
C10
C25
C22
N7
C35
C5
Cu 2
C9
O2
C24
C23
C30
O3
P
C34
C8
C6
C31
O4
O5
C33
C7
C32
C37
C36

DAPH6 - DAPHNE/CHIN - MAR 93

Space Group and Cell Dimensions Triclinic, P -1
a 13.250(3) b 13.891(5) c 15.575(3)
alpha 92.18(3) beta 114.883(15) gamma 109.452(24)
Volume 2398.4(11)A**3

Empirical formula : Cu2 C40 H47 N10 O15 P Cl2

Cell dimensions were obtained from 25 reflections with 2Theta angle in the range 27.00 - 33.00 degrees.

Crystal dimensions : 0.50 X 0.35 X 0.15 mm

FW = 1136.84 Z = 2 F(000) = 1168

Dcalc 1.574Mg.m-3, mu 1.11mm-1, lambda 0.70930A, 2Theta(max) 45.0

The intensity data were collected on a Rigaku diffractometer, controlled by TEXRAY software, using the theta/2theta scan mode.
The h,k,l ranges used during structure solution and refinement are :--
Hmin,max -14 13; Kmin,max 0 14; Lmin,max -16 16
No. of reflections measured 6624
No. of unique reflections 6289
No. of reflections with Inet > 2.5sigma(Inet) 4649
No correction was made for absorption

The last least squares cycle was calculated with
115 atoms, 631 parameters and 4649 out of 6289 reflections.
Weights based on counting-statistics were used.
The weight modifier K in KFo**2 is 0.000050

The residuals are as follows :--
For significant reflections, RF 0.049, Rw 0.050 GoF 2.22
For all reflections, RF 0.076, Rw 0.051.
where RF = Sum(Fo-Fc)/Sum(Fo),
Rw = Sqrt[Sum(w(Fo-Fc)**2)/Sum(wFo**2)] and
GoF = Sqrt[Sum(w(Fo-Fc)**2)/(No. of reflns - No. of params.)]
The maximum shift/sigma ratio was 0.302.

In the last D-map, the deepest hole was -0.510e/A**3,
and the highest peak 0.640e/A**3.

Standard intensities remained constant over the course of collection (average decrease 0.4%). Merging R was 1.0% for 335 pairs of symmetry related reflections. Structure was solved by direct methods followed by a difference map. Hydrogens were calculated except water protons which were omitted. Structure was refined by least-squares with all non-hydrogen atoms anisotropic. The asymmetric unit contains a complex cation, two perchlorates, one acetone and one water molecule of solvation. All computing done using the NRCVAX system of crystallographic software.

The following references are relevant to the NRCVAX System.

1. Full System Reference :
   NRCVAX, Gabe, E.J., Le Page, Y., Charland,.J.-P., Lee, F.l. and White, P.S. (1989) J. Appl. Cryst., 22, 384-387.

2. Scattering Factors from Int. Tab. Vol. 4 :
   International Tables for X-ray Crystallography, Vol. IV, (1974) Kynoch Press, Birmingham, England.

3. ORTEP Plotting :
   Johnson, C.K., (1976) ORTEP - A Fortran Thermal Ellipsoid Plot Program, Tehnical Report ORNL-5138, Oak Ridge Tennessee.

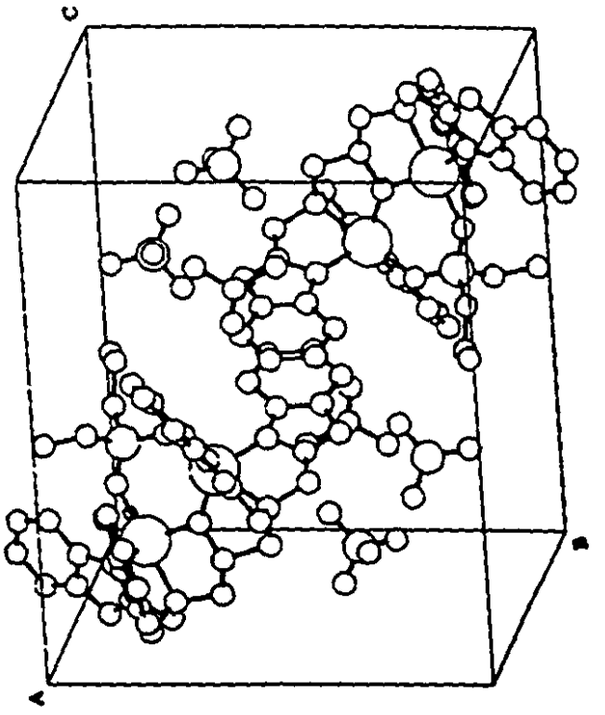
c
a

Table 2. Atomic Parameters x,y,z and Beq
E.S.Ds. refer to the last digit printed.

	x	y	z	Beq
Cu 1	0.46702(7)	0.67916(6)	0.71662(5)	3.12(4)
Cu 2	0.68982(6)	0.88176(6)	0.92593(5)	2.80(4)
P	0.61872(15)	0.90605(13)	0.70957(12)	3.15(10)
O 1	0.5788 (3)	0.7411 (3)	0.8563 (3)	3.01(24)
O 2	0.5339 (4)	0.7950 (3)	0.6656 (3)	4.3 (3)
O 3	0.6959 (3)	0.9390 (3)	0.8156 (3)	3.6 (3)
O 4	0.7072 (4)	0.9372 (3)	0.6642 (3)	4.5 (3)
O 5	0.5397 (4)	0.9735 (3)	0.6726 (3)	5.0 (3)
N 1	0.3907 (4)	0.5531 (4)	0.7696 (3)	3.2 (3)
N 2	0.2936 (4)	0.6620 (4)	0.6442 (3)	3.5 (3)
N 3	0.5205 (4)	0.5697 (4)	0.6705 (3)	3.3 (3)
N 4	0.1088 (4)	0.5939 (4)	0.6302 (4)	4.3 (3)
N 5	0.4996 (4)	0.4040 (4)	0.6530 (3)	3.7 (3)
N 6	0.6974 (4)	0.8244 (4)	1.0497 (3)	3.0 (3)
N 7	0.5283 (4)	0.9090 (4)	0.9335 (3)	3.0 (3)
N 8	0.8476 (4)	0.9856 (3)	1.0211 (3)	2.9 (3)
N 9	0.4164 (4)	0.8374 (4)	1.0060 (3)	3.3 (3)
N10	1.0027 (4)	1.0292 (4)	1.1678 (3)	3.7 (3)
C 1	0.5337 (5)	0.6848 (4)	0.9154 (4)	3.1 (4)
C 2	0.4807 (5)	0.5700 (4)	0.8704 (4)	3.3 (4)
C 3	0.2743 (5)	0.5520 (5)	0.7596 (5)	3.9 (4)
C 4	0.2254 (5)	0.6013 (5)	0.6778 (4)	3.7 (4)
C 5	0.2199 (5)	0.6989 (5)	0.5715 (4)	3.7 (4)
C 6	0.2464 (6)	0.7681 (5)	0.5157 (5)	4.6 (4)
C 7	0.1529 (6)	0.7923 (6)	0.4511 (5)	5.4 (5)
C 8	0.0373 (6)	0.7478 (6)	0.4417 (5)	6.4 (5)
C 9	0.0098 (6)	0.6803 (6)	0.4973 (5)	5.7 (5)
C10	0.1038 (5)	0.6548 (5)	0.5632 (5)	4.3 (4)
C11	0.3715 (5)	0.4550 (5)	0.7125 (4)	4.0 (4)
C12	0.4666 (5)	0.4763 (5)	0.6805 (4)	3.3 (4)
C13	0.5955 (5)	0.5577 (5)	0.6335 (4)	3.3 (4)
C14	0.6722 (6)	0.6307 (5)	0.6069 (4)	3.9 (4)
C15	0.7352 (6)	0.5959 (6)	0.5705 (5)	4.9 (5)
C16	0.7223 (6)	0.4918 (6)	0.5592 (5)	5.3 (5)
C17	0.6447 (6)	0.4191 (5)	0.5851 (5)	5.0 (5)
C18	0.5826 (5)	0.4541 (5)	0.6221 (4)	3.7 (4)
C19	0.6363 (5)	0.7093 (5)	1.0160 (4)	3.4 (4)
C20	0.6372 (5)	0.8709 (5)	1.0907 (4)	3.5 (4)
C21	0.5274 (5)	0.8747 (4)	1.0098 (4)	3.1 (4)
C22	0.4067 (5)	0.8907 (4)	0.8714 (4)	3.1 (4)
C23	0.3533 (5)	0.9076 (5)	0.7788 (4)	3.5 (4)
C24	0.2299 (6)	0.8793 (5)	0.7350 (5)	4.4 (4)
C25	0.1622 (6)	0.8358 (5)	0.7819 (5)	4.7 (5)
C26	0.2126 (6)	0.8174 (5)	0.8731 (5)	4.6 (5)
C27	0.3376 (5)	0.8458 (4)	0.9176 (4)	3.2 (4)
C28	0.8272 (5)	0.8583 (5)	1.1231 (4)	3.4 (4)
C29	0.8922 (5)	0.9590 (5)	1.1051 (4)	3.3 (4)
C30	0.9351 (5)	1.0811 (5)	1.0294 (4)	3.1 (4)
C31	0.9352 (5)	1.1454 (5)	0.9629 (4)	3.8 (4)
C32	1.0367 (6)	1.2380 (5)	0.9964 (5)	4.7 (5)
C33	1.1331 (5)	1.2641 (5)	1.0877 (5)	4.7 (4)
C34	1.1332 (5)	1.1996 (5)	1.1517 (5)	4.2 (4)
C35	1.0315 (5)	1.1078 (5)	1.1205 (4)	3.5 (4)
C36	0.6582 (7)	0.9189 (6)	0.5603 (5)	6.7 (6)
C37	0.5929 (7)	1.0837 (6)	0.7087 (7)	8.0 (7)

Table 2. (cont'd) Atomic Parameters x,y,z and Beq
E.S.Ds. refer to the last digit printed.

	x	y	z	Beq
OW	0.0329 (4)	0.0155 (5)	0.3611 (3)	8.2 (4)
Cl 1	0.24897(15)	0.16071(13)	0.62384(12)	4.14(10)
Cl 2	0.30327(18)	0.58886(16)	0.06028(15)	5.98(15)
O 6	0.3732 (4)	0.1837 (4)	0.6647 (4)	8.1 (4)
O 7	0.2182 (5)	0.2157 (4)	0.5490 (4)	7.8 (4)
O 8	0.2221 (5)	0.1949 (5)	0.6951 (4)	8.5 (5)
O 9	0.1832 (6)	0.0551 (4)	0.5855 (5)	10.8 (5)
O10	0.2883 (6)	0.5240 (4)	0.1214 (4)	9.0 (5)
O11	0.2655 (8)	0.6661 (6)	0.0627 (7)	16.6 (10)
O12	0.4218 (7)	0.6303 (7)	0.0852 (8)	20.2 (11)
O13	0.2676 (12)	0.5434 (10)	-0.0246 (6)	24.8 (15)
O14	0.0167 (5)	0.5374 (5)	0.2871 (4)	7.8 (5)
C38	0.0520 (6)	0.5349 (6)	0.2296 (5)	6.0 (6)
C39	0.0499 (8)	0.4407 (7)	0.1845 (7)	8.6 (7)
C40	0.1105 (11)	0.6319 (8)	0.2037 (8)	11.7 (11)

Beq is the mean of the principal axes of the thermal ellipsoid.

Table 3. Bond Distances in Angstroms

Cu(1)-O(1)	1.991(4)	C(3)-C(4)	1.476(9)
Cu(1)-O(2)	1.935(4)	C(5)-C(6)	1.378(9)
Cu(1)-N(1)	2.099(5)	C(5)-C(10)	1.399(9)
Cu(1)-N(2)	2.011(5)	C(6)-C(7)	1.384(9)
Cu(1)-N(3)	2.096(5)	C(7)-C(8)	1.387(10)
Cu(2)-O(1)	1.934(4)	C(8)-C(9)	1.365(12)
Cu(2)-O(3)	1.941(4)	C(9)-C(10)	1.405(9)
Cu(2)-N(6)	2.091(5)	C(11)-C(12)	1.488(8)
Cu(2)-N(7)	2.342(4)	C(13)-C(14)	1.390(9)
Cu(2)-N(8)	1.967(4)	C(13)-C(18)	1.387(9)
P-O(2)	1.493(4)	C(14)-C(15)	1.378(9)
P-O(3)	1.481(4)	C(15)-C(16)	1.394(10)
P-O(4)	1.563(4)	C(16)-C(17)	1.389(10)
P-O(5)	1.578(4)	C(17)-C(18)	1.375(9)
O(1)-C(1)	1.423(7)	C(20)-C(21)	1.490(8)
O(4)-C(36)	1.442(8)	C(22)-C(23)	1.384(8)
O(5)-C(37)	1.429(9)	C(22)-C(27)	1.396(8)
N(1)-C(2)	1.467(7)	C(23)-C(24)	1.381(9)
N(1)-C(3)	1.478(7)	C(24)-C(25)	1.389(10)
N(1)-C(11)	1.483(8)	C(25)-C(26)	1.368(10)
N(2)-C(4)	1.312(8)	C(26)-C(27)	1.399(9)
N(2)-C(5)	1.394(8)	C(28)-C(29)	1.485(8)
N(3)-C(12)	1.308(8)	C(30)-C(31)	1.394(8)
N(3)-C(13)	1.390(7)	C(30)-C(35)	1.379(8)
N(4)-C(4)	1.368(8)	C(31)-C(32)	1.394(9)
N(4)-C(10)	1.362(9)	C(32)-C(33)	1.381(10)
N(5)-C(12)	1.341(7)	C(33)-C(34)	1.367(10)
N(5)-C(18)	1.374(8)	C(34)-C(35)	1.390(8)
N(6)-C(19)	1.485(7)	Cl(1)-O(6)	1.403(5)
N(6)-C(20)	1.484(7)	Cl(1)-O(7)	1.408(5)
N(6)-C(28)	1.500(7)	Cl(1)-O(8)	1.410(5)
N(7)-C(21)	1.301(7)	Cl(1)-O(9)	1.383(6)
N(7)-C(22)	1.412(7)	Cl(2)-O(10)	1.364(5)
N(8)-C(29)	1.315(7)	Cl(2)-O(11)	1.332(7)
N(8)-C(30)	1.399(7)	Cl(2)-O(12)	1.348(7)
N(9)-C(21)	1.361(7)	Cl(2)-O(13)	1.258(9)
N(9)-C(27)	1.373(8)	O(14)-C(38)	1.176(9)
N(10)-C(29)	1.350(7)	C(38)-C(39)	1.448(12)
N(10)-C(35)	1.379(8)	C(38)-C(40)	1.479(12)
C(1)-C(2)	1.510(8)		
C(1)-C(19)	1.508(8)		

Table 4. Bond Angles in Degrees

O(1)-Cu(1)-O(2)	97.49(16)	N(2)-C(5)-C(10)	107.6(5)
O(1)-Cu(1)-N(1)	83.49(17)	C(6)-C(5)-C(10)	121.6(6)
O(1)-Cu(1)-N(2)	127.24(18)	C(5)-C(6)-C(7)	116.9(6)
O(1)-Cu(1)-N(3)	108.55(17)	C(6)-C(7)-C(8)	121.6(7)
O(2)-Cu(1)-N(1)	178.75(18)	C(7)-C(8)-C(9)	122.2(6)
O(2)-Cu(1)-N(2)	97.50(19)	C(8)-C(9)-C(10)	116.8(6)
O(2)-Cu(1)-N(3)	99.59(19)	N(4)-C(10)-C(5)	107.0(5)
N(1)-Cu(1)-N(2)	81.27(19)	N(4)-C(10)-C(9)	132.1(6)
N(1)-Cu(1)-N(3)	80.82(18)	C(5)-C(10)-C(9)	120.8(6)
N(2)-Cu(1)-N(3)	118.22(19)	N(1)-C(11)-C(12)	109.0(5)
O(1)-Cu(2)-O(3)	97.48(16)	N(3)-C(12)-N(5)	113.5(5)
O(1)-Cu(2)-N(6)	85.15(16)	N(3)-C(12)-C(11)	121.1(5)
O(1)-Cu(2)-N(7)	87.55(16)	N(5)-C(12)-C(11)	125.2(5)
O(1)-Cu(2)-N(8)	153.10(18)	N(3)-C(13)-C(14)	129.9(6)
O(3)-Cu(2)-N(6)	175.68(17)	N(3)-C(13)-C(18)	109.3(5)
O(3)-Cu(2)-N(7)	103.30(17)	C(14)-C(13)-C(18)	120.7(5)
O(3)-Cu(2)-N(8)	94.70(17)	C(13)-C(14)-C(15)	117.3(6)
N(6)-Cu(2)-N(7)	80.18(17)	C(14)-C(15)-C(16)	121.9(6)
N(6)-Cu(2)-N(8)	81.51(18)	C(15)-C(16)-C(17)	120.5(6)
N(7)-Cu(2)-N(8)	112.82(18)	C(16)-C(17)-C(18)	117.5(6)
O(2)-P-O(3)	120.01(24)	N(5)-C(18)-C(13)	105.6(5)
O(2)-P-O(4)	109.10(25)	N(5)-C(18)-C(17)	132.3(6)
O(2)-P-O(5)	105.9(3)	C(13)-C(18)-C(17)	122.1(6)
O(3)-P-O(4)	105.57(23)	N(6)-C(19)-C(1)	108.7(5)
O(3)-P-O(5)	110.7(3)	N(6)-C(20)-C(21)	108.9(4)
O(4)-P-O(5)	104.64(25)	N(7)-C(21)-N(9)	113.9(5)
Cu(1)-O(1)-Cu(2)	132.77(20)	N(7)-C(21)-C(20)	122.4(5)
Cu(1)-O(1)-C(1)	110.9(3)	N(9)-C(21)-C(20)	123.6(5)
Cu(2)-O(1)-C(1)	110.6(3)	N(7)-C(22)-C(23)	130.5(5)
Cu(1)-O(2)-P	133.9(3)	N(7)-C(22)-C(27)	108.6(5)
Cu(2)-O(3)-P	134.38(24)	C(23)-C(22)-C(27)	121.0(5)
P-O(4)-C(36)	118.9(4)	C(22)-C(23)-C(24)	117.1(5)
P-O(5)-C(37)	119.8(4)	C(23)-C(24)-C(25)	121.5(6)
Cu(1)-N(1)-C(2)	105.1(3)	C(24)-C(25)-C(26)	122.5(6)
Cu(1)-N(1)-C(3)	109.0(4)	C(25)-C(26)-C(27)	116.1(6)
Cu(1)-N(1)-C(11)	108.6(3)	N(9)-C(27)-C(22)	106.3(5)
C(2)-N(1)-C(3)	113.4(4)	N(9)-C(27)-C(26)	131.9(5)
C(2)-N(1)-C(11)	110.3(5)	C(22)-C(27)-C(26)	121.8(6)
C(3)-N(1)-C(11)	110.1(4)	N(6)-C(28)-C(29)	106.1(5)

Table S-2. Calculated Hydrogen Atom Parameters

	x	y	z	Biso
HN4	0.062	0.537	0.660	4.9
HN5	0.449	0.321	0.640	4.3
HN9	0.404	0.794	1.059	4.3
HN10	1.027	1.011	1.239	4.2
H 1	0.463	0.705	0.919	3.7
H 2A	0.442	0.522	0.910	3.7
H 2B	0.552	0.547	0.872	3.7
H 3A	0.285	0.594	0.825	4.5
H 3B	0.212	0.472	0.746	4.5
H 6	0.337	0.801	0.524	5.2
H 7	0.170	0.848	0.407	6.1
H 8	-0.035	0.766	0.391	6.8
H 9	-0.080	0.646	0.490	6.0
H11A	0.282	0.426	0.649	4.8
H11B	0.373	0.395	0.754	4.8
H14	0.680	0.711	0.614	4.4
H15	0.796	0.649	0.549	5.7
H16	0.773	0.467	0.531	5.7
H17	0.634	0.339	0.574	5.6
H19A	0.698	0.675	1.015	3.9
H19B	0.603	0.674	1.065	3.9
H20A	0.698	0.949	1.133	4.2
H20B	0.612	0.824	1.138	4.2
H23	0.406	0.944	0.743	4.2
H24	0.184	0.888	0.662	5.0
H25	0.067	0.818	0.747	5.0
H26	0.160	0.785	0.909	4.8
H28A	0.862	0.801	1.116	4.1
H28B	0.835	0.870	1.195	4.1
H31	0.859	1.124	0.890	4.4
H32	1.042	1.293	0.948	5.4
H33	1.209	1.335	1.109	5.1
H34	1.208	1.220	1.224	4.8
H36C	0.730	0.945	0.540	7.0
H36A	0.604	0.839	0.527	7.0
H36B	0.603	0.964	0.532	7.0
H37C	0.527	1.118	0.676	8.2
H37A	0.627	1.102	0.786	8.2
H37B	0.666	1.119	0.692	8.2
H39C	0.085	0.454	0.133	8.9
H39A	0.115	0.416	0.243	8.9
H39B	-0.034	0.378	0.155	8.9
H40C	0.136	0.619	0.149	11.7
H40A	0.058	0.679	0.183	11.7
H40B	0.196	0.681	0.269	11.7

Hydrogen positions calculated assuming C/N-H of 1.08A. Biso(H) is from Uiso(H) = Ueq(C/N) + 0.01.

Table S-3. Anisotropic u(i,j) values *100.
E.S.Ds. refer to the last digit printed

	u11	u22	u33	u12	u13	u23
Cu 1	3.44(4)	3.64(5)	4.25(5)	0.90(4)	1.65(4)	0.66(4)
Cu 2	3.33(4)	3.24(4)	3.35(4)	0.75(4)	1.28(4)	0.72(4)
P	3.71(10)	4.40(11)	3.99(10)	1.43(9)	1.93(8)	1.49(9)
O 1	3.85(25)	2.88(24)	3.68(24)	0.63(20)	1.34(20)	0.59(20)
O 2	5.8 (3)	4.5 (3)	4.2 (3)	0.42(24)	1.74(23)	1.22(23)
O 3	4.4 (3)	4.2 (3)	3.9 (3)	0.49(22)	1.55(22)	1.07(22)
O 4	5.2 (3)	6.8 (3)	5.1 (3)	1.3 (3)	3.28(25)	1.5 (3)
O 5	5.5 (3)	6.2 (3)	7.4 (3)	3.2 (3)	2.3 (3)	2.7 (3)
N 1	4.2 (3)	3.6 (3)	4.2 (3)	1.2 (3)	2.2 (3)	0.1 (3)
N 2	3.7 (3)	4.1 (3)	5.5 (3)	1.4 (3)	2.1 (3)	0.2 (3)
N 3	4.0 (3)	3.9 (3)	4.6 (3)	1.4 (3)	2.1 (3)	0.4 (3)
N 4	4.0 (3)	5.5 (4)	6.3 (4)	1.0 (3)	2.4 (3)	0.3 (3)
N 5	4.5 (3)	3.7 (3)	5.3 (3)	1.4 (3)	1.9 (3)	-0.4 (3)
N 6	3.5 (3)	3.1 (3)	4.1 (3)	0.49(25)	1.6 (3)	0.39(25)
N 7	3.9 (3)	3.5 (3)	4.3 (3)	1.4 (3)	2.2 (3)	0.6 (3)
N 8	3.0 (3)	3.4 (3)	3.9 (3)	0.66(25)	1.35(25)	0.45(25)
N 9	5.1 (3)	3.2 (3)	5.0 (3)	1.6 (3)	3.0 (3)	1.2 (3)
N10	4.2 (3)	4.6 (3)	4.1 (3)	1.5 (3)	1.0 (3)	0.4 (3)
C 1	4.4 (4)	3.0 (4)	4.4 (4)	1.0 (3)	2.6 (3)	0.7 (3)
C 2	4.7 (4)	3.2 (4)	4.7 (4)	1.4 (3)	2.5 (3)	1.0 (3)
C 3	3.5 (4)	4.7 (4)	6.5 (5)	0.8 (3)	2.7 (4)	0.5 (4)
C 4	3.5 (4)	4.1 (4)	5.7 (4)	1.3 (3)	1.8 (3)	-1.0 (3)
C 5	3.7 (4)	4.5 (4)	4.7 (4)	1.6 (3)	1.0 (3)	-0.9 (3)
C 6	5.1 (5)	6.0 (5)	6.3 (5)	2.9 (4)	1.7 (4)	1.1 (4)
C 7	6.6 (5)	6.4 (5)	6.9 (5)	3.4 (4)	1.8 (4)	1.4 (4)
C 8	6.0 (5)	9.3 (7)	7.8 (6)	4.5 (5)	0.9 (5)	0.4 (5)
C 9	4.1 (4)	8.7 (6)	8.1 (5)	3.3 (4)	1.5 (4)	-0.4 (5)
C10	3.9 (4)	5.6 (5)	5.7 (4)	1.8 (4)	1.5 (4)	-0.8 (4)
C11	5.4 (4)	2.9 (4)	5.8 (4)	0.3 (3)	2.8 (4)	-0.1 (3)
C12	3.3 (4)	4.3 (4)	4.3 (4)	1.1 (3)	1.5 (3)	-0.1 (3)
C13	3.7 (4)	5.2 (4)	3.1 (4)	1.9 (3)	1.2 (3)	0.3 (3)
C14	5.5 (4)	5.7 (5)	4.5 (4)	2.8 (4)	2.4 (4)	1.0 (4)
C15	5.5 (5)	8.2 (6)	5.8 (5)	2.8 (4)	3.2 (4)	1.7 (4)
C16	6.7 (5)	9.1 (6)	5.4 (5)	4.5 (5)	2.7 (4)	0.3 (4)
C17	6.8 (5)	6.4 (5)	6.3 (5)	3.5 (4)	2.8 (4)	0.2 (4)
C18	4.6 (4)	4.6 (4)	4.2 (4)	2.1 (4)	1.4 (3)	-0.2 (3)
C19	5.3 (4)	3.6 (4)	4.0 (4)	1.7 (3)	2.2 (3)	1.1 (3)
C20	4.7 (4)	4.1 (4)	3.8 (4)	1.2 (3)	1.9 (3)	0.2 (3)
C21	4.6 (4)	2.9 (4)	4.6 (4)	1.2 (3)	2.7 (3)	0.3 (3)
C22	4.8 (4)	3.0 (4)	4.8 (4)	1.6 (3)	2.7 (3)	0.4 (3)
C23	5.7 (4)	3.7 (4)	4.9 (4)	2.1 (4)	2.9 (4)	0.7 (3)
C24	6.0 (5)	5.4 (5)	5.1 (4)	2.9 (4)	1.8 (4)	-0.2 (4)
C25	4.1 (4)	5.4 (5)	7.5 (5)	1.8 (4)	2.1 (4)	-0.4 (4)
C26	4.8 (4)	4.9 (5)	7.9 (5)	1.4 (4)	3.6 (4)	0.7 (4)
C27	4.5 (4)	2.7 (4)	5.1 (4)	1.1 (3)	2.8 (3)	0.4 (3)
C28	4.0 (4)	4.2 (4)	3.9 (4)	0.9 (3)	1.5 (3)	1.0 (3)
C29	3.4 (4)	4.7 (4)	3.7 (4)	1.5 (3)	1.2 (3)	0.4 (3)
C30	3.4 (4)	3.9 (4)	4.3 (4)	1.3 (3)	1.6 (3)	0.5 (3)
C31	4.3 (4)	4.7 (4)	5.1 (4)	1.4 (4)	2.2 (3)	1.1 (4)
C32	5.8 (5)	4.4 (4)	8.4 (5)	1.6 (4)	4.2 (4)	2.2 (4)
C33	3.9 (4)	4.4 (4)	8.0 (5)	0.2 (4)	2.4 (4)	-0.6 (4)
C34	3.6 (4)	4.2 (4)	6.2 (5)	0.8 (3)	1.1 (4)	-0.8 (4)
C35	4.1 (4)	3.9 (4)	4.5 (4)	1.4 (3)	1.5 (3)	0.1 (3)
C36	9.3 (6)	9.5 (7)	6.2 (5)	1.4 (5)	5.1 (5)	1.4 (5)
C37	9.8 (7)	6.1 (6)	14.2 (9)	4.8 (6)	3.7 (6)	3.1 (6)

Table S-3. Anisotropic u(i,j) values *100.
E.S.Ds. refer to the last digit printed

	u11	u22	u33	u12	u13	u23
OW	7.1 (4)	16.2 (6)	5.1 (3)	2.0 (4)	2.2 (3)	2.2 (4)
Cl 1	5.18(11)	5.09(11)	5.07(11)	1.41(9)	2.41(9)	1.41(9)
Cl 2	8.21(15)	7.80(15)	9.50(16)	3.88(13)	5.70(13)	4.51(13)
O 6	5.0 (3)	10.2 (5)	14.6 (5)	3.3 (3)	3.3 (4)	3.1 (4)
O 7	12.1 (5)	11.3 (5)	7.1 (4)	5.5 (4)	4.2 (4)	5.4 (4)
O 8	12.5 (5)	16.4 (6)	7.7 (4)	7.3 (5)	6.8 (4)	3.8 (4)
O 9	13.3 (6)	5.0 (4)	16.6 (7)	-0.7 (4)	4.7 (5)	1.1 (4)
O10	15.0 (6)	9.5 (5)	15.4 (6)	5.2 (4)	11.4 (5)	7.9 (4)
O11	31.2 (10)	19.6 (8)	40.1 (13)	20.8 (8)	31.2 (11)	22.0 (9)
O12	16.2 (8)	23.3 (10)	50.2 (17)	12.0 (8)	21.7 (10)	26.8 (12)
O13	47.5 (18)	35.1 (16)	11.2 (7)	17.7 (15)	11.8 (10)	3.2 (9)
O14	9.0 (4)	11.7 (5)	11.7 (5)	3.7 (4)	7.4 (4)	2.9 (4)
C38	6.2 (5)	9.9 (7)	8.1 (6)	3.7 (5)	3.9 (5)	2.6 (5)
C39	8.9 (7)	9.2 (7)	12.3 (8)	1.7 (6)	4.7 (6)	-1.7 (6)
C40	23.6 (13)	12.3 (9)	16.6 (11)	9.7 (10)	13.6 (10)	9.0 (8)

Anisotropic Temperature Factors are of the form
Temp=-2*Pi*Pi*(h*h*u11*astar*astar+---+2*h*k*u12*astar*bstar+---)

Appendix 5: X-ray Supplemental Material for μ-dimethylphosphato-di-μ-hydroxy-bis[(1,4,7-triazacyclononane)cobalt(III)] triperchlorate·H_2O

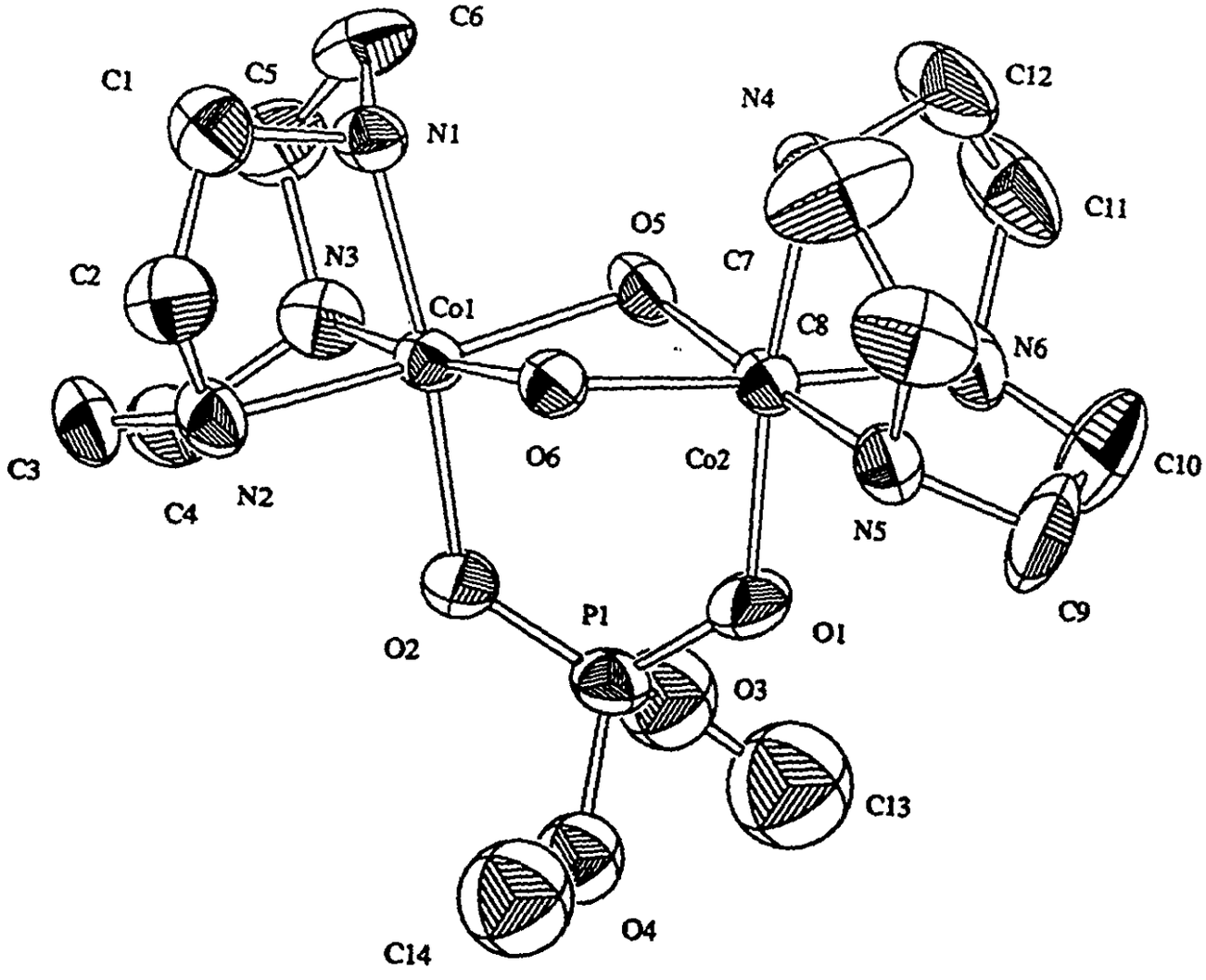
C6
C1
C5
N1
N4
C12
C11
O5
C7
N3
C2
Co1
C8
N6
O6
Co2
C3
C4
N2
N5
C10
C9
P1
O1
O2
O3
C13
O4
C14

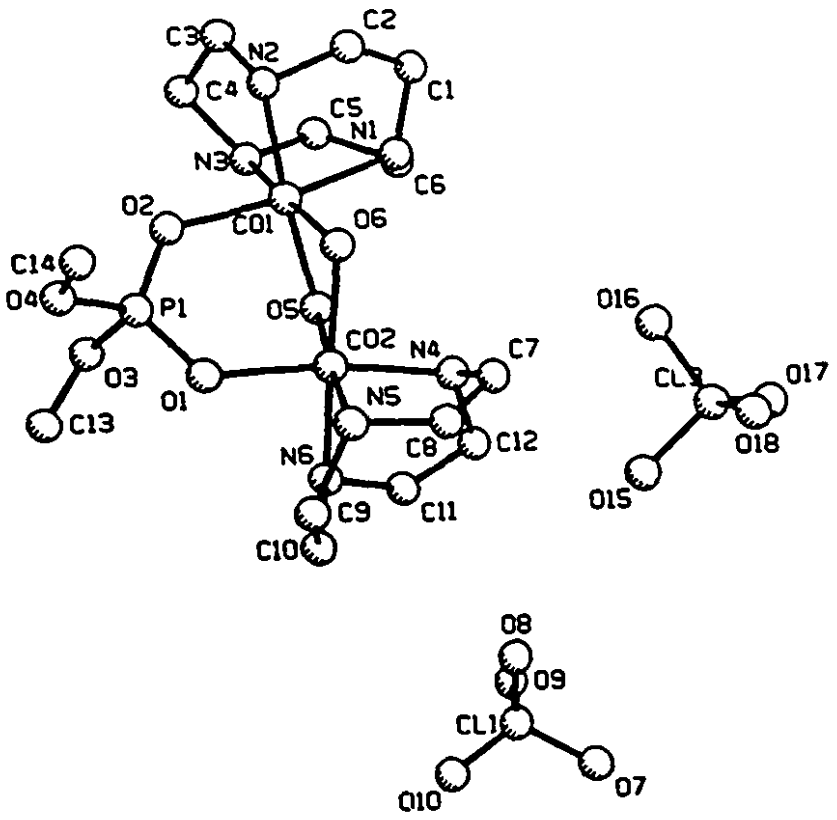
C3
N2
C2
C4
C1
C5
N1
N3
C6
O2
C01
O6
C14
O4
P1
O5
C02
N4
C7
O3
O1
N5
C13
C8
C12
N6
C9
C11
C10
O16
CL3
O17
O18
O15
O8
O9
CL1
O10
O7
O12
CL2
O11
O13
O14
O(W)

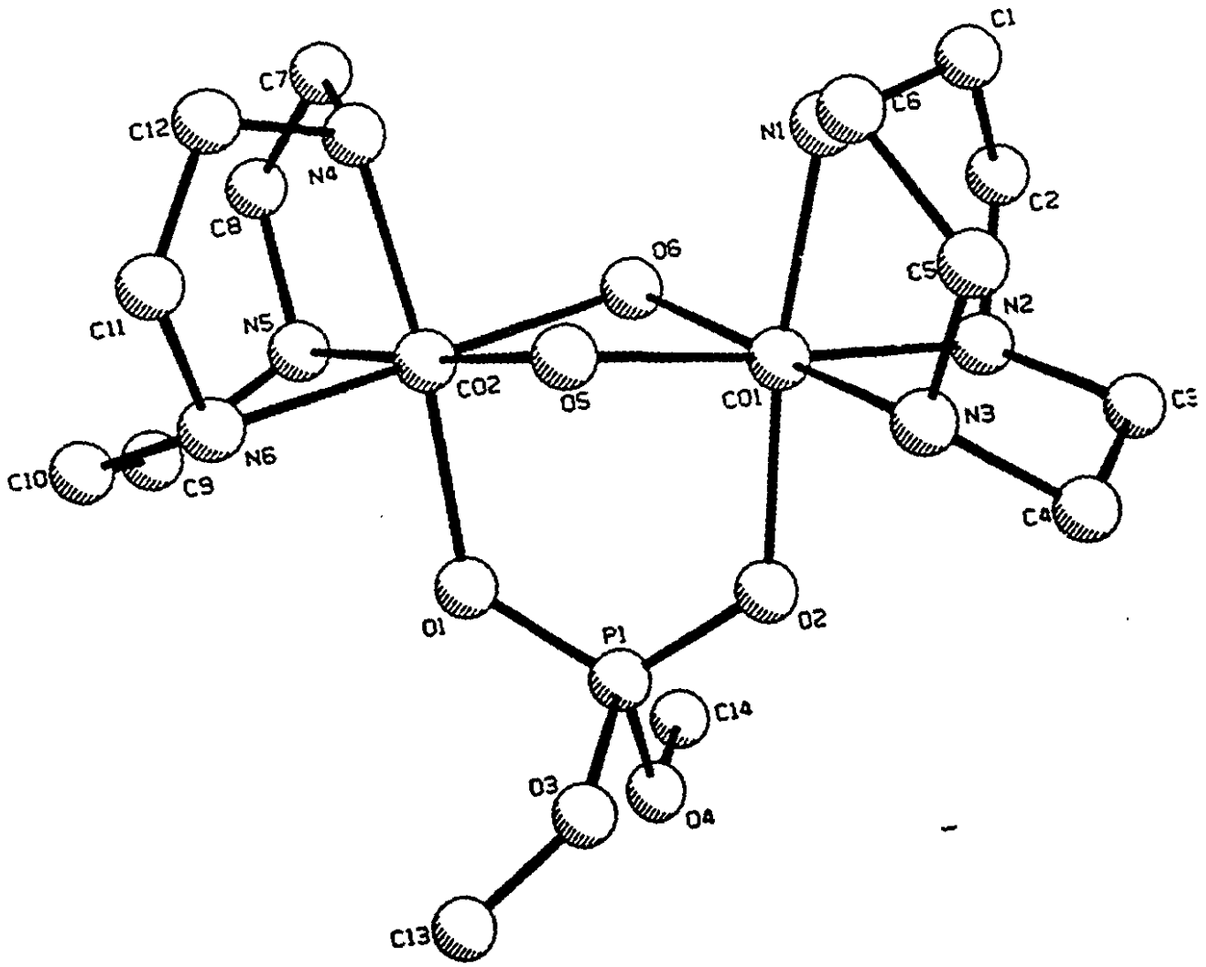
C1
C7
C12
C6
N1
N4
C2
C8
O6
C5
C11
N5
N2
CO2
O5
CO1
N3
C3
N6
C10
C9
C4
O1
P1
O2
C14
O3
O4
C13

[Co2 [9] and N3(OH)2PO2(OCH3)2 (C 104)3.H20

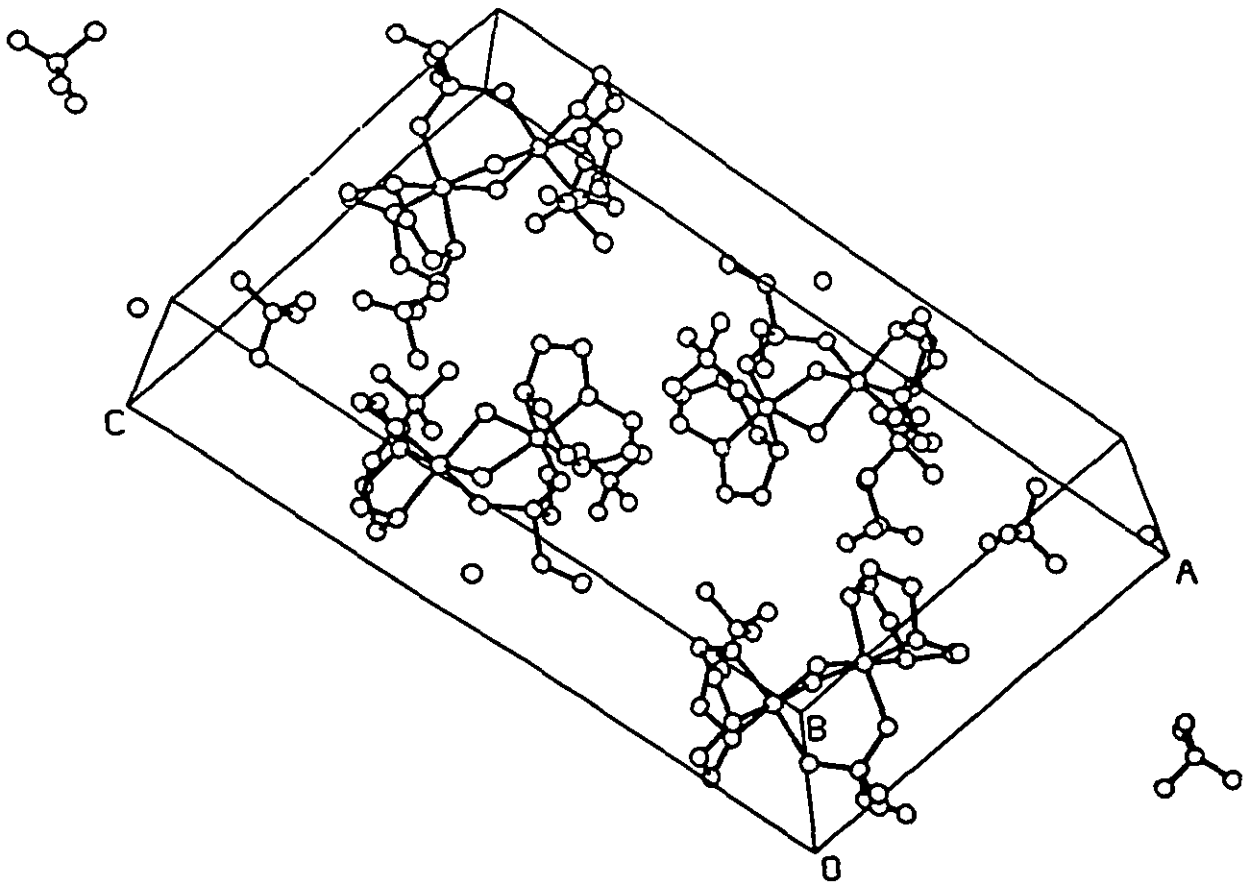

TABLE OF CONTENTS

INTRODUCTION

The compound was found to be the expected one with the dimethyl phosphate group in bridging position. Both O-CH3 groups on the phosphate ligand are disordered, occupancies for the disordered atoms refined to average values .58 and .42. These values were normalised to 0.60 and 0.40.

Compound crystallises as the monohydrate. Of the three perchlorate counter ions, no 2 and 3 are disordered, and are modeled with partial oxygen atoms. Refinement was on |F|, non-H atoms were refined anisotropically except for O-CH3 groups on the phosphate and oxygens from minor oriantation in ClO4 no2. Hydrogens on hydroxo ligands and on water molecule were not introduced in the model.

Final agreement factors including weak data are 0.154 and 0.081 for R and Rw respectively.

No absorption correction was applied since 4 empirical psi scans indicated variations of less than 5% between minimum and maximum transmission factors.

EXPERIMENTAL

DATA COLLECTION

A red block crystal of $C_{14}H_{40}O_{19}N_6PCl_3Co_2$ having approximate dimensions of 0.500 X 0.370 X 0.200 mm was mounted on a glass fiber. All measurements were made on a Rigaku AFC6S diffractometer with graphite monochromated Mo Kα radiation.

Cell constants and an orientation matrix for data collection, obtained from a least-squares refinement using the setting angles of 15 carefully centered reflections in the range $35.00 < 2\theta < 45.00°$ corresponded to a monoclinic cell with dimensions:

$a = 13.084\ (3)\text{Å}$
$b = 11.222\ (3)\text{Å}$ $\beta = 103.87\ (2)°$
$c = 22.784\ (5)\text{Å}$
$V = 3248\ (1)\text{Å}^3$

For $Z = 4$ and F.W. = 851.70, the calculated density is 1.742 g/cm^3. Based on the systematic absences of:

$h0l: l \neq 2n$
$0k0: k \neq 2n$

and the successful solution and refinement of the structure, the space group was determined to be:

$P2_1/c$ (#14)

The data were collected at a temperature of 20 ± 1°C using the ω-2θ scan technique to a maximum 2θ value of 50.0°. Omega scans of several intense reflections, made prior to data collection, had an average width at half-height of 0.20° with a take-off angle of 6.0°. Scans of (0.85 + 0.35 tan θ)° were made at a speed of 16.0°/min (in omega). The weak reflections ($I < 7.0\sigma(I)$) were rescanned (maximum of 9 rescans) and the counts were accumulated to assure good counting statistics. Stationary background counts were recorded on each side of the reflection. The ratio of peak counting time to background counting time was 2:1. The diameter of the incident beam collimator was 0.5 mm and the crystal to detector distance was 400.0 mm.

DATA REDUCTION

Of the 11987 reflections which were collected, 6043 were unique (R_{int} = .106); equivalent reflections were merged. The intensities of three representative reflections which were measured after every 150 reflections declined by 1.57%. A linear correction factor was applied to the data to account for this phenomena.

The linear absorption coefficient for Mo Kα is 14.0 cm^{-1}. Azimuthal scans of several reflections indicated no need for an absorption correction. The data were corrected for Lorentz and polarization effects. A correction for secondary extinction was applied (coefficient = 0.15242E-06).

STRUCTURE SOLUTION AND REFINEMENT

The structure was solved by the Patterson heavy atom method.[3] The non-hydrogen atoms were refined anisotropically. The final cycle of full-matrix least-squares refinement[4] was based on 2647 observed reflections ($I > 2.50\sigma(I)$) and 447 variable parameters and converged (largest parameter shift was 1.16 times its esd) with unweighted and weighted agreement factors of:

$$R = \Sigma \, ||Fo| - |Fc|| \, / \, \Sigma \, |Fo| = 0.057$$

$$R_w = [(\Sigma \, w \, (|Fo| - |Fc|)^2 \, / \, \Sigma \, w \, Fo^2)]^{1/2} = 0.068$$

The standard deviation of an observation of unit weight[5] was 1.77. The weighting scheme was based on counting statistics and included a factor (p = 0.03) to downweight the intense reflections. Plots of $\Sigma \, w \, (|Fo| - |Fc|)^2$ versus |Fo|, reflection order in data collection, $\sin\theta/\lambda$, and various classes of indices showed no unusual trends. The maximum and minimum peaks on the final difference Fourier map corresponded to 0.53 and -0.36 $e^-/Å^3$, respectively.

Neutral atom scattering factors were taken from Cromer and Waber[6]. Anomalous dispersion effects were included in Fcalc[7]; the values for Δf′ and Δf″ were those of Cromer[8]. All calculations were performed using the TEXSAN[9] crystallographic software package of Molecular Structure Corporation.

References

(1) PLUTO:
Motherwell,S. & Clegg,W.; PLUTO. Program for plotting molecular and crystal structures. Univ. of Cambridge, England (1978).

(2) ORTEP:
Johnson,C.K.; ORTEPII. Report ORNL-5138. Oak Ridge National Laboratory, Oak Ridge, Tennessee (1976).

(3) Structure Solution Methods:
PHASE
Calbrese,J.C.; PHASE - Patterson Heavy Atom Solution Extractor. Univ. of Wisconsin-Madison, Ph.D. Thesis (1972).
DIRDIF
Beurskens,P.T.; DIRDIF: Direct Methods for Difference Structures - an automatic procedure for phase extension and refinement of difference structure factors. Technical Report 1984/1 Crystallography Laboratory, Toernooiveld, 6525 Ed Nijmegen, Netherlands.

(4) Least-Squares:
Function minimized: $\Sigma w (|Fo| - |Fc|)^2$
where: $w = 4Fo^2/\sigma^2(Fo^2)$
$\sigma^2(Fo^2) = [S^2(C+R^2B) + (pFo^2)^2]/Lp^2$
S = Scan rate
C = Total Integrated Peak Count
R = Ratio of Scan Time to background counting time.
B = Total Background Count
Lp = Lorentz-polarization factor
p = p-factor

(5) Standard deviation of an observation of unit weight:

$$[\Sigma w(|Fo| - |Fc|)^2/(No - Nv)]^{1/2}$$

where: No = number of observations
Nv = number of variables

(6) Cromer,D.T. & Waber,J.T.; "International Tables for X-ray Crystallography", Vol. IV, The Kynoch Press, Birmingham, England, Table 2.2 A (1974).

(7) Ibers,J.A. & Hamilton,W.C.; Acta Crystallogr., 17, 781 (1964).

(8) D.T. Cromer, "International Tables for X-ray Crystallography", Vol/ IV, The Kynoch Press, Birmingham, England, Table 2.3.1 (1974).

(9) TEXSAN - TEXRAY Structure Analysis Package, Molecular Structure Corporation (1985).

EXPERIMENTAL DETAILS

A. Crystal Data

Empirical Formula	$C_{14}H_{40}O_{19}N_6PCl_3Co_2$
Formula Weight	851.70
Crystal Color, Habit	red, block
Crystal Dimensions (mm)	0.500 X 0.370 X 0.200
Crystal System	monoclinic
No. Reflections Used for Unit Cell Determination (2θ range)	15 (35.0 - 45.0°)
Omega Scan Peak Width at Half-height	0.20
Lattice Parameters:	a = 13.084 (3)Å b = 11.222 (3)Å c = 22.784 (5)Å β = 103.87 (2)° V = 3248 (1)Å^3
Space Group	$P2_1/c$ (#14)
Z value	4
D_{calc}	1.742 g/cm^3
F_{000}	1752
$\mu_{(MoK\alpha)}$	13.98 cm^{-1}

B. Intensity Measurements

Diffractometer	Rigaku AFC6S
Radiation	MoKα (λ = 0.71069 Å)
Temperature	20°C
Take-off Angle	6.0°
Detector Aperture	6.0 mm horizontal 6.0 mm vertical

Crystal to Detector Distance	40 cm
Scan Type	ω-2θ
Scan Rate	16.0°/min (in omega) (9 rescans)
Scan Width	(0.85 + 0.35 tanθ)°
$2\theta_{max}$	50.0°
No. of Reflections Measured	Total: 11987 Unique: 6043 (R_{int} = .106)
Corrections	Lorentz-polarization Decay (1.57% decline) Secondary Extinction (coefficient: 0.15242E-06)

C. Structure Solution and Refinement

Structure Solution	Patterson Method
Refinement	Full-matrix least-squares
Function Minimized	Σ w (|Fo| - |Fc|)^2
Least-squares Weights	$4Fo^2/\sigma^2(Fo^2)$
p-factor	0.03
Anomalous Dispersion	All non-hydrogen atoms
No. Observations (I>2.50σ(I))	2647
No. Variables	447
Reflection/Parameter Ratio	5.92
Residuals: R; R_w	0.057; 0.068
Goodness of Fit Indicator	1.77
Max Shift/Error in Final Cycle	1.16
Maximum Peak in Final Diff. Map	0.53 $e^-/Å^3$
Minimum Peak in Final Diff. Map	-0.36 $e^-/Å^3$

Positional parameters and B(eq) for
[Co2 [9]aneN3(OH)2PO2(OCH3)2](ClO4)3.H2O

atom	x	y	z	B(eq)
Co(1)	0.18787(11)	0.17138(11)	0.15764(06)	3.00(5)
Co(2)	0.37019(11)	0.23178(11)	0.11192(06)	3.21(5)
P(1)	0.1921(03)	0.0906(03)	0.03022(13)	4.3(1)
O(1)	0.2968(06)	0.1451(07)	0.0408(03)	5.5(4)
O(2)	0.1383(05)	0.0952(06)	0.0798(03)	4.3(3)
O(3)*	0.1205(14)	0.1800(16)	-0.0195(08)	7.4(4)
O(3A)#	0.1285(14)	0.0940(16)	-0.0331(08)	4.1(4)
O(4)*	0.1771(12)	-0.0249(12)	-0.0035(06)	5.6(3)
O(4A)#	0.247(02)	-0.052(03)	0.0313(14)	9.0(8)
O(5)	0.2472(05)	0.3064(05)	0.1265(03)	3.6(3)
O(6)	0.3310(05)	0.1182(05)	0.1673(03)	3.2(3)
N(1)	0.2209(06)	0.2393(07)	0.2372(03)	3.5(3)
N(2)	0.1359(07)	0.0367(07)	0.1944(04)	4.2(4)
N(3)	0.0506(07)	0.2406(08)	0.1490(04)	4.3(4)
N(4)	0.4587(07)	0.3176(07)	0.1769(04)	4.3(4)
N(5)	0.4964(07)	0.1575(08)	0.1023(04)	4.4(4)
N(6)	0.4003(07)	0.3554(08)	0.0600(04)	4.7(4)
C(1)	0.2060(10)	0.1523(11)	0.2836(05)	5.3(6)
C(2)	0.1982(10)	0.0293(10)	0.2569(05)	5.1(6)
C(3)	0.0207(10)	0.0480(10)	0.1894(06)	5.4(6)
C(4)	-0.0268(09)	0.1414(11)	0.1436(05)	5.3(6)
C(5)	0.0474(10)	0.3228(11)	0.1995(06)	5.6(6)
C(6)	0.1571(11)	0.3476(10)	0.2349(05)	5.4(6)
C(7)	0.5543(11)	0.2413(15)	0.2003(06)	8.8(9)
C(8)	0.5852(10)	0.1776(12)	0.1555(07)	7.1(7)
C(9)	0.5159(13)	0.2025(16)	0.0444(07)	9(1)
C(10)	0.4820(14)	0.3211(16)	0.0300(06)	9(1)
C(11)	0.4283(12)	0.4635(11)	0.0965(07)	7.8(7)
C(12)	0.4795(14)	0.4389(11)	0.1583(06)	8.7(8)
C(13)*	0.138(02)	0.195(03)	-0.0724(15)	11.0(9)
C(13A)#	0.047(04)	0.186(04)	-0.047(02)	10(1)
C(14)*	0.228(03)	-0.134(03)	0.0279(15)	9(1)
C(14A)#	0.176(03)	-0.147(03)	0.0336(15)	5.5(8)

* indicates occupancy of 0.60
# indicates occupancy of 0.40

Table 4. Bond Angles in Degrees
(cont'd)

Cu(1)-N(2)-C(4)	112.6(4)	N(8)-C(29)-N(10)	112.7(5)
Cu(1)-N(2)-C(5)	140.6(4)	N(8)-C(29)-C(28)	121.5(5)
C(4)-N(2)-C(5)	106.7(5)	N(10)-C(29)-C(28)	125.6(5)
Cu(1)-N(3)-C(12)	111.6(4)	N(8)-C(30)-C(31)	130.3(5)
Cu(1)-N(3)-C(13)	143.7(4)	N(8)-C(30)-C(35)	108.5(5)
C(12)-N(3)-C(13)	104.7(5)	C(31)-C(30)-C(35)	121.2(5)
C(4)-N(4)-C(10)	107.0(5)	C(30)-C(31)-C(32)	115.2(6)
C(12)-N(5)-C(18)	106.9(5)	C(31)-C(32)-C(33)	123.2(6)
Cu(2)-N(6)-C(19)	104.9(3)	C(32)-C(33)-C(34)	121.0(6)
Cu(2)-N(6)-C(20)	108.7(3)	C(33)-C(34)-C(35)	116.7(6)
Cu(2)-N(6)-C(28)	108.6(3)	N(10)-C(35)-C(30)	106.7(5)
C(19)-N(6)-C(20)	113.5(4)	N(10)-C(35)-C(34)	130.7(5)
C(19)-N(6)-C(28)	112.6(4)	C(30)-C(35)-C(34)	122.6(6)
C(20)-N(6)-C(28)	108.4(4)	O(6)-Cl(1)-O(7)	108.6(3)
Cu(2)-N(7)-C(21)	103.4(4)	O(6)-Cl(1)-O(8)	109.1(4)
Cu(2)-N(7)-C(22)	138.7(3)	O(6)-Cl(1)-O(9)	111.0(4)
C(21)-N(7)-C(22)	104.8(4)	O(7)-Cl(1)-O(8)	108.4(4)
Cu(2)-N(8)-C(29)	113.8(4)	O(7)-Cl(1)-O(9)	108.7(4)
Cu(2)-N(8)-C(30)	140.7(4)	O(8)-Cl(1)-O(9)	110.9(4)
C(29)-N(8)-C(30)	105.5(4)	O(10)-Cl(2)-O(11)	114.2(4)
C(21)-N(9)-C(27)	106.4(5)	O(10)-Cl(2)-O(12)	107.6(5)
C(29)-N(10)-C(35)	106.6(5)	O(10)-Cl(2)-O(13)	114.9(6)
O(1)-C(1)-C(2)	107.7(4)	O(11)-Cl(2)-O(12)	108.8(6)
O(1)-C(1)-C(19)	108.7(4)	O(11)-Cl(2)-O(13)	112.6(7)
C(2)-C(1)-C(19)	111.3(5)	O(12)-Cl(2)-O(13)	97.1(8)
N(1)-C(2)-C(1)	108.6(5)	O(14)-C(38)-C(39)	123.8(8)
N(1)-C(3)-C(4)	107.9(5)	O(14)-C(38)-C(40)	120.9(8)
N(2)-C(4)-N(4)	111.8(5)	C(39)-C(38)-C(40)	115.1(7)
N(2)-C(4)-C(3)	122.1(5)		
N(4)-C(4)-C(3)	126.0(5)		
N(2)-C(5)-C(6)	130.8(5)		

Positional parameters for [Co2 [9]aneN3(OH)2PO2(OCH3)2](ClO4)3.H2O

atom	x	y	z	occupancy
Co(1)	0.18787(11)	0.17138(11)	0.15764(06)	
Co(2)	0.37019(11)	0.23178(11)	0.11192(06)	
P(1)	0.1921(03)	0.0906(03)	0.03022(13)	
O(1)	0.2968(06)	0.1451(07)	0.0408(03)	
O(2)	0.1383(05)	0.0952(06)	0.0798(03)	
O(3)	0.1205(14)	0.1800(16)	-0.0195(08)	0.600
O(3A)	0.1285(14)	0.0940(16)	-0.0331(08)	0.400
O(4)	0.1771(12)	-0.0249(12)	-0.0035(06)	0.600
O(4A)	0.247(02)	-0.052(03)	0.0313(14)	0.400
O(5)	0.2472(05)	0.3064(05)	0.1265(03)	
O(6)	0.3310(05)	0.1182(05)	0.1673(03)	
N(1)	0.2209(06)	0.2393(07)	0.2372(03)	
N(2)	0.1359(07)	0.0367(07)	0.1944(04)	
N(3)	0.0506(07)	0.2406(08)	0.1490(04)	
N(4)	0.4587(07)	0.3176(07)	0.1769(04)	
N(5)	0.4964(07)	0.1575(08)	0.1023(04)	
N(6)	0.4003(07)	0.3554(08)	0.0600(04)	
C(1)	0.2060(10)	0.1523(11)	0.2836(05)	
C(2)	0.1982(10)	0.0293(10)	0.2569(05)	
C(3)	0.0207(10)	0.0480(10)	0.1894(06)	
C(4)	-0.0268(09)	0.1414(11)	0.1436(05)	
C(5)	0.0474(10)	0.3228(11)	0.1995(06)	
C(6)	0.1571(11)	0.3476(10)	0.2349(05)	
C(7)	0.5543(11)	0.2413(15)	0.2003(06)	
C(8)	0.5852(10)	0.1776(12)	0.1555(07)	
C(9)	0.5159(13)	0.2025(16)	0.0444(07)	
C(10)	0.4820(14)	0.3211(16)	0.0300(06)	
C(11)	0.4283(12)	0.4635(11)	0.0965(07)	
C(12)	0.4795(14)	0.4389(11)	0.1583(06)	
C(13)	0.138(02)	0.195(03)	-0.0724(15)	0.600
C(13A)	0.047(04)	0.186(04)	-0.047(02)	0.400
C(14)	0.228(03)	-0.134(03)	0.0279(15)	0.600
C(14A)	0.176(03)	-0.147(03)	0.0336(15)	0.400

Positional parameters and B(eq) for water and perchlorates in [Co2 [9]aneN3(OH)2PO2(OCH3)2](ClO4)3.H2O

atom	x	y	z	B(eq)	Occupancy
Cl(1)	0.7798(03)	0.4591(03)	0.06997(15)	5.4(2)	
O(7)	0.8729(09)	0.5112(13)	0.0977(07)	14(1)	
O(8)	0.7745(12)	0.3582(11)	0.0976(07)	16(1)	
O(9)	0.6984(10)	0.5286(12)	0.0808(06)	13.5(9)	
O(10)	0.7610(14)	0.4509(16)	0.0119(05)	19(1)	
Cl(2)	0.4759(04)	0.1641(03)	0.84918(17)	6.9(2)	
O(11)	0.4123(12)	0.1192(14)	0.7962(06)	15(1)	
O(12)	0.460(02)	0.1083(15)	0.8982(07)	13(1)	0.700
O(12A)	0.379(03)	0.131(04)	0.871(02)	8(1)	0.300
O(13)	0.5666(12)	0.1066(11)	0.8460(08)	16(1)	
O(14)	0.4660(13)	0.2796(11)	0.8314(10)	11(1)	0.700
O(14A)	0.523(03)	0.263(04)	0.886(02)	11(1)	0.300
Cl(3)	0.8406(03)	0.1900(03)	0.30841(17)	6.0(2)	
O(15)	0.817(03)	0.220(03)	0.2431(15)	11(2)	0.500
O(15A)	0.816(03)	0.140(02)	0.2530(15)	10(2)	0.500
O(16)	0.7486(18)	0.1198(17)	0.3091(13)	9(1)	0.500
O(16A)	0.840(03)	0.119(03)	0.3582(13)	12(2)	0.500
O(17)	0.849(03)	0.286(03)	0.340(02)	15(2)	0.500
O(17A)	0.781(02)	0.291(03)	0.3170(15)	8(1)	0.500
O(18)	0.926(02)	0.118(02)	0.3257(16)	11(1)	0.500
O(18A)	0.9452(18)	0.234(04)	0.3125(11)	14(2)	0.500
O((W))	0.0845(09)	0.0620(10)	0.5556(05)	10.3(6)	

U values for CHIN15 DAPHNEE

atom	U11	U22	U33	U12	U13	U23
H(N2)	0.0637					
H(2A)	0.0776					
H(2B)	0.0776					
H(N3)	0.0650					
H(3A)	0.0818					
H(3B)	0.0818					
H(N4)	0.0647					
H(4A)	0.0796					
H(4B)	0.0796					
H(N5)	0.0674					
H(5A)	0.0847					
H(5B)	0.0847					
H(N6)	0.0707					
H(6A)	0.0819					
H(6B)	0.0819					
H(7A)	0.1336					
H(7B)	0.1336					
H(8A)	0.1077					
H(8B)	0.1077					
H(9A)	0.1325					
H(9B)	0.1325					
H(10A)	0.1310					
H(10B)	0.1310					
H(11A)	0.1168					
H(11B)	0.1168					
H(12A)	0.1301					
H(12B)	0.1301					
H(131)	0.1664					
H(131A)	0.1544					
H(132)	0.1664					
H(132A)	0.1544					
H(133)	0.1664					
H(133A)	0.1544					
H(141)	0.0810					
H(141A)	0.0810					
H(142)	0.0810					

U values for CHIN15 DAPHNEE

atom	U11	U22	U33	U12	U13	U23
Co(1)	0.0441(08)	0.0326(07)	0.0354(08)	-0.0021(07)	0.0058(06)	0.0001(06)
Co(2)	0.0443(08)	0.0418(08)	0.0326(07)	-0.0081(07)	0.0023(06)	0.0032(06)
P(1)	0.067(02)	0.0531(18)	0.0363(16)	-0.0159(16)	0.0018(14)	-0.0059(13)
O(1)	0.066(05)	0.102(06)	0.039(05)	-0.024(05)	0.012(04)	-0.025(04)
O(2)	0.052(04)	0.068(05)	0.044(05)	-0.017(04)	0.009(04)	-0.013(04)
O(3)	0.094(05)					
O(3A)	0.052(05)					
O(4)	0.071(04)					
O(4A)	0.114(10)					
O(5)	0.050(04)	0.034(04)	0.050(04)	-0.013(03)	0.008(03)	0.003(03)
O(6)	0.044(04)	0.040(04)	0.037(04)	-0.003(03)	0.006(03)	0.002(03)
N(1)	0.057(05)	0.035(05)	0.040(05)	0.000(04)	0.009(04)	0.001(04)
N(2)	0.063(06)	0.035(05)	0.066(06)	-0.007(05)	0.023(05)	0.005(04)
N(3)	0.053(05)	0.054(05)	0.052(05)	0.004(05)	0.005(04)	0.001(05)
N(4)	0.058(06)	0.058(06)	0.039(05)	-0.020(05)	-0.001(04)	-0.002(04)
N(5)	0.057(06)	0.055(06)	0.057(06)	-0.013(05)	0.016(05)	0.003(05)
N(6)	0.057(06)	0.066(06)	0.051(06)	-0.023(05)	0.005(05)	0.015(05)
C(1)	0.084(09)	0.070(08)	0.042(07)	-0.013(07)	0.003(06)	0.018(06)
C(2)	0.094(10)	0.047(07)	0.052(08)	0.007(07)	0.014(07)	0.016(06)
C(3)	0.078(09)	0.050(07)	0.086(10)	-0.022(07)	0.037(08)	0.003(07)
C(4)	0.046(07)	0.081(09)	0.072(09)	-0.009(06)	0.013(06)	-0.016(07)
C(5)	0.072(09)	0.067(08)	0.077(09)	0.017(07)	0.024(07)	-0.007(07)
C(6)	0.093(10)	0.061(07)	0.052(08)	0.019(07)	0.019(07)	-0.014(06)
C(7)	0.078(10)	0.166(15)	0.070(10)	0.064(11)	-0.024(08)	-0.019(10)
C(8)	0.059(08)	0.089(10)	0.101(11)	0.018(08)	-0.023(08)	-0.007(09)
C(9)	0.125(14)	0.141(15)	0.089(12)	-0.006(12)	0.079(11)	0.011(10)
C(10)	0.139(15)	0.142(15)	0.060(10)	0.027(13)	0.051(10)	0.037(10)
C(11)	0.110(12)	0.063(08)	0.101(12)	-0.035(09)	-0.015(09)	0.037(08)
C(12)	0.186(17)	0.067(09)	0.066(10)	-0.061(10)	0.010(10)	0.016(07)
C(13)	0.139(11)					
C(13A)	0.130(16)					
C(14)	0.115(11)					
C(14A)	0.069(10)					
H(N1)	0.0533					
H(1A)	0.0805					
H(1B)	0.0805					

U values for CHIN15 DAPHNEE

atom	U11	U22	U33	U12	U13	U23
H(142A)	0.0810					
H(143)	0.1394					
H(143A)	0.0810					
Cl(1)	0.062(02)	0.082(02)	0.059(02)	-0.0034(18)	0.0125(17)	0.0034(17)
O(7)	0.077(08)	0.218(15)	0.241(17)	-0.029(09)	0.022(10)	0.018(13)
O(8)	0.194(15)	0.109(10)	0.257(18)	-0.014(10)	-0.013(13)	0.053(11)
O(9)	0.104(10)	0.198(13)	0.201(14)	-0.001(09)	0.019(09)	-0.106(12)
O(10)	0.30(02)	0.37(02)	0.050(08)	0.175(18)	0.009(11)	0.005(11)
Cl(2)	0.121(03)	0.069(02)	0.061(02)	0.022(02)	-0.002(02)	0.009(02)
O(11)	0.211(15)	0.217(15)	0.097(11)	0.022(12)	-0.033(10)	0.017(10)
O(12)	0.32(03)	0.108(13)	0.063(12)	0.013(17)	0.049(16)	0.009(10)
O(12A)	0.107(13)					
O(13)	0.161(13)	0.099(09)	0.31(02)	0.066(09)	-0.009(14)	-0.015(11)
O(14)	0.136(14)	0.039(08)	0.24(02)	0.038(09)	0.054(15)	0.040(11)
O(14A)	0.133(15)					
Cl(3)	0.076(02)	0.066(02)	0.081(03)	0.006(02)	0.012(02)	-0.001(02)
O(15)	0.13(02)	0.21(04)	0.09(02)	0.01(03)	0.037(17)	0.03(03)
O(15A)	0.20(03)	0.10(02)	0.08(02)	-0.01(02)	-0.00(02)	-0.008(17)
O(16)	0.111(18)	0.072(13)	0.16(02)	-0.032(13)	0.066(17)	0.024(15)
O(16A)	0.24(04)	0.14(02)	0.12(02)	0.05(03)	0.09(02)	0.060(19)
O(17)	0.21(04)	0.07(02)	0.28(05)	-0.03(03)	0.02(04)	-0.08(02)
O(17A)	0.094(18)	0.077(17)	0.16(03)	0.011(17)	0.06(02)	-0.005(17)
O(18)	0.077(16)	0.069(14)	0.22(03)	0.015(14)	-0.034(18)	-0.026(17)
O(18A)	0.065(15)	0.37(05)	0.11(02)	-0.05(03)	0.037(14)	-0.06(03)
O((W))	0.122(09)	0.161(10)	0.108(08)	-0.046(08)	0.028(07)	-0.043(08)

Intramolecular Distances [Co2[9]aneN3(OH)2PO2(OCH3)2](ClO4)3.H2O

atom	atom	distance	atom	atom	distance
Co(1)	O(2)	1.935(6)	N(2)	C(3)	1.49(1)
Co(1)	O(5)	1.915(6)	N(3)	C(4)	1.49(1)
Co(1)	O(6)	1.927(6)	N(3)	C(5)	1.48(1)
Co(1)	N(1)	1.918(7)	N(4)	C(7)	1.50(1)
Co(1)	N(2)	1.930(8)	N(4)	C(12)	1.47(1)
Co(1)	N(3)	1.924(9)	N(5)	C(8)	1.48(1)
Co(2)	O(1)	1.937(7)	N(5)	C(9)	1.49(1)
Co(2)	O(5)	1.912(7)	N(6)	C(10)	1.45(2)
Co(2)	O(6)	1.947(6)	N(6)	C(11)	1.47(2)
Co(2)	N(4)	1.907(8)	C(1)	C(2)	1.50(1)
Co(2)	N(5)	1.909(9)	C(3)	C(4)	1.51(2)
Co(2)	N(6)	1.925(8)	C(5)	C(6)	1.49(2)
P(1)	O(1)	1.466(8)	C(7)	C(8)	1.38(2)
P(1)	O(2)	1.469(7)	C(9)	C(10)	1.42(2)
P(1)	O(3)	1.63(2)	C(11)	C(12)	1.43(2)
P(1)	O(3A)	1.48(2)	Cl(1)	O(7)	1.36(1)
P(1)	O(4)	1.49(1)	Cl(1)	O(8)	1.30(1)
P(1)	O(4A)	1.75(3)	Cl(1)	O(9)	1.39(1)
O(3)	O(3A)	1.03(2)	Cl(1)	O(10)	1.29(1)
O(3)	C(13)	1.29(3)	Cl(2)	O(11)	1.39(1)
O(3A)	C(13A)	1.46(5)	Cl(2)	O(12)	1.34(2)
O(4)	C(14)	1.49(4)	Cl(2)	O(12A)	1.51(4)
O(4A)	C(14A)	1.42(5)	Cl(2)	O(13)	1.37(1)
N(1)	C(1)	1.49(1)	Cl(2)	O(14)	1.35(1)
N(1)	C(6)	1.47(1)	Cl(2)	O(14A)	1.44(4)
N(2)	C(2)	1.46(1)	Cl(3)	O(15)	1.48(3)

Distances are in angstroms. Estimated standard deviations in the least significant figure are given in parentheses.

Intramolecular Distances (cont)

atom	atom	distance	atom	atom	distance
Cl(3)	O(15A)	1.35(3)			
Cl(3)	O(16)	1.44(2)			
Cl(3)	O(16A)	1.39(2)			
Cl(3)	O(17)	1.28(3)			
Cl(3)	O(17A)	1.42(3)			
Cl(3)	O(18)	1.36(2)			
Cl(3)	O(18A)	1.44(2)			

Distances are in angstroms. Estimated standard deviations in the least significant figure are given in parentheses.

Intramolecular Bond Angles [Co2[9]aneN3(OH)2PO2(OCH3)2](ClO4)3.H2O

atom	atom	atom	angle	atom	atom	atom	angle
O(2)	Co(1)	O(5)	95.0(3)	O(6)	Co(2)	N(6)	174.3(3)
O(2)	Co(1)	O(6)	94.1(3)	N(4)	Co(2)	N(5)	85.9(4)
O(2)	Co(1)	N(1)	172.6(3)	N(4)	Co(2)	N(6)	86.4(4)
O(2)	Co(1)	N(2)	88.6(3)	N(5)	Co(2)	N(6)	86.2(4)
O(2)	Co(1)	N(3)	89.2(3)	O(1)	P(1)	O(2)	117.4(4)
O(5)	Co(1)	O(6)	79.5(3)	O(1)	P(1)	O(3)	102.4(7)
O(5)	Co(1)	N(1)	91.0(3)	O(1)	P(1)	O(3A)	115.6(8)
O(5)	Co(1)	N(2)	175.8(3)	O(1)	P(1)	O(4)	116.6(7)
O(5)	Co(1)	N(3)	95.4(3)	O(1)	P(1)	O(4A)	91(1)
O(6)	Co(1)	N(1)	91.3(3)	O(2)	P(1)	O(3)	102.2(7)
O(6)	Co(1)	N(2)	98.2(3)	O(2)	P(1)	O(3A)	119.2(7)
O(6)	Co(1)	N(3)	174.2(3)	O(2)	P(1)	O(4)	113.4(6)
N(1)	Co(1)	N(2)	85.6(3)	O(2)	P(1)	O(4A)	107(1)
N(1)	Co(1)	N(3)	85.9(4)	O(3)	P(1)	O(4)	101.2(8)
N(2)	Co(1)	N(3)	86.7(4)	O(3A)	P(1)	O(4A)	100(1)
O(1)	Co(2)	O(5)	95.5(3)	Co(2)	O(1)	P(1)	127.1(4)
O(1)	Co(2)	O(6)	93.4(3)	Co(1)	O(2)	P(1)	127.1(4)
O(1)	Co(2)	N(4)	172.0(3)	P(1)	O(3)	O(3A)	63(1)
O(1)	Co(2)	N(5)	87.3(4)	P(1)	O(3)	C(13)	122(2)
O(1)	Co(2)	N(6)	88.9(4)	P(1)	O(3A)	C(13A)	116(2)
O(5)	Co(2)	O(6)	79.1(3)	P(1)	O(4)	C(14)	118(2)
O(5)	Co(2)	N(4)	91.4(3)	P(1)	O(4A)	C(14A)	115(2)
O(5)	Co(2)	N(5)	176.7(3)	Co(1)	O(5)	Co(2)	98.7(3)
O(5)	Co(2)	N(6)	95.5(3)	Co(1)	O(6)	Co(2)	97.1(3)
O(6)	Co(2)	N(4)	91.9(3)	Co(1)	N(1)	C(1)	111.9(6)
O(6)	Co(2)	N(5)	99.1(3)	Co(1)	N(1)	C(6)	107.3(6)

Angles are in degrees. Estimated standard deviations in the least significant figure are given in parentheses.

Intramolecular Bond Angles (cont)

atom	atom	atom	angle	atom	atom	atom	angle
C(1)	N(1)	C(6)	113.5(9)	N(6)	C(11)	C(12)	113(1)
Co(1)	N(2)	C(2)	107.1(7)	N(4)	C(12)	C(11)	113(1)
Co(1)	N(2)	C(3)	110.8(7)	O(7)	Cl(1)	O(8)	107(1)
C(2)	N(2)	C(3)	113(1)	O(7)	Cl(1)	O(9)	108.4(8)
Co(1)	N(3)	C(4)	107.8(6)	O(7)	Cl(1)	O(10)	116(1)
Co(1)	N(3)	C(5)	111.8(7)	O(8)	Cl(1)	O(9)	106(1)
C(4)	N(3)	C(5)	112.6(9)	O(8)	Cl(1)	O(10)	114(1)
Co(2)	N(4)	C(7)	106.6(8)	O(9)	Cl(1)	O(10)	104.9(9)
Co(2)	N(4)	C(12)	111.4(7)	O(11)	Cl(2)	O(12)	112(1)
C(7)	N(4)	C(12)	116(1)	O(11)	Cl(2)	O(12A)	79(2)
Co(2)	N(5)	C(8)	111.7(8)	O(11)	Cl(2)	O(13)	97(1)
Co(2)	N(5)	C(9)	106.9(8)	O(11)	Cl(2)	O(14)	95(1)
C(8)	N(5)	C(9)	114(1)	O(11)	Cl(2)	O(14A)	151(2)
Co(2)	N(6)	C(10)	112.4(8)	O(12)	Cl(2)	O(13)	98(1)
Co(2)	N(6)	C(11)	107.9(8)	O(12)	Cl(2)	O(14)	132(1)
C(10)	N(6)	C(11)	112(1)	O(12A)	Cl(2)	O(13)	135(2)
N(1)	C(1)	C(2)	109(1)	O(12A)	Cl(2)	O(14A)	106(2)
N(2)	C(2)	C(1)	108.1(9)	O(13)	Cl(2)	O(14)	117(1)
N(2)	C(3)	C(4)	110.8(9)	O(13)	Cl(2)	O(14A)	98(2)
N(3)	C(4)	C(3)	107.6(9)	O(15)	Cl(3)	O(16)	99(2)
N(3)	C(5)	C(6)	109(1)	O(15)	Cl(3)	O(17)	109(3)
N(1)	C(6)	C(5)	109(1)	O(15)	Cl(3)	O(18)	113(2)
N(4)	C(7)	C(8)	113(1)	O(15A)	Cl(3)	O(16A)	119(2)
N(5)	C(8)	C(7)	112(1)	O(15A)	Cl(3)	O(17A)	116(2)
N(5)	C(9)	C(10)	114(1)	O(15A)	Cl(3)	O(18A)	102(2)
N(6)	C(10)	C(9)	111(1)	O(16)	Cl(3)	O(17)	115(2)

Angles are in degrees. Estimated standard deviations in the least significant figure are given in parentheses.

Intramolecular Bond Angles (cont)

atom	atom	atom	angle	atom	atom	atom	angle
O(16)	Cl(3)	O(18)	108(1)				
O(16A)	Cl(3)	O(17A)	104(2)				
O(16A)	Cl(3)	O(18A)	110(2)				
O(17)	Cl(3)	O(18)	113(2)				
O(17A)	Cl(3)	O(18A)	105(2)				

Angles are in degrees. Estimated standard deviations in the least significant figure are given in parentheses.

Intermolecular Distances

atom	atom	distance	ADC(*)
Co(1)	Co(2)	2.903(2)	1
N(6)	O(10)	3.20(2)	66503
O(5)	O((W))	2.77(1)	55404
O(7)	O((W))	3.25(2)	65404
N(1)	O(11)	3.00(2)	55404
N(2)	O(17)	2.93(4)	64502
N(2)	O(17A)	3.00(3)	64502
O(16A)	O((W))	2.83(3)	65603
N(3)	O((W))	3.18(1)	55404
O((W))	O((W))	3.25(2)	55603
N(4)	O(11)	3.01(2)	55404
N(5)	O(12)	3.04(2)	65603
N(5)	O(13)	3.36(2)	65603

Special Contacts Involving the Nonhydrogen Atoms

atom	atom	distance	ADC(*)	atom	atom	distance	ADC(*)
Co(1)	Co(2)	2.903(2)	1				

Contacts out to 4.00 angstroms. Estimated standard deviations in the least significant figure are given in parentheses.

Calculated Hydrogen Atoms Coordinates and B(eq) for
[Co2 [9]aneN3(OH)2PO2(OCH3)2](ClO4)3.H2O

atom	x	y	z	B(eq)
H(N1)	0.2929	0.2623	0.2467	4.2
H(1A)	0.2642	0.1559	0.3178	6.4
H(1B)	0.1431	0.1703	0.2958	6.4
H(N2)	0.1479	-0.0335	0.1738	5.0
H(2A)	0.1646	-0.0225	0.2795	6.1
H(2B)	0.2666	-0.0000	0.2578	6.1
H(N3)	0.0340	0.2850	0.1125	5.1
H(3A)	-0.0122	-0.0263	0.1775	6.5
H(3B)	0.0096	0.0701	0.2278	6.5
H(N4)	0.4223	0.3244	0.2081	5.1
H(4A)	-0.0906	0.1700	0.1515	6.3
H(4B)	-0.0406	0.1084	0.1041	6.3
H(N5)	0.4842	0.0742	0.0984	5.3
H(5A)	0.0145	0.3954	0.1837	6.7
H(5B)	0.0084	0.2874	0.2251	6.7
H(N6)	0.3377	0.3713	0.0298	5.6
H(6A)	0.1560	0.3712	0.2747	6.5
H(6B)	0.1866	0.4097	0.2159	6.5
H(7A)	0.6109	0.2913	0.2198	10.6
H(7B)	0.5390	0.1865	0.2289	10.6
H(8A)	0.6119	0.1025	0.1715	8.5
H(8B)	0.6388	0.2207	0.1432	8.5
H(9A)	0.5890	0.1989	0.0468	10.5
H(9B)	0.4792	0.1523	0.0126	10.5
H(10A)	0.4548	0.3277	-0.0125	10.3
H(10B)	0.5401	0.3734	0.0425	10.3
H(11A)	0.4743	0.5100	0.0794	9.2
H(11B)	0.3658	0.5071	0.0956	9.2
H(12A)	0.4550	0.4942	0.1834	10.3
H(12B)	0.5532	0.4482	0.1634	10.3
H(131)	0.2073	0.2263	-0.0680	13.1
H(131A)	0.0774	0.2625	-0.0385	12.2
H(132)	0.1313	0.1224	-0.0932	13.1
H(132A)	0.0099	0.1807	-0.0878	12.2
H(133)	0.0886	0.2516	-0.0944	13.1
H(133A)	-0.0018	0.1735	-0.0217	12.2
H(141)	0.1893	-0.1767	0.0734	6.4
H(141A)	0.1070	-0.1210	0.0199	6.4
H(142)	0.1903	-0.2095	0.0074	6.4
H(142A)	0.1903	-0.2095	0.0074	6.4
H(143)	0.3055	-0.1165	0.0380	11.0
H(143A)	0.1893	-0.1767	0.0734	6.4

Calculated Hydrogen Atoms Coordinates for
[Co2 [9]aneN3(OH)2PO2(OCH3)2](ClO4)3.H2O

atom	x	y	z	occupancy
H(N1)	0.2929	0.2623	0.2467	
H(1A)	0.2642	0.1559	0.3178	
H(1B)	0.1431	0.1703	0.2958	
H(N2)	0.1479	-0.0335	0.1738	
H(2A)	0.1646	-0.0225	0.2795	
H(2B)	0.2666	-0.0000	0.2578	
H(N3)	0.0340	0.2850	0.1125	
H(3A)	-0.0122	-0.0263	0.1775	
H(3B)	0.0096	0.0701	0.2278	
H(N4)	0.4223	0.3244	0.2081	
H(4A)	-0.0906	0.1700	0.1515	
H(4B)	-0.0406	0.1084	0.1041	
H(N5)	0.4842	0.0742	0.0984	
H(5A)	0.0145	0.3954	0.1837	
H(5B)	0.0084	0.2874	0.2251	
H(N6)	0.3377	0.3713	0.0298	
H(6A)	0.1560	0.3712	0.2747	
H(6B)	0.1866	0.4097	0.2159	
H(7A)	0.6109	0.2913	0.2198	
H(7B)	0.5390	0.1865	0.2289	
H(8A)	0.6119	0.1025	0.1715	
H(8B)	0.6388	0.2207	0.1432	
H(9A)	0.5890	0.1989	0.0468	
H(9B)	0.4792	0.1523	0.0126	
H(10A)	0.4548	0.3277	-0.0125	
H(10B)	0.5401	0.3734	0.0425	
H(11A)	0.4743	0.5100	0.0794	
H(11B)	0.3658	0.5071	0.0956	
H(12A)	0.4550	0.4942	0.1834	
H(12B)	0.5532	0.4482	0.1634	
H(131)	0.2073	0.2263	-0.0680	0.600
H(131A)	0.0774	0.2625	-0.0385	0.400
H(132)	0.1313	0.1224	-0.0932	0.600
H(132A)	0.0099	0.1807	-0.0878	0.400
H(133)	0.0886	0.2516	-0.0944	0.600
H(133A)	-0.0018	0.1735	-0.0217	0.400
H(141)	0.1893	-0.1767	0.0734	0.400
H(141A)	0.1070	-0.1210	0.0199	0.400
H(142)	0.1903	-0.2095	0.0074	0.400
H(142A)	0.1903	-0.2095	0.0074	0.400
H(143)	0.3055	-0.1165	0.0380	0.600
H(143A)	0.1893	-0.1767	0.0734	0.400